



Molecular and Functional Characterization of Endocannabinoid Hydrolases

Nada S Mahmood

M.B.Ch.B, M.Sc

This thesis is submitted to the University of Nottingham for the degree of

Doctor of Philosophy

June 2018

Abstract

Background: It is now widely accepted that cannabinoids (whether synthetic or endogenous ligands) have multiple physiological, psychological and pathological effects. One area of research is investigating how to increase endogenous cannabinoid levels for potential therapeutic benefit, principally by pharmacological inhibition. However, many enzymes within the endocannabinoid system are lacking pharmacological tools such as inhibitors and/or defined substrate/s. Therefore, the development of high throughput screening assays for compound libraries will pave the way for investigation of the biochemical and pharmacological properties of these enzymes and will open the door for further in vivo studies.

Monoacylglycerols, are subjected to hydrolysis by multiple lipases with monoacylglycerol lipase (MAGL) being the principle hydrolysing enzyme in the brain, alongside ‘minority’ enzymes, such as ABHD6 and ABHD12 (Blankman *et al.*, 2007). ABHD6 was recently described as having a potential role in 2-arachidonyl glycerol hydrolysis and its characterization is crucial for understanding and exploitation of endocannabinoid signalling pathways. This project aimed to identify the biochemical characteristics and the cellular and subcellular distribution of these hydrolysing enzymes (particularly ABHD6 and MAGL) and to generate potential high throughput screening assays (HTS).

Methods: A radiometric-based enzyme assay (using [³H]-2-oleoylglycerol as a substrate) was used to measure enzyme activity in rat tissues and cell lines using the reported selective inhibitors for MAGL and ABHD6. Cloning of human recombinant tagged and un-tagged versions of enzymes was done to assess functional activity and sub-cellular distribution of these enzymes. Lentiviral construct expressing ABHD6 was made to allow expression in primary cells. Expression of ABHD6, MAGL and X1MAGL (a splice variant for MAGL in rat) mRNA was determined by quantitative RT-PCR. Immunoblotting and activity based protein profile of over-expressed enzymes in host cells (HEK293) were conducted. A number of colorimetric and fluorescent esterase assays were set up and validated for high through screening of enzymes. Among them, the 4-

Methylumbelliferyl heptanoate (MUH) assay was extensively studied as an ABHD6 in *vitro* assay.

Results: The hydrolysis of 2OG in rat neural tissues appears to be mediated predominantly through MAGL and an as yet unidentified lipase/s, with little contribution from ABHD6. In contrast, high levels of ABHD6 activity were detected in rat intestines. Two isoforms of human MAGL were successfully cloned and characterized. Results for mRNA expression indicated both MAGL and ABHD6 were expressed in all of tissues tested. Notably, ABHD6 showed high level of mRNA expression in rat intestines in comparison to MAGL. Immuno-staining of flag-tagged ABHD6 showed significant cytoplasmic distribution of ABHD6. In addition, nuclear membrane distribution was evident in both transfected and primary cells. MUH hydrolytic assay results proved to be useful for ABHD6 modulators screening in recombinant systems.

Conclusion: The findings from this piece of work provide insight into the functional activities of hydrolase enzymes in a number of rat tissues and cell lines. It also provides a further step in the understanding of cellular and subcellular localization of ABHD6 and MAGLs. MUH assay offers the opportunity for the discovery of a new range of selective and potent ABHD6 inhibitors.

Acknowledgements

Thanks and praise to Allah, the Lord of all for helping me fulfil this work.

I would like to express my sincere gratitude and thanks to Dr. Steve Alexander for his kind supervision, guidance and support throughout this study.

My thanks and appreciation are to Dr. Andy Bennett, for his help and support. I would like also to thank my third supervisor, Dr. Vicky Chapman.

My debt is endless and I am grateful and sincere to my family for their unlimited support and patience (my beloved parents and brothers) and my husband (Dr. Ahmed Khalil), who gave the immense help, love and encouragement that I needed throughout the work. To my adorable daughters (Maghfra and Misk) and son (Seraj) I say, thanks for giving me unlimited happiness.

Finally, I wish to express my thanks to every person who, in one way or another, has contributed in the completion of the present study (I would put names down but I am too afraid of missing someone out by accident).

List of abbreviations

2-AG: 2-arachidonyl glycerol

2OG: 2-oleoylglycerol

ABHD12: α/β hydrolase domain 12

ABHD6: α/β hydrolase domain 6

AEA: arachidonylethanolamine (anadamide)

CB₁: Cannabinoid receptor 1

CB₂: Cannabinoid receptor 2

cDNA: Complementary deoxyribonucleic acid

COX-2: Cyclo-oxygenase 2

DAGL α/β : Diacylglycerol lipase α/β

dpm: disintegration per minute (a unit for radioactivity measure)

ECB: endocannabinoid

FAAH: fatty acid amide hydrolase

IC₅₀: Half maximal inhibitory concentration

MAFP: Methylarachidonoyl fluorophosphonate

MAGL: monoacylglycerol lipase

MAGs: monoacylglycerols

PG: Prostaglandin

ICC: immunocytochemistry

PFC: prefrontal cortex

Publications

Nada Mahmood, Andy J Bennett, Victoria Chapman and Steve PH Alexander. Exploring ABHD6 Genetic Expression in Rat Tissues. 25th Annual Symposium of the International Cannabinoid Research Society, Wolfville, Canada, June 28 – July 3, 2015.
<http://www.icrs.co/SYMPOSIUM.2015/ICRS2015.Programme.pdf>.

Nada Mahmood, Andy J Bennett, Victoria Chapman and Steve PH Alexander. 2-Oleoylglycerol Hydrolysis in the Rat Brain. 26th Annual Symposium of the International Cannabinoid Research Society, Bukovina, Poland, June 26 – July 1, 2016.
<http://www.icrs.co/SYMPOSIUM.2016/ICRS2016.PROGRAMME.PUBLIC.pdf>

Nada Mahmood, Yousra Abdul Maqsood, Sadia Shabnam, Andy J Bennett & Steve PH Alexander. In *vitro* esterase assays for human recombinant monoacylglycerol hydrolases (MAGL, ABHD6, ABHD12). 28th Annual Symposium of the International Cannabinoid Research Society, Montréal, Canada, 22 – 27 June 2017.
<http://www.icrs.co/SYMPOSIUM.2017/ICRS2017.FINAL.PROGRAMME.pdf>

Nada Mahmood, Yousra Abdul Maqsood, Andy J Bennett & Steve PH Alexander. The application of a fluorogenic substrate for recombinant $\alpha\beta$ hydrolase 6 (ABHD6) activity. 8th European Workshop on Cannabinoid Research, University of Roehampton, UK, 31 August – 2 September 2017.
<https://www.bps.ac.uk/BPSMemberPortal/media/BPSWebsite/Assets/EWCR2017-Roehampton-UPDATE.pdf>

Table of Contents

1.	General introduction.....	1
1.1	Introduction and background.....	1
1.1.1	History of Cannabis	1
1.1.2	Cannabinoid ligands	2
1.1.3	Cannabinoid receptors	2
1.2	Endocannabinoids Synthesis and metabolism	9
1.2.1	Synthesis.....	10
1.2.2	Metabolism.....	11
1.3	Neuro-physiological function.....	12
1.4	Clinical applications and restrictions.....	13
1.5	Focus on the main 2-AG hydrolysing enzymes.....	14
1.6	Role of ABHD6 in patho/physiological conditions.....	16
1.6.1	Metabolic disorders	16
1.6.2	Diabetes and insulin level	18
1.6.3	Schizophrenia	18
1.6.4	Inflammation and autoimmune diseases	18
1.6.5	Miscellaneous neurological conditions.....	19
1.6.6	Ewing tumours and other cancers	20
1.7	Role of MAGL in physio/pathological conditions.....	21
1.7.1	Pain and inflammation.....	22
1.7.2	Metabolic disorders	23
1.7.3	Stress, depression and addiction	24
1.7.4	Cancer and its related syndromes	25
1.8	ABHD6 inhibitors	25
1.9	MAGL inhibitors.....	27
1.10	Biochemical Characteristics of 2-AG hydrolases	30
1.10.1	Enzyme activity in Human	30
1.10.2	Enzyme activity in mice	30
1.10.3	Enzyme activity in Rats	31
1.11	Aim of thesis	33
2.	Material and Methods.....	35
2.1	Reagents	35
2.2	Cell culture methods.....	35
2.2.1	Primary cell culture	35
2.2.2	Cell line culture	35
2.2.3	Trans-well cell culture	36
2.2.4	Transfection.....	37
2.3	Radiometric enzyme assay	37
2.3.1	Samples preparation.....	38
2.3.2	Assay method	39
2.4	Molecular biology methods.....	40
2.4.1	Cloning Primers and thermal conditions.....	40
2.4.2	Polymerase chain reaction (PCR) and Cloning into plasmid vectors.....	42
2.4.3	Sub-cloning into mammalian expression vectors.....	43
2.4.4	RNA isolation and Agilent tests	43
2.4.5	Complementary DNA (cDNA) synthesis.....	43
2.4.6	TaqMan real-time quantitative PCR	44
2.5	Protein quantification	46
2.5.1	Bicinchoninic Acid (BCA) protein assay.....	46

2.5.2	Lowry test.....	46
2.6	Immunoblotting.....	47
2.6.1	Sample preparation.....	47
2.6.2	Gel electrophoresis.....	47
2.6.3	Immunoblot stripping.....	48
2.7	Immunocytochemistry.....	49
2.8	Activity Based Protein Profile (ABPP).....	50
2.9	Viral infection.....	50
2.9.1	Primers and PCR.....	50
2.9.2	Transfection.....	54
2.9.3	Harvesting.....	54
2.9.4	Infection.....	54
3.	Characterization of MAGL and ABHD6 in rat tissues, cell transfects and primary cultured cells..	56
3.1	Introduction.....	56
3.2	Aim of this Chapter.....	58
3.3	Methods.....	59
3.4	Results.....	59
3.4.1	Concentration inhibition curve of JJKK048 in rat neurological tissues.....	60
3.4.2	Concentration inhibition curve for WWL123 in spinal cord.....	61
3.4.3	Combination of WWL123 and JJKK048 in rat neurological tissues.....	62
3.4.4	[³ H]-2OG hydrolysis in rat intestine preparations: the effects of inhibitors and biological sex	64
3.4.5	Soluble 2OG hydrolase activity in the small intestine.....	67
3.4.6	Activity in Transfects.....	69
3.4.7	[³ H]-AEA as substrate.....	79
3.4.8	Activity with different inhibitors.....	80
3.4.9	Activity in native HEK293 cells.....	82
3.4.10	Activity in other cell lines.....	82
3.4.11	Activity in primary culture cells.....	84
3.5	Discussion.....	86
3.5.1	MAGL and ABHD6 in rat neural tissues.....	86
3.5.2	MAGL and ABHD6 in rat intestines.....	88
3.5.3	Activity in transfects.....	90
3.5.4	Native Enzyme Activities in cell lines.....	94
3.5.5	Activity in primary cell culture.....	95
4.	mRNA detection and subcellular localization of MAGLs and ABHD6.....	99
4.1	Introduction.....	99
4.1.1	Genetic expression in rat tissues.....	99
4.1.2	Subcellular localization of the enzymes.....	100
4.2	Aim of this Chapter.....	102
4.3	Methods.....	102
4.4	Results.....	103
4.4.1	Determination of mRNA level in rat tissues.....	103
4.4.2	Immunostaining of human recombinant tagged MAGLs.....	106
4.4.3	Immunostaining of human recombinant tagged ABHD6.....	110
4.4.4	Nuclear distribution of MAGL and ABHD6.....	116
4.4.5	Subcellular localization of ABHD6 in neurons and astrocytes.....	120
4.5	Discussion.....	124
4.5.1	Exploring mRNA in rat tissues.....	124
4.5.2	Subcellular localization of human MAGL1, MAGL2 and ABHD6 in transfected cells and primary cell culture.....	125
4.5.3	Focus on primary cell culture and viral infection.....	128
4.5.4	Implication of ABHD6 distribution.....	129
5.	MAGL and ABHD6 high throughput assays.....	135
5.1	Introduction.....	135
5.2	Aim of this Chapter.....	138
5.3	Methods.....	139
5.3.1	4-NPA assay.....	139

5.3.2	4-Methylumbelliferyloleate and 4-methylumbelliferylheptanoate assays.....	139
5.3.3	Glycerol detection assay	140
5.4	Results.....	141
5.4.1	4-NPA assay	141
5.4.2	4-MUO assay.....	144
5.4.3	Glycerol detection assay	146
5.4.4	4-MUH assay.....	148
5.5	Discussion	162
5.5.1	4-NPA.....	162
5.5.2	4-MUO assay.....	163
5.5.3	Glycerol detection assay	164
5.5.4	4-MUH assay.....	164
6.	General Discussion.....	170
6.1	Discussion	170
6.2	Limitations	174
6.3	Future perspectives.....	175
7.	References:.....	180
8.	Appendix.....	210
8.1	Section A.....	210
8.2	Section B	241

List of Figures

Figure 1.1 Chemical structure of cannabinoid ligand.	4
Figure 1.2 Schematic representation of the major pathways of anandamide and 2-arachidonyl glycerol synthesis, degradation and transformation.	11
Figure 1.3 Subcellular localization of MAGL, ABHD6 and ABHD12.	16
Figure 1.4 α/β -Hydrolase domain 6 (ABHD6) pathologies.	21
Figure 1.5 Chemical structure of some of ABHD6 and MAGL inhibitors.	27
Figure 2.1 Schematic illustration of cells on transwell (Adapted from transwell Corning.com).	37
Figure 2.2 Schematic of 2OG hydrolysis by MAGL and ABHD6 to generate glycerol and oleic acid.	40
Figure 2.3 A representative image of an acceptable standard curve.	45
Figure 3.1 Concentration inhibition curves of JKKK048 against [3H]-2OG hydrolysis in rat spinal cord and prefrontal cortex preparations.	61
Figure 3.2 Concentration inhibition analysis of WWL123 against [3H]- 2OG hydrolysis in both fractions of rat spinal cord.	62
Figure 3.3 Concentration inhibition curves of WWL123 with [3H]-2OG hydrolysis after complete inhibition of MAGL in rat spinal cord, pre-frontal cortex and hippocampus.	63
Figure 3.4 WWL123 inhibition of [3H]-2OG hydrolysis in the absence of MAGL activity in	65
Figure 3.5 Representative figure comparing stable versus transient transfection.	70
Figure 3.6 Representative images for co-transfection with GFP in HEK293.	71
Figure 3.7 Representative image for transfection with an empty vector.	71
Figure 3.8 Concentration inhibition curve of JKKK048 on [3H]-2OG hydrolysis in transfected HEK293 cells with MAGL1 and MAGL2.	72
Figure 3.9 Activity Based Protein Profile of MAGL transfects.	74
Figure 3.10 Concentration inhibition curve of WWL123 on [3H]-2OG hydrolysis in ABHD6 transfected HEK293 cell membranes.	75
Figure 3.11 Concentration inhibition curve of WWL70 on [3H]-2OG hydrolysis in soluble.	76
Figure 3.12 Activity Based Protein Profile of ABHD6-transfected HEK293 cells with.	78
Figure 3.13 Concentration inhibition curve of JKKK048 on [3H]-2OG hydrolysis in ABHD6- transfected HEK293 cells.	78
Figure 3.14 [3H] AEA hydrolysis in the membrane fractions of MAGL1, MAGL2 and ABHD6-transfected HEK293 and rat liver.	79
Figure 3.15 [3H]-2OG hydrolysis in both fractions of MAGL1 and MAGL2 transfected- HEK293 cells.	81
Figure 3.16 [3H]-2OG hydrolysis in both fractions of ABHD6 and ABHD12-transfected HEK293 cells.	81
Figure 3.17 [3H]-2OG hydrolysis in membranous fraction of MAGL1, MAGL2 and ABHD6-transfected HEK293.	82
Figure 3.18 [3H]-2OG hydrolysis in cells derived from rat brain (neurons, astrocytes and microglia).	85
Figure 4.1 RT-qPCR analysis of the distribution of rat MAGL, X1MAGL and ABHD6 mRNAs in 19 different rat tissues.	105
Figure 4.2 Comparison of the expression level of the three genes in rat tissues (visual correlation analysis).	106
Figure 4.3 Representative images of native HEK293 cells as negative controls.	107
Figure 4.4 Subcellular localization of C-terminal HA-tagged MAGL1 expressed in HEK293 cells.	107
Figure 4.5 Subcellular localization of N-terminal HA-tagged MAGL1 expressed in HEK293 cells.	107
Figure 4.6 Subcellular localization of C-terminal HA-tagged MAGL2 expressed in HEK293 cells.	108
Figure 4.7 Subcellular localization of N-terminal HA-tagged MAGL2 overexpressed in HEK293 cells.	108
Figure 4.8 Representative immunoblot of HA-tag and β -actin in un-transfected and MAGL1-transfected HEK293 cells.	109
Figure 4.9 Representative immunoblot showing expression of tagged MAGL2 in two fractions, cytosol and membrane in transfected HEK293.	109
Figure 4.10 Representative immunostaining of empty vector transfected HEK293 cells.	111
Figure 4.11 Localization of C-terminus HA-tag protein in transfected HEK293 cells.	112
Figure 4.12 Localization of N-terminus HA-tag protein in transfected HEK293 cells.	113
Figure 4.13 Microscopy of C-terminus HA-ABHD6 in HEK293 cells.	114
Figure 4.14 Microscopy of N-terminus HA-ABHD6 in HEK293 cells.	114
Figure 4.15 Immunoblotting of cytosolic and membrane fractions of HEK293 cells transfected with empty vector or N- or C-terminal HA-tagged ABHD6. α -tubulin was used as a loading control.	115
Figure 4.16 Western blot of nuclear and plasma membrane fractions of HA-ABHD6 transfects and native HEK293.	118
Figure 4.17 Stripping of nuclear and membranous blots of HA-ABHD6 transfects and native HEK293.	119
Figure 4.18 Re-probing of above stripping blots.	119
Figure 4.19 Western blot of nuclear fraction of HA-ABHD6 transfects and native HEK with the two membrane markers.	120
Figure 4.20 Western blot of nuclear and membranous fractions of HA-MAGL1 probed with the two membranous marker antibodies.	120

Figure 4.21 Representative image of mice neonatal cortical neurones.	121
Figure 4.22 Viral expression of GFP in mice neonatal cortical neurones.	121
Figure 4.23 Localization of virally expressed N-terminus HA-tagged ABHD6 in mice neonatal cortical neurones.	122
Figure 4.24 Viral expression of GFP in rat neonatal cortical astrocytes.	123
Figure 4.25 Viral expression of N-terminus HA-tagged ABHD6 in rat neonatal cortical astrocytes.	123
Figure 5.1 A schematic of the α/β hydrolase fold protein superfamily.	135
Figure 5.2 The glycerol detection assay of endocannabinoid hydrolysing enzymes.	138
Figure 5.3 Schematic clarify the chemical reaction of 4-NPA hydrolysis.	139
Figure 5.4 Schematic clarify the chemical reaction of 4-MUO hydrolysis.	140
Figure 5.5 Schematic clarify the chemical reaction of 4-MUH hydrolysis.	140
Figure 5.6 Michaelis-Menten analysis of 4-NPA hydrolysis by two fractions of recombinant MAGL1 transiently expressed in HEK293 cells.	142
Figure 5.7 Hydrolysis of 2mM 4-NPA by two fractions of recombinant enzymes.	143
Figure 5.8 Hydrolysis of 4-NPA by 5 points protein dilution of recombinant MAGL1 and control.	144
Figure 5.9 Hydrolysis of different concentrations of 4-MUO by rat liver soluble fraction.	145
Figure 5.10 Hydrolysis of 4-MUO by doubling protein dilutions of rat liver and control.	145
Figure 5.11 Hydrolysis of 4-MUO by two fractions of recombinant enzymes.	146
Figure 5.12 Linearity of glycerol standard plot in lab generated kit and commercial kit assays at various time points.	147
Figure 5.13 Hydrolysis of three 2-monoacylglycerol substrates in lab generated kit.	148
Figure 5.14 Hydrolysis of 4-MUH by two fractions of recombinant enzymes at 250 μ M final concentration.	149
Figure 5.15 Michaelis-Menten analysis of 4-MUH in ABHD6-HEK293 membrane preparations.	150
Figure 5.16 Hydrolysis of MUH by 1 μ M concentrations of eleven different inhibitors in ABHD6-HEK293 membrane preparation.	151
Figure 5.17 Concentration inhibition curves of MAFP, JKKK048, WWL123 and.	152
Figure 5.18 Blind screening of a range of drugs as potential inhibitors of MUH.	153
Figure 5.19 Concentration inhibition curve of orlistat for MUH.	154
Figure 5.20 Hydrolysis of 4-MUH by putative substrates (at 100 μ M).	154
Figure 5.21 Hydrolysis of 4-MUH by 125X fold protein dilution of rat intestine membranes.	156
Figure 5.22 Michaelis-Menten analysis of 4-MUH in rat intestine membranes.	156
Figure 5.23 Michaelis-Menten analysis of 4-MUH hydrolysis in rat hippocampus membranes.	157
Figure 5.24 MUH Hydrolysis in rat hippocampus membranes in the presence of 1 μ M concentrations of eleven different inhibitors.	159
Figure 5.25 Concentration inhibition curve of WWL70 for 4-MUH hydrolysis in rat hippocampus membranes.	159
Figure 6.1 Chemical structure of arachidonoyl-1-thioglycerol.	178

List of Tables

Table 1.1 Biochemical aspects of ABHD6 inhibitors from literature.	26
Table 1.2 Biochemical aspects of miscellaneous MAGL inhibitors from literature	29
Table 2.1 Primer sequences and vectors used in cloning. Red font indicates restriction enzyme cutting sites. Coding DNA Sequence (CDS) is on the rightmost column. T _m was calculated by using http://tmcaculator.neb.com	41
Table 2.2 primers sequence, vectors and restriction enzymes used in cloning the Tagged version of human MAGL1, MAGL2 and ABHD6 genes. Red font identifies the sites for restriction DNA cutting enzymes while the blue font represents the HA-tag.....	41
Table 2.3 Thermal conditions for the cloned genes.	42
Table 2.4 Thermal cycle for the tagged genes.	42
Table 2.5 Taqman mixture reaction	44
Table 2.6 Primer and probe sequences of rat Taqman gene expression	45
Table 2.7 List of antibodies used in immunoblotting.....	48
Table 2.8 List of antibodies used in ICC.	49
Table 2.9 PCR condition for the amplification attB N-ABHD6.	50
Table 2.10 Primers for ABHD6 and GFP for entry clone.	52
Table 2.11 The components of colony PCR.	53
Table 2.12 Colony PCR conditions for entry clone.	53
Table 2.13 Colony PCR conditions for expression clone.	53
Table 3.1 [3H]-2OG hydrolysis in two fractions of rat spinal cord and prefrontal cortex.	60
Table 3.2 [3H]-2OG hydrolysis in rat spinal cord.	62
Table 3.3 [3H]-2OG hydrolysis in particulate and soluble fractions of rat tissues in the presence of 100 nM JJKK048 and increasing concentrations of WWL123.	63
Table 3.4 [3H]-2OG hydrolysis in male and female rat intestine.	66
Table 3.5 The hydrolytic activity of [3H]-2OG in rat small intestine treated with serial concentrations of Protease Inhibitors.	67
Table 3.6 [3H]-2OG hydrolytic activity assayed in rat small intestine homogenized with and without protease inhibitors (P.I.).....	68
Table 3.7 [3H]-2OG hydrolytic activity in epithelial and muscular layers of rat small intestine.	68
Table 3.8 [3H]-2OG hydrolytic activity in epithelial layer of rat small intestine.	69
Table 3.9 [3H]-2OG hydrolytic activity assayed in membrane fractions of transient vs stable transfection in HEK293.	70
Table 3.10 [3H]-2OG hydrolysis in HEK293 cells transfected with MAGL1 and MAGL2 in four independent experiments performed in duplicate.....	73
Table 3.11 [3H]-2OG hydrolysis in ABHD6-transfected HEK293 cells.	77
Table 3.12 [3H]-2OG hydrolysis in both fractions of ABHD6-transfected HEK293 cells in the presence of fixed concentrations of different inhibitors.....	77
Table 3.13 [3H]-2OG hydrolysis in both fractions of native HEK293 cells.	82
Table 3.14 [3H]-2OG hydrolysis in fractions of HCA-7 cells.	83
Table 3.15 [3H]-2OG hydrolysis in fractions of N2a cells.	83
Table 3.16 [3H]-2OG hydrolysis in fractions of Caco-2 cells.	83
Table 3.17 [3H]-2OG hydrolysis in both fractions of rat astrocytes, neurons and microglia.....	85
Table 4.1 Hydrolytic activity in tagged MAGL1 and MAGL2 transfected HEK293 cells.	110
Table 4.2 Hydrolytic activity in tagged ABHD6 transfected HEK293.	115

Table 4.3 Hydrolytic activity in nuclear fractions of native HEK, MAGL1, MAGL2 and ABHD6 transfects in response to three inhibitors and mitochondrial fraction in native HEK and ABHD6 transfects in response to WWL123.	117
Table 5.1 Master mix component and final concentrations in glycerol detection assay.	141
Table 5.2 Km values for MUH hydrolysis in rat hippocampal membranes.	157

Chapter One

General Introduction

1. General introduction

1.1 Introduction and background

This Chapter will start with a concise description of cannabinoids and the endocannabinoid (ECB) system, including ligands, enzymes, receptors and associated signalling mechanisms. This will then be followed by a review of key areas in ECB synthesis and metabolism. The review will continue with an overview of the potential roles of ABHD6 and MAGL and their inhibitors in patho/physiological conditions. The final Section will describe biochemical aspects of the main 2-AG hydrolases in different species and recombinant systems.

1.1.1 History of Cannabis

Cannabis sativa has been exploited for centuries to obtain relief from pain and improvement in mood status. Every part of the plants (flower, leaves, seeds and hemp fibre) has been used in different forms (smoked, inhaled and orally consumed) by many nations over many years. The Chinese Emperor Shennong Bencao Jing, 5000 years ago, was reported to be the first person to recommend *Cannabis* as a medicinal remedy (Earleywine, 2002).

Due to the psychotropic effects of *Cannabis* intake, it was prohibited by the Dangerous Drugs Act of 1925 in UK. The first trial to extract cannabinoids was conducted in the mid-twentieth century (Cunha *et al.*, 2011; Uchigashima *et al.*, 2007). In the sixties, Mechoulam managed to isolate and describe the chemical structure of Δ^9 -tetrahydrocannabinol (THC) (Gaoni *et al.*, 1964) (Figure 1.1) as the principle psychoactive ingredient of *Cannabis* and the prototype among the 60-100 bioactive metabolites (highly lipophilic bi- or tricyclic ringed structures); extracted from this plant, it is the focus of the majority of cannabinoid studies conducted since its discovery (Alexander, 2014; Ameri, 1999; Biegon, 2004; Hanus, 2009; Irving *et al.*, 2002). Synthetic analogues of THC, which, together with THC itself, were shown to act mainly on two types of GPCR (G protein-coupled receptors): CB₁ and CB₂ receptors (see below). Together with the enzymes responsible for synthesising, hydrolysing and controlling endocannabinoid levels in the body, this has been collectively called the

endocannabinoid system and has been revealed to play important physiological and pathophysiological roles (Di Marzo, 2008). Two main endocannabinoids have been studied so far: 2-arachidonylglycerol (2-AG) and anandamide (AEA). Recently, a number of non-cannabinoid plant products have also been shown to display cannabinoid receptor ligand-like activity. It has been suggested, therefore, that “phytocannabinoid is now defined as any plant-derived natural product capable of either directly interacting with cannabinoid receptors or sharing chemical similarity with cannabinoids or both” (Gertsch *et al.*, 2010).

1.1.2 Cannabinoid ligands

The ligands that bind to CB₁ and CB₂ receptors can be classified according to chemical structure and pharmacological activity (Howlett *et al.*, 2002):

- 1) Agonists
 - a) Classical cannabinoids: it includes derivatives of dibenzopyran. The class includes both natural and synthetic analogue compounds. The best examples are Δ^9 -THC and 11 hydroxy- Δ^8 -THC –dimethyl (HU-210) (Pertwee *et al.*, 2010) (see Figure 1.1).
 - b) Non-classical cannabinoids: the same basic structure as the classical types but lacking the pyran ring of THC. It includes the series of bicyclic and tricyclic cannabinoid analogues (Melvin *et al.*, 1984; Pertwee *et al.*, 2010). The example here is CP55940 (see Figure 1.1).
 - c) Aminoalkylindoles: These are structurally not related to THC. The prototype is R-(+)-WIN55212 (see Figure 1.1).
 - d) Fatty acid derivatives: derivatives of arachidonic acid. Anandamide and 2-AG are representative examples.
- 2) Cannabinoid receptor antagonists or inverse agonists: Diarylpyrazoles (rimonabant /SR141716A and SR144528) and related chemical series (Howlett *et al.*, 2002).

1.1.3 Cannabinoid receptors

1.1.3.1 Introduction

To date, there are two types of classical cannabinoid receptors defined; distinguished by their amino acid sequences, tissue distribution and signalling mechanisms. Both receptors are coupled through pertussis toxin-sensitive G_{i/o}

proteins to inhibit adenylyl cyclase and stimulate mitogen-activated protein kinases (Howlett *et al.*, 2002). The earliest study showing targeting of GPCR by cannabinoids was conducted by Howlett and colleagues in 1986 (Howlett *et al.*, 1986). GPCRs have a common structure of seven hydrophobic trans-membrane segments with an extracellular amino terminus and an intracellular carboxyl terminus and they are of 5 families: the rhodopsin family (including the cannabinoid receptors), the adhesion family, the frizzled/ taste family, the glutamate family, and the secretin family (Fredriksson *et al.*, 2003). These receptors mediate a wide range of intracellular signalling pathways that facilitate cellular development, differentiation, proliferation and migration.

1.1.3.2 CB₁ and CB₂ receptors

The determination and characterization of a cannabinoid receptor from brain was first reported in 1988 (Devane *et al.*, 1988). In 1990, the CB₁ receptor was identified by cloning at a molecular level from rat brain (Matsuda *et al.*, 1990). Soon after, CB₁ receptors were identified in both human and mouse (Gerard *et al.*, 1991) (Chakrabarti *et al.*, 1995). These species share 97 %-99 % similarity in amino acid sequences (Howlett *et al.*, 2002). In man, however, the CB₁ receptor shares only 48 % homology of protein sequence with CB₂ (Howlett *et al.*, 2002). The CB₁ receptor has an extensive distribution in the central nervous system and it is the most densely expressed GPCR in the brain (Herkenham *et al.*, 1990; Matsuda *et al.*, 1990). The CB₁ receptor is highly expressed in the cerebellum, cortex and hippocampus, areas responsible for cognitive control, motor and emotional function, therefore, activation of CB₁ receptors leads to the behavioural and psychotropic actions of cannabinoids. CB₁ receptors are also found in the hypothalamus and brainstem, with an action on perception of pain and thermoregulation (Patel *et al.*, 2010) and expressed in the spinal cord as well (Farquhar-Smith *et al.*, 2000). In neurones, the CB₁ receptor is positioned pre-synaptically (Egertova *et al.*, 2000) to control neurotransmitter release (for example: acetylcholine, 5-hydroxytryptamine, noradrenaline, dopamine, glutamate and GABA) (Pertwee, 2009).

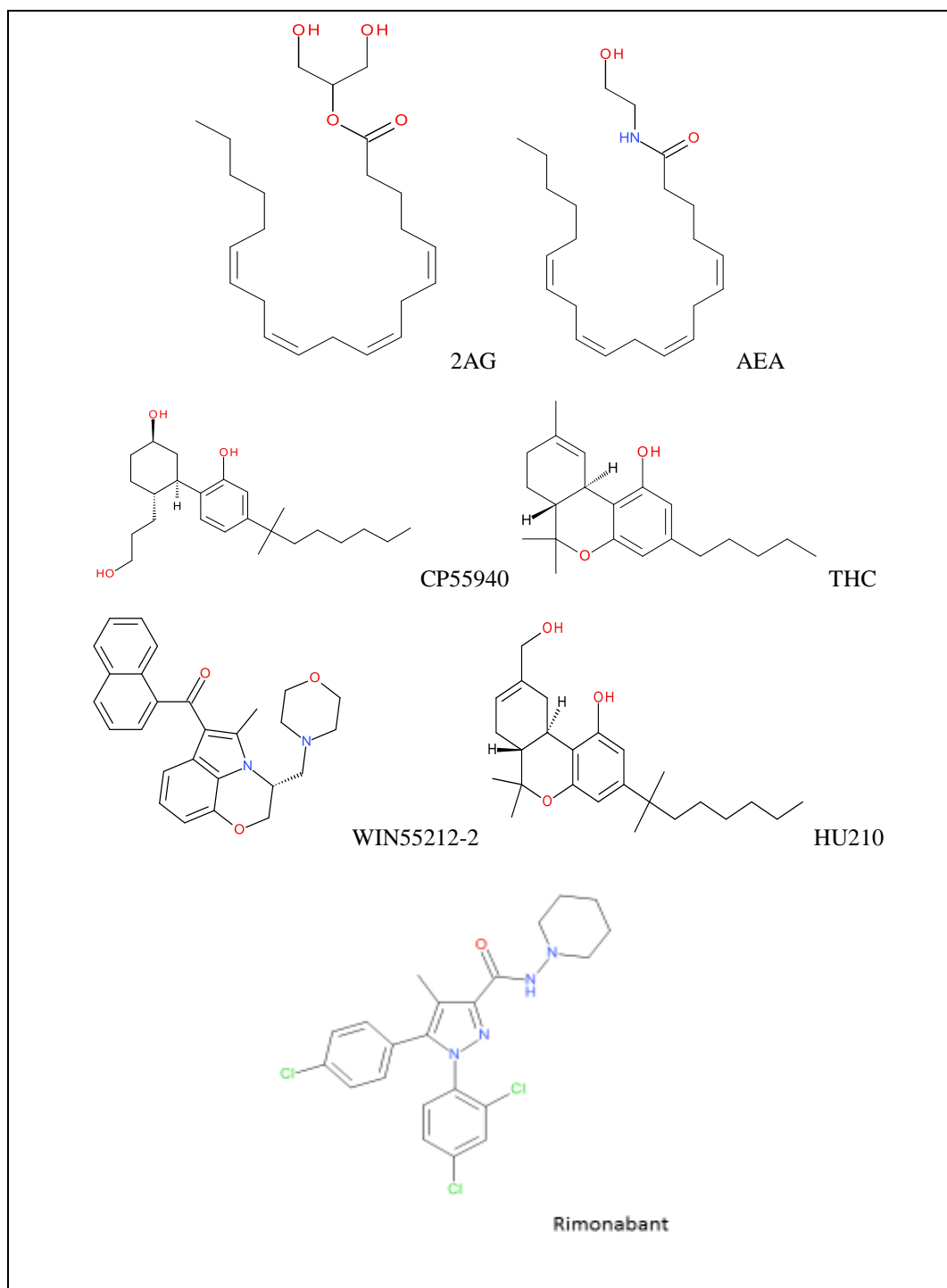


Figure 1.1 Chemical structure of cannabinoid ligand.

The distribution of CB₁ receptors explains the wide range of effects associated with its global activation through *Cannabis* intake. These comprise hypomotility (Adams *et al.*, 1996), short term memory disruption (Hall *et al.*, 1998), anti-nociception (Agarwal *et al.*, 2007b), euphoria and intoxication (Ameri, 1999) and

distorted time perception (Mathew *et al.*, 1998). In addition, it also plays a positive role in controlling nausea, vomiting, appetite, intra-ocular pressure and decreases muscle spasticity; in contrast, it exhibits adverse effects on memory and cognition (Howlett *et al.*, 2002).

Peripherally, the CB₁ receptor has been found in the uterus, adipocyte, liver (Patel *et al.*, 2010), adrenal, heart, ovary and prostate (Galiegue *et al.*, 1995) and in nociceptive terminals (Agarwal *et al.*, 2007a); mRNA encoding for CB₁ receptors has been reported in testis (Gerard *et al.*, 1991) and in immune cells (Howlett *et al.*, 2002) to regulate different physiological process such as energy control and reproduction. Interestingly, CB₁ receptors are mostly absent in the respiratory area of the brainstem and that is why there are no respiratory symptoms upon overdose of cannabinoids (Tsou *et al.*, 1998).

A CB₂ cannabinoid receptor was cloned from HL-60 cells (human lymphoblast cells) (Munro *et al.*, 1993) and was reported to be a peripheral receptor for cannabinoids, expressed mainly in immune cells, osteoblasts and osteoclasts. Therefore, it was proposed to have a role in immune function (modulation of cytokine release) and bone remodelling (Howlett *et al.*, 2002). In addition, the CB₂ receptor has been detected in other immune cells; mast cells (Samson *et al.*, 2003), T-cells (Schatz *et al.*, 1997) and B-lymphocytes (Galiegue *et al.*, 1995). The distribution of these receptors in healthy central nervous system tissue is quite controversial; it has been suggested that the extent of its expression in human brain is limited (Benito *et al.*, 2008) as well as in rat spinal cord (Zhang *et al.*, 2003). Some recent evidence exists for central neural expression of CB₂ receptors reported to be expressed in glial cells within the CNS (Beltramo *et al.*, 2006; Maresz *et al.*, 2005; Stella, 2010; Stella, 2004).

1.1.3.3 Signalling

Inhibitory G proteins (G_{i/o}) play a role in cannabinoid receptor signalling function. Subsequently, this will lead to inhibition of adenylyl cyclase and reduced adenosine 3',5'-cyclic monophosphate, increased K⁺ efflux and reduced calcium influx (Elphick *et al.*, 2001), hence, reduced neurotransmitter release.

Both CB₁ and CB₂ receptors also activate extracellular signal-regulated protein kinases (Bouaboula *et al.*, 1995).

1.1.3.4 Other cannabinoid receptors

Endocannabinoids not only work through CB₁ and CB₂ receptors; there are other receptors that can be activated by cannabinoids.

1.1.3.4.1 GPR55

This receptor has been emerged as a putative “CB₃” cannabinoid receptor although it shares less than 15% sequence homology with CB₁ and CB₂ (Yang *et al.*, 2016). Its mRNA is widely distributed centrally and peripherally. GPR55 has been implicated in inflammation (Yang *et al.*, 2016) and in neuropathic pain (Staton *et al.*, 2008).

1.1.3.4.2 GPR119

OEA (an analogue of AEA) and 2OG (an analogue of 2-AG) are natural agonists for GPR119 (Hansen *et al.*, 2011). This receptor has been implicated in obesity, as its activation reduced food intake and weight gain in rodent (Overton *et al.*, 2006). GPR119 receptors are expressed in human and rodent pancreas, brain and intestine. Activation of GPR119 stimulates glucagon like peptide-1 (GLP-1) release which regulates glucose and insulin levels, as well as satiety status (Prasad-Reddy *et al.*, 2015).

1.1.3.4.3 GPR18

Three cannabinoids were reported as full agonists of GPR18: AEA, N-arachidonoyl glycine (NAGly) and THC (McHugh *et al.*, 2010). GPR18 mRNA expression was reported in human spleen and testis while it was not detected in many other tissues: liver, brain, kidney, pancreas, heart, lung and colon (Gantz *et al.*, 1997). 2-AG was reported to be ineffective on GPR18 (Yin *et al.*, 2009). There is limited amount of information available about this receptor and further research is needed.

1.1.3.4.4 Ion channels

Ion channels play an important role in cannabinoid actions, which may be either direct or indirect. Evidence for the role of anion channels is very limited when

compared to cation channels and the evidence supports involvement of Ca^{2+} and K^+ channels more than Na^+ channels. It is well reviewed in (Pertwee, 2010).

1.1.3.4.5 Calcium channels

2-AG (and other ECB) can bind to L-type voltage-gated calcium channels ($\text{Ca}_v1.2$), possibly in a non-competitive/allosteric manner; their reported IC_{50} or apparent K_i value range from 3.2 to 40 μM (Johnson *et al.*, 1993; Oz *et al.*, 2004; Oz *et al.*, 2000; Shimasue *et al.*, 1996). 2-AG induced an inhibitory effect on P-type calcium channel current peak amplitude (by 78 %) at 10 μM (Fisyunov *et al.*, 2006).

1.1.3.4.6 Potassium channels

Potassium channels modulate neuronal and muscle excitability. Human cardiac $\text{K}_v1.5$ channels were reported to be inhibited by 2-AG with an IC_{50} value of 2.5 μM (Barana *et al.*, 2010). In parallel, AEA and THC directly inhibited $\text{K}_v1.2 \text{ K}^+$ channels (ubiquitously found in the mammalian brain) with IC_{50} values of 2.7 and 2.4 μM , respectively (Poling *et al.*, 1996).

1.1.3.4.7 Sodium channels

2-AG, arachidonoyl glycerol ether (noladin ether), N-arachidonoyl-dopamine (NADA) have been found to cause functional inhibition of mouse brain synaptoneurosomal voltage-gated sodium channels with relatively high IC_{50} values of 90, 51 and 20 μM , respectively (Duan, Liao, *et al.*, 2008; Duan, Zheng, *et al.*, 2008).

1.1.3.4.8 TRPV1 channels

The transient receptor potential vanilloid subfamily member 1 (TRPV1, capsaicin receptor) is one of the transient receptor potential (TRP) superfamily of nonselective cation channels which has six members (TRPV1-6) that mediates pain sensations; is commonly activated by a wide variety of exogenous and endogenous, physical and chemical stimuli (for example: acidic pH and heating) and it is densely expressed in sensory neurons (Tominaga *et al.*, 1998).

Most of the literature shows very little functional activity of 2-AG at TRPV1 receptors (Abood *et al.*, 2012) in comparison to anandamide and its analogues (reviewed in (Basso *et al.*, 2017)). Recently, it has been suggested that MAG may

play several physiological roles via TRPV1 depending upon the cellular and tissue context (Iwasaki *et al.*, 2008; Poursharifi *et al.*, 2017; Zygmunt *et al.*, 2013)

1.1.3.4.9 Nuclear hormone receptors

PPARs (peroxisome proliferator-activated receptors) belong to the family of nuclear hormone receptors comprising three isoforms: α , β and γ (O'Sullivan, 2007). PPARs are sensors of fatty acid levels and, as endocannabinoids are fatty acid derivatives, it is not surprising that endocannabinoids activate PPARs (O'Sullivan, 2007). Generally, there are three mechanisms by which cannabinoids are reported to activate PPARs: direct binding, metabolism to other compounds that directly bind to PPARs or via intracellular signalling processes.

The first evidence of the ability of 2-AG to interact with PPARs came from a study conducted by Kozak (Kozak *et al.*, 2002) which showed that lipoxygenase (LOX) metabolism of 2-AG lead to formation of 15-hydroxyeicosatetraenoic acid glyceryl ester, 15-HETE-G, at concentrations of 1–10 μM that increased the transcriptional activity of PPAR α , as shown in a reporter gene assay. Recently, it was shown that induction of adipose tissue browning (by 1-MAG) is mediated in part through the activation of PPAR α and γ (Zhao *et al.*, 2016). On the other hand, AEA, PEA and OEA are also agonists of PPAR α and play roles in regulation of inflammation and feeding (Bisogno *et al.*, 2002; Fowler *et al.*, 2001).

PPAR γ is involved in the regulation of insulin sensitivity, inflammation and adipocyte formation. Ligands of PPAR γ , such as the thiazolidinediones, are used clinically in the treatment of type 2 diabetes to improve insulin sensitivity. 2-AG was reported to bind to PPAR γ with the same potency as anandamide ($\text{IC}_{50} = 10 \mu\text{M}$) (Bouaboula *et al.*, 2005). In addition, Rockwell (Rockwell *et al.*, 2006) found that 2-AG activated PPAR γ to produce anti-inflammatory effects. In that study, it was shown that 2-AG had an EC_{50} value of 30 μM in a reporter gene assay in 3T3-L1 cells (mice adipose tissue) expressing recombinant receptors. Furthermore, 2-AG also activated PPAR γ transcriptional activity and stimulated the differentiation of fibroblasts into adipocytes (Fievet *et al.*, 2006); Stienstra *et al.*, 2007).

PPAR β (also known as PPAR δ) is ubiquitously expressed. Evidence suggests that this receptor has a metabolic regulatory function (Barish *et al.*, 2006), but has not been extensively examined for activation by cannabinoids.

1.2 Endocannabinoids Synthesis and metabolism

All the endocannabinoids (endogenous cannabinoids) that have been identified till now are of lipid origin and allocated in two main lipid families: N-acylethanolamines (NAEs) and 2-monoacyl-glycerols (2-MAGs) which show similar pharmacological profiles, but little structural similarity, to THC (van der Stelt *et al.*, 2003). The prototypes for the above two families are N-arachidonylethanolamine (anandamide, AEA) (Devane *et al.*, 1992) and N-arachidonoyl dopamine (NADA) (Huang *et al.*, 2002) for NAEs and 2-arachidonoylglycerol (2-AG) (Mechoulam *et al.*, 1995), and 2-oleoylglycerol (2OG) (Dinh *et al.*, 2002a) as representative of MAGs (Figure 1.1).

The discovery of the two principle most abundant, well-established, polyunsaturated fatty acid derivatives, AEA and 2-AG dated back to the mid-nineties. Both act as agonists with nanomolar affinity to CB₁ and CB₂ receptors (like THC) (Devane *et al.*, 1992; Mechoulam *et al.*, 1995) in both man and other mammals (Di Marzo *et al.*, 2007).

Anandamide was discovered in 1992 from extracts of pig brain (Devane *et al.*, 1992) and it is a partial agonist at CB₁ receptors (although of high affinity) and a relatively weak ligand at CB₂ receptors (Pertwee, 2006). AEA concentration is 1000 fold lower than 2-AG in mammalian neuronal tissue (Buczynski *et al.*, 2010). 2-AG was identified from canine gut (Mechoulam *et al.*, 1995). It is a full agonist at both receptors (Gonsiorek *et al.*, 2000) and is much more abundant than anandamide in the brain (Pertwee, 2006). It exhibits higher intrinsic efficacy than anandamide at both CB₁ and CB₂ receptors (Pertwee, 1999) and has a relatively higher affinity for CB₁ than CB₂ receptors (Howlett *et al.*, 2002).

The action of the ECB system is tightly controlled by the rapid synthesis and the fast transport or metabolism by the corresponding enzymes.

1.2.1 Synthesis

The two endocannabinoids AEA and 2-AG have distinct synthetic pathways. One proposed mechanism for AEA synthesis is comprised of transference (by transacylation) of an arachidonoyl sidechain of phosphatidylcholine to the free amine of phosphatidylethanolamine to form *N*-arachidonoylphosphatidylethanolamine, NAPE, a membrane lipid. A second step is the hydrolysis of this phospholipid by a distinct phospholipase D activity, called NAPE-PLD, to generate anandamide and phosphatidic acid (Sugiura *et al.*, 1996). Importantly, both steps require an elevation of intracellular calcium levels (Di Marzo *et al.*, 1994). However, genetic deletion of NAPE-PLD showed no alteration in mice brain AEA level suggested the presence of an alternative pathway (Leung *et al.*, 2006). Indeed, it has been shown that phospholipase C is able to catalyse the cleavage of NAPE (Liu *et al.*, 2006) (Figure 1.2).

2-AG synthesis involves 2 steps also; hydrolysis of phosphatidylinositol 4,5-bisphosphate to generate 1,2-diacylglycerol and inositol 1,4,5-trisphosphate by phosphatidylinositol specific phospholipase C (PLC), then 1,2-diacylglycerol can be hydrolysed by diacylglycerol lipases (DAGL α/β) (Bisogno, 2008) to generate 2-arachidonoylglycerol and free fatty acids. Notably, endocannabinoids are proposed to be synthesized on demand (not stored in vesicles like other neurotransmitters).

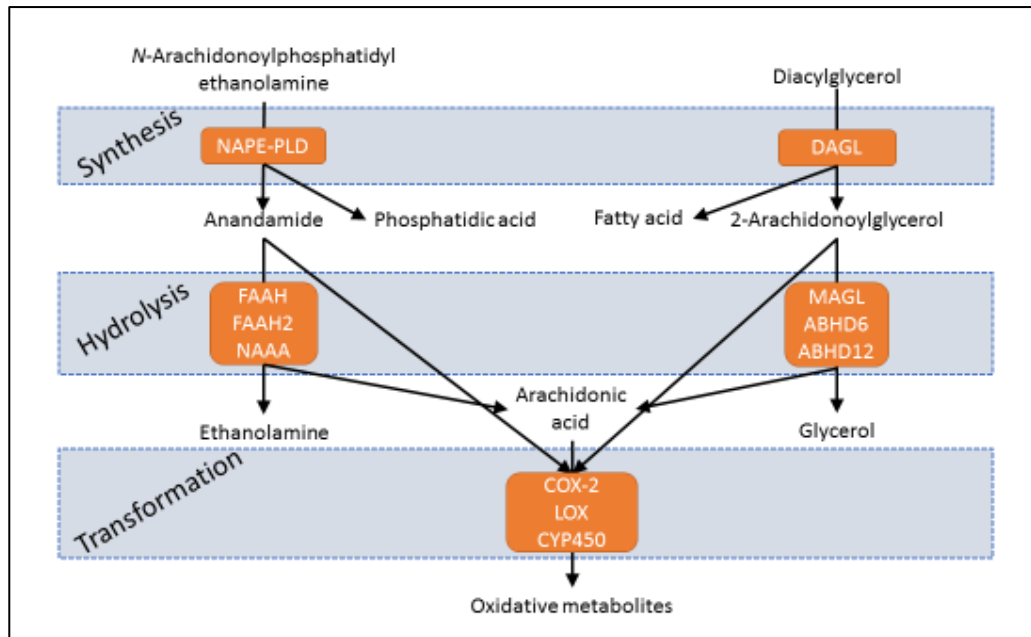


Figure 1.2 Schematic representation of the major pathways of anandamide and 2-arachidonyl glycerol synthesis, degradation and transformation.

Adapted from (Fowler et al., 2017).

1.2.2 Metabolism

There appear to be two steps for endocannabinoids to be removed from the synaptic cleft: cellular uptake and intracellular enzymatic hydrolysis (Matias *et al.*, 2007). Cellular uptake occurs through simple membranous diffusion as ECB are highly lipophilic compounds (Hillard *et al.*, 1985). The involvement of specific transporter process is a matter of controversy. FAAH-like anandamide transporter 1 (FLAT-1) was suggested as a carrier for AEA (Fu *et al.*, 2011), but its existence has been disputed (Fowler, 2014).

Intracellularly, anandamide in the nervous system is metabolized primarily by the microsomal enzyme fatty acid amide hydrolase (FAAH) (Ahn *et al.*, 2008), a membrane-bound, amidase subfamily of serine hydrolase, found abundantly in liver and brain (Deutsch *et al.*, 1993), to give arachidonic acid and ethanolamine. There is a second isoform of FAAH, FAAH2, that has been identified in man, rabbits and elephants but not in rats, mice and dogs (Wei *et al.*, 2006). FAAH2 and *N*-acyl ethanolamine hydrolysing acid amidase (NAAA) may contribute to the hydrolysis of AEA in particular cell types (Ahn *et al.*, 2008). On the other hand, 2-AG has been reported to be hydrolysed by several enzymes, but primarily by monoacylglycerol lipase (MAGL), from the lipase subfamily of serine

hydrolase, which has been reported in many tissues including brain and adipose tissue to generate arachidonic acid and glycerol (Dinh *et al.*, 2002a). Two other serine hydrolases, α/β -hydrolase domain 6 (ABHD6) and ABHD12 are also thought to be responsible for 2-AG degradation (Blankman *et al.*, 2007) (Figure 1.2).

Oxidative metabolism of the arachidonoyl moiety (found in both anandamide and 2-AG) has also been reported by lipoxygenases (LOX) (Kozak *et al.*, 2002), cytochrome P450 isoforms (Snider *et al.*, 2009) and cyclooxygenase-2 (COX-2) (Fowler, 2007) to generate bioactive products (Bisogno, 2008; Ho *et al.*, 2007) that exert their effects through a mechanism other than CB₁ receptors. For example, cyclooxygenase-2 transforms both anandamide and 2-AG to prostaglandin-like metabolites which regulate endocannabinoid tone at particular hippocampal pathways (Kim *et al.*, 2004) and have a wide array of roles in cellular responses (Manna *et al.*, 2014). However, biotransformation of both endogenous cannabinoids by lipoxygenase results in unclear physiological roles of the metabolites (Bisogno, 2008; Ho *et al.*, 2007) (Figure 1.2).

1.3 Neuro-physiological function

Synaptic plasticity is one of the important neurochemical foundations for different physiological brain activities, first described in 1973 (Bliss *et al.*, 1973; Xu *et al.*, 2015). It occurs in both excitatory and inhibitory synapses in response to various stimuli and events and its efficacy is dependent on the synaptic densities of receptors (Xu *et al.*, 2015).

Endocannabinoids contribute to short-term (seconds to minutes) (Alexander, 2014) and long-term synaptic plasticity (5-10 minutes) (Kano, 2014). These are phenomena dependent on cannabinoid receptors. The emerging evidence strongly suggests that 2-AG is considered the main messenger for these events (Kano, 2014) while AEA involvement is still controversial (Pan *et al.*, 2009a; Xu *et al.*, 2015). Depolarisation-evoked suppression of excitation (DSE) and depolarisation-evoked suppression of inhibition (DSI) are consequences of endocannabinoid release and action, both of which are representative of short-term plasticity.

In brief, synthesis of ECB in postsynaptic neurons occurs in response to post-synaptic depolarization and/or receptor activation, this in turn in a retrograde manner activates pre-synaptic CB₁ receptors which inhibit neurotransmitter release (glutamate or GABA as the primary excitatory or inhibitory CNS neurotransmitters, respectively, and hence the name DSE and DSI, respectively) at a variety of synapses throughout the central and peripheral nervous systems.

1.4 Clinical applications and restrictions

The wide array of therapeutic uses of *Cannabis* over the centuries was the impetus behind focusing research on cannabinoids to discover either new analogues or new pharmacological applications. Initially, there has been a drive to produce synthetic agonists that help to alleviate medical disorders such as nausea and pain; however, psychological side effects (sedation, dissociation and other psychotropic activity impairment) remain an obstacle. These side effects probably occurred through activation of the central CB₁ receptor. The first trials of cannabinoid receptor agonists in the clinical field were less than 40 years ago (Pertwee, 2009). Sativex® was the first medication licenced in UK for treating multiple sclerosis spasticity and peripheral neuropathic pain as an add-on drug (Nurmikko *et al.*, 2007). Nabilone (Cesamet®), Dronabinol (synthetic Δ⁹-THC) (Marinol®) have therapeutic applications (to treat chemotherapy-induced nausea and vomiting, to increase appetite and to provide neuropathic pain relief in multiple sclerosis or advanced cancer) (Pertwee, 2009) in some countries with some limitations. Rimonabant (a CB₁ receptor antagonist) (Rinaldi-Carmona *et al.*, 1994) was used for 2 years before being abandoned because of depression and suicidal ideation (Alexander, 2014; Hanus, 2009).

The rapid inactivation of endocannabinoids *in vivo* and/or their short life within the synapse stand behind the difficulty of exploiting the therapeutic characterisation of AEA and 2-AG (Deutsch *et al.*, 1993). The failure of drugs targeting cannabinoid receptors directly has lead researchers to investigate the therapeutic potential of compounds targeting specific enzymes within the cannabinoid system (Marrs *et al.*, 2011). Selective inhibitors of fatty acid amide hydrolase and monoacylglycerol lipase have been identified and there is evidence to suggest potential therapeutic actions, although till now, no successful clinical

trials have been reported (Alexander, 2014). MAGL is thought to be the main contributor to 2-AG hydrolysis and its inhibition leads to 2-AG accumulation which exerts its effects on cannabinoid receptors. However, on chronic inactivation, this leads to desensitization of CB₁ receptors and behavioural tolerance (Savinainen *et al.*, 2012). This appears not to happen with FAAH inhibitors in either acute or chronic administration (Ahn *et al.*, 2009a; Schlosburg *et al.*, 2010) or just became less effective on repeated administration (Okine *et al.*, 2012). One of the promising areas in this regard are ABHD6 and ABHD12 inhibitors. In mouse whole brain, these enzymes have been reported to be responsible for hydrolysing 4% and 9% of 2-AG activity respectively (Savinainen *et al.*, 2012). An ABHD6 inhibitor, in particular, generated a moderate reduction of 2-AG hydrolysis and no desensitization of receptors. Thus, it produced a fine tuning of 2-AG levels and a key role “within the therapeutic window of enhanced 2-AG signalling” (Marrs *et al.*, 2011).

1.5 Focus on the main 2-AG hydrolysing enzymes

One of the largest enzyme superfamilies is the α/β hydrolase fold superfamily. It has at least 19 members (Todd *et al.*, 2001). These enzymes have unrelated sequences, different substrates and different kinds of catalytic activities (Holmquist, 2000). However, a catalytic triad invariably comprises a nucleophile (serine), an acidic residue (aspartate) and a conserved histidine (Todd *et al.*, 2001). The serine hydrolases include lipases, proteases, esterases and others (Long *et al.*, 2011; Simon *et al.*, 2010), where the substrates are esters, amides or thioester bonds (Long *et al.*, 2011). For a recent review, see (Lord *et al.*, 2013).

ABHD6 belongs to the serine hydrolase family, with a typical GxSxG motif in the active site (Max *et al.*, 2009). The active site is expected to be inside the cell, thus this enzyme may be important in controlling intracellular pools of endocannabinoid (Savinainen *et al.*, 2012) (Figure 1.3). RT-PCR of human tissues showed high expression of ABHD6 in liver, kidney and ovary (Li *et al.*, 2009). Based on the primary sequence, it has 337 amino acids with a predicted molecular weight of 38 kDa, but is observed to range from 30-38 kDa (see Introduction of Chapter 3). There is, as yet, no evidence as to whether acute or chronic ABHD6 inhibition can desensitize CB receptors. However, there is

evidence that acute or chronic treatment with an ABHD6 inhibitor prevented spontaneous behavioural seizures (in a mouse model of Huntington's disease (HD)) without inducing drug tolerance (Naydenov *et al.*, 2014). In addition, acute and chronic ABHD6 antisense oligonucleotide (ASO) inhibition did not desensitize CB₁ receptors in mouse liver (Thomas *et al.*, 2013), but whether ECB desensitization occurred in other tissues and organs is unknown. It is important to mention that ABHD6 is known to only be responsible for a minor proportion of 2-AG hydrolysis (Blankman *et al.*, 2007) and this probably is beneficial in avoiding 2-AG overload, CB receptor desensitization and behavioural tolerance; hence, there is accumulating evidence for developing ABHD6 as a drug target.

MAGL was initially described in the context of lipid metabolism, serving a house-keeping function (Navia-Paldanius *et al.*, 2012), before it was recognised to have a role in endocannabinoid turnover (Labar *et al.*, 2010b). In the adipocyte, triacylglycerols are packaged into lipid droplets, and subsequently are hydrolysed into fatty acids which are released into the blood circulation on demand (Lafontan *et al.*, 2009). At the beginning of the 1960s, several studies showed the involvement of two enzymes in lipolysis not related to lipoprotein lipase (Vaughan *et al.*, 1964). They are hormone sensitive lipase, which cleaves triacylglycerols to monoacylglycerols, and MAGL which converts the latter to generate free fatty acids for release to the circulation (Fredrikson *et al.*, 1981). MAGL is a soluble enzyme and is reported to be found in both cytosolic and plasma membrane fractions (see Figure 1.3). High expression levels of mRNA (in rat) have been reported in adipose tissue, kidney and testis (Karlsson *et al.*, 1997). It has 303 amino acids and is approximately 33 kDa. Acute MAGL inhibition has anti-nociceptive effects while chronic blockade causes 2-AG elevation which desensitizes CB₁ receptor causing undesirable effects, for example, hypothermia, hypomotility and hyperreflexia (Schlosburg *et al.*, 2010).

ABHD12 is a 398 residue protein (45 kDa) and predicted to be a single-pass integral membrane protein with its active site facing the extracellular space (Blankman *et al.*, 2007) (Figure 1.3). Although widely distributed in many tissues, the highest mRNA expression is found in mouse brain (Lord *et al.*, 2013), especially the microglia (Savinainen *et al.*, 2012). However, little is known about

its functional activity and physiological role/s. Similarly to ABHD6, ABHD12 ASO treated mice were found to be protected from diet induced obesity, hepatic steatosis and insulin resistance (Thomas, 2014). ABHD12 mutations have been shown to be associated with polyneuropathy, hearing loss, ataxia, retinitis pigmentosa and cataract (PHARC) in humans (Fiskerstrand *et al.*, 2010). However, the lack of selective inhibitors and /or substrate has limited exploration of this enzyme. To this end, a versatile activity assay is required to allow profiling of a large library of potential inhibitors/substrates. In fact, 2-AG hydrolase activity is the only feature potentially linking ABHD12 to the endocannabinoid system (Navia-Paldanius *et al.*, 2012). This doctoral thesis will focus mainly on 2-AG hydrolases enzymes, in particular, MAGL and ABHD6.

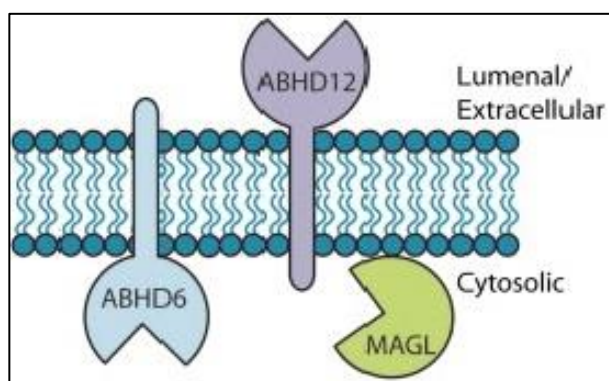


Figure 1.3 Subcellular localization of MAGL, ABHD6 and ABHD12. Adapted from (Blankman *et al.*, 2007).

1.6 Role of ABHD6 in patho/physiological conditions

There are studies suggesting that ABHD6 may have a role in certain illnesses. Accordingly, this infers that inhibition of ABHD6 might have potential therapeutic implications. In many cases, ABHD6 seemed to follow similar (if not identical) therapeutic approaches/aspects to MAGL and research is still ongoing to unveil ABHD6 role/s. Below is a summary of this research, disease/pathology involved (Figure 1.4), techniques used and the investigated species.

1.6.1 Metabolic disorders

A study exploring ABHD6's biochemistry and physiology in certain peripheral tissues (liver, adipose tissue and kidney) (Thomas *et al.*, 2013) provided key information about ABHD6 and metabolic disorders. Harlan male mice

(maintained either on standard rodent chow or switched to high fat diet) were injected simultaneously with murine specific ABHD6 antisense oligonucleotides (ASO) for an ABHD6 knockdown study, in either dietary setting, without altering expression in the brain. Quantitative Real-Time PCR showed that ABHD6 mRNA expression was up regulated by high fat diet in the liver and small intestine and ABHD6 knockdown protected against body weight gain induced by fatty diet after 4 weeks of treatment. There was, in addition, significant reduction of the total hepatic triacylglycerol in high fat diet mice and protection from high fat diet-induced hyperglycaemia, hyper-insulinemia and improvement in glucose and insulin tolerance (by mass spectrometry of liver lipids and glucose and insulin tolerance tests) as well as protection from hepatic steatosis. Furthermore, this ABHD6 knockdown did not alter hepatic ECB levels or cause CB₁ desensitization). Inhibition of ABHD6 suggested a role in lysophospholipid metabolism (increased their hepatic level) and protected against obesity (Thomas *et al.*, 2013).

Later on, the same research group confirmed that whole-body ABHD6 knockout mice on a high fat diet were protected from obesity, hyperinsulinemia (see below), hepatic steatosis and they had elevated energy expenditure attributed in part to browning of white adipose tissue and brown adipose tissue activation (Zhao *et al.*, 2016).

Recently, using viral mediated knockdown of ABHD6 and pharmacological approaches, ABHD6 inhibition was identified as a regulator of fasting, nutrient excess, cold, and dieting (Fisette *et al.*, 2016). Mice lacking ABHD6 from neurons of the ventromedial hypothalamus were characterized by an impaired feeding response to fasting, reduced cold induced thermogenesis and increased susceptibility to hypothermia, resistance to diet-induced weight loss (transition from high fat diet to regular chow) and increased susceptibility to high fat diet-induced obesity (Fisette *et al.*, 2016).

Finally, it has been reported that ABHD6 is a part of late endosomal/lysosomal lipid sorting machinery (Pribasnig *et al.*, 2015). ABHD6, in mouse and human, was found to degrade bis(monoacylglycerol)phosphate with high specific activity (both *in vivo* and *in vitro*, using antisense oligoneucleotides and the selectively

reported ABHD6 inhibitor KT182, respectively). Bis(monoacylglycerol)phosphate is enriched in late endosomes/lysosomes with a profound role in lipid metabolism (digesting and sorting).

1.6.2 Diabetes and insulin level

Pancreatic islets were isolated from male Wistar rats and from man; insulin secretion was studied in isolated islets and in INS82/13 cell (rat insulin secreting cell line). Overexpression and RNAi silencing knockdown of ABHD6 and MAGL were conducted together with assays of insulin secretion, HPLC and western blot analysis. The 1-MAG was generated near the plasma membrane of β cells during glucose metabolism, acting as a signalling molecule to enhance insulin secretion. 1-MAG was hydrolyzed by ABHD6 and the genetic deletion of ABHD6 was associated with enhanced *ex vivo* and *in vivo* glucose stimulated insulin secretion (GSIS) and total monoacylglycerols (Zhao *et al.*, 2014; Zhao *et al.*, 2015). In contrast, inhibition of MAGL activity pharmacologically or via siRNA knockdown of the enzyme did not affect GSIS. Importantly, administration of WWL70 (ABHD6 selective inhibitor) restored normal glucose tolerance and GSIS in an animal model of diabetes (injected with low-dose streptozotocin to induce diabetes) (Zhao *et al.*, 2014).

1.6.3 Schizophrenia

mRNA encoding ABHD6 was assessed by quantitative RT-PCR in human prefrontal cortex from otherwise healthy controls and schizophrenics *post-mortem*. Elevated levels were identified in younger subjects with shorter illness duration, compared to older subjects treated with antipsychotics. In parallel, prefrontal cortices from macaque monkeys exposed to haloperidol, olanzapine, THC or vehicle were assessed for ABHD6 mRNA expression but no differences were observed in any treatment group (Volk *et al.*, 2013).

1.6.4 Inflammation and autoimmune diseases

It has been found that there is physiological interaction between the ECB system and the prostanoid system, in that pharmacological blockade of ABHD6 (via WWL70) in macrophages (J774, murine cell line) and *in vivo* lead to increased 2-AG (dose dependent) and this increased prostaglandin D2 (PG-D2) (via COX-2) which has anti-inflammatory benefits both *in vivo* and *in vitro* (Alhouayek *et*

al., 2013). The macrophages were treated with lipopolysaccharide (LPS), a potent immune system activator. Macrophages activated with LPS release several pro-inflammatory cytokines, such as IL-1 β , IL-6, and TNF- α , and produce nitric oxide. All of these cytokines and the PGs were quantified by enzyme-linked immunosorbent assay (ELISA) and Liquid chromatography–mass spectrometry (HPLC-MS), respectively. An anti-inflammatory profile of WWL70 was also unveiled in another study where it was shown to decrease PG-E2 glycerol ester both *in vivo* and *in vitro* (Tanaka *et al.*, 2017).

In another recent study (Wen *et al.*, 2015), pharmacological inhibition of ABHD6 increased 2-AG/CB₂ signalling to exert anti-inflammatory effects. This study examined the role of WWL70 administration in experimental autoimmune encephalomyelitis (an animal model of multiple sclerosis). The neuroprotective effects reported here are reduced demyelination and axonal loss and increased survival of mature oligodendrocytes.

In addition, it is reported that there was a strong association between the high expression of ABHD6 and the development of Systemic Lupus Erythematosus (SLE), an autoimmune disease (Oparina *et al.*, 2014). Furthermore, the study also revealed that this robust correlation was specifically related to subjects of European origins and that single nucleotide polymorphisms (SNP) variant with lower ABHD6 expression is protective against it (Poursharifi *et al.*, 2017).

1.6.5 Miscellaneous neurological conditions

The first study reporting the beneficial aspects of ABHD6 inhibition was in a mouse model of traumatic brain injury (TBI) (Tchantchou *et al.*, 2013). It was found that selective inhibition of ABHD6 (using WWL70) significantly increased CB₁ and CB₂ receptor expression to 40% and 60% in the ipsilateral cerebral cortex post TBI, respectively, compared to control. In order to assess blood brain barrier function, which represent an important hallmark of TBI pathology, two steps were needed: expression of ICNA-1 (marker of leukocyte transmigration) was carried out and showed up-regulation, and fluorometric analysis of Evans blue extravasation of brain tissue which showed higher levels when compared with control groups. However, both these parameters were significantly decreased by WWL70 treatment. WWL70 reduced brain lesions and the effect

was blocked by a CB₁ receptor antagonist. Further functional recovery tests were conducted to assess motor and memory brain function and all collectively showed that fine tuning of 2-AG by ABHD6 could exert anti-inflammatory and neuroprotective effects (Tchantchou *et al.*, 2013). It is reasonable to believe that there are other beneficial aspects of ABHD6 blocking for treating patients with neurodegenerative diseases (Poursharifi *et al.*, 2017), multiple sclerosis (Wen *et al.*, 2015) and other neurological conditions.

Furthermore, selective blocking of ABHD6 is beneficial in epilepsy models. Three types of mouse were used: (WT) Wild Type mice, (Cnr1^{-/-} and Cnr2^{-/-}) mice lacking CB₁ and CB₂ receptors, treated with pentylenetetrazole (to induce seizure) and R6/2 mice (a genetic model of juvenile Huntington's disease). The study showed that selective inhibition of ABHD6 (using WWL123) exerted antiepileptic activity in these seized mice (by video EEG monitoring) mediated by GABA receptors rather than CB₁ or CB₂ receptors. Other semi-quantitative procedures were also carried out for further confirmation (Naydenov *et al.*, 2014).

It is interesting to note that during the preparation of this thesis that a novel anti-nociceptive and anti-inflammatory mechanisms of WWL70 treatment in neuropathic pain model mice was uncovered using a range of techniques: qRT-PCR, enzyme-linked immunosorbent assay (ELISA), immunohistochemistry and liquid chromatography coupled with tandem mass spectrometry (LC-MS/MS). It revealed the interaction between endocannabinoid and eicosanoid pathways and that WWL70 exert its effects via decreasing PG-E2 and COX-2 production and expression, rather than through cannabinoid receptors. Blocking ABHD6 also significantly alleviated thermal hyperalgesia and mechanical allodynia in these models (Wen *et al.*, 2018).

1.6.6 Ewing tumours and other cancers

ABHD6 is highly expressed in certain type of tumours, however, unlike MAGL, its knockdown did not inhibit abnormal cell growth (Navia-Paldanius *et al.*, 2012). EFT (Ewing Family Tumors) cell line and normal tissues underwent quantitative RT-PCR for ABHD6 expression which showed an exceptionally high expression of ABHD6 in Ewing tumours. However, knockdown of ABHD6 did not inhibit cell growth of Ewing family tumours (Max *et al.*, 2009).

It is also reported that Epstein-Barr virus (EBV) antigen 2 (which is associated with lymphomas and other EBV-associated malignancies) target ABH6 gene (Maier *et al.*, 2006). Furthermore, semi-quantitative PCR was performed among other 7 tumour cell lines, from mouse and human origin, to study DNA and protein sequence. High expression of ABHD6 was found in bone, prostate and leukocyte cancer cell lines (Li *et al.*, 2009).

In addition, ABHD6 was identified as being highly expressed, via the functional proteomic technology of activity based protein profiling, in one of the most fatal cancers which is pancreatic ductal adenocarcinoma (PDAC) (Gruner *et al.*, 2016). It was investigated in both human and mouse PDAC cell lines, *in vivo* and *in vitro* and its inhibitors, reduced both tumour proliferation and metastasis. Finally, RNAseq data and screening among liver tumour genes, ABHD6 was found as a potential anti-oncogene marker (with low ABHD6 expression in advanced hepatocellular carcinoma) (Yu *et al.*, 2016).

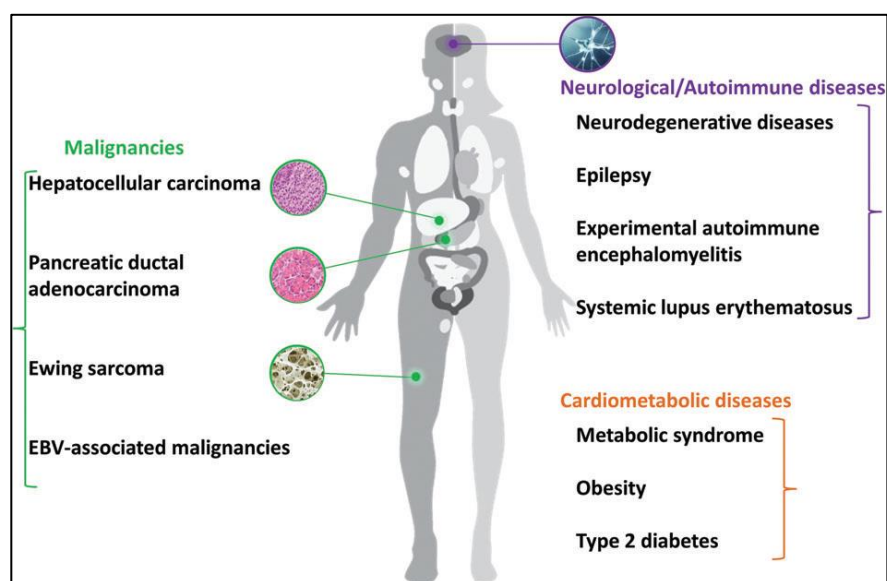


Figure 1.4 α/β -Hydrolase domain 6 (ABHD6) pathologies. On the left side, the image shows ABHD6 relation with different kinds of cancers. On the right side, it shows its involvement with various neural, immunological and metabolic diseases. Adapted from (Poursharifi *et al.*, 2017).

1.7 Role of MAGL in physio/pathological conditions

More than 50 years have passed since the first description of MAGL. MAGL research started from fat metabolism and, within recent years, it has moved toward endocannabinoid signalling and arachidonic acid metabolism (Grabner *et al.*

al., 2017). This enzyme is known to have several potential therapeutic benefits both *in vivo* and *in vitro* (as will be shown below). However, doubts and/or concerns arose as its chronic inhibition (genetic or pharmacologic) lead to, for example, functional antagonism of brain CB₁ receptor, physical dependence, impaired endocannabinoid-dependent synaptic plasticity and neuropsychiatric adverse effects (Schlosburg *et al.*, 2010).

MAGL serves a critical node within the health and disease context. Understanding metabolic, biochemical and physiological roles of MAGL, would help to accelerate the discovery of selective and potentially potent inhibitors and apply careful examination to their pathways. Below is a summary of the therapeutic potential of MAGL inhibition:

1.7.1 Pain and inflammation

It has been shown that acute MAGL inhibition exerted anti-nociceptive effects, via CB₁ receptors, in chemical, inflammatory, thermal and neuropathic pain mouse models using various MAGL inhibitors and receptor agonists (Guindon *et al.*, 2011; Kinsey *et al.*, 2009; Long *et al.*, 2009a; Mulvihill *et al.*, 2013). Interestingly, an oral MAGL inhibitor (SAR127303) was also tested. It is reported to exert anti-nociceptive effect even at repeated administration and have potential anti-epileptic properties with no tolerance detection in rodent (Griebel *et al.*, 2015).

MAGL conversely regulates 2-AG and arachidonic acid (AA) levels in several tissues (Dinh *et al.*, 2002a) and AA oxidation (COX-1, COX-2, cytochrome P450 and LOG) can convert it to other signalling molecules, such as prostaglandins (Grabner *et al.*, 2017). Non-steroidal anti-inflammatory drugs (NSAID) such as aspirin and ibuprofen, are widely used to treat pain and inflammation by blocking COX-1 and COX-2 and subsequently decreasing PGs (Rouzer *et al.*, 2011). Anti-inflammatory effects of MAGL ablation come from two levels: firstly by directly increasing 2-AG which acts on cannabinoid receptors which has been shown to have many central and peripheral anti-inflammatory effects (Bridges *et al.*, 2001; Ibrahim *et al.*, 2003; Valenzano *et al.*, 2005)(for review, see (Grabner *et al.*, 2017; Klein, 2005; Mulvihill *et al.*, 2013; Turcotte *et al.*, 2015). Secondly, by reducing AA availability for ECB independent pro-inflammatory processes (Grabner *et al.*,

2017). Indeed, reducing the supply of AA and subsequent PGs synthesis and cytokine production has been shown to be protective in LPS-induced neuroinflammation mice with both pharmacological and genetic deletion of MAGL (Nomura *et al.*, 2011b). In addition, one of the major advantages of MAGL inhibition over NSAIDs, is a lack of risk of GIT bleeding and ulcers, (Sostres *et al.*, 2013). Indeed, it was shown that JZL184, a MAGL inhibitor, protected from NSAID-induced gastric haemorrhage (Kinsey *et al.*, 2013).

It is now well known that genetic or pharmacological blockade of MAGL has profound impact in terms of neurophysiology, synaptic plasticity, inflammation and behaviour (Blankman *et al.*, 2013; Murataeva *et al.*, 2014; Viader *et al.*, 2015). In particular, it has been found that MAGL in astrocytes, rather than in neurons or microglia, is mainly responsible for converting 2-AG to neuroinflammatory PGs (Viader *et al.*, 2015). The study indicated that astrocytes exert a fundamental part in facilitating ECB-eicosanoid crosstalk in the nervous system and that selective genetic deletion of MAGL in these cultured cells was coupled to elevation of 2-AG and reduction in AA and PGs in mice.

Furthermore, MAGL blockade (by JZL184) has been shown to be beneficial in inflammatory bowel disease (trinitrobenzene sulfonic acid (TNBS)-induced colitis) mouse model in terms of restoring intestinal integrity and barrier function, reducing both histologically and macroscopically colon alternations and pro-inflammatory cytokine levels (Alhouayek *et al.*, 2011).

1.7.2 Metabolic disorders

Metabolic syndrome is a major health problem and includes combinations of pathological conditions of: high blood pressure, abdominal obesity, insulin resistance and high blood sugar and abnormal cholesterol and triglyceride level and it directly increases the risk of cardiovascular diseases and diabetes (Kaur, 2014). MAGL is well known in the context of lipolysis; triglycerides are hydrolysed by hormone sensitive lipase and adipose tissue triacylglycerol lipase into monoacylglycerols which in turn are hydrolysed by MAGL to fatty acids and glycerol (Labar *et al.*, 2010b). Furthermore, MAGL has been implicated in insulin secretion. It has been reported that MAGL inhibition (pharmacologically with 1 μ M JZL184) or RNAi silencing knockdown) or over-expression does not alter

glucose-sensitive insulin secretion in β cells (Zhao *et al.*, 2014). In contrast, MAGL inhibition using three different MAGL inhibitors (JZL184 (10 μ M), MJN110 (10 μ M) and URB602 (50 μ M)) caused GSIS blocking in the same cell line (INS82/13 cell) (Berdan *et al.*, 2016). This discrepancy was explained by the first group of researchers by the high dose of the inhibitors applied in the experiment.

While acute MAGL inhibition caused hyperphagy, as shown by Woodhams and colleagues, that single administration of JZL184 significantly increased food intake in rats (Woodhams *et al.*, 2012), long term inhibition (MAGL- knockout) decreased diet induced obesity and insulin resistance in mice (Taschler *et al.*, 2011). Furthermore, a recent study demonstrated that MAGL global deletion reduced body weight in high fat diet fed mice and that MAGL controls energy homeostasis via mobilization of fat stores (Douglass *et al.*, 2015).

1.7.3 Stress, depression and addiction

MAGL inhibitors, similarly to direct cannabinoid agonists and FAAH inhibitors, showed promising response in neuro-behavioural diseases, such as: anxiety, stress and addiction (Grabner *et al.*, 2017). It has been reported that chronic MAGL inhibition prevents stress- induced anxiety-like behaviours, while acute inhibition has little effect (Sumislawski *et al.*, 2011). The mechanism included augmentation of 2-AG levels by JZL184 and consequent activation of CB₁ receptors which prevented both behavioural and synaptic adaptations to chronic stress in mice.

In addition, chronic JZL184 treatment improved chronic stress-induced depression-like behaviour through enhancement of ECB-mammalian target of rapamycin (mTOR) signalling (Zhong *et al.*, 2014) where the mTOR signalling pathway plays a major role in depression development (Abelaira *et al.*, 2014).

Furthermore, MAGL plays a role in drug withdrawal symptoms. By enhancing ECB levels, MAGL inhibition (by JZL184) reduced withdrawal signs and ileal contractions intensity in opioid dependent mice (in a dose-dependent manner) (Ramesh *et al.*, 2011), significantly reduced the intensity of withdrawal signs precipitated in THC-dependent mice (with acute administration) (Schlosburg *et*

al., 2009) and nicotine somatic withdrawal signs in mice (dose-dependently) (Muldoon *et al.*, 2015).

1.7.4 Cancer and its related syndromes

MAGL is upregulated, providing free fatty acids (FFA) in aggressive human cancer cells and primary tumours, which is in turn implicated in escalating oncogenic lipid signalling and cancer aggressiveness (Mulvihill *et al.*, 2013). These authors also demonstrated that MAGL's blocking role in cancer was operated by ECB independent signalling; it is by reducing FFA and pro-tumorigenic lipids, for example: PG-E2 and lysophosphatidic acid (Kopp *et al.*, 2010; Mulvihill *et al.*, 2013). Impairment of cellular migration, invasiveness and aggressiveness in breast, ovarian and melanoma cancer cells was influenced by MAGL ablation (Nomura *et al.*, 2010). On the other hand, another report supported dual inhibitory actions of MAGL (using JZL184) in decreasing prostatic cancer pathogenicity by ECB signalling and low FFA pathways and they also reported high MAGL activity in aggressive prostate cancer cells (Nomura *et al.*, 2011a). High MAGL expression was reported in nasopharyngeal carcinoma (Hu *et al.*, 2014), hepatocellular carcinoma (Zhu *et al.*, 2016) and colorectal carcinoma (Ye *et al.*, 2011); in these carcinomas, it has been shown that MAGL upregulation caused increased cellular growth, invasiveness abilities and metastasis, while its downregulation decreased these characteristics. MAGL inhibition (with type II topoisomerase) also was revealed to reduce neuroblastoma cell growth (Matuszak *et al.*, 2012).

In addition, JZL184 dose-dependently suppressed vomiting in a lithium chloride model using shrews by elevating 2-AG which has anti-emetic or anti-nausea potential (Sticht *et al.*, 2012).

1.8 ABHD6 inhibitors

There are many non-selective ABHD6 inhibitors but there has been little success in developing potent and selective inhibitors (Patel *et al.*, 2015). Examples of non-selective inhibitors are: MAFP (a useful reference compound as it inhibits nearly all serine hydrolases, (Deutsch *et al.*, 1997), orlistat (THL) and RHC-80267 (DAG lipase inhibitors) and pristimerin (MAGL inhibitor, (Navia-

Paldanius *et al.*, 2012). In 2007, by screening a library of carbamate derivatives, Li et al identified WWL70 as a potent selective ABHD6 inhibitor using functional proteomic strategy (Li *et al.*, 2007). Later on, an isosteric analogue of WWL70, WWL123 (Bachovchin *et al.*, 2010) (Figure 1.5), showed adequate blood brain penetration and anti-epileptic effects (described above). KT182 and KT185 belong to triazole urea based ABHD6 inhibitors. KT 182 showed selectivity and potency in Neuro2A cells (< 5 nM, but is not commercially available) while KT185 had orally bioavailability with good selectivity against other brain and liver serine hydrolases *in vivo* (Hsu *et al.*, 2013). A dual FAAH and ABHD6 inhibitor, UCM710, was also reported (Marrs *et al.*, 2011). Table 1.1 describes the biochemical aspects of ABHD6 inhibitors.

Table 1.1 Biochemical aspects of ABHD6 inhibitors from literature.

Inhibitor	IC ₅₀ value (μM)	Tissue type	Study	Substrate/ final concentration	Detection method
WWL70	0.07	Recombinant human ABHD6 in COS-7 cells	(Li <i>et al.</i> , 2007)	FP-Rh 1 μM	ABPP
WWL123	0.43	Recombinant human ABHD6 in COS-7 cells	(Bachovchin <i>et al.</i> , 2010)	FP-Rh 2 μM	ABPP
KT182	0.002	Mouse brain membrane proteomes	(Hsu <i>et al.</i> , 2013)	FP-Rh 1 μM	ABPP
UCM710	2.4	Recombinant human ABHD6 in COS-7 cells homogenates	(Marrs <i>et al.</i> , 2011)	[3H]-2-AG ~1 nM	radiometric enzyme assay

(ABPP) Activity Based Protein Profile, (FP- Rh) Fluorophosphonate -rhodamine probe (further details in methodology Chapter).

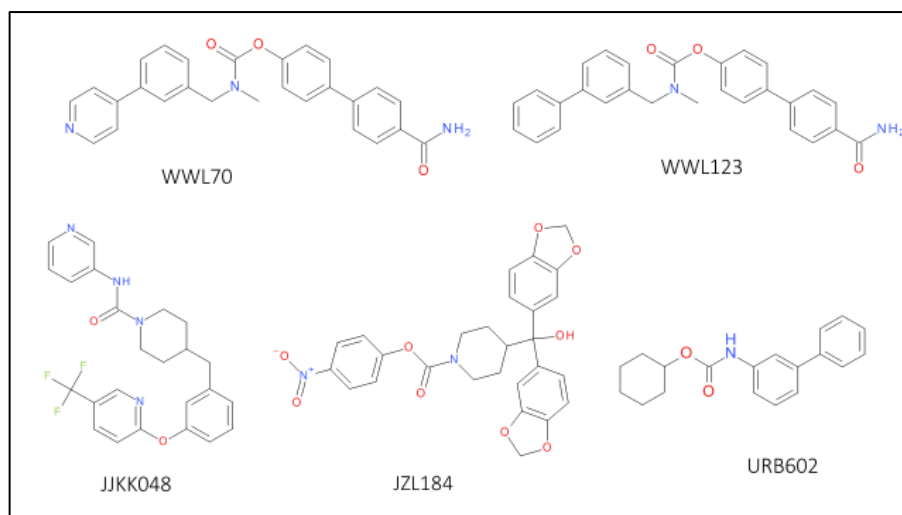


Figure 1.5 Chemical structure of some of ABHD6 and MAGL inhibitors.

1.9 MAGL inhibitors

As discussed above, pharmacological inhibition of MAGL has been reviewed and suggested to have many potential benefits. Different classes of MAGL inhibitors (based on chemical structure) have been identified; they share their inhibitory action by either binding to the nucleophilic cysteine residue (Cys¹²²) or to cysteine residues near the catalytic site (Cys²⁰¹, Cys²⁰⁸ and Cys²⁴²) (King *et al.*, 2009; Saario *et al.*, 2005; Zvonok *et al.*, 2008).

NAM belongs to a maleimide group of MAGL inhibitors. Mass spectrometry and site directed mutagenesis have revealed that NAM forms a Michael conjugate with Cys²⁴² of human MAGL thereby causing its inhibition (Zvonok *et al.*, 2008) while pristimerin (a naturally occurring terpenoid), another reported MAGL inhibitor, interacts with Cys²⁰⁸ to inhibit MAGL. However, ABHD6 was reported as an off target (IC₅₀ 98 nM) (King *et al.*, 2009).

Carbamate-based MAGL inhibitors consist of a long list of inhibitors, notable among them are JZL184, URB602, JW642 and KML29; all of them have off targets with variable affinities (Chang *et al.*, 2012). JZL184 carbamoylates (covalent modification) MAGL's serine nucleophile and hence, evokes irreversible inhibition (Figure 1.5). JZL184 showed off target effects, although the level of cross reactivity is relatively low, including FAAH (IC₅₀ 4.7 μM), ABHD6 (IC₅₀ 3.3 μM) (Long *et al.*, 2009a) and carboxylesterases especially in

peripheral tissues such as liver (Long *et al.*, 2009a; Zhang *et al.*, 2007). URB602 is another example of an inhibitor exerting off target activity with FAAH inhibition detected in rat brain homogenate by [³H]-AEA hydrolysis assay (IC₅₀ 17 μM) (Vandevoorde *et al.*, 2007). Urea based MAGL inhibitor, JJKK048, also has been reported to have FAAH as an off target (IC₅₀ 4.8 μM) (Aaltonen *et al.*, 2013) (Figure 1.5). Table 1.2 summarizes biochemical characteristics of MAGL inhibitors.

Table 1.2 Biochemical aspects of miscellaneous MAGL inhibitors from literature

Inhibitor	IC ₅₀ value (μM)	Tissue type	Study	Substrate/ Final concentration	Detection method
NAM	0.14	Rat cerebellar membranes	(Saario <i>et al.</i> , 2005)	2-AG 50 μM	AA detection by HPLC
Pristimerin	0.093	Purified E. coli recombinant rat MAGL	(King <i>et al.</i> , 2009)	2OG 10 μM	LC/MS
URB602	28	Cytosolic fraction of rat membrane	(Hohmann <i>et al.</i> , 2005)	[3H]-2OG/ Not stated	Radiometric enzyme assay
JZL184	0.010 and 0.006, respectively	Mouse brain membranes and human MAGL recombinant in COS-7 cells, respectively	(Long <i>et al.</i> , 2009a)	FP-Rh 2 μM and 2-AG 100 μM	ABPP and LC/MS
JW642	0.008 and 0.004, respectively	Mouse brain membranes and human MAGL recombinant in HEK293 cells, respectively	(Chang <i>et al.</i> , 2012)	FP-Rh 1 μM	ABPP
KML29	0.015 and 0.006, respectively	Mouse brain membranes and human MAGL recombinant in HEK293 cells, respectively	(Chang <i>et al.</i> , 2012)	FP-Rh 1 μM	ABPP
JJKK048	IC ₅₀ < 0.4 nM	Mouse, rat brain membranes and human recombinant MAGL in HEK293 cells	(Aaltonen <i>et al.</i> , 2013)	2-AG 25 μM	Fluorescent glycerol detection
MJN110	0.009	Mouse brain proteome	(Chang <i>et al.</i> , 2013)	FP-Rh 50 μM	ABPP

Activity Based Protein Profile (ABPP), Fluorophosphonate -rhodamine (FP- Rh) probe (further details in methodology Chapter), Liquid chromatography/ mass spectrometry (LC/MS)

1.10 Biochemical Characteristics of 2-AG hydrolases

Generally, since the discovery of endocannabinoids, many studies have attempted to explore biochemical aspects of these ligands and the associated enzymes, including substrate affinities, inhibitor potencies, assay methodologies and tissue distribution in particular species. However, only a few have shed light on ABHD6, ABHD12 and to some extent MAGL, in terms of biochemical or pharmacological aspects of these enzymes.

Below is a general quantitative summary (where possible) for *in vitro* experiments reported from the literature. It is described on the base of their relevance to the materials used in this thesis to give the base for the comparisons in the subsequent Chapters.

1.10.1 Enzyme activity in Human

Generally, there are limited reports of hydrolase activities in humans or human relevant recombinants. Using a glycerol detection assay in transfected HEK293 lysates, V_{max} values for hMAGL, hABHD6 and hABHD12 were 120, 45 and 42 nmol/mg/min, respectively (Navia-Paldanius *et al.*, 2012). In a comparison of different inhibitor profiles between hABHD6 and hABHD12 (with 25 μ M final concentration of 2-AG), it was found that MAFP was the most potent inhibitor (pIC_{50} values of ~ 7.77 and ~ 7.06), followed by orlistat (7.32 and 6.72) for hABHD6 and hABHD12, respectively, highlighting non selectivity of both agents. WWL70 had a pIC_{50} value of 7.07 in hABHD6 but showed no activity toward hABHD12. Pristimerin inhibited hABHD6 ($pIC_{50}=5.8$) whereas hABHD12 was resistant to this compound. Previously, pristimerin had been reported as a reversible MAGL inhibitor with a potency of ~ 7 in rat recombinant Hela lysates (King *et al.*, 2009).

1.10.2 Enzyme activity in mice

Using LC-MS detection with 2-AG (100 μ M) as a substrate, the hydrolase activities of ABHD6 and ABHD12 in brain membranes was determined as 2.6 and 5.9 nmol/min/mg, respectively (Blankman *et al.*, 2007). 10 μ M of WWL70 blocked only 5 % (non-significantly) of total brain activity (potentially reflecting

ABHD6), while orlistat (20 μM) blocked about 10 %; combination of the inhibitors appeared additive (~16 %). URB597 (FAAH inhibitor) at 10 μM failed to cause a significant inhibition (2 %).

In another study with intact mouse neurons in culture, it was reported that WWL70 (10 μM) and JZL184 (1 μM) inhibited ~ 40% and 60 % of total activity, respectively, (potentially represent ABHD6 and MAGL in those cells). This was investigated by using [^3H]-2-AG (100 μM) as substrate (Marrs *et al.*, 2010).

1.10.3 Enzyme activity in Rats

Rat cerebellar membrane hydrolysed 50 μM 2-AG at a rate of 32 nmol/min/mg protein determined using LC-MS (Saario *et al.*, 2004). URB597 was a weak inhibitor (70% control at 1 mM) of 2-AG degradation while MAFP had a pIC_{50} value of 8.7. Using 2OG as substrate and LC-MS detection in the same tissue, MAFP (1 μM) was found to inhibit ~ 92 % of MAGL activity, while URB602 (0.1 mM) exhibited ~10% inhibition (King *et al.*, 2007). In the same study, concentration inhibition analysis for URB602 conducted in both purified and non-purified rat recombinant MAGL in Hela lysates showed a statistical difference in potency (IC_{50} = 223 μM versus 81 μM , respectively). This suggested the presence of another 2OG-hydrolyzing enzyme or a post-translation modification (King *et al.*, 2007).

In rat ileum, it was shown that MAGL-like activity (100 μM [^3H]-2OG hydrolysis) was higher in the mucosal layer (521 nmol/min/mg protein) in comparison to its muscular layer (140 nmol/min/mg protein) (Duncan *et al.*, 2008). The authors reported that the soluble fractions appeared more sensitive to the inhibitory actions of URB602 than membranes where URB602 (100 μM) evoked a significant inhibition of ileum soluble MGL activity (reduced to $56 \pm 4\%$ of control activity levels). In the same study, UBR602 was able to dose-dependently attenuate whole gut transit and slow colonic propulsion in mice and these functions were absent in CB_1 receptor deficient mice (Duncan *et al.*, 2008).

As has been shown above, there are limited studies investigating the biochemical aspects of these 2-AG metabolising enzyme (especially ABHD6 and ABHD12). This represents a significant gap in our knowledge and impairs translational

research in the field. Here, it is hypothesized that there is a potential role for ABHD6 in the turn-over and signalling of endocannabinoids. To investigate this, the use of the recombinant enzymes would allow the generation of an assay that enable us to study the native enzyme in real tissues.

1.11 Aim of thesis

Currently, the role of the endocannabinoid system is well-recognised in health and disease, but less is known about the catalytic enzymes that control ECB levels in the body. While many examples of FAAH and MAGL characterization exist (Hanus *et al.*, 2010; Sugiura *et al.*, 2006), there is much less focus on ABHD6. Therefore, the main aim of this study was to gain a deeper understanding of these monoacylglycerol hydrolases by the characterization, cellular and subcellular localization of ABHD6 and MAGL using molecular, biochemical, immunocytochemical and functional assays in tissue and recombinant systems.

The major objectives of this thesis are:

- 1- To identify the distribution of ABHD6, MAGL and other enzyme activities in preparations from animal tissues
- 2- To characterize ABHD6 and MAGL biochemically in recombinant systems
- 3- To study the subcellular localization of these enzymes.
- 4- To generate high throughput screening assays for 2-AG hydrolysing enzymes.

Chapter Two

Materials and Methods

2. Material and Methods

2.1 Reagents

All of the inhibitors stocks were stored at -80 °C freezer at 10 mM concentration. DMSO and/or ethanol was used as a diluent following manufacturer's instruction. JZL184 was bought from CAYMAN (Cambridge Biosciences, Cambridge, UK) while all other inhibitors were purchased from Tocris (Bristol, UK). [³H]-2OG was obtained from American Radio-labelled Chemicals, Inc. (St Louis, MO, USA) and scintillation fluid from PerkinElmer (Emulsifier-Safe, Waltham, CA/USA).

2.2 Cell culture methods

2.2.1 Primary cell culture

Neonatal (1-2 days old male Wistar rat pups) cortical astrocytes isolation and culture (for radiometric enzyme assay and for ICC) were kindly generated by Rawan Hareeri following a protocol of (Croft *et al.*, 2016). Neonatal male Wistar rat and mouse (C57/BL6) cortical neurons (for radiometric enzyme assay and ICC) were kindly provided by Raquel Ribeiro according to the method of (Dajas-Bailador *et al.*, 2008). Rat cortical microglia (from male Sprague Dawleys) for radio-assay were donated kindly by Amer Imraish following the protocol of (Yip *et al.*, 2009) and (Bronstein *et al.*, 2013) with minor modifications. It is all done under local ethical committee Schedule 1 approval.

2.2.2 Cell line culture

All cell techniques were performed under sterile conditions in class II laminar flow cabinets. All culture reagents were warmed to 37 °C before use. Cells were grown in culture flasks at 37 °C and 95% O₂, 5% CO₂ in a humidified atmosphere.

2.2.2.1 Thawing cells

Cells were taken from liquid nitrogen and thawed by incubating the cryovial at 37 °C for 2-3 minutes before adding them to warm media in a Sterilin tube and

centrifuging at 1000 rpm for 5 min to wash and pellet the cells. After aspiration of the supernatant, one ml of media was added to the cells, which were then transferred to 15 ml media in a T175 cm² flask for overnight incubation. After 24 h, the growth media was replaced with fresh media. Cells were passaged every 2-3 days upon reaching ~90% confluency.

2.2.2.2 Subcultural passaging

The cells were washed with phosphate buffered saline (PBS) and incubated with 2 ml of warmed trypsin–EDTA (Sigma Aldrich, UK) for less than 5 min in the incubator. The cells were then collected by the addition of 8 ml of media (to neutralize trypsin) and pelleted at 1000 rpm for 5 minutes. The supernatant layer was aspirated, the pellet re-suspended with 5 ml fresh media and (with usually 1:5 dilution) transferred into the new flask. The following media and additions were used:

- HEK293: Dulbecco's Modified Eagle Medium, DMEM (Sigma, M2279) with 10% FBS, 2 mM L-glutamine and 1% Non-Essential Amino Acids (NEAA).
- CaCo2: Dulbecco's Modified Eagle Medium, DMEM (Sigma, M2279), with 10% FBS, 2 mM L-glutamine.

2.2.2.3 Cryopreservation

Freezing of cells was conducted followed the same steps of sub-culturing till re-suspension, which was achieved by the addition of freezing solution (90 % (v/v) FBS and 10 % (v/v) dimethylsulphoxide (DMSO) followed by filtration through a 0.2 µm filter (Sartorius). Cells were then transferred into labelled cryo-vials (Sarstedt, UK) and placed into a Mr. Frosty™ Freezing Container in a -80 °C freezer for 24 h and afterward transferred into liquid nitrogen.

2.2.3 Trans-well cell culture

Caco2 cells have been used to study many physiological functions of the intestinal epithelia such as transport, absorption and secretion. They spontaneously develop mature villi characteristic of the small intestinal epithelium (Ho *et al.*, 2002) when grown in conditions resembling the *in vivo* state. For this purpose, 12 well plates with poly carbonated trans-well inserts were used to culture Caco2 cells for 14–

18 days after confluence; with an insert growth area of 1.12 cm² and pore size of 0.4 μm (Corning Incorporated Costar, 3460, USA) following the manufacturer's instruction (Figure 2.1).

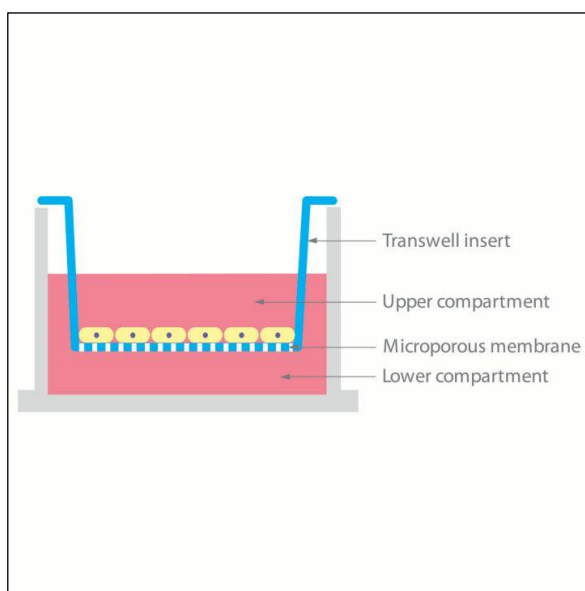


Figure 2.1 Schematic illustration of cells on transwell (Adapted from transwell Corning.com).

2.2.4 Transfection

Cells were cultured as monolayers in 6-well plates one day before transfection. Transfection was conducted following manufacturer's recommendations (X-tremeGENE HP, Roche, 06 366 546 001) in a ratio of 3:1 (w/w X-tremeGENE: DNA). After 48 h, cells were harvested.

Co-transfection with green fluorescent protein (GFP) in a ratio of 1:1 was also conducted to check transfection efficiency of the experiment, then the number of cells was assessed under fluorescent microscopy (Axiovert ZEISS, 4.8 version-40X lenses).

2.3 Radiometric enzyme assay

A radiometric enzyme-assay was carried out using 2-oleoyl-[³H]-glycerol (2OG) as substrate to determine monoacylglycerol hydrolase enzymatic activity in different tissues and cell lines.

2.3.1 Samples preparation

2.3.1.1 Tissue preparation

Selected rat tissues were chosen: prefrontal cortex, hippocampus and spinal cord as representative of rat neural tissues, while small (duodenum) and large intestine (colon) were chosen as they appeared to express the highest ABHD6 mRNA levels relative to MAGL. For each of these tissues, soluble and membrane fractions were isolated by high speed centrifugation, and tested following a standard assay protocol (Vandevoorde *et al.*, 2007) with a minor modification involving charcoal separation (Boldrup *et al.*, 2004) (Björklund *et al.*, 2010). Tissue was homogenised in 10 volumes of TE buffer (50 mM Tris-1 mM EDTA, pH 7.4) using a glass homogenizer, except for the intestines where an Ultra Turrax homogenizer was used (T25, IKA®-Labortechnik), followed by centrifugation at 30 000 g at 4 °C for 30 min to obtain the supernatant layer - the soluble fraction. The pellet was re-suspended with the same buffer volume and a second centrifugation was conducted. The second soluble fraction was discarded (except for the small intestine, where it was combined with the first fraction (Duncan *et al.*, 2008)). To the membrane fraction (second pellet), the same volume of TE buffer was added (except for small intestine where three times the volume were added (Duncan *et al.*, 2008)). Samples were quantified for protein content, labelled and stored as aliquots at -80 °C.

2.3.1.2 Homogenization of cultured cell lines

Transfected cells and other cultured cell lines were washed twice with ice cold PBS before the addition of 750 µl TE buffer to each well of a 6 well plate (50 mM Tris-1 mM EDTA, pH 7.4) and scraped to collect cells into a 1.5 ml Eppendorf for brief sonication. The cells were then centrifuged at 30 000 g for 30 min at 4 °C to obtain the supernatant layer, which was subsequently kept as aliquots at -80 °C. The pellet was re-suspended with 500 µl Tris, sonicated again and kept at -80 °C till used.

2.3.1.3 Homogenization of epithelial vs muscular fraction of small intestine

Two to four cm pieces of small intestine were irrigated with PBS and cut longitudinally. The tissue was gently stretched (to allow better access to the surface area) followed by carefully removal by scraping off the very top layer -

the epithelial (mucosal) layer. The remaining piece was the muscular layer which consists of: submucosa, muscular (circular and longitudinal) layers and serosa. These two parts were suspended separately in 5 volumes of TE buffer for one mass of tissue (for the muscular layer, Ultra Turrax homogenizer was used) followed by centrifugation and resuspending the pellet with 2 volumes of TE buffer.

2.3.2 Assay method

2-Oleoyl-[³H]-glycerol as a substrate is hydrolysed by enzymes (such as MAGL and ABHD6) to give [³H]-glycerol and free oleic acid. The un-hydrolysed 2-acylglycerol can be adsorbed to charcoal while the [³H]-glycerol remains in the aqueous phase, which was removed for scintillation counting and hence measurement of the enzyme activity. Assays were conducted in duplicate and the activity calculated as nmol/min/mg protein according to this equation:

$$(\text{Test-Blank})/(\text{Standard-Blank}) \times 10 (\text{final 2OG amount in nmoles})/[30 (\text{min}) \times \text{protein amount (mg)}].$$

Tissue was diluted with 0.1% BSA in TE buffer before each experiment. Ninety microliters of tissue were pre-incubated for 15 min at 37 °C on a shaker with 5 µl of inhibitor. For blank (without homogenate - to assess non-enzymatic hydrolysis of radio-labelled substrate) and control samples, the vehicle (typically DMSO) was used in place of the inhibitor. Then 5 µl of tritium-labelled 2OG (diluted with unlabelled 2OG to allow a final concentration of 100 µM) was added, vortexed and incubated for another 30 min on the warmed shaker. The reaction was stopped by the addition of 400 µl charcoal (8% w/v charcoal in 0.5 M HCl), vortexed and centrifuged for up to 5 minutes at 13 000 rpm to pellet the charcoal (to which is bound un-hydrolysed [³H]-2OG). Removal of 200 µl aliquots of the supernatant layer into scintillation insert vials was followed by the addition of 3-4 ml scintillation fluid and counting in a [³H] channel in a scintillation counter. Figure 2.2 represents the reaction underlying the enzymatic hydrolysis of 2OG by monoacylglycerol hydrolases.

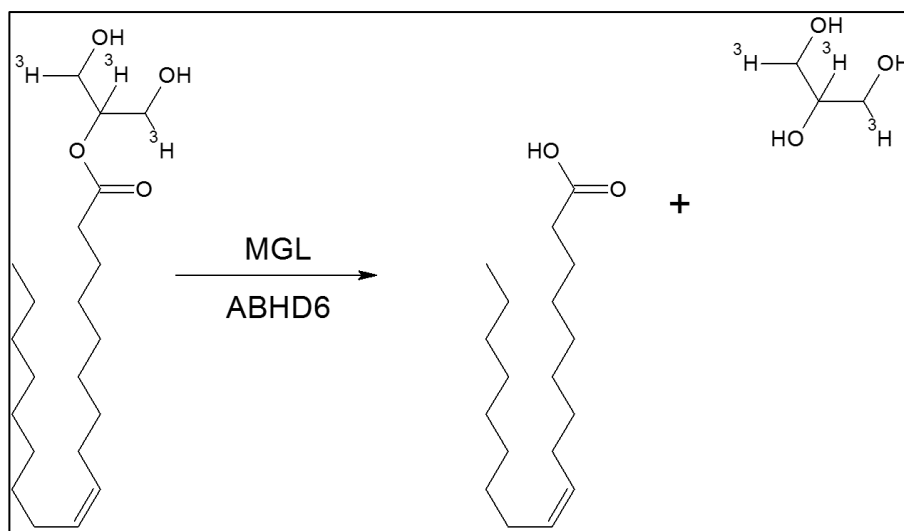


Figure 2.2 Schematic of 2OG hydrolysis by MAGL and ABHD6 to generate glycerol and oleic acid.

2.4 Molecular biology methods

2.4.1 Cloning Primers and thermal conditions

Human MAGL1, MAGL2 (a splice variant of MAGL), ABHD6 and ABHD12 were cloned in this study. In addition, tagged versions (N- and C-terminus each) with human influenza virus hemagglutinin (HA-tag) for these genes were also generated for MAGL1, MAGL2 and ABHD6. Primer sequences are shown in Table 2.1 and 2.2 (further details in Appendix Table A.1). Two further human genes encoding endocannabinoid hydrolases (FAAH1 and FAAH2) were also cloned for completeness (see Appendix-Table A.1).

Table 2.1 Primer sequences and vectors used in cloning. Red font indicates restriction enzyme cutting sites. Coding DNA Sequence (CDS) is on the rightmost column. Tm was calculated by using <http://tmcalculator.neb.com>.

Gene Name	Primer Sequence	Vector	CDS	Tm
Human MAGL1 NM_007283.6 (313 aa)	FW: ACAGGATCCGGCTGAGCGCCCCAGCCCGA (BamHI-HF®) Rev: ACA AAGCTT GGAGAGGCAGGGCAGAGGCTTGGC (HindIII)	pcDNA3.1(-)	565-1506	81 79
Human MAGL2 NM_001003794.2 (303 aa)	FW: ACAGGATCCGCGCTCGTGGCCCCGGACCT (BamHI-HF®) Rev: ACA AAGCTT CCCCAGACCATGAGCCGGGCA (HindIII)	pcDNA3.1(-)	188-1099	80 81
Human ABHD6 NM_020676.5 (337 aa)	FW: ACAGGATCCGGCTGGTCAGGAGTCAGCCAGCCT (BamHI-HF®) Rev: ACA AAGCTT TGGTGGCTGCGTCAGACTTGGGGG (HindIII)	pcDNA3.1(-)	411-1424	76 80
Human ABHD12 NM_001042472.2 (398 aa)	FW: ACAGGATCCGCGGCCTGGGCTGGGATGTGAGG (BamHI-HF®) Rev: ACA CTCGAG ACGGGAGGAGGGCAGAGGTCTTCA (XhoI)	pcDNA3.1(+)	280-1476	81 76

Table 2.2 primers sequence, vectors and restriction enzymes used in cloning the Tagged version of human MAGL1, MAGL2 and ABHD6 genes. Red font identifies the sites for restriction DNA cutting enzymes while the blue font represents the HA-tag.

Gene Name	Primer Sequence
MAGL1 –HA- N-terminus tag pcDNA3.1(-)	FW:gatc GGTACCATG TACCCATACGATGTTCCAGATTACGCT GGAAGTGGTgaaacaggacctgaagacct (KpnI) Rev:ACA AAGCTT GGAGAGGCAGGGCAGAGGCTTGGC (HindIII)
MAGL1 –HA- C-terminus tag pcDNA3.1(-)	FW: ACAGGATCCggctgagcgccccagccgaaaggcag (BamHI-HF®) Rev:gatc GGTACCTTAAGCGTAATCTGGAACATCGTATGGGTA ACCACTTCCGGGTGGGGACGCAGTTCCTGC (KpnI)
MAGL2 –HA- N-terminus tag pcDNA3.1(-)	FW:gatc GGTACCATG TACCCATACGATGTTCCAGATTACGCT GGAAGTGGTCCAGAGGAAAGTTCCTCCAGG (KpnI) Rev: ACA AAGCTT CCCCAGACCATGAGCCGGGCA (HindIII)
MAGL2 –HA- C-terminus tag pcDNA3.1(-)	FW: ACAGGATCCGCGCTCGTGGCCCCGGACCT (BamHI-HF®) Rev:gatc GGTACCTTAAGCGTAATCTGGAACATCGTATGGGTA ACCACTTCCgggtggggacgcagttcctgc (KpnI)
ABHD6 –HA- N-terminus tag pcDNA3.1(-)	FW:gatc GGTACCATG TACCCATACGATGTTCCAGATTACGCT GGAAGTGGTgatcttgatgtggttaacatg (KpnI) Rev: ACA AAGCTT TGGTGGCTGCGTCAGACTTGGGGG (HindIII)
ABHD6 –HA- C-terminus tag pcDNA3.1(-)	FW: ACAGGATCCGGCTGGTCAGGAGTCAGCCAGCCT (BamHI-HF®) Rev:gatc GGTACCTTAAGCGTAATCTGGAACATCGTATGGGTA ACCACTTCCgtccagcttctgtgtgctc (KpnI)

Primers were ordered from Eurofins (Germany). The PCR reaction was conducted using a T100 Thermal Cycler (Bio-Rad) and Phusion™ High-Fidelity DNA polymerase (New England BioLabs, M0530L) to amplify the studied genes. Human brain total RNA (M7962, Life Technology) was converted to cDNA and used as a template for amplification of MAGLs and ABHD12 while for ABHD6, human adipose tissue cDNA (provided by colleagues in the FRAME LAB) was used. For the tagged genes, the original plasmids (untagged) were used as a template. Thermal cycles are shown in Tables 2.3 and 2.4.

Table 2.3 Thermal conditions for the cloned genes.

Initial denaturation	98 °C	2 minutes
Cycling: 35x	98 °C	30 seconds
	72 °C (for ABHD12: 69.5 °C)	2 minutes
Final extension	72 °C	7 minutes
Hold	4 °C	∞

Table 2.4 Thermal cycle for the tagged genes.

Initial denaturation	98 °C	30 seconds
Cycling: 35x	98 °C	10 seconds
	72 °C	30 seconds
Final extension	72 °C	10 minutes
Hold	4 °C	∞

2.4.2 Polymerase chain reaction (PCR) and Cloning into plasmid vectors

PCR products (stained with SYBR® Green dye) were then run on an 0.8 % (w/v) agarose gel (Tris-Acetate-EDTA 1%) alongside appropriate markers at a constant voltage, cut, cleaned up by GenElute™ Gel Extraction Kit (SIGMA) and digested by two Restriction endonuclease enzymes (following manufacturer's instructions) as well as for the vector.

After purification with phenol-chloroform, sequences were ligated first to compatible restriction sites of bacterial vector p-Bluescript SK II and the plasmid was introduced into compatible competent *Escherichia coli* (XL-10 Gold) using a compatible antibiotic in agar and bacteria suspension. White colonies were picked, small scale plasmid DNA preparation (mini-prep) was done by QiAprep®

Spin Mini-prep kit (Qiagen) and sent to Gene Sequencing service - Nottingham UK. Sequences were analysed by Chromas 2 software.

2.4.3 Sub-cloning into mammalian expression vectors

Once the coding sequence identities were confirmed by Nucleotide BLAST, the plasmid was double cut (double digestion protocol, NEB) and then sub-cloned (ligation using T₄ DNA ligase, NEB) into eukaryotic expression vector pcDNA 3.1 (Invitrogen). The plasmid was then transformed in *Escherichia coli* (Genlantis-SolBL21) following the manufacturers instruction and plated onto an LB-agar plate containing ampicillin (100 µg/ml) for overnight incubation at 37°C. At this point, plasmid DNA was purified for miniprep scale for sequencing confirmation followed by plasmid Midi-prep kit (Qiagen) to obtain high quality and quantity DNA.

2.4.4 RNA isolation and Agilent tests

RNA was extracted from 19 different rat tissues using Tri-reagent® (Ambion Inc, USA) according to the manufacturer's instructions. To check the integrity and quality of RNA, samples were subjected to Agilent 2100 Bioanalyzer (Agilent Technologies, USA) following the manufacturer's protocol. It has been highly recommended to run an Agilent test as routine in every RNA extraction (Bustin, 2002). This is especially important in "unclean" tissues, for example: colon. Any samples with a RIN value below 7 were not used for cDNA synthesis (see Appendix Figure A-2).

2.4.5 Complementary DNA (cDNA) synthesis

Complementary DNA (cDNA) was made first by mixing 500 ng/µl of RNA with 3 µl of random primers (100 ng) and RNAase-free water up to 14 µl total volume and left for 5 min at 65 °C, followed by a rapid chill on ice. Whilst on ice, master mix was made by the addition of 2 µl of AffinityScript™ RT buffer (10X), 2 µl of DTT (100 mM), 1 µl of dNTP mix (100 mM) and 1 µl of AffinityScript™ Reverse Transcriptase (cat: 600109). The reaction was then left at 25 °C for 10 min, 50 °C for 1 hour and 70 °C for 15 min in a Thermocycler (MWG-Biotech Primus 69 Plus) for the reverse transcription reaction to proceed. The cDNA resulting was stored at -20 °C.

2.4.6 TaqMan real-time quantitative PCR

Probes and primers for rat ABHD6, MAGL and one variant of MAGL (X1MAGL) were designed using Primer Express 3 Software (Applied Biosystems, UK). Primers were synthesized by Eurofins Genomics (Germany). The probes were dual labelled with FAM (6-carboxy fluorescein) as a dye at the 5' end and with TAMRA (6-carboxytetramethylrhodamine) as a quencher at the 3' end. This allow fluorescent light emission. The intensity of this light is measured in real time and represents the number of DNA copies in the samples.

Using Step-One Plus™ Real Time PCR system (Applied Biosystems), mRNA levels of these genes were quantified using 96 well format based on the relative standard curve method (Biosystems, 2008). Master mix components are shown in Table 2.5.

Table 2.5 Taqman mixture reaction

Reagents	Volume (µl)
TaqMan® Universal Fast PCR Master Mix (Applied Biosystems, 4352042)	6.5
cDNA	3
Forward primer (10 µM)	0.4
Reverse primer (10 µM)	0.4
Probe (10 µM)	0.25
HPLC H ₂ O	2.45
Total Volume	13

Thermo-cycling was carried out as follows:

- 1- 95°C for 10 minutes (polymerase activation).
- 2- 95°C for 15 seconds and 60°C for one minute repeated for 40 cycles, (denaturation/annealing, elongation temperature).

An assay was excluded that did not have a standard curve with a slope between -3.0 and -3.6, efficiency of 90-100%, more than 0.5 Ct value difference between triplicates or showed detectable amplification signal in the negative controls. Figure 2.3 shows an example of accepted parameters of TaqMan PCR. Three reference genes were used in Taqman PCR (GAPDH, β-ACTIN and TBP), as no single reference gene was expressed equally across the tissues (Vandesompele *et al.*, 2002; Warrington *et al.*, 2000). Therefore, the geometric mean for the

reference genes was calculated (Vandesompele *et al.*, 2002). Table 2.6 shows primers and probes of rat MAGL, X1MAGL and ABHD6.

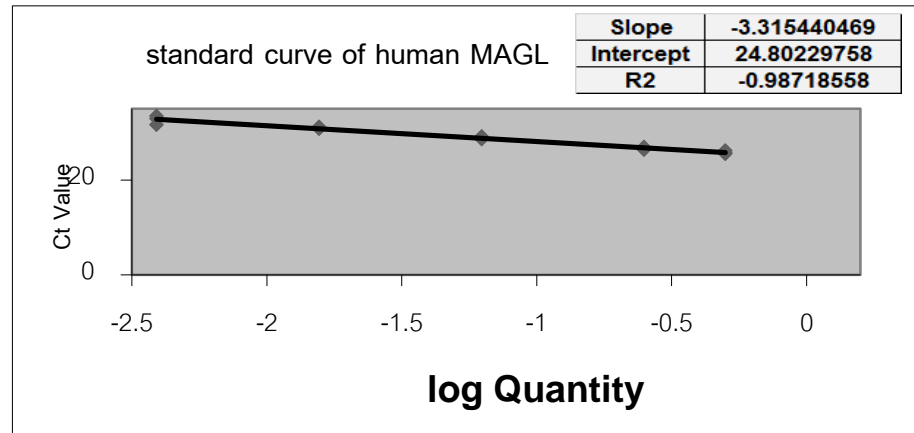


Figure 2.3 A representative image of an acceptable standard curve.

Linear regression showing a slope value of -3.3 and correlation coefficient (R^2) value of 0.98.

Table 2.6 Primer and probe sequences of rat Taqman gene expression

Name	Sequence	length	Tm (°C)	GC (%)
Rat MAGL NM-138502.2	FW:AAGTCGGAGGTTGACCTGTACAA	23	59	48
	Rev: GGATGCCAAAGCATACCTTCA	21	59	48
	Probe:CCGACCCACTCATCTGCCACGC	22	70	68
Rat X1 MAGL XM-008763053.2	FW: GGCGGTAGTGGAATGCAAAA	20	60	50
	Rev: GGAGTTCGCCTGGGTGAA	18	58	61
	Probe:CCAAGACTAATGGAAACAGGGCC CAAA	27	68	48
Rat ABHD6 NM-001007680.1	FW: GCTCGTACGTCCGCTTCAA	19	59	58
	Rev: ATTTCCGGTAGAAGCTGTTGTGA	23	59	43
	Probe:TCAAGGTCTTGTGCGACGTTCCGCAT CC	26	70	54
Rat b-actin Frame database	FW: GTGAAAAGATGACCCAGATCATGT	24	59	42
	Rev: CACAGCCTGGATGGCTACGT	20	61	60
	Probe: TGAGACCTTCAACACCCCAGCCATG	25	66	56
Rat GAPDH Frame database	FW: TCTGCTCCTCCCTGTTCTAGAGA	23	62	52
	Rev: CGACCTTCACCATCTTGTCTATGA	24	61	46
	Probe: ATCTTCTTGTGCAGTGCCAGCCTCGT	26	66	54
Rat TBP Frame database	FW: TTCGTGCCAGAAATGCTGAA	20	55	45
	Rev: GTTCGTGGCTCTTATTCTCATG	24	61	46
	Probe:ATCCAAGCGTTTGCTGCAGTCA	24	64	54

2.5 Protein quantification

Two assays were used to measure protein concentrations; Bicinchoninic Acid (BCA) protein assay for immunoblot samples while the Lowry test was used for the biochemical radiometric assay.

2.5.1 Bicinchoninic Acid (BCA) protein assay

The BCA method is a colorimetric protein quantification assay first described by (Smith *et al.*, 1985). It is based on reduction of cupric salts to cuprous versions by protein in an alkaline medium (biuret reaction) and then selective detection by BCA containing reagents to produce a purple colour which absorbs at 562 nm, quantified using a POLARstar Omega. Standard curves were made from a provided stock of BSA (BCA Protein Assay Kit, Thermo Scientific, 23225) from 2-0.025 µg/ml (1:2 serial dilution) alongside the unknowns following the manufacturer's protocol. Assays were run on 96 well plates, in triplicate, calculating the sample protein concentration from the standard curve using linear regression analysis.

2.5.2 Lowry test

The Lowry method is based on measuring the amount of proteins with Folin phenol reagent in the presence of alkaline copper conditions (Lowry *et al.*, 1951). The final blue colour was measured at 750 nm using a Spectra-MAX 340pc plate reader (Molecular Devices, CA).

A stock BSA standard was made (300 mg/ml) in 0.5 M sodium hydroxide and serial dilutions were prepared to produce a standard curve. Two hundred µl of diluted samples (1:100) and BSA standards were mixed with Lowry A solution (1 ml) (2% (w/v) sodium carbonate, 0.2% sodium potassium tartrate and 0.2% (w/v) copper sulphate) for 10 min at room temperature followed by the addition of 100 µl of Folin Ciocalteu's solution (1:1 in water) with vortexing for another 45 min at room temperature. Samples and standard were then loaded in triplicate into clear 96-well assay plates to measure the absorbance; sample concentrations were interpolated from the BSA standard curve using linear regression analysis.

2.6 Immunoblotting

2.6.1 Sample preparation

2.6.1.1 Sample homogenisation and solubilisation

Samples were washed twice with ice cold PBS before homogenization using RIPA buffer (Radio Immuno Precipitation Assay) [1 % Triton X-100, 150 mM NaCl, 50 mM Tris-HCl pH 7.6, containing 10 mM NaF, 1 % sodium deoxycholate, 0.1 % SDS, 1 mM Na₃VO₄, and stock 25 × Complete Protease inhibitor (Roche)]. Afterward, samples were sonicated three times for 10 s each and rotated on a daisy wheel at 4 °C for 45 min before centrifugation at 30 000 g for 30 minutes at 4 °C to separate solubilised material. Then each fraction was assayed for protein quantification.

2.6.1.2 Subcellular fractionation of transfected cells

Was carried out with minor modifications using the protocol of (Yu Z *et al.*, 2013) and Abcam protocol (online), nuclear, cytosolic and membrane fractions were extracted from transfected cells.

Cells were first washed with ice cold PBS, scraped and centrifuged at 1000 rpm for 5 min to obtain a pellet to which sucrose-containing buffer was added (250 mM sucrose, 20 mM HEPES pH 7.4, 10 mM KCl, 1.5 mM EDTA, 1 mM EGTA, 1 mM dithiothreitol and Protease inhibitor). Using a 25 G needle (and a 1 mL syringe), cellular lysates were triturated 10 times and then kept on ice for 20 min followed by centrifugation at 720 g for 5 min. After gentle removal of the supernatant layer, RIPA buffer was added to the pellet (the nuclear fraction). The supernatant layer was centrifuged for 100 000 g for one hour (Beckman Coulter). The resultant supernatant layer was the cytosol fraction while the pellet (non-nuclear membranes) was extracted with RIPA buffer and subsequently, all three fractions were quantified for protein content.

2.6.2 Gel electrophoresis

Samples were mixed with 6X solubilisation buffer (24 % (w/v) sodium dodecyl sulphate, 30 % (v/v) glycerol, 5 % (v/v) 2-mercaptoethanol, 2.5 % (v/v) bromophenol blue, 1.5 M Tris HCl, pH 6.8) before boiling at 95 °C for 5 min and centrifuging briefly to eliminate condensates.

Mini-PROTEAN® Precast Gels of 4-20% Tris-Glycine (PAGE) (Bio-Rad, Hercules, CA, U.S.A.) were loaded with about ~10 µg protein per lane and 5 µl of protein markers (Precision Plus Protein™ Standards, Kaleidoscope, Bio-Rad). Proteins were separated at 150 V for about one hour before transferring to a nitrocellulose membrane. The transfer was confirmed by Ponceau Red (Sigma) staining to visualize protein bands. To minimize non-specific binding, blocking was conducted for 1 h with 5 % skimmed milk (w/v) in TBS with 0.1 % Tween 20. The membrane was then incubated with primary antibodies at the recommended concentrations overnight at 4 °C with gentle shaking. The next day, the membrane was washed three times for 10 min each, with Tris-buffered saline containing 0.1 % (v/v) Tween 20, followed by incubation with anti-rabbit or anti-mouse IRDye® secondary antibodies for 1 h at room temperature (Li-Cor Biosciences, Biotechnology, Lincoln, NE, USA) and finally washed again as above. Proteins were visualised using the LI-COR® Odyssey infrared imaging system (Biosciences, Lincoln, NE/USA) at 700 nm for red channel and 800 nm for green channel. Table 2.7 shows the antibodies used in this study.

Table 2.7 List of antibodies used in immunoblotting.

Note: all secondary antibody concentrations were 1:10 000 for one hour at room temperature.

Primary antibody	Source	Cat#	Dilution	Approximate MW
Rabbit polyclonal anti-laminB1	Abcam, UK	16048	10:7000	68
Mouse monoclonal anti-HA	Abcam, UK	ab18181	1:1000	-
Mouse monoclonal anti-β-actin	Sigma, UK	A5441	1:5000	42
Mouse monoclonal anti-α-tubulin	Sigma, UK	T9026	1:5000	50
Rabbit monoclonal anti-sodium potassium ATPase	Abcam, UK	EP1845Y	1:20000	113

2.6.3 Immunoblot stripping

Stripping and re-probing of the immunoblots was conducted as follows. Mild stripping buffer (15 g/L glycine, 1 g/L SDS, 1 % v/v Tween20, pH 2.2) was used for membrane fraction blots. Harsh stripping buffer (2 % w/v SDS, 0.8 % v/v 2-mercaptoethanol in 62.5 mM Tris, pH 6.8) was used for nuclear protein blots (as these were not efficiently stripped with mild buffer). Complete removal of signal

was checked after each step using the LI-COR® Odyssey infrared imaging system.

2.7 Immunocytochemistry

HEK293 cells were seeded on cover slips pre-treated with poly-D-lysine (Sigma) at a density of 0.5×10^5 cells per well in 6-well plates. Transfection was described above in Section 2.2.4. The cells were washed with PBS before fixation with 4 % (w/v) paraformaldehyde (PFA) for 10 min and then washed twice again with PBS. Cells were permeabilized with 0.1% v/v Triton X-100 in 0.5% BSA for another 10 min at room temperature followed by three washes with PBS. Samples were incubated with 0.5 % w/v BSA for 1 h at room temperature then with primary antibodies overnight at 4°C. The next day, samples were first washed three times with PBS then incubated with secondary antibodies (with a light protection cover) for 45 min at room temperature with gentle shaking and washed again three times for five min each. DAPI (4',6-diamidino-2-phenylindole dihydrochloride) staining of nuclei at 1 µg/ml was conducted for 10 min followed by washing. Finally, cover slips were dried before being turned upside down on top of a drop of DABCO Fluorescent mounting media (1,4-diazabicyclo-2-2-2-octane (200 mg) + glycerol (90 ml) + PBS (10 ml)) on slides and fixed with nail polish all around the rim. Images were acquired using confocal microscopy (Zeiss LSM880C, Germany) with 63X objective (with oil) (NA 1.4). Post-acquisition processing (multi-channel overlay, scale bar addition) was performed using ImageJ 1.5 software. Images presented in JPEG format. An appropriate negative control was included with each experiment. Dilutions of primary antibodies (Table 2.8) were the same as for immunoblotting while secondary antibodies were 1:1000 diluted.

Table 2.8 List of antibodies used in ICC.

Primary antibody	Cat#	Secondary antibody
Mouse anti-HA	31665	Goat anti-mouse Rhodamine
Rabbit antilamin1	4110088	Goat anti-rabbit Alexa Fluor 488

Rhodamine was used for all experiments except for neurons viral imaging where donkey anti-mouse Alexa Fluor 568 was used instead (Cat#: A10037).

2.8 Activity Based Protein Profile (ABPP)

The protocol was optimized until the desired results were achieved. To 20 μ l sample (of around 100 μ g protein), 5 μ l inhibitor/vehicle was added then pre-incubated on a shaker at 37 °C for 20 min. Then 2 μ l (equivalent to 2 μ M final concentration) of serine hydrolase FP probe (Thermo Scientific, cat#88318) were added and incubated for 30 min under the same conditions. The reaction was stopped by adding 2X Laemmli reducing sample buffer. Samples then were loaded on Mini-PROTEAN® Precast Gels of 4-20% (Bio-Rad, Hercules, CA, U.S.A.). Running time and voltage were 1 h and 150 V. Scanning of the gel (Typhoon, Amersham Pharmacia Biotech) was conducted by a fellow PhD student, Nuha Anajirih.

2.9 Viral infection

2.9.1 Primers and PCR

Primers for N-ABHD6 and GFP (as positive control) are shown in the Table 2.10. Further details can be found in Appendix-Section B.

Using Phusion™ High-Fidelity enzyme DNA polymerase (New England Bio Labs), PCR was conducted using a thermal cycler (T100 TM, BIORAD, UK) following the thermal conditions indicated below (Table 2.9).

Table 2.9 PCR condition for the amplification *attB* N-ABHD6.

Step	Temperature	Time
Initial denaturation	98°C	30 seconds
Denaturation	98°C	30 seconds
Annealing	72°C	15 seconds
Extension	71°C	45 seconds
Final extension	72°C	5 minutes
Storage	4°C	∞

PCR products were checked for the presence of the correct band size in an agarose gel and the remaining amount was cleaned up using polyethylene glycol magnesium chloride solution (PEG-MgCl₂; 30% PEG in 30 mM MgCl₂) following Gateway® Technology protocol. In the presence of Gateway™ BP, Clonase™ II Enzyme mix (Invitrogen™, 11789-013) and pDONR™221 vector (Addgene, 12536-017), generation of the entry clone was carried out (with

positive and negative controls alongside) and reactions were kept at 25 °C for 16 h. Treatment with Proteinase K was also followed as well as transformation into OmniMax™ 2-T1^R *E. coli* (ThermoFisher, C8540-03) (positive and negative controls were run with the experiment according to manufacturer's instructions). The presence of insert DNA in plasmid construct was confirmed by conducting colony PCR using BIOTAQ™ DNA polymerase kit (Bio line, BT-516212) prior to miniprep scaling plasmid and sending for sequencing using M13 primers. Table 2.11 and 2.12 show components of colony PCR and its thermal condition.

Once sequencing results were confirmed, linearization of the entry clone (outside *attB* region) was carried out following the NEB protocol of single restriction enzyme digestion, DNA precipitation by sodium acetate and ethanol and dissolving the DNA pellet in Tris/EDTA buffer pH 8 to a final concentration of 150 ng/μl.

Table 2.10 Primers for ABHD6 and GFP for entry clone.

The length of FW- forward and Rev- reverse primers for N-ABHD6 was 20 and 19, respectively. For GFP primers, it was 20 and 26 nucleotides respectively. All primers did not have Hairpin self-dimerization, heterodimer, more than four repeats, runs properties upon blast calculation. Annealing T_m for N-ABHD6 was 59 °C and for GFP was 71 °C. PCR product length for N-ABHD6 was 1037 base pairs.

Name	Sequence	GC (%)	T _m (°C)
hu221pDONRNABHD6_Fw	GGGGACAAGTTTGTACAAAAAAGCAGGCTTCGCCACCATGTAC CCATACGATGTTCC	45	59
hupDONR221ABHD6_Rev	GGGGACCACTTTGTACAAGAAAGCTGGGTTTCAGTCCAGCTTC TTGTTG	47	59
pDONR221-GFP-FW	GGGGACAAGTTTGTACAAAAAAGCAGGCTTCGCCACC ATGGTGAGCAAGGGCGAGGA	60	71
pDONR221-GFP-Rev	GGGGACCACTTTGTACAAGAAAGCTGGGTTTTACTTGTACAGC TCGTCCATGCCGA	50	73

Table 2.11 The components of colony PCR.
M13 FW: (TGTAACGACGGCCAGT) and M13 Rev:
(CAGGAAACAGCTATGACC).

Component	Volume (μ l)
10X buffer	2
10 mM dNTP	0.4
10 μ M forward primer	1
10 μ M reverse primer	1
MgCl ₂	0.6
Enzyme	0.25
Nuclease free water	Up to 20 μ l

Table 2.12 Colony PCR conditions for entry clone.

Step	Temperature	Time
Initial denaturation	96°C	5 minutes
Denaturation	96°C	15 seconds
Annealing	52°C	20 seconds 30X repeats
Extension	72°C	45 seconds
Final extension	72°C	5 minutes
Storage	4°C	∞

In the presence of Gateway™ LR Clonase™ II Enzyme mix (Invitrogen™, 11791-091), creation of expression clones was performed by mixing the entry clone (*attL* site) with the destination vector pINDUCER20 (*attR* site)(Addgene, 44012) for overnight incubation followed by treatment with Proteinase K on the next day. Then, transformation into One shot™ Stbl3 *E. coli* (ThermoFisher, C7373-03) at 30 °C and performing colony PCR were conducted before sending for sequencing confirmation using LNX and pINDUCER 20 as forward and reverse primers (thermal condition shown in Table 2.13). At this stage, the plasmid was ready for transfection alongside packaging plasmids to create the virus.

Table 2.13 Colony PCR conditions for expression clone.
LNCX-FW: AGCTCGTTTAGTGAACCGTCAGATC and PIND20-REV:
GGTACTCCAGACTGCCTTGG as forward and reverse primers respectively.

Step	Temperature	Time
Initial denaturation	96°C	5 minutes
Denaturation	96°C	15 seconds
Annealing	56°C	50 seconds 30X repeats
Extension	72°C	90 seconds
Final extension	72°C	5 minutes
Storage	4°C	∞

2.9.2 Transfection

1.2×10^6 HEK293T cells were seeded in 10 cm dishes (CORNING). Two μg from each plasmid were used (GFP and N-ABHD6), as well as packaging and envelop materials, to a total of 300 μl with a diluent of reduced serum media (Opti-MEM®, Thermo Fischer). After mixing with polyethyleneimine (PEI), the mixture was incubated for 20 min at room temperature in the hood before adding to 6 ml of Opti-MEM® in the dish. The two dishes were kept in the incubator for 6 h before changing to normal media (DMEM with 10% FBS and NEAA).

2.9.3 Harvesting

Part of the supernatant (media) was used directly for infection after filtration through 0.45 μm filters (2 wells of a 6 well plate). The remaining media was concentrated by pelleting the virus using 20% sucrose as viscous liquid (as Cushioning buffer as it helps in gradient centrifugation (Jiang *et al.*, 2015)) in a chilled rotor (Beckman) followed by centrifugation at 100 000 g for 2.5 h.

2.9.4 Infection

Rat astrocytes and/or mouse neurons were seeded on cover slips in 6-well plates treated with poly-D-Lysine. Two wells were allocated for infection by the virus supernatant while the remaining wells were infected with the pelleted virus (using Opti-MEM®). After 4 h, replacement with normal media was carried out, as well as addition of doxycycline at 1 $\mu\text{g}/\text{ml}$. Fixation and preparation of slides were done after 48 h following the protocol described above (see Immunocytochemistry- Section 2.9- above).

Chapter Three

Characterization of MAGL and ABHD6 in rat tissues, cell transfects and primary cultured cells

3. Characterization of MAGL and ABHD6 in rat tissues, cell transfects and primary cultured cells

3.1 Introduction

In the CNS, endocannabinoids are characteristically synthesized post-synaptically (on demand) in response to increased neuronal activity and then diffuse in a retrograde manner to activate presynaptic cannabinoid receptors. Their action is limited by hydrolysis by lipase-like enzymes. The inhibition of these lipases allows longer retention of these ligands in the active areas potentially amplifying their effects in a manner which may generate therapeutic benefit. Therefore, exploring these enzymes may allow novel therapeutic exploitation of the endocannabinoid system. This study focusses on the enzymes that hydrolyse 2-AG, which include MAGL, ABHD6 and ABHD12. These together account for about 99% hydrolysis of 2-AG in the rodent CNS (Blankman *et al.*, 2007; Savinainen *et al.*, 2012). These enzymes are reported to have different subcellular and tissue distributions, suggesting that they may have unique roles in controlling the lifetime and action of 2-AG (Blankman *et al.*, 2007).

MAGL is relatively well characterized among the 2-AG hydrolysing enzymes, presumably as it was the first identified. It has wide tissue distribution (Karlsson *et al.*, 1997) and is abundant in adipose tissue where it plays an important role in lipid metabolism (Dinh *et al.*, 2002a). MAGL is a soluble enzyme that also associates with membranes (Blankman *et al.*, 2007; McKinney & Cravatt, 2005). Immunoblotting showed that MAGL can be identified in both fractions of mouse brain (Marrs *et al.*, 2010). In many tissues and cell types, MAGL is detected in both the soluble and the membrane fractions (Savinainen *et al.*, 2012).

Several MAGL inhibitors have been investigated with regard to selectivity and potency, including JZL184 ($IC_{50}=8$ nM in mouse brain membranes and $IC_{50}=6$ nM with human recombinant MAGL)(Long *et al.*, 2009a), URB602 ($IC_{50}=\sim 223$ μ M in human recombinant MAGL (King *et al.*, 2007) and $IC_{50}=\sim 28$ μ M in rat brain (Hohmann *et al.*, 2005)), and most recently JJKK048 as the most potent and

selective designed so far (IC_{50} less than 0.4 nM in human and rodent (Aaltonen *et al.*, 2013)) (see Table 1.2 in the Introduction). Both genetic and pharmacological MAGL inhibition has been found to be beneficial in models of Alzheimer disease (Chen *et al.*, 2012), anxiety (Kinsey *et al.*, 2011; Sumislawski *et al.*, 2011), neuro-inflammation- (Mulvihill *et al.*, 2013), cancer (Nomura *et al.*, 2011a; Ye *et al.*, 2011) and other therapeutic effects (see General Introduction Chapter) (Grabner *et al.*, 2017; Hohmann, 2007; Mulvihill *et al.*, 2013; Scalvini *et al.*, 2016).

MAGL (313 amino acid) migrates as two bands on SDS-PAGE gel in rodent brains of 33 and 35 kDa (Blankman *et al.*, 2007; Dinh *et al.*, 2002c; Karlsson *et al.*, 2001; Long *et al.*, 2009b). In addition, double bands were also observed in mice testes and rat proximal colon (Duncan *et al.*, 2008), however, a single band was found in other organs like lung, liver, kidney, heart and spleen. It is not fully understood how this variation occurs, although the presence of splice variants was proposed in these tissues (Labar *et al.*, 2010b).

Much less is known about ABHD6 and ABHD12 regarding their biochemical characteristics, structural information and physiological function. Both are predicted to be integral membrane enzymes, based on the presence of a trans-membrane domain in hydropathy plot. Immunoblotting suggested that ABHD6 was only found in the membrane fraction (Marrs *et al.*, 2010). The active site of ABHD6 was predicted to be facing the cell interior – a cytoplasmic orientation – and for ABHD12 to be facing the extracellular space – a luminal orientation (Blankman *et al.*, 2007). Recent evidence implicates ABHD6 in metabolic syndrome (Thomas *et al.*, 2013), diabetes (Zhao *et al.*, 2014), systemic lupus erythematosus (Oparina *et al.*, 2014), protection against neuro-inflammation and neuro-degeneration of experimental autoimmune encephalitis (an animal model of multiple sclerosis) (Wen *et al.*, 2015) and epilepsy (Naydenov *et al.*, 2014), while mutations of the catalytic activity of ABHD12 gene have been causally linked to a neurodegenerative disease, namely PHARC (polyneuropathy, hearing loss, ataxia, retinitis pigmentosa and cataract) (Fiskerstrand *et al.*, 2010).

ABHD6 has 337 amino acids and was reported to be detected at different molecular weights ranging from ~30 kDa (Blankman *et al.*, 2007) to 35 kDa (Li

et al., 2007) on activity based protein profile (ABPP) gels, 36 kDa with a doublet band-for the only time in ABPP (Navia-Paldanius *et al.*, 2012), at 37 kDa in immunoblots (Zhao *et al.*, 2014), ~40 kDa with His-tagged immunoblot (Pribasnig *et al.*, 2015) and most recently as 38 kDa (Poursharifi *et al.*, 2017). ABHD12 (398 aa) was detected at ~45 kDa (Blankman *et al.*, 2007; Navia-Paldanius *et al.*, 2012).

Although recent years have witnessed the development of many relatively selective MAGL inhibitors, a more limited number of ABHD6 inhibitors have been identified. The first to be reported as potent and selective was WWL70 (Li *et al.*, 2007) with $IC_{50}=70$ nM against human recombinant ABHD6. Later on, the Cravatt group disclosed WWL123 ($IC_{50}=426$ nM in human recombinants) (Bachovchin *et al.*, 2010), and KT182 ($IC_{50}< 5$ nM in mouse and neuroblastoma N2a)(Hsu *et al.*, 2010) as potent and selective inhibitors. More recently, JZP-430 was reported with an $IC_{50}=44$ nM in recombinant ABHD6 system (Patel *et al.*, 2015).

Other inhibitors reported as non-selective for both ABHD6 and ABHD12 were orlistat (tetrahydrolipostatin), MAFP, pristimerin and RHC-80267 (Naydenov *et al.*, 2014) (Table 1.1).

3.2 Aim of this Chapter

In order to explore the roles of these enzymes and their physiological functions, selective and potent inhibitors of the enzymes are needed. In addition, cell lines and/or tissues enriched with the enzyme of interest are also required for a more complete biochemical characterization.

In this Chapter, a radioisotope-based enzyme assay was used as a “Gold standard” method to measure and validate the different biochemical aspects of MAGL, ABHD6 and ABHD12. Inhibitor profiles were assessed in selected rat tissues and cloned enzymes to allow comparison with expression data and published literature. The main objectives of this study were therefore:

- To generate cell lines selectively expressing the enzyme of interest.
- To measure enzyme activities in selected rat tissues using the reported selective inhibitors; JJKK048 for MAGL and WWL123 for ABHD6.
- To investigate the subcellular distribution of the enzymes compared with the reported/ predicted pattern.

3.3 Methods

In this Chapter, the radiometric monoacylglycerol hydrolase assay was performed following the steps described in Section (2.3.2). Harvesting and fractionation of rat tissue and transfected cells followed Sections (2.3.1.1 and 2.3.1.2). Separation of epithelia and muscular layer of small intestine may be found in Section (2.3.1.3). Male rats were used to investigate neural tissues and to isolate primary cultured cells. Primary cell preparation followed Section (2.2.1). Transfection protocols and protein quantification were done according to Section (2.2.4) and (2.5.2), respectively. ABPP was done according to Section 2.8. Briefly, ABPP has been introduced in the last two decades (Liu *et al.*, 1999b) to investigate many classes of enzyme, with particular attention on probes that investigate the serine hydrolase family. The technique can also be applied to the screening of potential inhibitors. In general, ABPP probes have two important components: a reactive head for mechanistically reacting with the active site of the enzyme (in this case, a serine nucleophile) and a reporter tag for visualization (Simon *et al.*, 2010). An inhibitor could be added and the reaction products visualized and quantified by scanning on an SDS/PAGE gel.

3.4 Results

In order to investigate the distribution of enzyme activity compared to the preliminary data obtained for mRNA expression, a radio-active assay was conducted, with a focus on rat neural tissues (where these enzymes activities was first reported (Blankman *et al.*, 2007) and intestinal tract (where our qRT-PCR results showed the highest expression of ABHD6 mRNA, Section 4.4.1). These tissues included rat spinal cord, hippocampus, prefrontal cortex and small and large intestine. Four biological repeats assessing both fractions (soluble and membrane) were tested examining the potential inhibitory effects of the

reportedly-selective MAGL inhibitor JJKK048, or the reportedly-selective inhibitor WWL123 or combinations of both.

3.4.1 Concentration inhibition curve of JJKK048 in rat neurological tissues

To confirm the presence of MAG hydrolase activity in both particulate and soluble fractions in rat spinal cord and prefrontal cortex, [³H]-2OG hydrolysis was assayed. Serial dilutions of JJKK048 up to 100 nM were used in the radiometric assay (Figure 3.1 and Table 3.1).

Table 3.1 shows that [³H]-2OG hydrolysis was measurable in both fractions in these two tissues, with the highest level of [³H]-2OG activity in prefrontal cortex of 62.8 ± 3 nmol/min/mg protein. The majority of hydrolase activity was detected in particulate fractions in both prefrontal cortex and spinal cord. In both preparations from both tissues, JJKK048 produced a concentration-dependent inhibition with very high potency (Figure 3.1). In all four preparations, JJKK048 failed to inhibit [³H]-2OG hydrolysis completely, with between 17-43 % of activity resistant to inhibition (Table 3.1). In both tissues, JJKK048-resistant activity appeared to be proportionally higher in the soluble fraction (Figure 3.1, Table 3.1).

Table 3.1 [³H]-2OG hydrolysis in two fractions of rat spinal cord and prefrontal cortex. Data are mean \pm SEM from four independent experiments performed in duplicate.

Tissue source	Total 2OG hydrolysis nmol/min/mg	JJKK048 potency pIC ₅₀ value	JJKK048-sensitive		JJKK048-insensitive	
			nmol/min/mg	% total	nmol/min/mg	% total
Spinal cord soluble	6.0 \pm 0.3	10.3 \pm 0	3.4 \pm 0.3	57 \pm 3	2.6 \pm 0.2	43 \pm 3
Spinal cord particulate	20.6 \pm 1	10.3 \pm 0.1	15.5 \pm 1	75 \pm 3	5.1 \pm 0.6	25 \pm 3
PFC soluble	8.4 \pm 1.6	9.9 \pm 0.2	5.9 \pm 0.5	74 \pm 3	2.6 \pm 1.1	27 \pm 3
PFC particulate	62.8 \pm 3	9.7 \pm 0.2	52.5 \pm 1.2	84 \pm 2	10.9 \pm 1.8	17 \pm 2

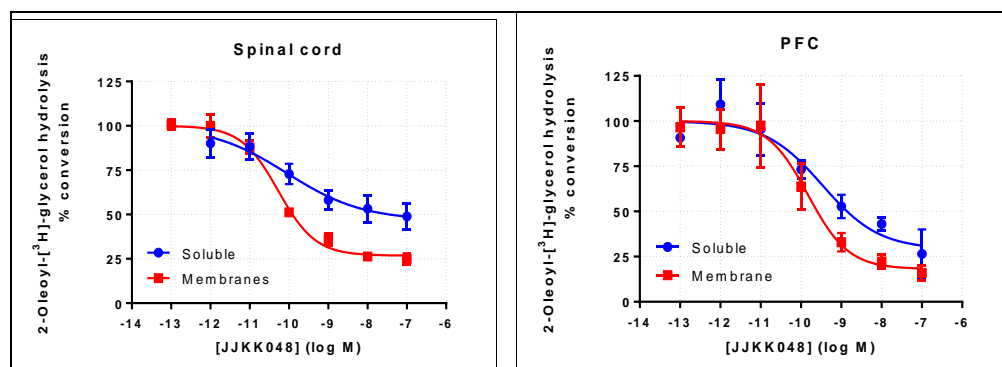


Figure 3.1 Concentration inhibition curves of JJKK048 against [³H]-2OG hydrolysis in rat spinal cord and prefrontal cortex preparations.

Data are mean ± SEM from four independent experiments performed in duplicate.

Given the reported expression of ABHD6 and its contribution to MAG hydrolysis (Blankman et al., 2007), there arose the attractive possibility that ABHD6 might be responsible, at least in part, for the JJKK048-resistant activity in these tissues.

3.4.2 Concentration inhibition curve for WWL123 in spinal cord

Using WWL123 as a reportedly-selective inhibitor of ABHD6, both fractions of rat spinal cord were investigated for ABHD6 activity using [³H]-2OG hydrolysis. However, only a marginal inhibition was observed (Table 3.2). In both preparations, WWL123 failed to significantly inhibit [³H]-2OG hydrolysis with between 77-81 % of activity resistant to inhibition (Table 3.2). Curve fitting using the four parameter logistic equation (GraphPad Prism) was inconclusive, which might be a reflection of the minor contribution of ABHD6 to [³H]-2OG hydrolysis (Figure 3.2). Alternatively, WWL123 may not be an effective inhibitor of ABHD6 in these tissues.

Table 3.2 [³H]-2OG hydrolysis in rat spinal cord.

Data are mean ± SEM from four independent experiments performed in duplicate.

Tissue	Total 2OG hydrolysis	WWL123-sensitive		WWL123-insensitive	
		nmol/min/mg	% total	nmol/min/mg	% total
Spinal cord soluble	10.2 ± 0.9	2.5 ± 0.6	24 ± 3	7.6 ± 0.3	77 ± 3
Spinal cord particulate	31.8 ± 2.6	5.9 ± 0.6	19 ± 2	25.9 ± 2.6	81 ± 2

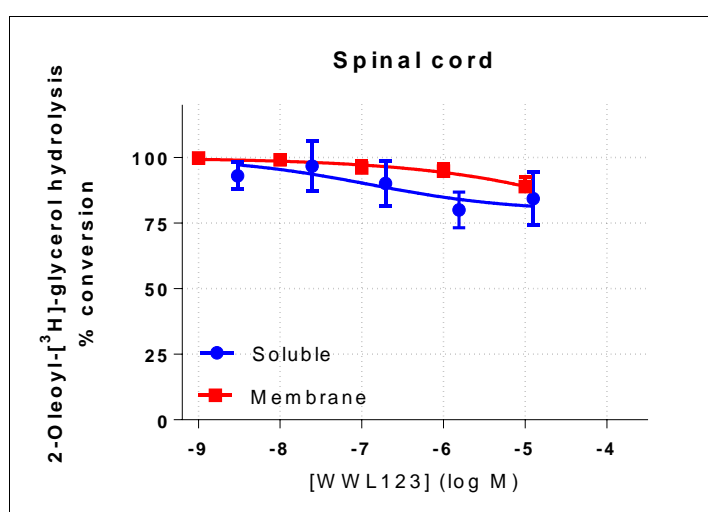


Figure 3.2 Concentration inhibition analysis of WWL123 against [³H]-2OG hydrolysis in both fractions of rat spinal cord.

Data are mean ±SEM of four independent experiments performed in duplicate.

3.4.3 Combination of WWL123 and JJKK048 in rat neurological tissues

Given that MAGL is expected to be a predominant contributor to MAG hydrolysis in the brain (Blankman *et al.*, 2007), the effect of WWL123 was examined in the absence of MAGL hydrolysis. The contribution of ABHD6 to the hydrolysis of [³H]-2OG, after complete inhibition of MAGL by 100 nM JJKK048, with serial dilutions of WWL123 was investigated in three tissues; spinal cord, prefrontal cortex and hippocampus. For most tissues, WWL123 only inhibited 1-2% of total [³H]-2OG hydrolysis (Table 3.3). In all three tissues, either soluble or particulate fractions, WWL123-evoked inhibition of [³H]-2OG

hydrolysis was minimal; curve fitting to a four parameter logistic equation of the WWL123 concentration-response curves was inconclusive (Figure 3.3).

Table 3.3 [³H]-2OG hydrolysis in particulate and soluble fractions of rat tissues in the presence of 100 nM JJKK048 and increasing concentrations of WWL123.

Data are mean ± SEM of four independent experiments performed in duplicate.

Tissue	Total 2OG hydrolysis	JJKK048sensitive		WWL123-sensitive		Residual activity	
	nmol/min/mg	nmol/min/mg	% total	nmol/min/mg	% total	nmol/min/mg	% total
Spinal Cord soluble	14.3 ± 0.4	10.0 ± 0.3	70 ± 2	0.1 ± 0.4	1 ± 3	4.1 ± 0.2	29 ± 1
Spinal Cord particulate	21.3 ± 1.1	18.0 ± 0.9	85 ± 1	0.3 ± 0.1	1 ± 0	3.0 ± 0.2	14 ± 1
Hippocampus soluble	14.3 ± 0.7	10.7 ± 0.8	74 ± 3	0.2 ± 0.1	1 ± 1	3.4 ± 0.1	24 ± 2
Hippocampus particulate	30.5 ± 2.8	24.4 ± 2.2	80 ± 3	0.2 ± 0.1	1 ± 0	6.0 ± 1.1	19 ± 3
PFC soluble	22.8 ± 1.4	16 ± 0.4	71 ± 3	0.2 ± 0.1	1 ± 0	6.5 ± 1.1	28 ± 3
PFC particulate	30.6 ± 0.7	24.6 ± 1.0	76 ± 3	0.7 ± 0.1	2 ± 1	6.9 ± 0.7	23 ± 3

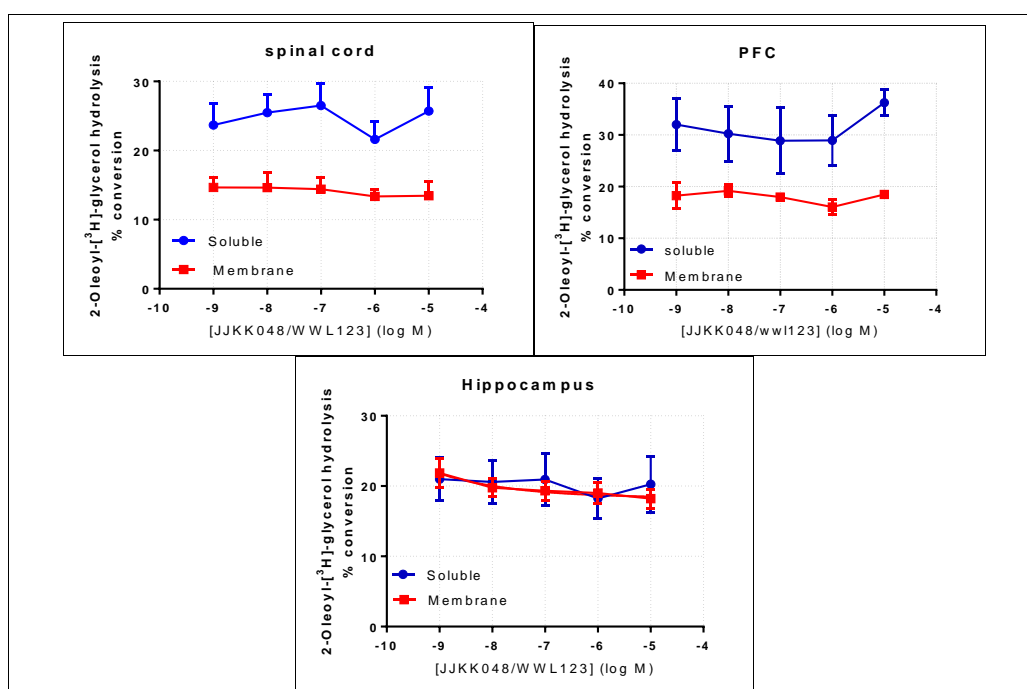


Figure 3.3 Concentration inhibition curves of WWL123 with [³H]-2OG hydrolysis after complete inhibition of MAGL in rat spinal cord, pre-frontal cortex and hippocampus.

Data are from four independent experiments performed in duplicate.

3.4.4 [³H]-2OG hydrolysis in rat intestine preparations: the effects of inhibitors and biological sex

The previous experiments using rat neural tissues identified difficulties in the identification of ABHD6 activity in these tissues. This might be attributed to the presence of high MAGL activity in those tissues relative to ABHD6. Pilot investigations provided qRT-PCR results (Section 4.4.1) that showed neural tissues to express relatively similar mRNA levels for MAGL and ABHD6. In contrast, mRNA from small and large intestines showed significantly higher expression levels of ABHD6 versus MAGL. Hence, the next step was to investigate ABHD6 and MAGL activity in rat small and large intestine using the radiometric assay. Preliminary experiments on female rat intestine suggested an interesting difference in functional activity between male and female intestines. Therefore, the study was expanded further to investigate potential sexual dimorphism in rat intestine.

The radiometric assay appeared to indicate the presence of both MAGL (JJKK048-sensitive 2OG hydrolysis) and ABHD6 (WWL123-sensitive 2OG hydrolysis) functional activities in both male and female intestine with the highest activity found in female small intestinal particulate fraction (62.5 ± 1.5 nmol/min/mg) as shown in Table 3.4. As in the CNS tissues, there were lower activities observed in the soluble compared to the particulate fractions (Table 3.4).

Relatively high remaining activity was detected in male small intestine membranes of $47 \pm 5\%$, indicating the presence of unidentified 2OG hydrolase enzyme(s). Table 3.4 below also summarized pIC₅₀ values for each fraction and showed an unexpected high potency of WWL123 in both sexes and in all intestinal fractions; pIC₅₀ values ranged from 7.5-8.4. This suggested, for the first time, a relatively high activity of ABHD6 in the soluble fraction of the intestine. Indeed, ABHD6 activity (WWL123 sensitive) was greater than MAGL (JJKK048 sensitive) in the soluble fraction of small intestine of both sexes (Table 3.4) while MAGL activity was predominant in the particulate fraction of the large intestine from both sexes.

In general, there were similar patterns/slopes for inhibitor activity in male and female rat intestinal preparations, with the exception of the small intestine particulate fraction (Figure 3.4) which showed a statistical difference between genders.

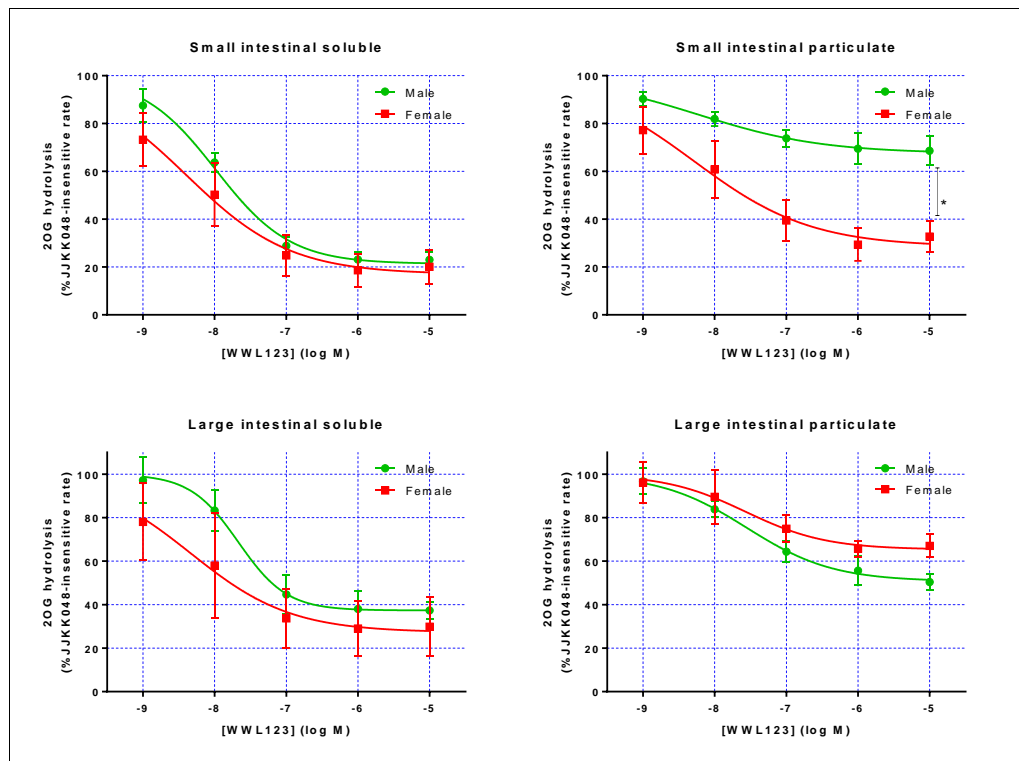


Figure 3.4 WWL123 inhibition of [³H]-2OG hydrolysis in the absence of MAGL activity in female and male rat small and large intestine.

Data are mean ± SEM from four independent experiments performed in duplicate. *P<0.01 unpaired T- test.

Table 3.4 [³H]-2OG hydrolysis in male and female rat intestine.

Data are mean ± SEM of three-five independent experiments performed in duplicate.

Male	Total 2OG hydrolysis	JJKK048-sensitive hydrolysis		WWL123-sensitive hydrolysis			Residual hydrolysis	
	nmol/min/mg	nmol/min/mg	% total	nmol/min/mg	% total	pIC ₅₀	nmol/min/mg	% total
Small intestine soluble	14.9 ± 1.7	4.6 ± 0.8	30 ± 3	7.7 ± 1.1	51 ± 2	8 ± 0.1	2.6 ± 0.5	19 ± 4
Small intestine particulate	23.2 ± 1.9	7.3 ± 1.4	31 ± 4	5.3 ± 0.8	24 ± 5	8.1 ± 0.2	10.8 ± 1.5	47 ± 5
Large intestine soluble	8.8 ± 0.7	3.3 ± 0.3	38 ± 5	3.4 ± 0.6	39 ± 4	7.7 ± 0.2	2.1 ± 0.4	23 ± 3
Large intestine particulate	11.0 ± 0.7	5.2 ± 0.7	47 ± 4	2.9 ± 0.2	26 ± 2	7.5 ± 0.2	2.9 ± 0.4	27 ± 3
Female								
Small intestine soluble	21.5 ± 1.4	9.0 ± 1.4	41 ± 4	10.2 ± 0.9	48 ± 5	8.4 ± 0.4	2.4 ± 0.9	11 ± 4
Small intestine particulate	62.5 ± 1.5	19.8 ± 2.8	32 ± 5	28.3 ± 0.8	45 ± 2	8.2 ± 0.3	16.8 ± 2.1	27 ± 3
Large intestine soluble	14.0 ± 1.3	6.6 ± 0.8	47 ± 5	5.2 ± 1.5	35 ± 6	8.3 ± 0.3	2.4 ± 0.5	19 ± 5
Large intestine particulate	23.0 ± 1.7	11.8 ± 2.1	49 ± 5	4.3 ± 0.7	17 ± 3	7.6 ± 0.5	6.9 ± 0.9	34 ± 5

3.4.5 Soluble 2OG hydrolase activity in the small intestine

The appearance of WWL123-sensitive MAG hydrolase activity, which might equate with ABHD6, in the soluble fraction was an unexpected observation since ABHD6 is reported to be a membrane bound enzyme (Blankman *et al.*, 2007; Marrs *et al.*, 2010; Poursharifi *et al.*, 2017; Savinainen *et al.*, 2012). One potential explanation for the presence of ABHD6 in the soluble fraction could be proteolytic modification. To investigate the potential influence of proteolysis, Protease Inhibitors cocktail tablet (Complete, Roche) was used in the Tris-EDTA buffer for homogenization of male rat small intestine in a pilot study. The combination of inhibitors in this tablet is designed to target a broad spectrum of serine and cysteine proteases. At first, serial dilution of this reagent was used (as an inhibitor) in ordinary homogenized tissue in radio-assay starting from undiluted tablet (1X) followed by 10X fold dilution from the previous stock. Results showed the maximum inhibitory effect with 1X concentration in both fractions followed by progressive recovery as the dilution of inhibitor increased (Table 3.5).

Table 3.5 The hydrolytic activity of [³H]-2OG in rat small intestine treated with serial concentrations of Protease Inhibitors.

Data are % control from a single experiment performed in duplicate.

	Soluble	Membrane
Control	100%	100%
Top conc. (1X)	16%	39%
10 fold dilution	39%	60%
100 fold dilution	67%	67%
1000 fold dilution	77%	67%

The next step was to investigate whether the proteolysis inhibitor cocktail inhibited the enzyme directly and whether it could change the distribution of the enzymes when the tissue was homogenized. The female small intestine was divided into two fragments and one piece homogenised in the presence of undiluted protease inhibitor (top concentration). Fractions from both sources were tested against fixed concentrations of different inhibitors (1 μ M MAFP, 100 nM JKKK048 and 1 μ M WWL123). In these experiments, the final concentration of

the protease inhibitor cocktail was 100x in the reaction mixture. Results showed no differences with and without Protease Inhibitor addition (Table 3.6).

Table 3.6 [³H]-2OG hydrolytic activity assayed in rat small intestine homogenized with and without protease inhibitors (P.I).

Data are % control from a single experiment performed in duplicate.

Inhibitor	Soluble	Soluble + P.I	Membrane	Membrane +P.I
Control	100%	100%	100%	100%
MAFP (1 μM)	4%	1%	1%	2%
JJKK048 (100 nM)	57%	54%	58%	43%
WWL123 (1 μM)	14%	15%	69%	61%

To further investigate this soluble activity of ABHD6 in the intestine, a pilot study involved separating the mucosal (epithelial) from submucosal layers (muscular) of a small intestine sample, before fractionation into soluble and membrane fractions and quantification by the radiometric enzyme assay. Inhibitors were investigated at 1 μM, as before (Table 3.7).

Table 3.7 [³H]-2OG hydrolytic activity in epithelial and muscular layers of rat small intestine.

Data are % control from a single experiment performed in duplicate.

	Epithelial soluble	Epithelial membrane	Muscular soluble	Muscular membrane
Control	100%	100%	100%	100%
MAFP (1 μM)	2%	2%	13%	4%
JJKK048 (1 μM)	33%	64%	54%	59%
WWL123 (1 μM)	27%	76%	64%	90%

Results showed that, in the soluble fraction of the epithelial layer, WWL123 appeared as effective as JJKK048. In the muscular layer, the activity inhibited by JJKK048 was more than WWL123 in both fractions (Table 3.7).

The epithelial layer of small intestine (both soluble and membrane fractions) were investigated further, combining JJKK048 and WWL123 (Table 3.8). MAFP appeared to completely inhibit the activities in both fractions, as before (Table 3.7). Particularly in the soluble fraction, WWL123 appeared to evoke a substantial inhibition. In the membrane fraction, however, the combination of JJK048 and WWL123 failed to inhibit 2OG hydrolysis completely, suggesting another serine hydrolase might be present.

Table 3.8 [³H]-2OG hydrolytic activity in epithelial layer of rat small intestine. Data are % control from a single experiment performed in duplicate.

	Epithelial soluble	Epithelial membrane
Control	100%	100%
MAFP (1 μM)	2%	2%
JJKK048 (1 μM)	22%	34%
WWL123 (1 μM)	11%	63%
JJKK048+WWL123	6%	28%

3.4.6 Activity in Transfects

3.4.6.1 Introduction

One of the aims of this study was to generate stable cell lines that independently express the three human serine hydrolases. However, many efforts at producing stable cell lines for enzyme expression were attempted and screened using the radiometric assay (Figure 3.5 and Table 3.9). Optimization was attempted using a variety of approaches, for example:

- Different plasmid source: two sources of plasmids was tried: a commercial version (GeneCopoeia, V0321) and a plasmid made in house.
- Different host cells: three type of host cells were used, HEK293 human kidney fibroblasts, SH-SY5Y human neuroblastoma cells and Chinese hamster ovary (CHO) fibroblasts.
- Different concentrations of selected antibiotics: although the killing curve indicated a fixed concentration to be used for each cell line, variable concentrations of antibiotic were examined.
- Different antibiotic: neomycin and G418 were used.
- Different vectors: pReceiver-M02 and pcDNA3.1

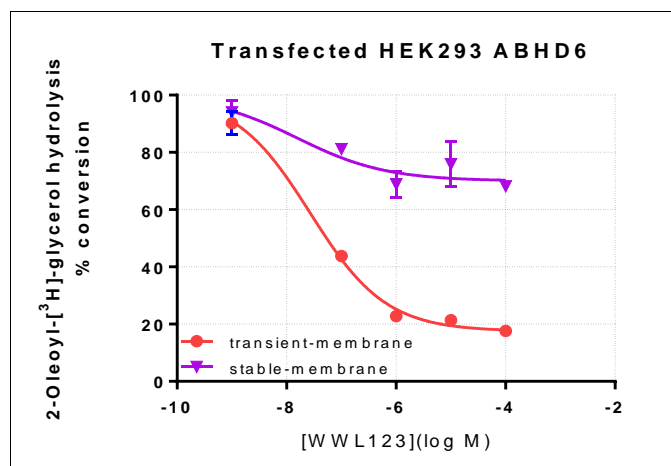


Figure 3.5 Representative figure comparing stable versus transient transfection. Data are from a single experiment performed in duplicate.

Table 3.9 [³H]-2OG hydrolytic activity assayed in membrane fractions of transient vs stable transfection in HEK293.

Data (from Figure 3.5) are mean values from a single experiment performed in duplicate.

Transfection type	Total 2OG hydrolysis nmol/min/mg	WWL123-sensitive hydrolysis nmol/min/mg	Residual hydrolysis nmol/min/mg
Transient	10.8	8.5	2.3
Stable	14.4	3.5	10.9

Transient transfection (of all of the cloned genes) was assessed with different approaches; first co-transfection with GFP (see Section 2.2.4) to indicate transfection efficiency. Results showed that there were ~20-30% fluorescent cells within the seeded HEK293 cell population (Figure 3.6) which was considered satisfactory for continuing with transient transfection. Next, ABPP (with and without the use of relevant inhibitors) also confirmed successful transient transfection (Figure 3.9 and 3.12). Finally, functional testing of these cells with the radiometric assay using fixed and or/ serial dilutions of relevant inhibitors (Figures 3.8, 3.10 and 3.11; Tables 3.9 and 3.10) confirmed efficient transient transfection. Figure 3.7 (representative for transient ABHD6 transfection in comparison to an empty vector, pcDNA 3.1 alone) showed [³H]-2OG hydrolysis was inhibited with high potency in the presence of WWL123. Therefore, transient transfection was used through the remainder of this study.

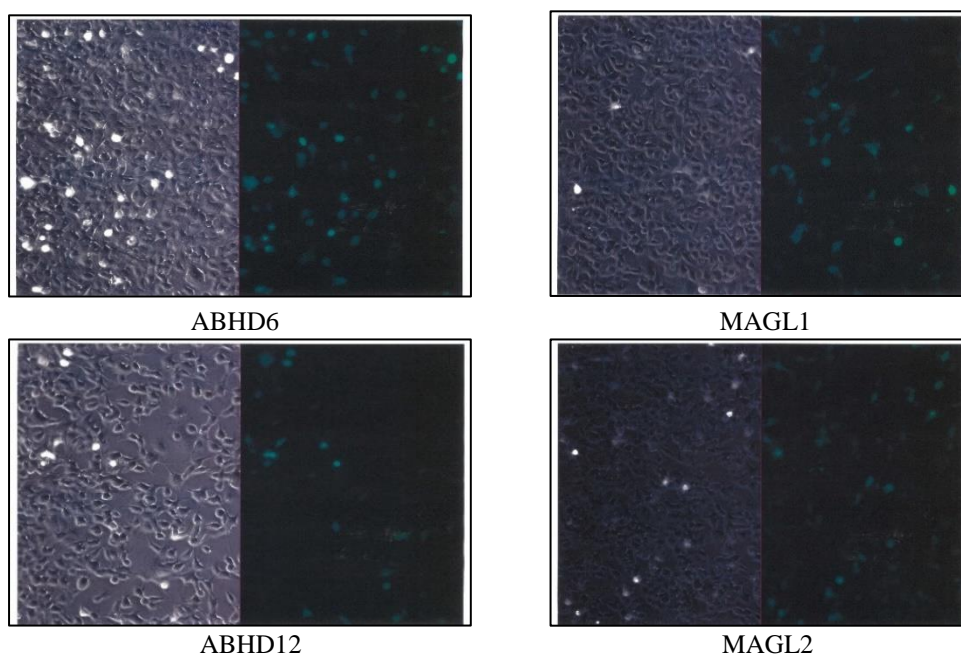


Figure 3.6 Representative images for co-transfection with GFP in HEK293. Cells were viewed under fluorescent microscopy after 28 h. Left column for ABHD6 and ABHD12. Right column for MAGL1 and MAGL2. Co-transfections with empty vectors were also done (image not shown) with similar results.

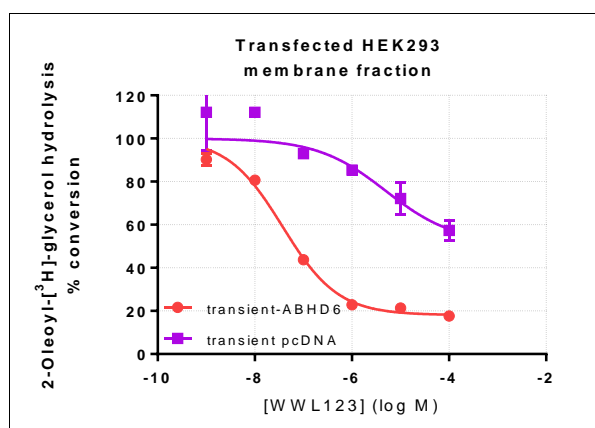


Figure 3.7 Representative image for transfection with an empty vector. Concentration inhibition curve of WWL123 on $[^3\text{H}]$ -2OG hydrolysis in membrane preparations of HEK293 cells transiently transfected with ABHD6 and control, performed in duplicate.

3.4.6.2 MAGL activity in transfected HEK293

Two isoforms of human MAGL were successfully cloned followed by over expression in HEK293 cells. Cloning, transfection, harvesting and separation of the lysate into soluble and membrane fractions with its protein quantification were described in the second Chapter. The transfects were then assayed using the radiometric method and investigated using serial dilutions of JJKK048 as a reported MAGL-selective inhibitor (Figure 3.8 and Table 3.10).

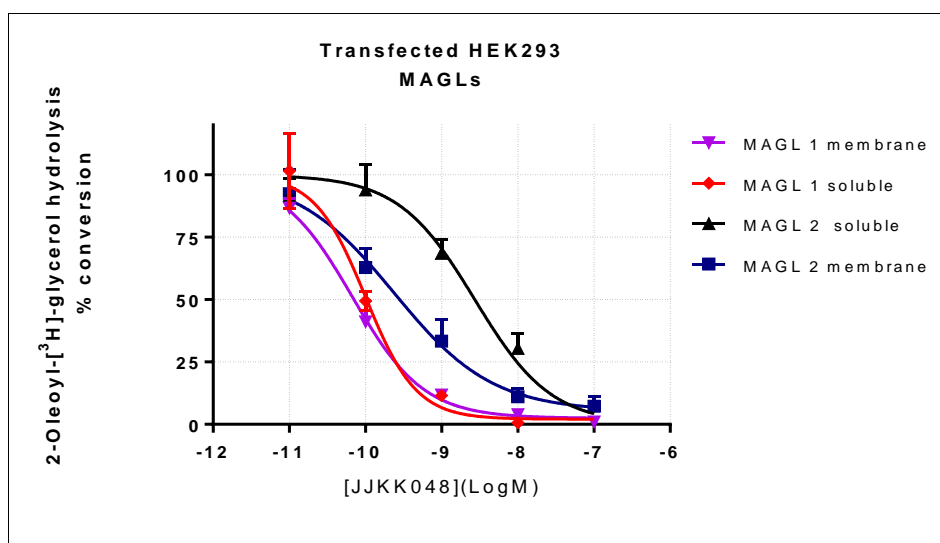


Figure 3.8 Concentration inhibition curve of JJKK048 on $[^3\text{H}]$ -2OG hydrolysis in transfected HEK293 cells with MAGL1 and MAGL2.

Data are mean \pm SEM from 4-6 independent experiments performed in duplicate.

Table 3.10 [³H]-2OG hydrolysis in HEK293 cells transfected with MAGL1 and MAGL2 in four independent experiments performed in duplicate.

	Total activity	JJKK048 sensitive activity				Residual activity	
	nmol/min/mg	nmol/min/mg	% inhibition	pIC ₅₀	Slope	nmol/min/mg	% control
MAGL1 soluble	181.7 ± 1.2	181.0 ± 1.2	100 ± 0	10.1 ± 0.1	-0.90 ± 0.06	0.65 ± 0.5	0
MAGL1 membrane	81.6 ± 2.4	80.6 ± 2.3	99 ± 1	9.8 ± 0.3	-0.78 ± 0.03	1.0 ± 0.5	1 ± 1
MAGL2 soluble	8.1 ± 0.6	7.4 ± 0.8	91 ± 4	8.7 ± 0.2	-1.00 ± 0.30	0.7 ± 0.2	9 ± 3
MAGL2 membrane	18.7 ± 0.9	16.8 ± 1.3	90 ± 5	9.3 ± 0.5	-0.82 ± 0.23	1.9 ± 0.9	10 ± 5

JJKB048 was able to fully inhibit both isoforms at 100 nM. The two fractions of MAGL1 exhibited almost identical properties, while the soluble and membrane activities of MAGL2 were also similar to each other (Figure 3.8). However, comparison of the two splice variants suggested that they displayed slightly different pIC₅₀ and slopes which might reflect different biochemical and pharmacological properties between the two isoforms. The two isoforms also showed differences in their subcellular distributions; MAGL1 appeared to have a greater proportion of activity in the soluble fraction, while MAGL2 appeared predominantly associated with the membrane fraction (Table 3.10).

Activity-based protein profiling (ABPP) analysis confirmed the inhibitory effect of JJKB048 on both isoforms. It also showed the doublet characteristic of MAGL1 reported in the literature (Blankman *et al.*, 2007; Dinh *et al.*, 2002a; Karlsson *et al.*, 2001; Long *et al.*, 2009b)(Figure 3.9).

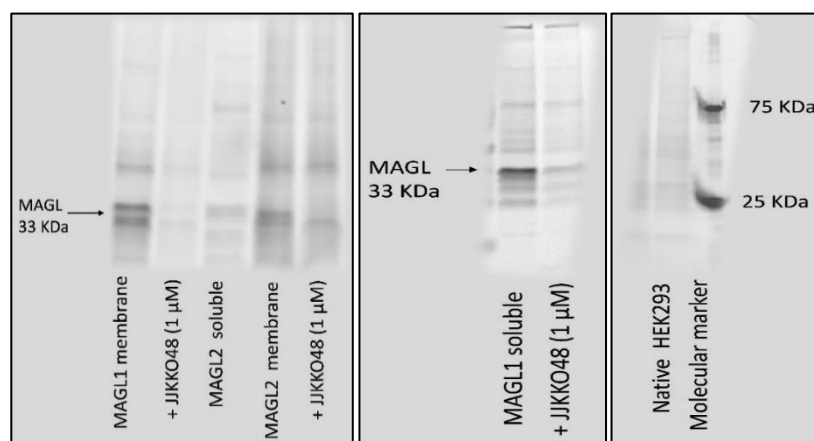


Figure 3.9 Activity Based Protein Profile of MAGL transfects.

Right side image showed the molecular marker and native (un-transfected) HEK293 as a control. Middle image showed the soluble fraction of transfected HEK293 with MAGL1 with and without JJKB048. Left hand side image showed the membranous fraction of transfected MAGL1 HEK293 and MAGL2 with and without JJKB048.

3.4.6.3 ABHD6 activity in transfected HEK293 cells

Parallel to the hMAGLs, human ABHD6 was the subject of the same methodologies for pharmacological and biochemical characterization. WWL123 was chosen as a selective inhibitor for ABHD6 (Bachovchin *et al.*, 2010) to be investigated, with a reportedly improved blood brain barrier penetration (Bachovchin *et al.*, 2010) compared to WWL70 (Poursharifi *et al.*, 2017). The profile of WWL123 with ABHD6 membrane transfects is shown in Figure 3.10 and Table 3.11. In addition, ABHD6 transfects (soluble and membrane) were challenged with another selective ABHD6 inhibitor - WWL70 (Figure 3.11). Noticeably, there was 20% control activity resistant to WWL123 or WWL70 at 10^{-4} M (Figure 3.10 and 3.11).

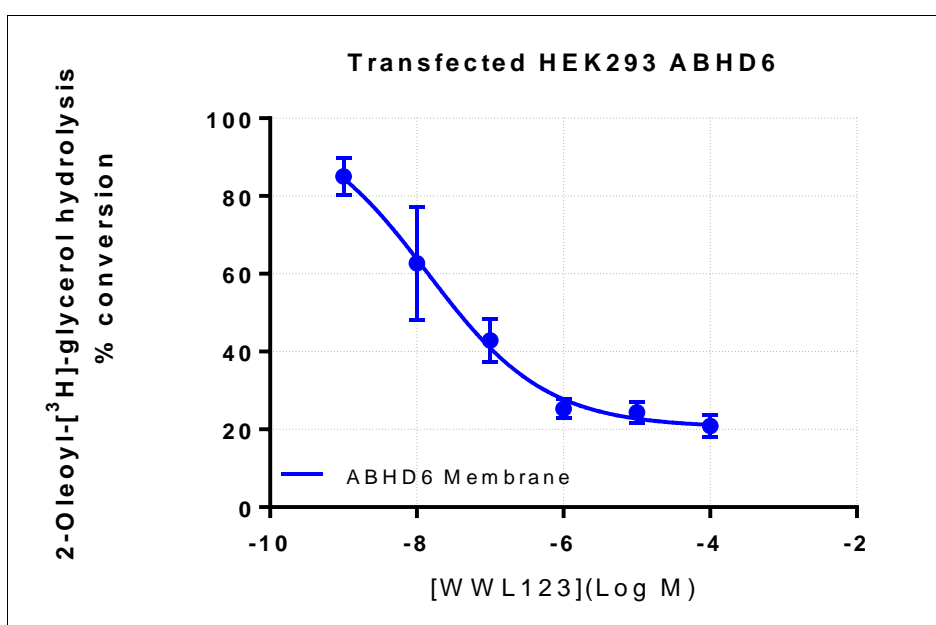


Figure 3.10 Concentration inhibition curve of WWL123 on [3 H]-2OG hydrolysis in ABHD6 transfected HEK293 cell membranes.

Data are mean \pm SEM from three independent experiments performed in duplicate.

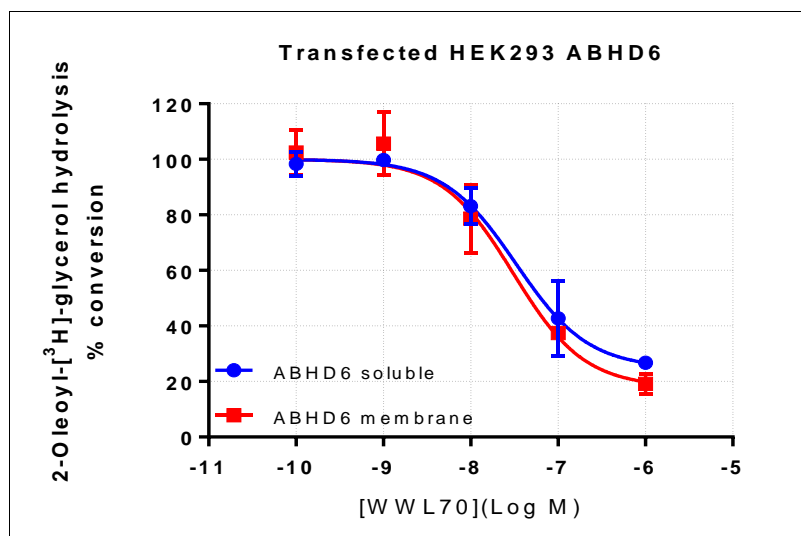


Figure 3.11 Concentration inhibition curve of WWL70 on [3H]-2OG hydrolysis in soluble and particulate fractions of an ABHD6-transfect.

Data are from a single experiment performed in duplicate, pIC_{50} 7.5 and slope -1.1 in both fractions. Total 2OG activity for the membrane was 7.4 nmol/mg/min, ABHD6 was 6.4 nmol/mg/minute and 1.0 nmol/mg/minute was the insensitive fraction.

Fixed concentrations of different inhibitors were assessed using soluble and membrane fractions of ABHD6 transfects in four independent experiments (Table 3.12). These inhibitors are MAFP (as a nonselective irreversible inhibitor of many serine hydrolases (Deutsch *et al.*, 1997)), JKKK048 (as a selective MAGL inhibitor (Aaltonen *et al.*, 2013)) and WWL123 (a selective ABHD6 inhibitor (Bachovchin *et al.*, 2010)). Results showed that MAFP produced almost complete inhibition in both fractions. Both JKKK048 (100 μ M) and WWL123 (1 μ M) displayed an inhibition on ABHD6 transfects and on both fractions, though to variable extent (Table 3.12).

The inhibitory effect of 1 μ M JKKK048 was clearly observed in the membrane fraction in the ABPP gel (Figure 3.12) as a complete inhibition of ABHD6, similar to MAFP. This is consistent with reports of ABPP using mouse brain membrane with 10^{-6} M JKKK048 which clearly inhibited labelling of both ABHD6 and FAAH (Aaltonen *et al.*, 2013). In a further analysis, ABHD6 activity in both fractions was also inhibited at 100 nM JKKK048 to roughly similar levels (Table 3.12).

Table 3.11 [³H]-2OG hydrolysis in ABHD6-transfected HEK293 cells.

Data are mean ± SEM from four independent experiments performed in duplicate.

	Total activity	WWL123 sensitive activity				Residual activity	
	nmol/min/mg	nmol/min/mg	% control	pIC ₅₀	Slope	nmol/min/mg	% control
ABHD6 particulate	11.6 ± 0.6	8.8 ± 0.5	76 ± 1	7.8 ± 0.2	-0.62 ± 0.09	2.8 ± 0.2	24 ± 1

Table 3.12 [³H]-2OG hydrolysis in both fractions of ABHD6-transfected HEK293 cells in the presence of fixed concentrations of different inhibitors.

Data are from 3-4 independent experiments performed in duplicate.

	ABHD6 soluble		ABHD6 membrane	
	nmol/min/mg	% control	nmol/min/mg	% control
Control	4.7 ± 0.5	100	11.1 ± 0.8	100
MAFP (1 μM)	0.4 ± 0.1	9 ± 2	0.1 ± 0.1	1 ± 1
JJKK048 (100 nM)	1.4 ± 0.2	30 ± 5	3.8 ± 0.7	34 ± 5
WWL123 (1 μM)	1.6 ± 0.2	35 ± 4	2.5 ± 0.3	23 ± 1

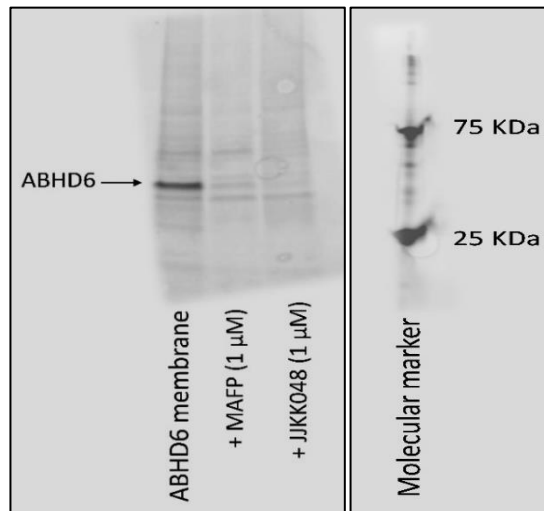


Figure 3.12 Activity Based Protein Profile of ABHD6-transfected HEK293 cells with 1 μ M of MAFP and JJKK048.

Consequently, concentration inhibition curves of JJKK048 in membrane fractions of ABHD6 transfects were assessed (Figures 3.13). However, the effects of the inhibitor did not show the typical sigmoidal curve expected. It showed that JJKK048 at 100 nM evoked an inhibition to 37 ± 5 % control.

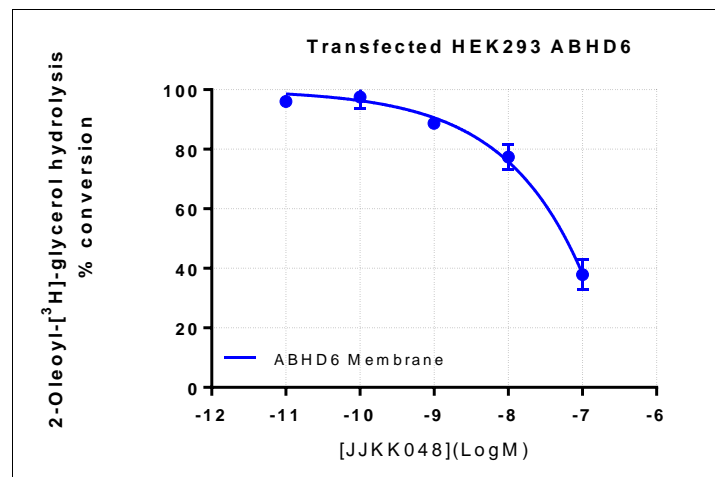


Figure 3.13 Concentration inhibition curve of JJKK048 on $[^3\text{H}]$ -2OG hydrolysis in ABHD6- transfected HEK293 cells. Data are from a single experiment performed in duplicate. Total $[^3\text{H}]$ -2OG hydrolysis was 12.4 nmol/min/mg.

3.4.6.4 ABHD12 transfection

The absence of a selective inhibitor for ABHD12 has limited its further exploration. In this study, MAFP (an inhibitor of serine hydrolases) was used for checking transfected cells. Total [^3H]-2OG hydrolysis in ABHD12 transfects was 51.5 nmol/mg/min and upon using MAFP, it dropped to 0.6 nmol/mg/min (1% control).

ABHD12 was also investigated with different inhibitors (in the radiometric assay) (Figure 3.16).

3.4.7 [^3H]-AEA as substrate

To exclude any potential amidase activity in the MAGLs and ABHD6 transfects, 5 μM AEA was used as a substrate, instead of 2OG, with rat liver membrane as a positive control (Figure 14).

There was high level of activity detected in liver compared to transfects. Liver hydrolysed AEA which was blocked in the presence of URB597 –as expected– which indicate FAAH like activity. AEA hydrolysis was not altered in the presence of JJKK048 in liver and slightly reduced with WWL123 (Figure 14). The three transfects (MAGL1, MAGL2 and ABHD6) showed negligible AEA hydrolysis indicating that AEA is not a substrate for these enzymes.

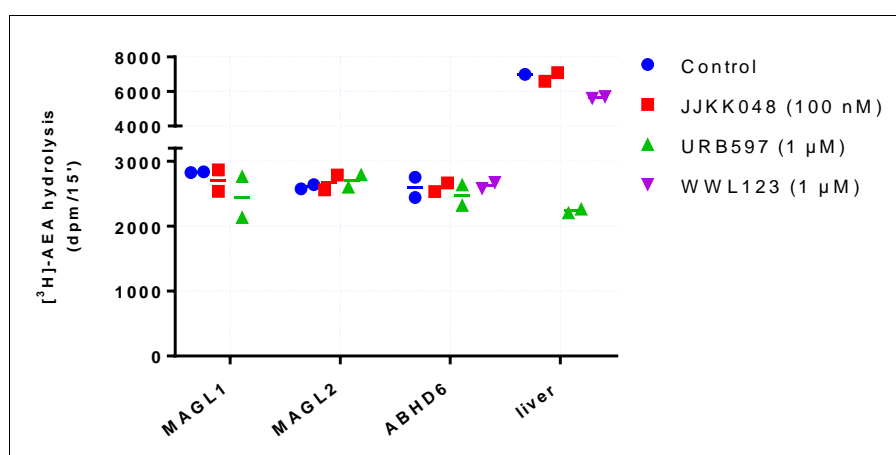


Figure 3.14 [^3H] AEA hydrolysis in the membrane fractions of MAGL1, MAGL2 and ABHD6-transfected HEK293 and rat liver.

Data are radioactive counts (dpm) from a single experiment conducted in duplicate.

3.4.8 Activity with different inhibitors

In this Section, samples from different types of transfects and cellular fractions were used to assess the selectivity of a series of inhibitors. The final concentration of these inhibitors was 1 μM , except for URB602 which was examined at 100 μM . Inhibitors were

- URB597 – a selective FAAH inhibitor (Piomelli *et al.*, 2006)
- JZL184 -a selective MAGL inhibitor (Long *et al.*, 2009b)
- URB602 -a selective inhibitor of MAGL (King *et al.*, 2007)
- WWL123 and WWL70-as selective ABHD6 inhibitors

There has been a controversy about the selectivity (and potency) of URB602 for MAGL over FAAH. Therefore, 100 μM (a relatively high concentration) was used as the final concentration. Hohmann and co-workers used 100 μM URB602 and failed to show FAAH inhibition (Hohmann *et al.*, 2005). In addition, (King *et al.*, 2007) used 100 μM URB602 as the optimal concentration for definition of MAGL. Later on, 100 μM of URB602 was used to assess the activity in rat ileum and liver (which is known to be rich in FAAH). (Duncan *et al.*, 2008) showed that this inhibitor evoked significant inhibition of ileum soluble MAGL activity, in contrast, URB602 evoked much more modest inhibition of rat liver particulate FAAH activity (Vandevoorde *et al.*, 2007). Based on this evidence, 100 μM of URB602 was chosen as a final concentration to measure MAGL.

The data in Figures 3.15 show that JZL184 and URB602 displayed approximately similar levels of near-complete inhibition in MAGL transfects (Figure 3.15) similar to the levels described in the literature though it appeared less sensitive with membranous MAGL2. URB597 showed negligible interference with 2OG hydrolysis in these preparations (Figures 3.15, 3.16 and 3.17). WWL70 showed minor inhibition to similar levels in both MAGLs and ABHD12 transfects, which might represent the endogenous ABHD6 in HEK293 cells (Table 3.13 and Figure 3.16). In Figure 3.16, URB602 caused an inhibition in ABHD6 and ABHD12 activity, although it appeared not to be as active compared to the MAGL isoforms. WWL70 caused considerable level of inhibition in ABHD6 fractions with negligible inhibition in ABHD12 and MAGLs transfects (Figure 3.15 and 3.16).

JJJK048 evoked complete inhibition of MAGLs and modest inhibition of ABHD6 (Figure 3.17), while WWL123 showed considerable level of inhibition in the ABHD6 transfect.

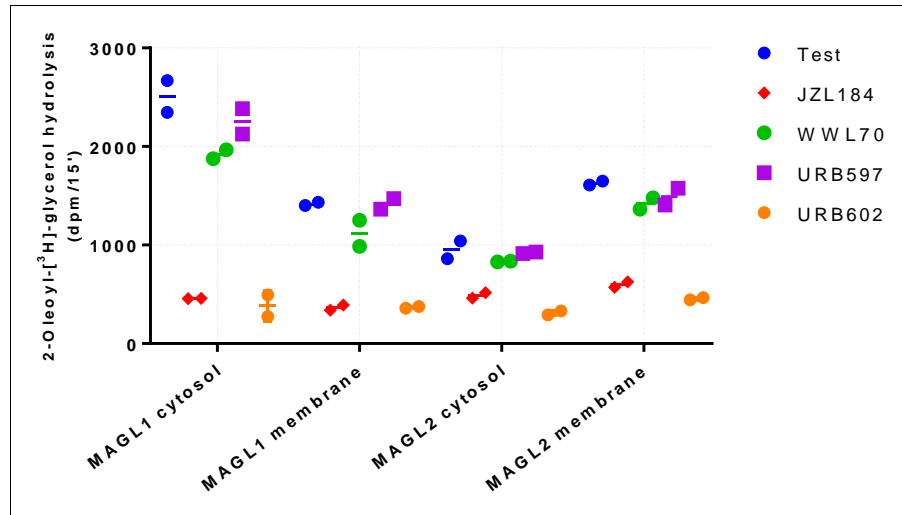


Figure 3.15 $[^3\text{H}]$ -2OG hydrolysis in both fractions of MAGL1 and MAGL2 transfected-HEK293 cells.

Data are radioactive counts (dpm) from a single experiment conducted in duplicate

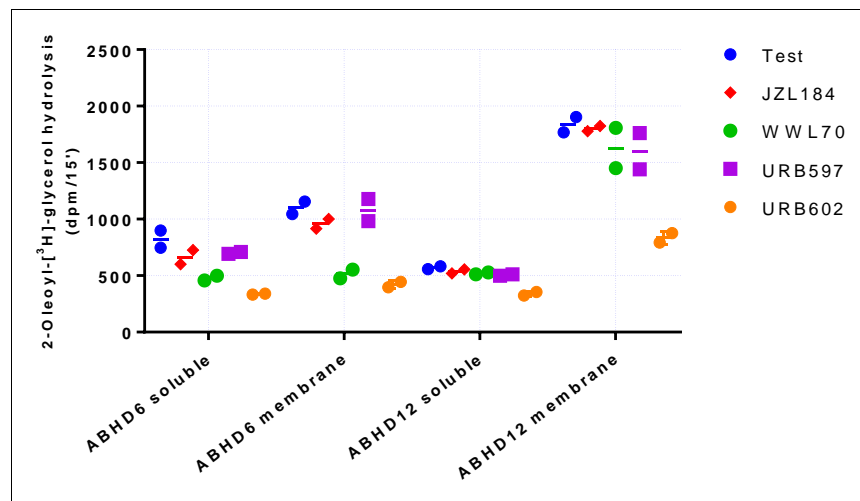


Figure 3.16 $[^3\text{H}]$ -2OG hydrolysis in both fractions of ABHD6 and ABHD12-transfected HEK293 cells.

Data are radioactive counts (dpm) from a single experiment conducted in duplicate.

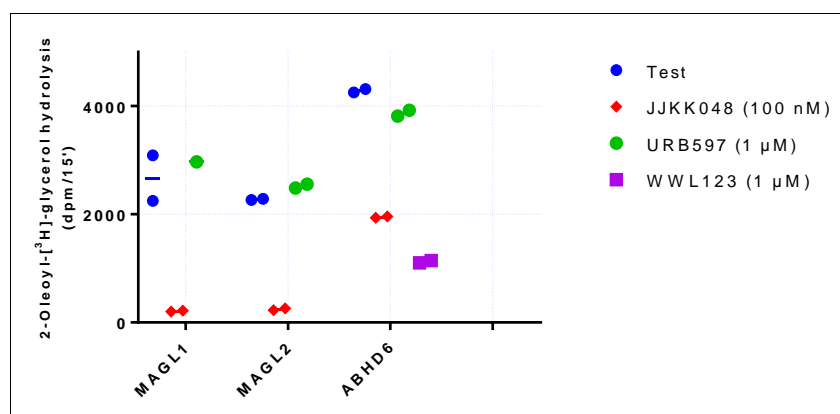


Figure 3.17 [3H]-2OG hydrolysis in membranous fraction of MAGL1, MAGL2 and ABHD6-transfected HEK293.

Data are radioactive counts (dpm) from a single experiment conducted in duplicate.

3.4.9 Activity in native HEK293 cells

[3H]-2OG hydrolysis was also investigated in native HEK293 cells in soluble and particulate fractions (and with different passage number) to measure the background activity before transfection. Fixed concentrations of inhibitors were used: 1 μM MAFP, JJKK048 and WWL123 (Table 3.13). Results showed that MAFP displayed almost complete inhibition, while the other two inhibitors displayed more modest inhibitions.

Table 3.13 [3H]-2OG hydrolysis in both fractions of native HEK293 cells.

Data are mean ± SEM from 4-5 independent experiments performed in duplicate.

	HEK293 soluble		HEK293 membrane	
	nmol/min/mg	% control	nmol/min/mg	% control
Control	1.6 ± 0.2	100	2.4 ± 0.2	100
MAFP (1 μM)	0.3 ± 0.0	16 ± 3	0.1 ± 0.0	4 ± 1
JJKK048 (1 μM)	1.0 ± 0.1	62 ± 1	1.8 ± 0.2	74 ± 5
WWL123 (1 μM)	1.4 ± 0.2	89 ± 3	1.7 ± 0.3	69 ± 5

3.4.10 Activity in other cell lines

Different cell lines were assayed with the aim of identifying a cell line that expressed ABHD6 activity intrinsically, by using the radiometric assay and fixed concentrations of selected inhibitors as indicated in Tables 14, 15 and 16. Soluble

and membrane fractions were prepared and examined in the presence of fixed concentrations of inhibitors. These cells were: N2a mouse neuroblastoma cells, which were suggested to express ABHD6 in ABPP experiments (Baggelaar *et al.*, 2015), HCA-7 human colon cancer and Caco-2 human Caucasian colon adenocarcinoma cells; both as representatives of human intestinal tissue.

Table 3.14 [³H]-2OG hydrolysis in fractions of HCA-7 cells.

Data are mean ± SEM from three independent experiments performed in duplicate.

	HCA-7 soluble		HCA-7 membrane	
	nmol/min/mg	%	nmol/min/mg	%
Control	0.5 ± 0.3	100	1.3 ± 0.1	100
MAFP (1 µM)	0.1 ± 0.0	11 ± 1	0.0 ± 0.0	1 ± 3
JJJK048 (1 µM)	0.2 ± 0.2	33 ± 5	0.7 ± 0.1	53 ± 2
WWL123 (1 µM)	0.5 ± 0.2	93 ± 3	1.1 ± 0.1	84 ± 5
JJJK048 + WWL123	0.3 ± 0.1	62 ± 3	0.5 ± 0.0	39 ± 3

Table 3.15 [³H]-2OG hydrolysis in fractions of N2a cells.

Data are mean ± SEM from 2-5 independent experiments performed in duplicate. (MAFP and JJJK048 were not analysed for the soluble fraction).

	N2a Soluble		N2a Membrane	
	nmol/min/mg	%	nmol/min/mg	%
Control	9.8 ± 0.5	100	13.2 ± 1.0	100
MAFP (1 µM)	Not investigated	-	3.3 ± 0.7	23 ± 1
JJJK048 (1 µM)	Not investigated	-	7.5 ± 1.6	53 ± 3
WWL123 (1 µM)	8.7 ± 0.8	94 ± 1	10.7 ± 1.2	80 ± 4

Table 3.16 [³H]-2OG hydrolysis in fractions of Caco-2 cells.

Data are mean ± SEM of 2-5 independent experiments performed in duplicate. Data presented as mean ± SE. (MAFP and JJJK048 were not analysed for the soluble fraction).

	Caco-2 Soluble		Caco-2 Membrane	
	nmol/min/mg	%	nmol/min/mg	%
Control	3.6 ± 0.7	100	9.1 ± 1.0	100
MAFP (1 µM)	Not investigated	-	0.3 ± 0.2	2 ± 1
JJJK048 (100 nM)	Not investigated	-	4.2 ± 0.6	40 ± 5
WWL123 (1 µM)	1.6 ± 0.4	43 ± 2	5.8 ± 0.7	64 ± 2

HCA-7 and Caco-2 cells are human colon cancer cell lines of an epithelial type, although they were derived from different stages of differentiation. HCA-7 cells are a well differentiated cell line often used to investigate COX-2 activity, while Caco-2 cells are often used in the literature as a model of the small intestinal epithelial barrier and intestinal absorption.

Because of the low levels of total activity in HCA-7 cells, the influence of the inhibitors is likely to be more variable, and hence less reliable (Table 14).

Caco-2 cells were grown (in different passage number) in trans-well plates and harvested after 15 and 22 days (to allow cell differentiation and villi maturation) (see Methodology Chapter). Caco-2 cells were also grown in T-75 flasks for 7 days. Both conditions yielded similar results using the radiometric assay; Table 3.16 identifies the combined data from both conditions. These cells were the best in terms of expressing WWL123-sensitive 2OG hydrolysis (presumably ABHD6) among the cells tested, although they expressed MAGL as well.

N2a cells showed the highest measurable total [³H]-2OG hydrolysis among other selected cells in both fractions with JJKK048 insensitive and WWL123 insensitive activities of 53% and 80% in the membrane partition, respectively (Table 15).

3.4.11 Activity in primary culture cells

For more focus on the individual cell types that comprise the rat brain, astrocytes, neurons and microglia, were tested in the radiometric assay (Figure 3.18).

Microglia exhibited the lowest 2OG hydrolysis activity within these three primary cell types. Relatively high hydrolytic activity insensitive to MAFP appeared in its soluble fraction. No WWL123-sensitive (ABHD6) activity was detected in the soluble fraction and only ~ 10 % in the membrane fraction (Figure 3.18). Neurons expressed the highest activity sensitive to WWL123 (ABHD6) in both fractions (Table 3.17). The level of activity (as nmol/min/mg protein) sensitive to WWL123 (ABHD6) in the membrane fractions in astrocytes was close to that in the neuronal membrane fraction (Table 3.17).

MAGL activity (i.e. that inhibited by JJKK048) was highest in the membrane fraction of astrocytes, followed by neuronal membranes, while JJKK048 inhibited ~20-40% of hydrolysis in microglia (Figure 3.18). A similar level of JJKK048-sensitive MAGL activity was apparent in the soluble fraction of both neurones and astrocytes (3.4 and 3.6 nmol/min/mg, respectively) (Table 17).

Table 3.17 [³H]-2OG hydrolysis in both fractions of rat astrocytes, neurons and microglia.

Data are mean ± SEM from 3-4 independent experiments performed in duplicate.

	2OG hydrolysis (nmol/min/mg protein)					
	Astrocytes		Neurons		Microglia	
	Soluble	Membrane	Soluble	Membrane	Soluble	Membrane
Control	4.8 ± 0.3	10.1 ± 1.0	5.2 ± 0.2	7.2 ± 0.1	0.9 ± 0.3	1.4 ± 0.4
MAFP (1 μM)	0.7 ± 0.3	1.1 ± 0.8	0.3 ± 0.0	0.1 ± 0.1	0.3 ± 0.1	0.1 ± 0.0
JJKK048 (100 nM)	1.2 ± 0.3	2.7 ± 0.5	1.8 ± 0.2	3.1 ± 0.4	0.7 ± 0.2	0.8 ± 0.1
WWL123 (1 μM)	4.5 ± 0.4	8.4 ± 0.4	4.1 ± 0.3	5.2 ± 0.2	0.9 ± 0.3	1.1 ± 0.2

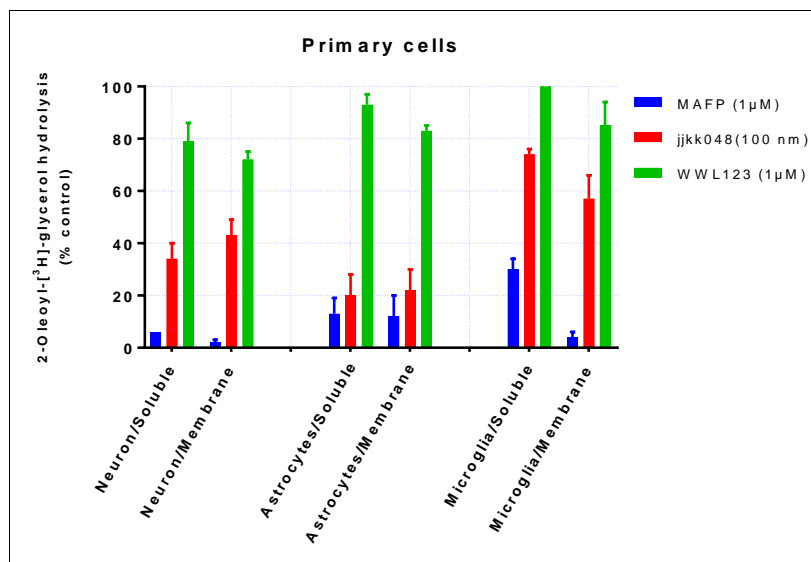


Figure 3.18 [³H]-2OG hydrolysis in cells derived from rat brain (neurons, astrocytes and microglia).

Data are mean ± SEM from 3-4 expressed as a percentage of the response in the absence of inhibitors.

3.5 Discussion

This Chapter described characterization of MAGL and ABHD6 activities in multiple rat tissues, multiple cell lines and in primary cells. Successful cloning allowed generation of MAG hydrolase enzymes (and for the first time MAGL2) in HEK293 as host cells and confirmed by different techniques. Using radiometric assay, MAGL and ABHD6 like activities were detected; being the highest in rat intestines for ABHD6 while high MAGL was measured in rat brain.

3.5.1 MAGL and ABHD6 in rat neural tissues

In this study, the use of a well-established assay of monoacylglycerol turnover, using 2-oleoyl-³H-glycerol as substrate, was applied in order to investigate the biochemical characterization of MAGL, ABHD6 and ABHD12. JJKK048 was used to define the contribution of MAGL as it has previously been described as the most potent and selective MAGL inhibitor (Aaltonen *et al.*, 2013) commercially available. Using this inhibitor, about 60 and 75 % of hydrolase activity in the soluble and membrane fractions of rat spinal cord could be ascribed to MAGL (Table 3.1). In the PFC, corresponding activities appeared higher at ~ 75 and 85 %, respectively.

Many reports in the literature have provided evidence for MAGL as the main MAG hydrolase in different parts of the nervous system. Thus, immune depletion of MAGL in soluble fractions of rat brain inhibited about 50% of total 2-AG-hydrolysis (Dinh *et al.*, 2004). Rat cerebellar membranes treated with N-arachidonoyl maleimide (an irreversible MAGL inhibitor) showed a ~85% decreased 2-AG hydrolysis (Saario *et al.*, 2005). ABPP identified that MAGL was responsible for ~85% of 2-AG hydrolase in mouse brain membranes (Blankman *et al.*, 2007) and MAGL activity was the most pronounced in mouse prefrontal cortex (Baggelaar *et al.*, 2017). However, this study described the remaining activity in three parts of brain. Using the same enzyme assay reported in this study, (Woodhams *et al.*, 2012) reported ~ 25% activity resistant to a selective MAGL inhibitor in both tissue fractions of Sprague Dawley rat spinal cord.

JJKK048 potencies for inhibition of 2OG hydrolysis (Table 3.1) were comparable or higher than those described for 2-AG hydrolysis (based on glycerol detection) in

rat cerebellar membranes and hMAGL overexpressing HEK293 lysates, with reported pIC₅₀ values of 9.67 and 9.44, respectively (Aaltonen *et al.*, 2013). In addition, in the lysate of HEK293 cells transfected with empty plasmid, JJKK048 pIC₅₀ value was 9.39 (Laitinen *et al.*, 2014).

The next step was to investigate whether ABHD6 activity was responsible for the 2OG hydrolysis in the JJKK048-insensitive fraction in the two tissues (Figure 3.2). WWL123 has been described as a selective ABHD6 inhibitor (Bachovchin *et al.*, 2010) where ABPP identified a pIC₅₀ value of 6.3 in lysate from recombinant expression in COS7 (monkey fibroblast). This inhibitor has also been administered *in vivo*, where it was able to reduce the severity of seizures in a mouse model of epilepsy (Naydenov *et al.*, 2014). As yet, there appear to be no reports of the use of WWL123 and/or an investigation of ABHD6 activity in rat tissues. The results showed a limited contribution of ABHD6 to 2OG hydrolysis in spinal cord or PFC. This might be attributed to the predominance of MAGL in these tissues, therefore, the following experiments were designed to investigate ABHD6 (or other enzymes) activity in the absence of MAGL activity. In the presence of 100 nM JJKK048, a serial dilution curve to WWL123 was constructed (Figure 3.3). As expected, JJKK048-sensitive MAGL activity appeared responsible for the bulk of hydrolysis ranging from 70-85% total activity, while WWL123-sensitive ABHD6 activity appeared to be only 1-2% of total hydrolysis in these tissues. Noticeably, the highest remaining activity was detected in the soluble fraction of rat spinal cord (Figure 3.3).

It is important to mention that there were variable levels of total [³H]-2OG hydrolysis detected in spinal cord and prefrontal cortex (Tables 3.1 and 3.3). This might be attributed to variations in substrate concentration in each experiment. 2OG is reported to be a low affinity substrate for MAGL (IC₅₀ value of 15 μM in rat brain against 2 μM 3H-2OG (Ghafouri *et al.*, 2004) and the concentration of substrate used in the present series of experiments is likely to be a non-saturating one.

To summarize, the hydrolysis of 2OG in rat spinal cord and PFC appears to be mediated predominantly through MAGL activity and an unidentified lipase/s, with little contribution from ABHD6. The attempt to detect ABHD6 in the presence of JJKK048 inhibition of MAGL failed. One potential explanation for the absence of

detectable ABHD6 activity in these regions is that 2OG may not be a ‘good’ substrate for ABHD6, while previous investigations have focussed on the use of 2AG as substrate or ABPP using -rhodamine-FP.

3.5.2 MAGL and ABHD6 in rat intestines

The next aim was to determine whether it was possible to distinguish the activities of MAGL and ABHD6 in rodent intestine, comparing mRNA expression levels and enzyme activities. Monoacylglycerols (and fatty acids) are present in the intestinal lumen following pancreatic lipase digestion of dietary fat as a major source of calories and cell membrane building blocks (Chon *et al.*, 2007; Storch *et al.*, 2008).

MAGL mRNA has been detected in rodent small intestine mucosa, full thickness ileum and in Caco-2 cell lines (Duncan *et al.*, 2008; Ho *et al.*, 2002) while MAGL protein was widely distributed throughout the length of gut co-localized with enteric neurons, based on fluorescence microscopy. During a high fat diet, 2OG was found to be formed in abundance in the intestine (Hansen *et al.*, 2011). MAG expression was found to be elevated as well (Chon *et al.*, 2007), which might indicate dietary control of MAGL expression levels. Another role for MAGL *in vivo* was identified following URB602 inhibition; there were trends to slow both upper GI transit and colonic propulsion (Duncan *et al.*, 2008). Furthermore, MAGL has been predicted to have an anti-inflammatory role by decreasing arachidonic acid in the gut (Nomura *et al.*, 2008).

This is the first study to demonstrate the presence of ABHD6 in small and large intestine, in soluble and membrane fractions of male and female rats. The results in Figure 3.4 and Table 3.4 confirmed principally the consistency of mRNA expression and activity for ABHD6. There appeared to be a higher level of ABHD6 activity over MAGL in some tissues, for example, in female small intestine and cytosol of male small intestine. The activities were almost equal in the soluble fractions of large intestine of both sexes. Whether the higher levels of ABHD6 activity in female intestine is relatively to a sex-specific role needs further investigation.

Previous results showed that, in rodent, the highest activity of 2OG hydrolysis was present in the soluble fraction of the duodenum and the lowest was in the distal colon

in male Sprague-Dawley rats (Duncan *et al.*, 2008). This is consistent with the male rat results observed here, nevertheless, the reverse was found in female rat. In the published study, URB602 was able to inhibit MAGL in both fractions of ileal mucosa, though the soluble part was more sensitive to the inhibitor and the authors predicted the presence of a “novel MAGL” in the membrane fraction.

Interestingly, WWL123 exhibit higher potency than is reported in the literature (Bachovchin *et al.*, 2010). At the moment, there is no obvious explanation for this. One possibility is that it may be related to the assay method, although a similar potency was found in ABHD6 HEK293 transfects. Alternatively, it may be a species related phenomenon or due to differences in post-translational modification. It would be useful to further explore this point, for example using tissues from mice with and without targeted disruption of the ABHD6 gene to compare the selectivity and potency of WWL123.

It was slightly surprising to identify this high level of ABHD6 activity in the soluble fractions of the gut, because ABHD6 was initially defined as a membrane-bound enzyme. As an example (Marrs *et al.*, 2010) identified ABHD6 in membrane fractions of mouse brain by immunoblotting. For some proteins, there is a proteolytic step which generates a soluble product from a membrane-bound enzyme. To investigate whether the soluble activity was generated by the action of proteolytic enzymes, protease inhibitors were mixed with the tissue before homogenization, and also during the enzyme assay to identify whether they might interfere directly (Tables 3.5 and 3.6). Added directly to the assay, the protease inhibitor combination inhibited 2OG hydrolysis in a concentration-dependent fashion in both soluble and membrane fractions of the rat small intestine (Table 3.5). However, incubation with protease inhibitors during the homogenization process and dilution in the enzyme assay failed to show any effect on the proportions of MAGL or ABHD6 in either membrane or soluble fractions (Table 3.6). This implies that protease activity is not an influence for generation of soluble ABHD6 activity.

There is very limited evidence in the literature supporting the presence of active ABHD6 in the soluble fraction. (Blankman *et al.*, 2007) highlighted the presence of a predicted trans-membrane domain in ABHD6 and ABHD12 by hydropathy study.

Further, they determined the average peptide spectral counts in mouse brain proteome showed that ABHD6 had 149 ± 7 and 5 ± 1 arbitrary units for the membrane versus soluble fraction, respectively. Fluorescence from an ABHD6-GFP fusion protein was identified in the cytoplasm of transfected AD293 cells (Li *et al.*, 2009). In another study; ABHD6 activity was measured in the soluble fraction of INS832/13 (rat pancreatic- β cells) that could be inhibited by 10 μ M WWL70 to ~60% (Zhao *et al.*, 2014). Taken together, the appearance of ABHD6 protein and activity in the soluble fraction appears reproducible, although it appears more abundant in the membrane fraction.

On separation of the epithelial layer of small intestine and subsequent enzymatic assay, it appeared most of the activity was inhibited with WWL123 more than JJKK048, with complete inhibition with MAFP. However, the combination of the inhibitors did not reach the level of MAFP inhibition indicating the presence of another 2OG (serine) hydrolase in the intestine.

In summary, it appears that multiple serine hydrolases, including MAGL and ABHD6, are active as monoacylglycerol hydrolases in the rat intestine. Whether these enzymes play metabolic or signalling roles will need to be examined in further experiments.

3.5.3 Activity in transfects

Searching the NCBI database for human genes identified three MAGL isoforms, one ABHD6 and two ABHD12 isoforms. In this study, MAGL1, MAGL2, ABHD6 and ABHD12 were successfully sub-cloned according to the map shown in Appendix-Table A.1.

MAGL3 isoform (NM_001256585.1) was described in NCBI as “a shorter form than MAGL 1 and it lacks an exon in the 3' coding region”. However, alignment comparison (using APE software) of the coding DNA sequence (CDS) of the MAGL1 and MAGL3 isoforms showed that they shared identical starting codon and stopping sequence. However, the difference is located in the middle fragment (90 base pair missing as shown in Appendix-Table A.3), then maintains again the reading frame. This result would make MAGL3 protein shorter than MAGL1 by 30

amino acids. To date, there are no published data on the presence of MAGL3 and whether or not there is in fact MAGL3.

Regarding a second isoform of ABHD12 (NM_015600.4), many trials to amplify the gene by PCR were conducted without detection on agarose gels. This means that it is either not present or another template (e.g. eye cDNA) might be more successful.

Many trials for making stable cell lines expressing these enzymes using different optimization methods were unsuccessful. In fact, until recently, there were no literature reports of stable cell transfects for ABHD6 and ABHD12. The exception is a very recently published work of (Chicca *et al.*, 2017). A MAGL stable cell line (with tagged 3HA) was reported (Savinainen *et al.*, 2010) and in two papers using a retrovirus system (Hu *et al.*, 2014; Nomura *et al.*, 2010). The difficulty in expressing these enzymes stably might indicate the protein or its products might be toxic in the host cells, or that the substrate/s are essential for cell survival.

The transfected cells were visualised by fluorescence detection after co-transfection with GFP (Figure 3.6) and assessed by measuring 2OG hydrolysis. As mentioned, the transient transfection system was found to be more efficient than the stable one (Figure 3.5). Results also showed that the transfects hydrolysed 2OG extensively compared to empty vector transfection (Figure 3.7) or non-transfected HEK293 cells (Table 3.13).

This is the first study to clone and determine the activity of MAGL2. MAGL2 lacks exon 5 and has a shorter N-terminus compared to the first isoform. This missing segment encodes for the lid region of MAGL and is implicated in substrate selectivity and membrane localization (Bertrand *et al.*, 2010; Labar *et al.*, 2010a; Labar *et al.*, 2010b; Scalvini *et al.*, 2016). This might explain the biochemical differences observed (see below) between MAGL1 and MAGL2.

Two research groups have reported two distinct crystal structures of MAGL and determined its catalytic site (Bertrand *et al.*, 2010; Labar *et al.*, 2010a). Both of them described two protein molecules per asymmetric unit with its catalytic region facing the phospholipid membrane (Scalvini *et al.*, 2016).

Over-expression of MAGL1 and MAGL2 isoforms in HEK293 cells showed they could be completely inhibited by the “ultra-potent” MAGL inhibitor JJKK048 (Figures 3.8 and 2.9 and Table 3.10) (Aaltonen *et al.*, 2013) although a slight difference in pIC₅₀ values between the two isoforms was observed. Total [³H]-2OG activity was higher in MAGL1 than MAGL2 transfects. MAGL1 appeared to be more active in the soluble fraction. Previously reported MAGL overexpression by adenovirus revealed equal activity in cytoplasm and membrane of host cells (Dinh *et al.*, 2002b). MAGL2 appeared much less active in both fractions than MAGL1, although it was more active in the membranes. The consistency in the absolute levels of JJKK048-resistant hydrolysis between MAGL1 and MAGL2 (in nmol/min/mg) suggests there is no difference in background hydrolysis between the two cells. The difference in biochemical parameters (substrate hydrolysis and enzyme inhibitor potency) may result from conformational changes in the enzyme around the active site (see Figures A.4, A.5 and A.6 in Appendix- for 3D structure of MAGL). Indeed, very recently it has been reported that mutation in the lid region of MAGL (where MAGL2 truncation occurs) can change substrate selection (Riccardi *et al.*, 2017). Obtaining crystal structures of the enzyme splice variants would allow a more detailed analysis of any change to be examined.

Both MAGL1 and MAGL2 were shown to have two bands on migration on ABPP gels (Figure 3.9) and both were inhibited in the presence of 1 μM JJKK048. This might indicate the presence of novel variants for each isoform (Labar *et al.*, 2010b) or it might be attributed to post-translational modification. Further investigation using inhibitors of glycosylation or the addition of glycosidase enzymes could examine the role of this particular post-translation modification.

ABHD6 transfects were used to identify the potency of inhibitors and enzyme distribution within the cell. The potency of WWL123 (Table 3.11) was slightly higher than with the only previously reported study (in ABPP) (Bachovchin *et al.*, 2010) (-7.8 versus -6.3, respectively). A similar potency (pIC₅₀ ~8) was observed in rat intestines (Table 3.4). This might be attributed to the enzyme assay system used or WWL123 might also affect another off target enzyme. Future studies should

investigate other tissues or other species (for example, human) or whether similar potency would be detected in tissues from ABHD6 disrupted animals.

In ABHD6 transfects, 20% of total 2OG hydrolysis was insensitive to the presence of 10^{-4} M WWL123. To follow up this point and check ABHD6 selectivity, a pilot study with WWL70 was conducted and a similar result was found. This is in line with a previous report of WWL70 inhibition of [3 H]-2-AG hydrolysis in mice brain homogenate with 20% activity remaining (Marrs *et al.*, 2010). On the other hand, (Patel *et al.*, 2015) detected ~5% insensitive fraction using a fluorescent glycerol detection assay using lysates of HEK293 cells transiently overexpressing ABHD6 and using 1-AG instead of 2-AG as a preferred substrate. This might indicate the limited ability of the host cells to over-express ABHD6, which also express another 2OG hydrolysing enzyme/s insensitive to either WWL70 or WWL123. Arguably, this discrepancy in residual activity might be attributed to the different substrates used in each experiment.

A number of experiments were done to exclude the role of AEA-hydrolysing enzymes and to assess the selectivity of different inhibitors with different transfects (Figures 3.14, 3.15, 3.16 and 3.17). Generally, the results were consistent with the expected role of the relevant inhibitor, yet, with some limited variabilities.

ABHD6 activity was measured in the presence of fixed concentrations of MAFP, JJKK048 and WWL123 in the two subcellular fractions (Table 3.12). The total measured activity was lower in the soluble compared to the membrane fraction. MAFP showed complete inhibition in both fractions. Because 1 μ M JJKK048 affected ABHD6 activity in the ABPP assay (Figure 3.12), 100 nM was examined (Table 3.12) and concentration inhibition curves to JJKK048 in ABHD6 transfects (Figure 3.13) were constructed to assess its inhibition profile.

The Aaltonen group reported that JJKK048 had a “moderate” inhibition of hABHD6 with a selectivity ratio of hMAGL over hABHD6 of ~630 fold making ABHD6 the “closest” off target. However, ABPP in the mouse brain membrane proteome showed that even at 10^{-7} M JJKK048, a reduced activity band of ABHD6 appeared, indicating poor selectivity of JJKK048 at this concentration. This might explain the

effects of JJKK048 on ABHD6 transfects in the present study (Table 3.12 and Figure 3.12).

There were variable effects of the FAAH inhibitor URB597 in the different transfects, although none of the enzymes exceeded 20% inhibition in the best condition (Figure 3.15, 3.16 and 3.17). While one group described URB597 with a lack of selectivity (Alhouayek *et al.*, 2014), others described URB597 as a selective FAAH inhibitor with no MAGL effect (Kathuria *et al.*, 2003). However, in a wide proteome study, URB597 has been identified as having off-target enzyme effects (Lichtman *et al.*, 2004), possibly among them ABHD6 and ABHD12 (Bosier *et al.*, 2013).

Finally, exploration of ABHD12 in transfected cells was limited in this thesis because of a lack of availability of selective inhibitors.

3.5.4 Native Enzyme Activities in cell lines

With the aim to find endogenous ABHD6 expression, a number of cell lines (N2a, HCA-7 and Caco-2) were enzymatically assayed HEK293 cells as potential hosts were assayed to determine background levels ABHD6 and MAGL like activity before transfection. This is the first study to determine the activity of ABHD6 and MAGL activities in these cell lines using the 2OG radioisotope enzyme assay as N2a was reported to express ABHD6 (Baggelaar *et al.*, 2015) while HCA-7 and Caco-2 were used as intestinal model (as an additional step for ABHD6 exploration in human gut after its characterization in rat intestine (Table 3.4 and Figure 3.4).

HEK293 cells almost equally expressed low activities of ABHD6 and MAGL like activities in the membrane fraction while MAGL like activity was more elevated in the soluble fraction (Table 3.13). HCA-7 cells had the lowest total 2OG hydrolysis in both fractions (Table 3.14), suggesting that results from investigating inhibitors effects were unlikely to be dependable.

In contrast, enzyme assay of N2a cells showed the total [³H]-2OG hydrolysis was measurable in both fractions –Table 3.15. MAFP largely inhibited the hydrolysis in membranes which indicates the presence of serine hydrolase enzymes, while JJKK048 at the relatively high concentration of 1 μM only inhibited ~ 50%

indicating the presence of multiple enzyme activities in these cells. While no detectable ABHD6 like activity could be measured in the soluble portion, nearly - and unexpectedly- only 20% of total 2OG in membrane fraction could be attributed to ABHD6 (Table 3.15). This was in contrast to ABHD6 detection using the ABPP method (Baggelaar *et al.*, 2015).

Caco-2 cells appeared to have the highest ABHD6-like activity in radioisotope enzyme assay among the selected cell lines (Table 3.16). MAFP was shown to completely inhibit 2OG hydrolysis in the particulate fraction. The detection of ABHD6 like activity (WWL123 inhibition) in the soluble fraction and ABHD6 and MAGL activities in the membrane fraction were in line with our previous results of ABHD6 and MAGL detection in rat gut (Table 3.4).

3.5.5 Activity in primary cell culture

Because measuring activities in neural tissues failed to identify ABHD6-like enzyme activities, the next step was to investigate individual cell types within these tissues. There were previous studies (Baggelaar *et al.*, 2015; Grabner *et al.*, 2016; Marrs *et al.*, 2010; Viader *et al.*, 2015; Viader *et al.*, 2016) investigating the distribution of 2-AG hydrolases in these types of cells using various assays and immunostaining tools especially in mice brain, nevertheless, this is the first study to measure the activity of 2OG as substrate.

It was reported that in mice primary microglial homogenates, MAGL and ABHD6 did not contribute to [³H]-2-AG hydrolysis, using JZL184 and WWL70 as inhibitors (Marrs *et al.*, 2010). However, in this Chapter, it has been shown that MAGL was responsible for ~40% and 20% of 2OG hydrolysis in microglial membranes and cytosol, respectively (Figure 3.18 and Table 3.17). This can be explained by the relatively low levels of total 2OG hydrolysis in microglia and thus, the less reliable data of ABHD6 and MAGL like activity in these cells.

ABHD6 was not detected by immunostaining in mouse primary microglia while it was present in the mouse microglial BV-2 cell line using quantitative PCR (Marrs *et al.*, 2010) . However, another study identified ABHD6 in microglia in cross sections of spinal cord of an experimental autoimmune encephalomyelitis mice

model, co-localized with F4/80 (a marker for macrophages/microglia) (Wen *et al.*, 2015). The authors hypothesized that ABHD6 was upregulated during inflammation. Another group reported the presence of ABHD6 in J774, RAW267.7 and BV-2 microglial cell lines of mice (Alhouayek *et al.*, 2014). Although these cells were used as surrogates for different functional aspects of microglia, their phenotypes were reported by many laboratories to be quite different from primary microglia (Marrs *et al.*, 2010). BV-2 cells are reported to express functional ABHD6; suggested to be responsible for ~50% of 2-AG hydrolysis (as indicated by WWL70 inhibition) in two separate research group (Marrs *et al.*, 2010) and (Tanaka *et al.*, 2017) while primary microglia were not.

Regarding MAFP in these primary cells, the results (Figure 3.18) showed almost complete inhibition, except in microglia and astrocyte cytosols with ~20% and 15% insensitive fractions, respectively. Further biochemical analysis would be required to define enzymes involved.

In neurons (Figure 3.18), MAGL represented ~60% of 2OG hydrolysis, while in astrocytes, it represented ~80%. (Dinh *et al.*, 2002a) reported MAGL 2-AG hydrolysis in rat neurons in soluble (0.3) and particulate (0.2 pmol/min/mg protein) fractions, respectively. With another study, it was shown that in neuronal homogenates, JZL184 alone inhibited ~50% of the total 2-AG hydrolysis whereas in combination with WWL70, it suppressed almost all of the hydrolysis. In the same study, the combination of 10 μ M WWL70 and 1 μ M JZL184 inhibited all 2-AG hydrolysis in intact neurons measured by [³H]-glycerol production (Marrs *et al.*, 2010). In mouse astrocytes, the Stella group reported that MAGL was expressed, using 2-AG as a substrate in radiometric assay and in immunoblotting (Walter *et al.*, 2004). These data are in agreement with results in this study (Figure 3.18).

ABHD6 appeared responsible for ~30% and 20% in membrane fractions of neurons and astrocytes, respectively. The Cravatt group have shown ABHD6 was responsible for ~50% of hydrolysis of 2-AG in neurons using the maximally effective concentration of 10 μ M WWL70. They confirmed the expression of ABHD6 mRNA in primary neuron and microglia with the radiometric assay (Marrs *et al.*, 2010). In

addition, they conducted immunocytochemistry of mouse primary cells and showed that ABHD6 was expressed in neurons and astrocytes, but not in microglia.

As mentioned earlier, the lack of available ABHD12 inhibitors limits its characterization in these cells. It has been reported in the literature that ABHD12 was greatly responsible for 2-AG hydrolysis in microglia (Savinainen et al., 2012) (and astrocyte) but not in neurons using an ABHD12 knockout mouse (Viader *et al.*, 2016).

In conclusion, this Chapter gave an indication of the subcellular distribution of MAGL, ABHD6 and other “unknown” MAG metabolising enzymes in various cellular and tissue contexts. In order to expand and draw complete picture, genetic expression and protein visualization would be required. The next Chapter, the mRNA expression of MAGL and ABHD6 in various rat tissues will be investigated. In addition, visualization of these proteins in recombinant expression will be assessed.

Chapter Four

mRNA detection and subcellular localization of MAGLs and ABHD6

4. mRNA detection and subcellular localization of MAGLs and ABHD6

4.1 Introduction

4.1.1 Genetic expression in rat tissues

The wide distribution of mRNA encoding for MAGL has been described. MAGL was reported to be expressed in many rat tissues including ovary, heart, spleen, lung, liver, skeletal muscle with the highest expression in adipose tissue, adrenal glands, kidney and testis (Karlsson *et al.*, 1997). In rat brain, MAGL mRNA was high in hippocampus, cerebellum, thalamus and cortex which also express high levels of the CB₁ receptor (Dinh *et al.*, 2002a; Tsou *et al.*, 1998). In rat intestine, MAGL mRNA was higher in submucosa and myenteric plexus than in the mucosal layer (Duncan *et al.*, 2008).

In an interesting study using mouse intestinal MAGL, dramatic changes in mRNA levels and activity took place during ontogeny (Chon *et al.*, 2007). There was a relative abundance of mRNA expression at the early stage of life, which was in contrast to MAGL activity at the same age. There was a gradual decrease to low but detectable levels of expression which appeared opposite to enzyme function (high activity measured) at 100 days old. Both expression and activity were elevated after administration of a high fat diet, but not starvation, suggesting a potential role in dietary lipid control. This discrepancy between MAGL mRNA and activity has also been reported in adult rat neurones, astrocytes and microglia where the activity was inverted with respect to mRNA levels (Viader *et al.*, 2016). This raises the possibility that MAGL in this tissue undergoes some further editing at the translational or post-translational levels.

Regarding mRNA for ABHD6, it has also been shown to be widely expressed. It has been described in liver, heart, lung, brown adipose tissue, kidney, spleen, small intestine, testis, brain and skeletal muscle of mice; with the highest levels found in small intestine followed by adipose tissue and liver (Thomas *et al.*, 2013). As with MAGL, ABHD6 expression appears to be influenced in diet.

Thus, high fat diet feeding in mice lead to increased ABHD6 mRNA expression in the small intestine and liver (Thomas *et al.*, 2013). ABHD6 mRNA was highly expressed in neonatal mouse primary hippocampal neurons and increased until adulthood when it remained stable (Wei *et al.*, 2016) with no sex differences observed between male and female mice (Chesworth *et al.*, 2018).

Upon searching for rat MAGL mRNA on the NCBI database, two transcripts appear: MAGL and a predicted variant termed X1MAGL. X1MAGL exhibits a 16 amino acid deletion at the beginning of the 5' region in comparison to MAGL. It is not known for now whether the rat MAGL has similar variants to human as no data are available regarding the second variant of MAGL (X1 MAGL) in rat.

4.1.2 Subcellular localization of the enzymes

It has been postulated that ABHD6 and MAGL might be located in the nuclear membrane and mitochondria (Marrs *et al.*, 2007). However, this suggestion remains to be confirmed. This speculation was based on the presence of 2-AG hydrolytic activity in different fractions from intact cells, for example; in plasma membrane, nuclear membrane and mitochondria, suggesting different subcellular localization of the enzymes was responsible for a distinct pool of 2-AG hydrolysis (Marrs *et al.*, 2007).

For MAGL, the subcellular localization was first studied in 1981 in rat fat cells where the activity was detected in multiple cellular fractions (Sakurada *et al.*, 1981). These were (in descending order): in cytosolic fraction, membranes, microsomes, nuclear and mitochondrial fractions. Later, different studies reported the presence of MAGL in the cytoplasm (Dinh *et al.*, 2002a; Dinh *et al.*, 2004), in membranes (Saario *et al.*, 2005; Woodhams, 2012) and in both fractions (Blankman *et al.*, 2007; Labar *et al.*, 2010b; Long *et al.*, 2009a). MAGL was found to be equally distributed between the cytosolic, nuclear, mitochondrial and microsomal fractions of mice neurons (Muccioli *et al.*, 2007). Given these alternatives, it is possible that MAGL might have different localization in different species and cell types.

Muccioli *et al.* (2007) identified a novel MAGL-like activity enriched in mitochondrial and nuclear fractions in BV-2 mouse microglial cells (Muccioli *et al.*, 2007). ABHD6 was later found to be responsible for ~ 50% of 2-AG hydrolysis in these cells and hence suggested to represent the previously reported “novel MAGL” activity (Marrs *et al.*, 2010). An ABHD6-GFP fusion protein was detected in cytoplasm in host transfecting cells (Li *et al.*, 2009). Most recently, ABHD6 was reported to be enriched in endoplasmic reticulum membranes and in the perinuclear area of transfected COS-7 cells (Pribasnig *et al.*, 2015). Given the detection of ABHD6 in the cytoplasm in this study (Chapter 3 with rat intestines and in human transfects), the identification of the subcellular localization of this enzyme in different conditions (native and overexpressed condition) and in different types of cells (cell line and primary cell culture) would be important to complete an understanding of the function of the activity.

Because of the constraints in finding a specific ABHD6 antibody to study its distribution (see Section 4.3 below) and because of the lack of a selective antibody to discriminate the two MAGL isoforms, HA-tagging at both termini (N- and C-) of each gene was conducted (primers and methods were described in Chapter Two, Sections 2.4.1 and 2.4.3).

A link between ABHD6 and neuronal cells has been described in the literature (Marrs *et al.*, 2010; Straiker *et al.*, 2009; Viader *et al.*, 2016). However, these studies did not investigate the subcellular location of ABHD6. Keeping in mind the difficulties of introducing genes in primary cell cultures, viral infection has been used in this Chapter to identify subcellular localization of ABHD6 in multiple cell types.

4.2 Aim of this Chapter

The aim of this Chapter was mainly to provide a dataset combining different techniques and tissue sources. The objectives were to:

- Quantify gene expression in different rat tissues.
- Identify the subcellular localization of human ABHD6, MAGL1 and MAGL2 in recombinant expression using immunostaining, immunoblotting and radiometric enzyme assay.
- Investigate the subcellular localization of ABHD6 in primary neuronal cell culture cells using viral infection.

4.3 Methods

RNA isolation and conversion to cDNA were described in Sections 2.4.4 and 2.4.5, respectively. Specific Taqman primers and probes were designed for the two MAGL variants, as well as for rat ABHD6, and for three reference genes (β -actin, TBP and GAPDH). The mRNA expression levels of selected genes were quantified in this Chapter using TaqMan®-Based Detection qRT-PCR (Section 2.4.6).

There were many attempts in this study to measure ABHD6 protein using two polyclonal antibodies (anti-ABHD6 antibody abcam, 74681 and Gene Tex, GTX87697), using different dilutions, different blocking buffers and different sources of enzyme (tissues and cell lines). All failed to provide evidence for functional antibodies (see Figure A.7 in Appendix as a representative image). HA-tagging of the enzyme by cloning was attempted, attaching at both C- and N-terminals for ABHD6. The HA-tag (human influenza hemagglutinin) is 9 amino acids in length and in common use due to its immunogenicity and easy detection without apparently interfering with protein function. In addition, HA-tagging was conducted with human MAGL1 and MAGL2 at both termini. Stripping and re-probing of immunoblots was performed as described in Section 2.6.3. Subcellular localization of ABHD6 in primary cell cultures by viral infection was conducted.

Primary cell culture represents a more physiological model, in terms of the physiological relevance of protein distribution, compared to CHO and HEK cells. It is, however, accompanied by the difficulties of culturing enough cell numbers for investigation and there is less efficient expression when transiently transfected. Therefore, this study aimed to introduce the ABHD6 gene using viral vectors into rat primary cell cultures, namely neurones and astrocytes, for the first time in literature. The use of viral vectors represents a powerful tool of transferring a gene into a hosting genome (Hwang *et al.*, 1984) and it is efficient to deliver the gene of interest into primary and other hard-to-transfect mammalian cells.

The virus type produced here was pseudo particles of retrovirus taking advantage of the Gateway® Technology system (details of viral infection are described in Section 2.9 and Appendix, Section B). In order to produce a lentivirus, transfection of a suitable host cell line (HEK293FT) with three types of plasmids is needed: first a transfer plasmid (N-ABHD6). The second one is the packaging system plasmid (pxPAX2) and finally the envelope plasmid (pMD2.G). pINDUCER system was chosen as a destination vector of the virus as it is well known to provoke a rapid and doxycycline dependent expression of different genes in different cell types (Meerbrey *et al.*, 2011). GFP-virus was used as a control.

Subcellular fractionation and protein quantification followed Sections 2.6.1.2 and 2.5.1. Immunostaining and details of antibodies used are described in Sections 2.7 and 2.6. All images were captured in the SLIM unit of the School of Life Sciences using confocal microscopy (Zeiss LSM880C, Germany).

4.4 Results

4.4.1 Determination of mRNA level in rat tissues

RT-qPCR was used to characterize gene expression levels of selected genes (Figure 4.1). The highest levels of ABHD6 gene expression, compared to MAGL and X1MAGL, were found in the gut (large and small intestine), where MAGL levels appeared the lowest level among the tissues investigated. ABHD6 was also

highly expressed in liver and kidney. An intriguing observation of the three genes in neural tissues was that they appeared to be equally well expressed. MAGL showed highest levels in adipose tissue, kidney and testis in broad agreement with another study that reported that MAGL mRNA levels were particularly high in those tissues (Karlsson *et al.*, 1997), although that study did not investigate the levels of X1MAGL expression. The X1MAGL variant was highest in testis and lowest in small intestine. Comparing MAGL and X1MAGL expression, kidney (both cortex and medulla) and adipose tissue had greater relative levels of MAGL, while X1MAGL appeared much higher than MAGL in testis (Figure 4.1).

In addition, mRNA detection were conducted for abdominal, thoracic and mesenteric rat aorta. Results are shown in the Appendix -Figure A.3.

The rank orders of individual gene expression levels were assessed and the results were then compared (Figure 4.2). The range of mRNA expression of ABHD6 was more limited (range 0.20-2.04 arbitrary units) compared to MAGL (0.15-8.66) and the X1 MAGL variant (0.08-10.36).

In comparing rank orders of expression of MAGL and ABHD6 (left graph of Figure 4.2), the testes, kidney cortex, mid brain and heart were tissues where MAGL ranked higher than ABHD6. On the other hand, ABHD6 expression ranked higher than MAGL in large, small intestine and the hippocampus. Similarly, by comparing X1MAGL and ABHD6 (right of Figure 4.2), the same above-mentioned tissues for MAGL (testes, midbrain and heart) ranked higher than ABHD6 while ABHD6 ranked higher in intestine (both the small and large one), liver and kidney medulla.

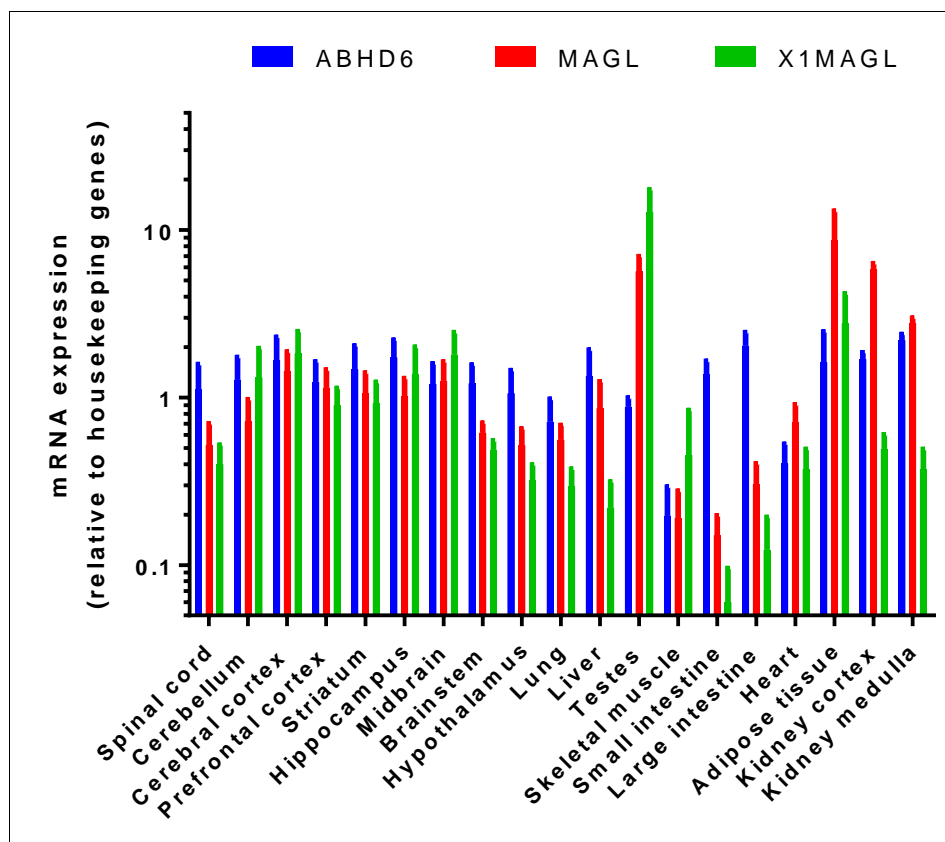


Figure 4.1 RT-qPCR analysis of the distribution of rat MAGL, X1MAGL and ABHD6 mRNAs in 19 different rat tissues.

Data were normalized to the geometric mean of three reference genes (β -actin, TBP and GAPDH). Data represent means \pm SEM of three technical separate experiments from a single male rat.

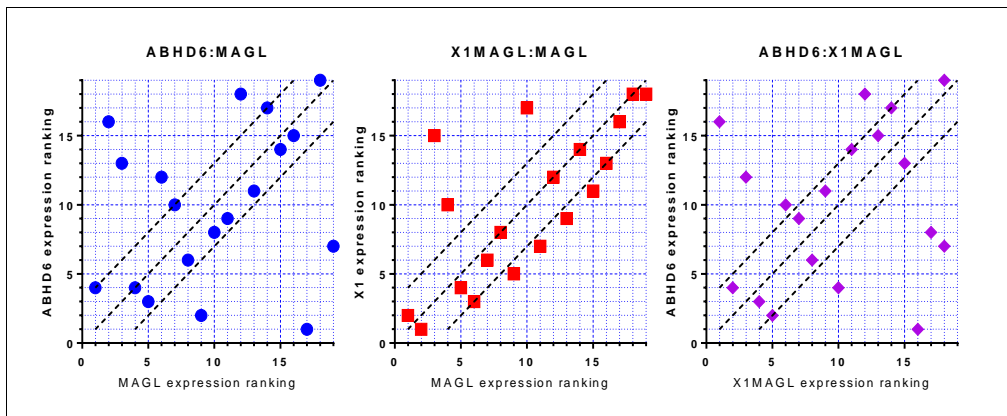


Figure 4.2 Comparison of the expression level of the three genes in rat tissues (visual correlation analysis).

Rank level of MAGL, X1MAGL and ABHD6 in 19 rat tissues were graphically compared. The middle dashed lines in each graph represents an arbitrary line of unity while the outer lines represent three rank units of the independent variable.

Generally, there was a level of independence between ABHD6 and the MAGLs while there was good correlation of the rank order of expression of mRNA encoding the two MAGLs (middle graph of Figure 4.2) except in kidney cortex & medulla and liver which showed MAGL ranked noticeably higher than the X1 variant (figure 4.2).

4.4.2 Immunostaining of human recombinant tagged MAGLs

Appropriate negative controls (native HEK293 and empty vector transfection; omitting primary and/or secondary antibodies) were identified to have no detectable background signal (Figure 4.3) using Zeiss SM880 confocal microscopy.

The results of human MAGL1 HA-tagged at both terminals are shown in Figures 4.4 and 4.5. The images revealed that the distribution of the C-tagged version was reasonably diffuse and occasionally punctate through the cytoplasm, without obvious association with either nuclear or plasma membranes. For the N-tagged version, the distribution is fairly similar, maybe with a more punctate appearance.

For MAGL2, the results for HA-tagging from both sides were shown in Figures 4.6 and 4.7. Notably, a weak fluorescent signal was detected with anti-HA staining in the red channel compared to that of MAGL1. MAGL2 appeared to be more associated with membranes, with a relatively minor cytoplasmic distribution.

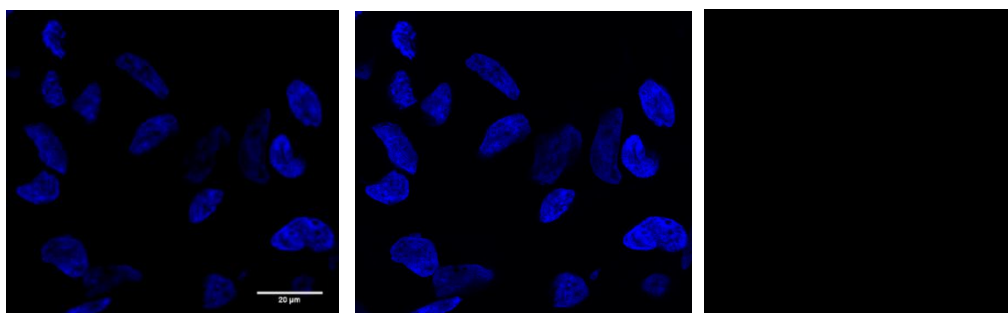


Figure 4.3 Representative images of native HEK293 cells as negative controls. Right image: Anti-HA (red). Middle: DAPI (blue). Left: Merge image. Scale bar = 20 μm .

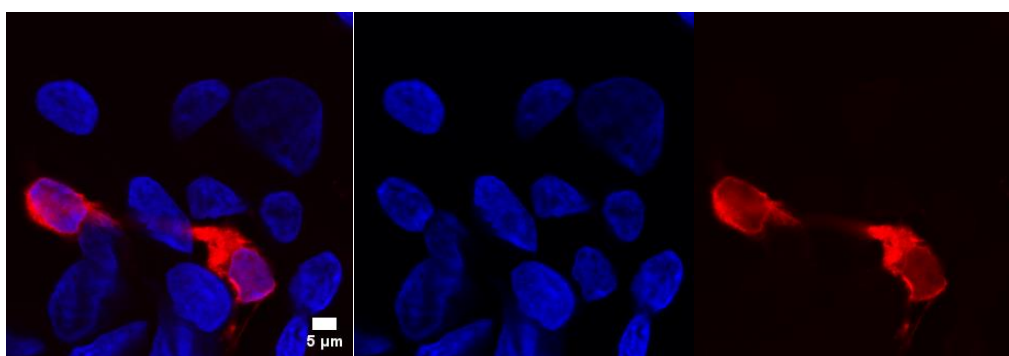


Figure 4.4 Subcellular localization of C-terminal HA-tagged MAGL1 expressed in HEK293 cells. Right image: Anti-HA (red). Middle: DAPI (blue). Left: Merge image. Scale bar = 5 μm .

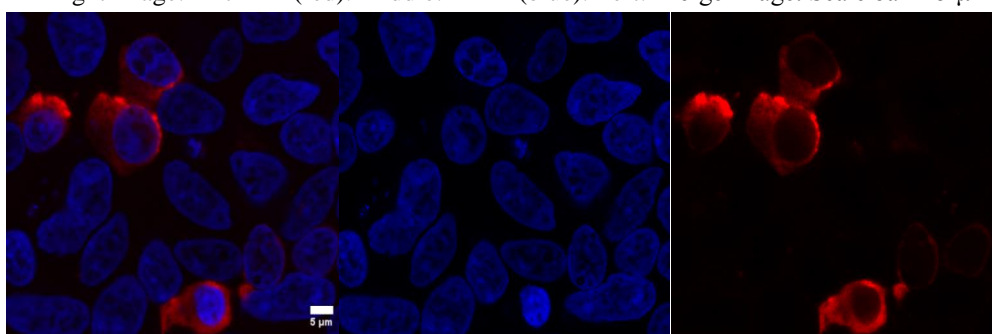


Figure 4.5 Subcellular localization of N-terminal HA-tagged MAGL1 expressed in HEK293 cells. Right image: Anti-HA (red). Middle: DAPI (blue). Left: Merge image. Scale bar = 5 μm .

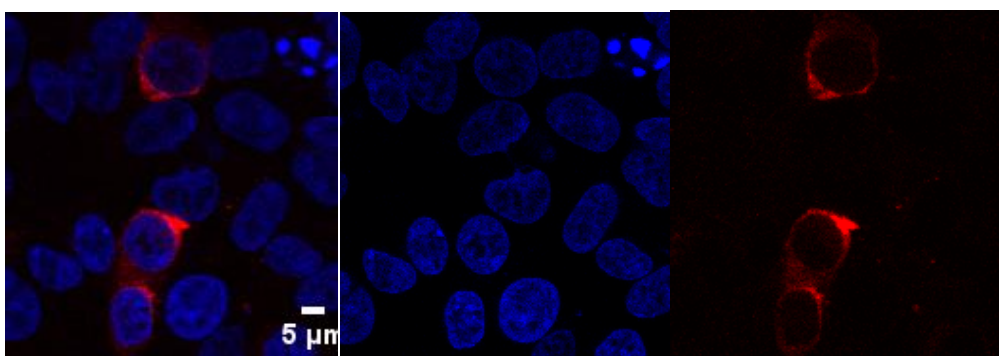


Figure 4.6 Subcellular localization of C-terminal HA-tagged MAGL2 expressed in HEK293 cells.
 Right image: Anti-HA (red). Middle: DAPI (blue). Left: Merge image. Scale bar = 5 μm .

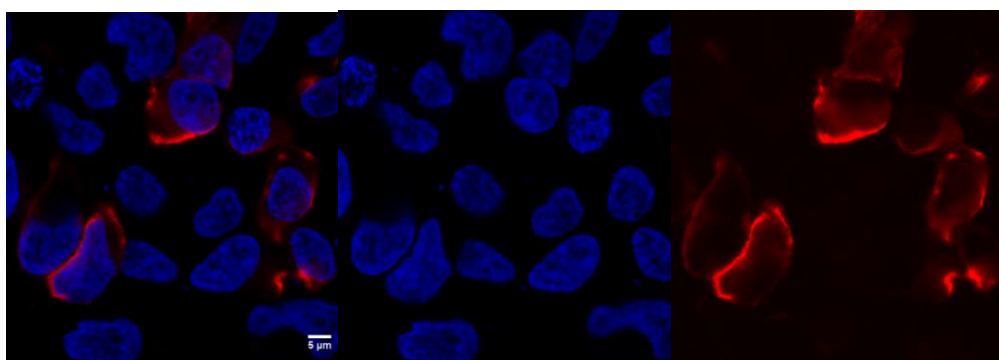


Figure 4.7 Subcellular localization of N-terminal HA-tagged MAGL2 overexpressed in HEK293 cells.
 Right image: Anti-HA (red). Middle: DAPI (blue). Left: Merge image. Scale bar = 5 μm .

In a parallel investigation, immunoblotting was carried out on these tagged transfects using two simple cellular fractions: cytosol and membranes (Figures 4.8 and 4.9). Native un-transfected HEK293 cells were used as a negative control and β -actin as a whole cell cytoskeleton marker according to the Abcam guide (Loading Control Guide). Both N- and C-terminal tags (with the same amount of protein was run for each sample) were detected for each gene (Figures 4.8 and 4.9). For MAGL1, the N-terminal tagged version appeared fainter than the C-terminal version, with a possible definition of a doublet for the C- but not N-terminal tag (Figure 4.8). Similarly for MAGL2, the C-terminal tagged version appeared to be more densely expressed (Figure 4.9), although both versions appeared to be present as a single band only.

Functional activity of these tagged enzymes was assessed by [³H]-2OG hydrolysis, in a pilot study, and the results are shown in Table 4.1. The transfected enzymes (MAGL1 and MAGL2), unexpectedly, produced high levels of activity (more than 15% of substrate was hydrolysed within the 30 min incubation period, indicating non-linear kinetics). However, both fractions were sensitive to 100 nM JJKK048, indicating primarily MAGL activity. Table 4.1 indicates that N- or C-terminal tagged versions of MAGLs were expressed to similar levels and displayed a similar, and evenly balanced, subcellular distribution.

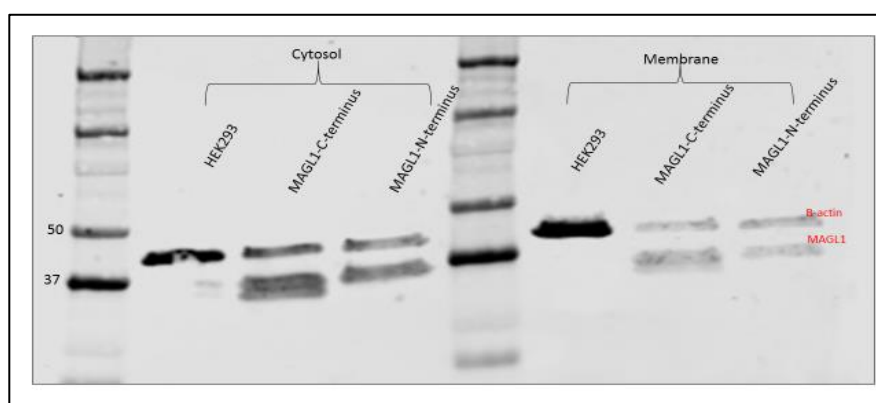


Figure 4.8 Representative immunoblot of HA-tag and β -actin in un-transfected and MAGL1-transfected HEK293 cells.

Data are from a single experiment, which are representative of two experiments with similar profiles.

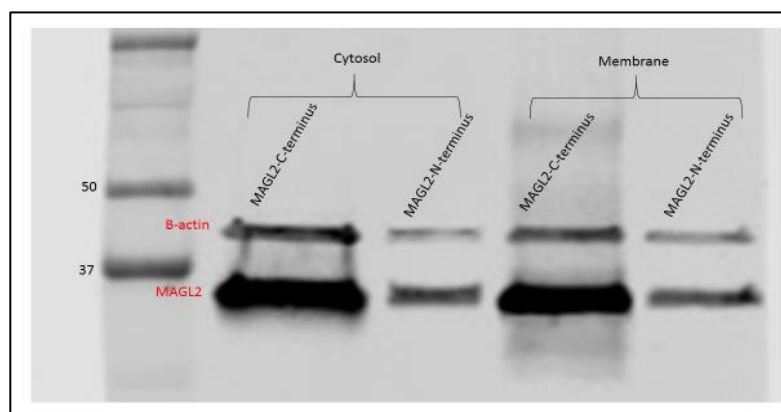


Figure 4.9 Representative immunoblot showing expression of tagged MAGL2 in two fractions, cytosol and membrane in transfected HEK293.

B-actin was used as a loading control.

Table 4.1 Hydrolytic activity in tagged MAGL1 and MAGL2 transfected HEK293 cells.

Data are mean % conversion of [³H]-2OG to glycerol from a single experiment performed in duplicate. Raw data were multiplied by the sample volume (adjusting for recovery) and divided by the total radioactivity present to calculate the amount of glycerol produced from 2OG.

	MAGL1	Control	JJKK048 (100 nM)	MAGL2	Control	JJKK048 (100 nM)
C-tag	cytosol	60.2%	2.7 %	cytosol	61.4%	2.4%
	membrane	58.7 %	3.8 %	membrane	61.3%	2.6%
N-tag	cytosol	53.7 %	1.6%	cytosol	46.6%	0.5%
	membrane	54.1%	2%	membrane	51.4%	1.8%

4.4.3 Immunostaining of human recombinant tagged ABHD6

Immunostaining was applied as a further step toward investigating ABHD6 subcellular distribution beyond the two fractions (cytoplasmic and membrane), Making use of an anti-lamin β 1 antibody as a nuclear envelope marker. Figure 4.10 represent an empty vector transfected HEK293 cells immunostaining as a control.

C- and N-terminal HA-tagged clones of ABHD6 were expressed in HEK293 cells (Figures 4.11 and 4.12). Using the anti-lamin β 1 antibody, there was good overlap of immunostaining with the DAPI stain (Figure 4.11B and 4.11C; Figure 4.12B and 4.12C). Assessing the distribution of the C- and N-tagged versions of ABHD6, immunostaining was evident on or in close proximity to the nuclear membrane identified by the anti-lamin β 1 antibody. In addition, immunoreactivity was also evident extending into the cytoplasm, possibly involving the plasma membrane.

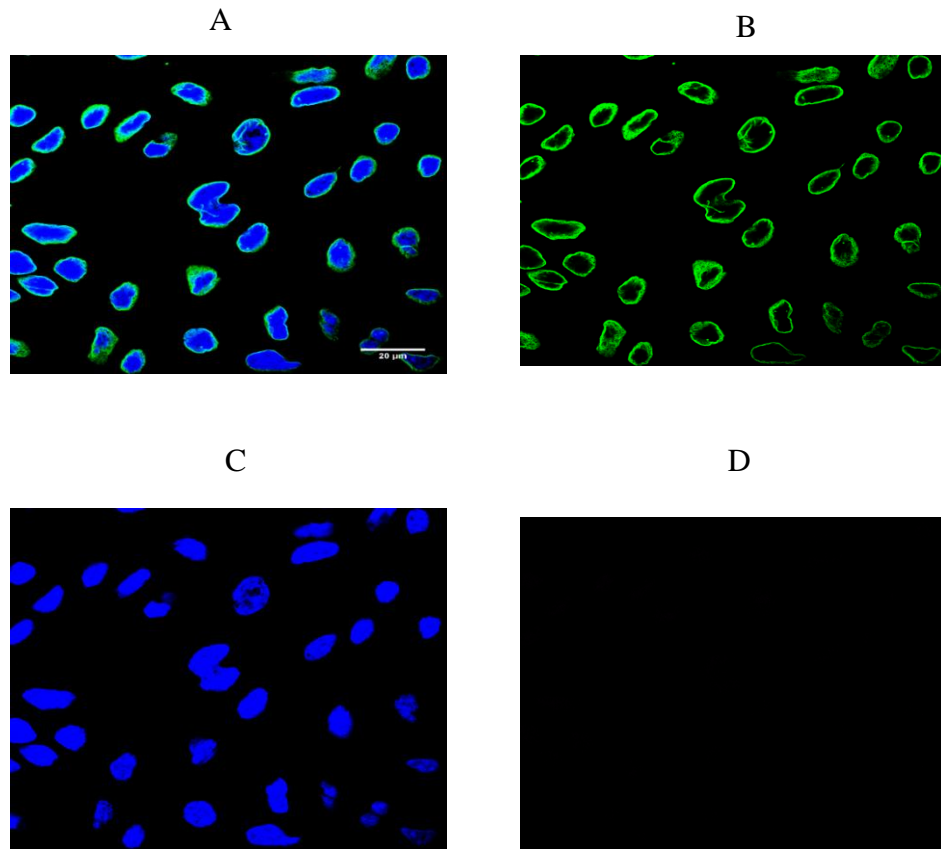


Figure 4.10 Representative immunostaining of empty vector transfected HEK293 cells. A- Merge image. B-Anti-Lamin B1 antibody as nuclear membrane marker (green). C-DAPI (blue) and D- Anti-HA antibody. Scale bar = 20 μ m.

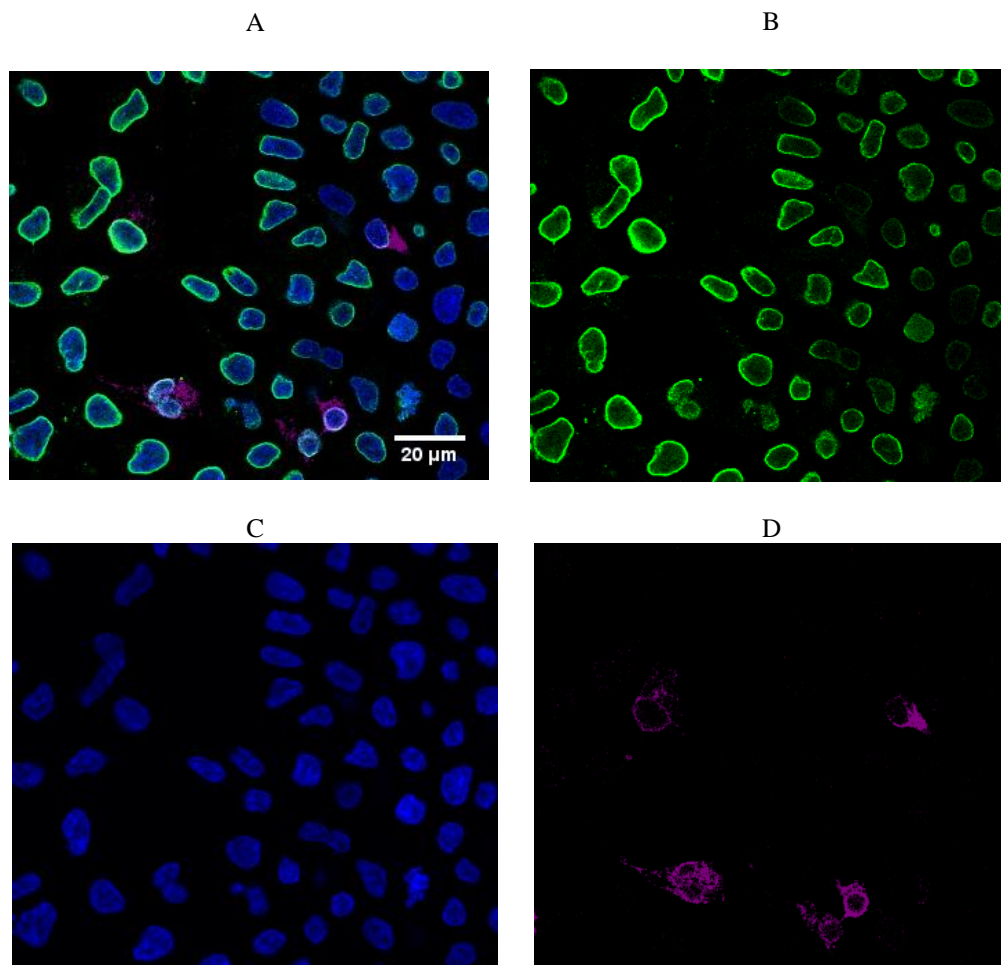


Figure 4.11 Localization of C-terminus HA-tag protein in transfected HEK293 cells. A-Merge. B- Anti-Lamin β 1 antibody as nuclear membrane marker (green). C-DAPI (blue) and D- Anti-HA antibody (magenta). Scale bar = 20 μ m.

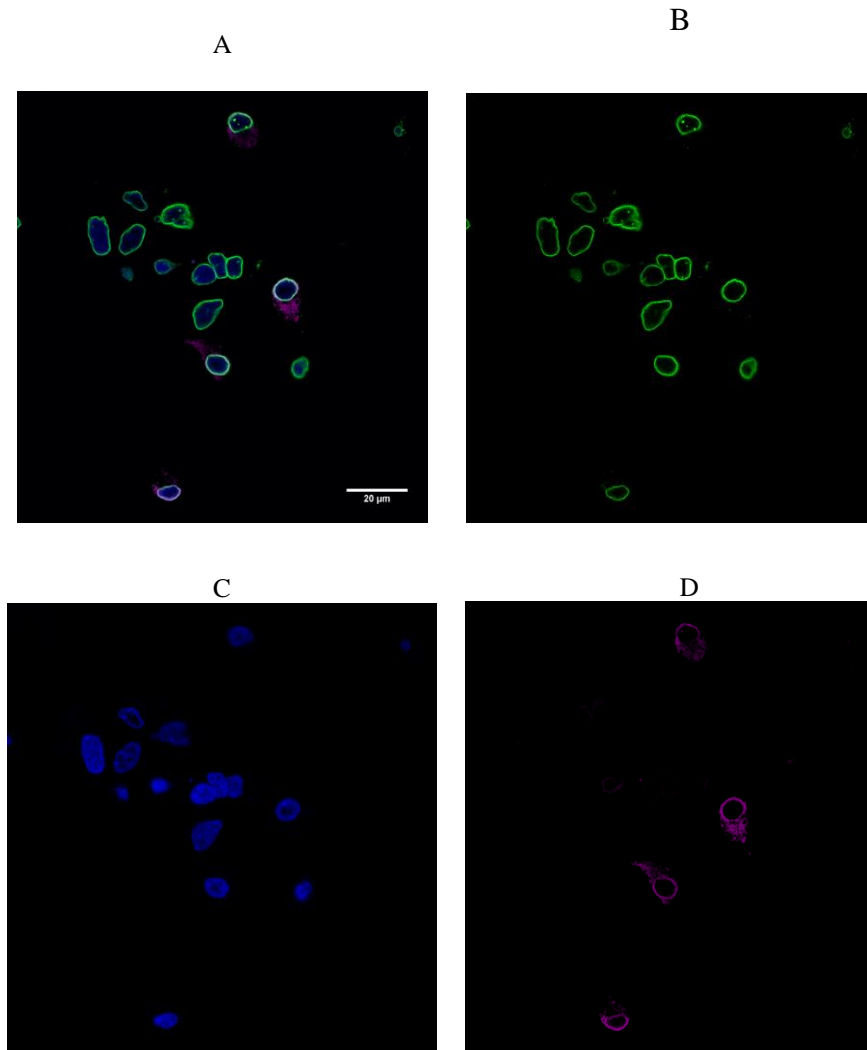


Figure 4.12 Localization of N-terminus HA-tag protein in transfected HEK293 cells. A-Merge. B- Anti-Lamin β 1 antibody as nuclear marker (green). C-DAPI (blue) and D- Anti-HA antibody (magenta). Scale bar = 20 μ m.

Because HEK293 cells have large nuclei relative to the cell size, it is often difficult to discriminate between nuclear and plasma membranes. Imaging was, therefore, repeated with differential interference contrast (DIC) microscopy (Figures 4.13 and 4.14). Using this technique, an association of a proportion of C-terminus HA-tagged ABHD6 immunoreactivity with the plasma membrane was evident (Figure 4.13). This was not so obvious with N-terminal HA-tagged ABHD (Figure 4.14).

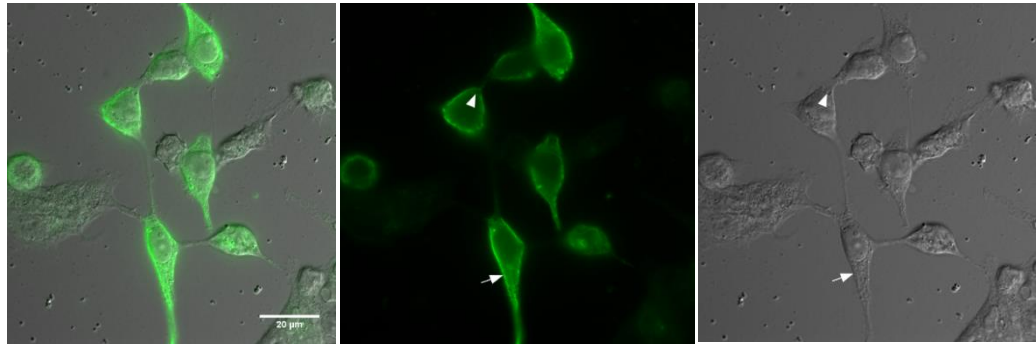


Figure 4.13 Microscopy of C-terminus HA-ABHD6 in HEK293 cells. Arrows indicate plasma membranes. Scale bar=20 μm . Right side image: Differential interference contrast, middle image: fluorescence and left side image: merge.

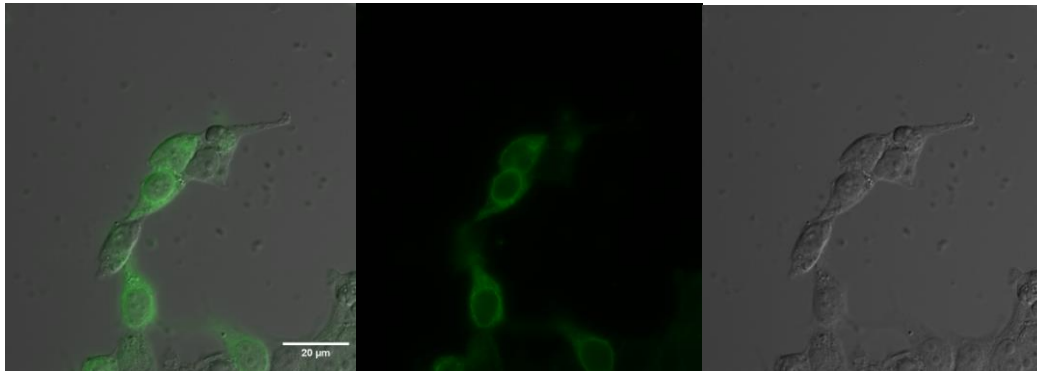


Figure 4.14 Microscopy of N-terminus HA-ABHD6 in HEK293 cells. Arrows indicate plasma membranes. Scale bar=20 μm . Right side image: Differential interference contrast, middle image: fluorescence and left side image: merge.

Alpha-tubulin, a cytoplasmic marker (Planès *et al.*, 2016) was used as a loading control for immunoblotting of the two tagged versions of ABHD6 (Figure 4.15). α -Tubulin was apparent in cytoplasmic fractions from empty vector and N- and C-terminus tagged ABHD6-expressing cells (Figure 4.15). Immunoreactivity in the membrane fractions from the same cells was absent. Both cytosolic and membrane fractions of the ABHD6-transfected cells showed immunoreactivity for HA-tags in both N- and C-terminals.

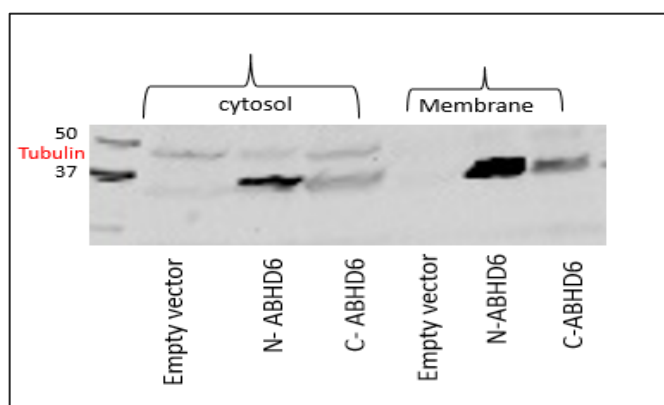


Figure 4.15 Immunoblotting of cytosolic and membrane fractions of HEK293 cells transfected with empty vector or N- or C-terminal HA-tagged ABHD6. α -tubulin was used as a loading control.

To check whether tagged versions of ABHD6 retained functional activity, cell fractions were assessed in the radiometric enzyme assay (Table 4.2). In general, 1 μ M WWL70 evoked an incomplete inhibition of 2OG hydrolysis in all fractions of the transfected cells. N-terminal tagged ABHD6 appeared more highly expressed than C-terminally tagged versions, with a predominant association with the membrane, rather than cytosolic fraction.

Table 4.2 Hydrolytic activity in tagged ABHD6 transfected HEK293. Data are % conversion of [3 H]-2OG to glycerol. Representative data are from a single experiment performed in duplicate, representative of three experiments.

	ABHD6	Control	WWL123 (1 μ M)
C-tag	Cytosol	1.8%	1.3%
	Membrane	8.6%	2.5%
N-tag	Cytosol	6.5%	1.9%
	Membrane	16.3%	4.4%

4.4.4 Nuclear distribution of MAGL and ABHD6

As the N-terminal HA-tagged version of ABHD6 showed the greatest hydrolase activities and there was no obvious difference between tagging MAGLs, the C-terminal HA tagged version of MAGLs were chosen for further experiments to investigate the potential nuclear localisation of these enzymes and mitochondrial activity of ABHD6 -Table 4.3.

In un-transfected HEK293 cells, 2OG hydrolysis was evident in the nucleus and was almost completely inhibited in the presence of MAFP. The activity was partly sensitive to WWL123, but was unaltered in the presence of JKKK048 (Table 4.3). This suggests the potential endogenous expression of ABHD6 in these cells.

In HEK293 cells transfected with ABHD6, there was a modest increase in nuclear 2OG hydrolysis. Activity was substantially inhibited in the presence of either JKKK048 or WWL123. This suggests a modest localization of ABHD6 to the nuclear fraction.

In HEK293 cells transfected with MAGL1 and MAGL2, there was a large increase in nuclear 2OG hydrolysis, which was unaffected by WWL123, but was almost completely inhibited in the presence of JKKK048. This suggests that MAGL1 and MAGL2 can be expressed in the nuclear fraction, at least under conditions of overexpression.

In native HEK293 cells, 2OG hydrolysis in the mitochondrial fraction was low and was only modestly inhibited in the presence of WWL123 (Table 4.3) while 2OG hydrolysis in the mitochondrial fraction was elevated following ABHD6 transfection, but was only partly sensitive to WWL70. This suggests that increased expression of ABHD6 is associated with increased activity in the mitochondrial fraction.

Table 4.3 Hydrolytic activity in nuclear fractions of native HEK, MAGL1, MAGL2 and ABHD6 transfects in response to three inhibitors and mitochondrial fraction in native HEK and ABHD6 transfects in response to WWL123.

Data are mean % conversion of [³H]-2OG to glycerol from a single experiment performed in duplicate.

		Control	MAFP (1 μM)	JJKB048 (100 nM)	WWL123 (1 μM)
Nuclear fraction	Native HEK 293	4.8%	0.7%	4.2%	3.2%
	ABHD6	9.6 %	0.4 %	7%	4.7%
	MAGL1	63.6 %	1%	1.9%	62.5
	MAGL2	59.8%	0.9%	2.8%	56.5%
Mitochondria	Native HEK293	2.3%	-	-	1.5%
	ABHD6	11.2%	-	-	5.6%

Subcellular fractionation to isolate nuclei and plasma membranes was assessed using antibodies directed against lamin β1 (a nuclear envelope marker) and Na⁺/K⁺-ATPase (as a plasma membrane marker) (Figures 4.16). In the plasma membrane fraction, both native and N-terminal HA-tagged ABHD6-transfected cells showed immunoreactivity for Na⁺/K⁺-ATPase (100 kDa, Figure 4.16), while the same samples exhibited immunoreactivity for lamin β1 in the nuclear fraction (66 kDa, Figure 4.16). Both plasma membrane and nuclear fractions from ABHD6-transfected, but not native, HEK293 cells showed immunoreactivity for HA (Figure 4.16).

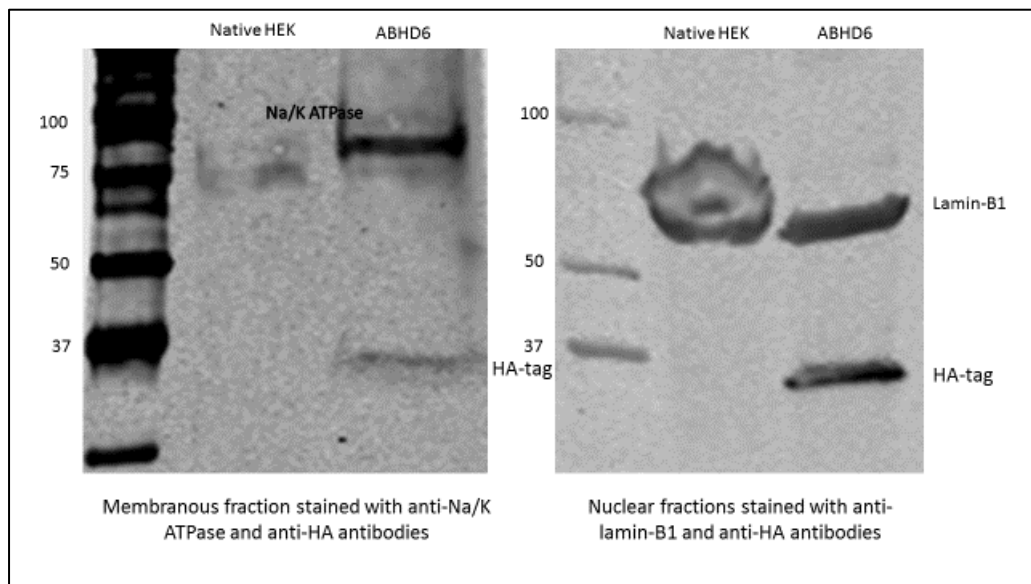


Figure 4.16 Western blot of nuclear and plasma membrane fractions of HA-ABHD6 transfects and native HEK293.

Samples were probed for Na⁺/K⁺-ATPase, lamin β 1 and HA, as indicated.

To confirm the ability of the cell fractionation methodology to differentiate plasma membrane and nuclear fractions, blots were stripped (Figure 4.17) and then re-probed with the contrary antibody (i.e. plasma membrane fractions were probed with anti-lamin β 1 antibodies). Re-probing (Figure 4.18) showed that there was minor contamination between plasma and nuclear membranes in ABHD6 transfects and native cells. To further clarify this point with more focus on the plasma membrane marker, another experiment was done. Two blots of nuclear fraction only of ABHD6 transfects and control (Figure 4.19) were probed with the two markers and the results showed that there was clear labelling of nuclear fractions with plasma membrane marker, indicating either impurity of the nuclear membrane with plasma membrane or low specificity of the primary marker antibody. In another trial with nuclear and membrane extracts of HA-MAGL1, similar results for Na/K ATPase marker were obtained as it was evident in both fractions, while Lamin-B1 appeared only in the nuclear fraction of HA-MAGL1 and native control (Figure 4.20).

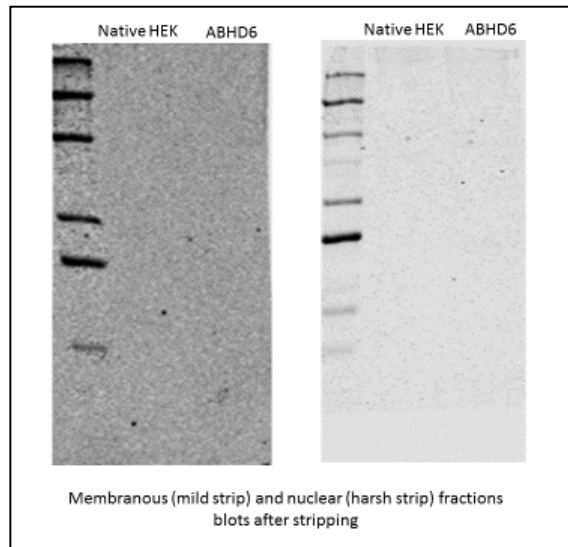


Figure 4.17 Stripping of nuclear and membranous blots of HA-ABHD6 transfects and native HEK293. Mild stripping was required for the membranous blot while harsh treatment was needed for the nuclear blot to remove primary and secondary antibodies.

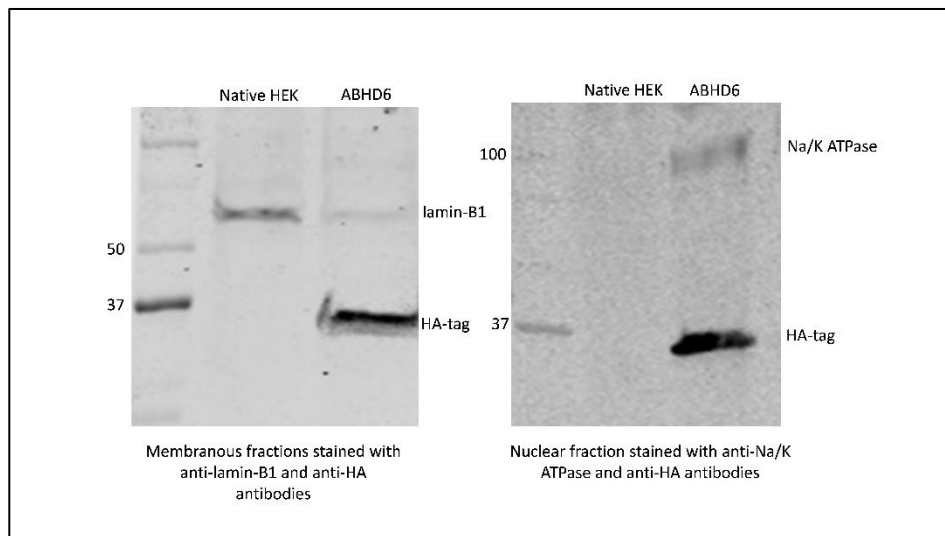


Figure 4.18 Re-probing of above stripping blots. Using nuclear marker antibody for membranous fraction of HA-ABHD6 and native control cells and plasma membrane antibody for nuclear fraction of ABHD6 and Native control cells.

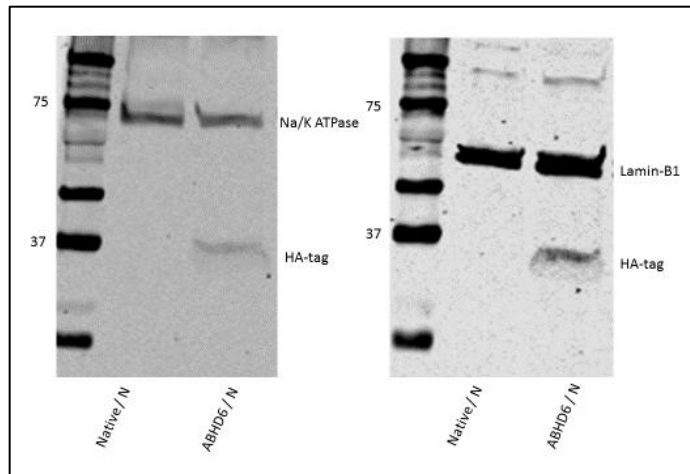


Figure 4.19 Western blot of nuclear fraction of HA-ABHD6 transfects and native HEK with the two membrane markers.
N=nuclear fraction.

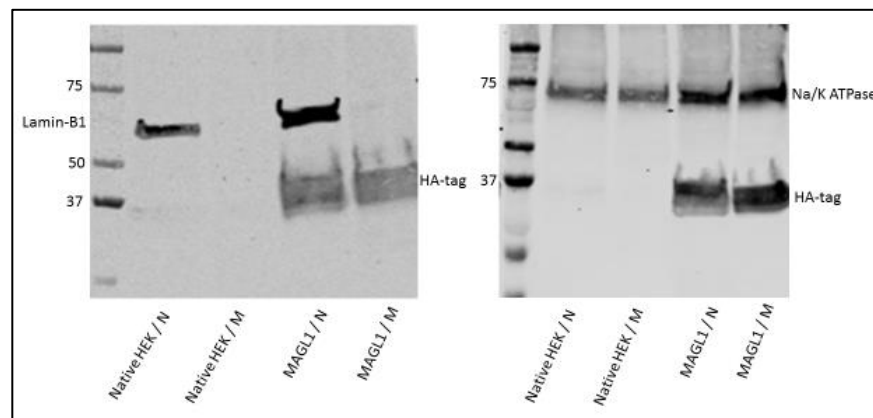


Figure 4.20 Western blot of nuclear and membranous fractions of HA-MAGL1 probed with the two membranous marker antibodies.
N=nuclear fraction and M=membrane fraction.

4.4.5 Subcellular localization of ABHD6 in neurons and astrocytes

The experiments described in this Section were conducted with the kind assistance of Dr. Alex Tarr, and Monika Owen.

Control (un-infected) mice cortical neurones were stained with DAPI and anti-lamin β 1 to visualize nuclei and nuclear membranes, respectively (Figure 4.21). Lamin β 1 was detected across the nuclei, while DAPI staining was more punctate, presumably picking out nucleoli. Viral infection of GFP in these neurones was used to illustrate successful application of the technique (Figure 4.22). GFP, although not expressed in every cell in the field of view, appeared to be present

throughout the cell body and extended through the cytoplasm into axons. Viral infection of N-terminus HA-tagged ABHD6 appeared to show immunoreactivity present in the cytoplasm of cerebral cortical neurones, extending into the axons, with some concentration around or on the nuclear membrane (Figure 4.23).

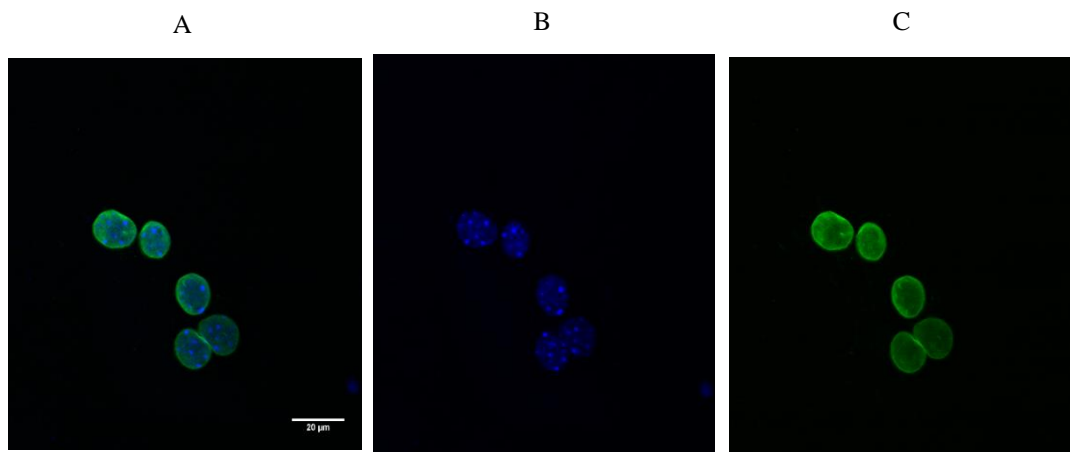


Figure 4.21 Representative image of mice neonatal cortical neurones. Neurones stained with DAPI (blue) (B) and anti-lamin β 1 (green) (C); merge image (A). Scale bar=20 μ m.

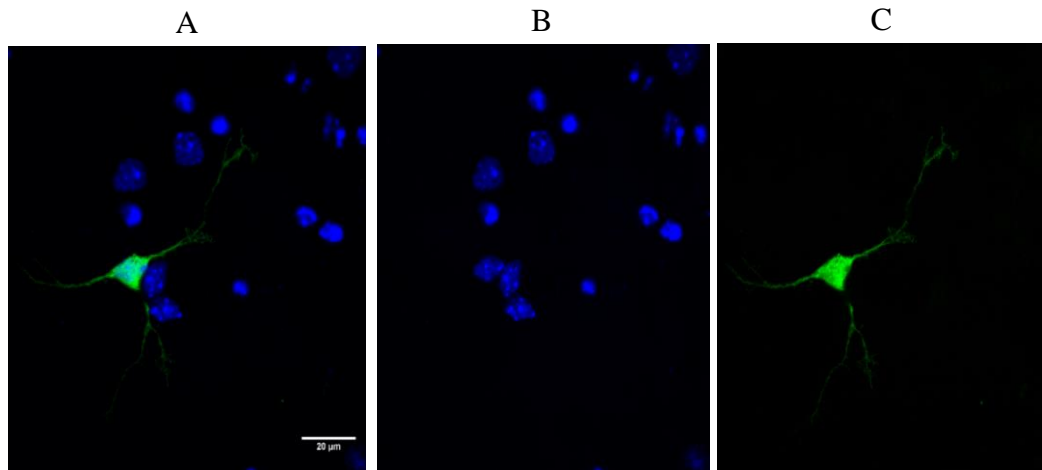


Figure 4.22 Viral expression of GFP in mice neonatal cortical neurones. A-Merge. B- DAPI (blue) and C- GFP (green). Scale bar = 20 μ m.

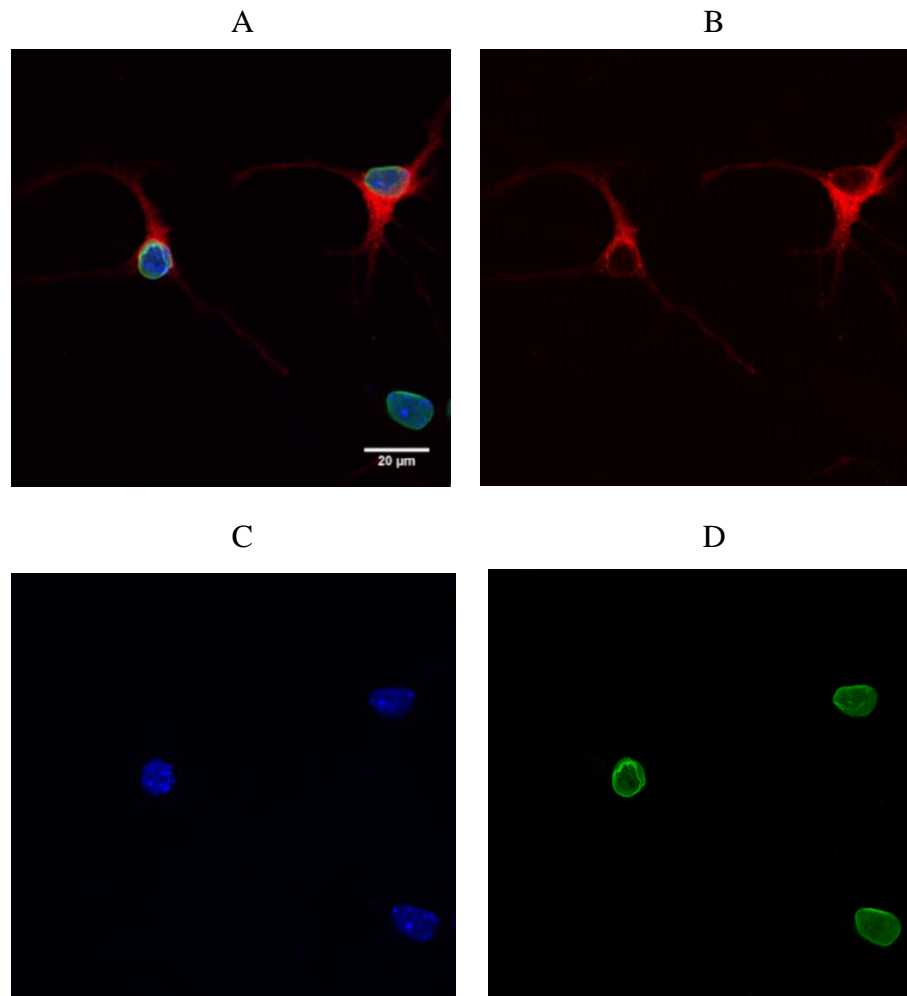


Figure 4.23 Localization of virally expressed N-terminus HA-tagged ABHD6 in mice neonatal cortical neurones.

A-Merge. B- HA (red). C- DAPI (blue) and D lamin β1 (green). Scale bar = 20 μm.

Viral transfection of astrocytes with GFP was also conducted (Figure 4.24) as a control. GFP was expressed throughout the cytosol in astrocytes, at times with a striped appearance. Viral infection with ABHD6 allowed identification of cytosolic expression with some concentration on or close to the nuclear membrane (Figure 4.25).

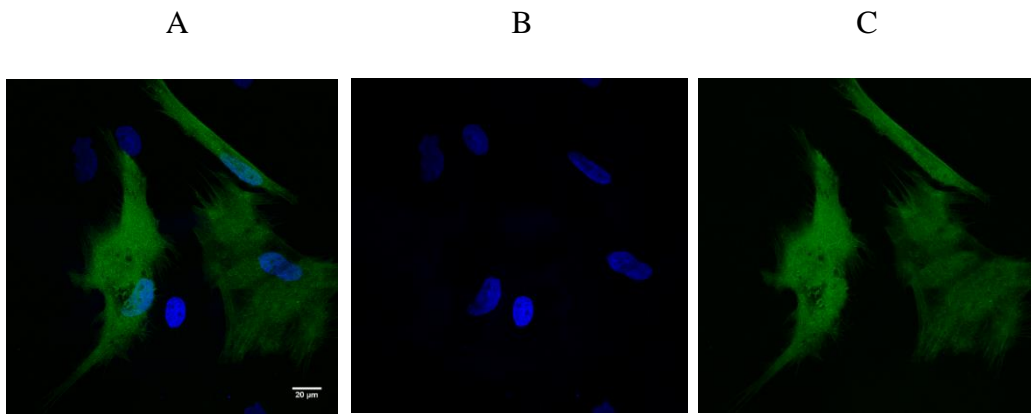


Figure 4.24 Viral expression of GFP in rat neonatal cortical astrocytes. A-Merge. B- DAPI (blue) and C- GFP (green). Scale bar = 20 μ m.

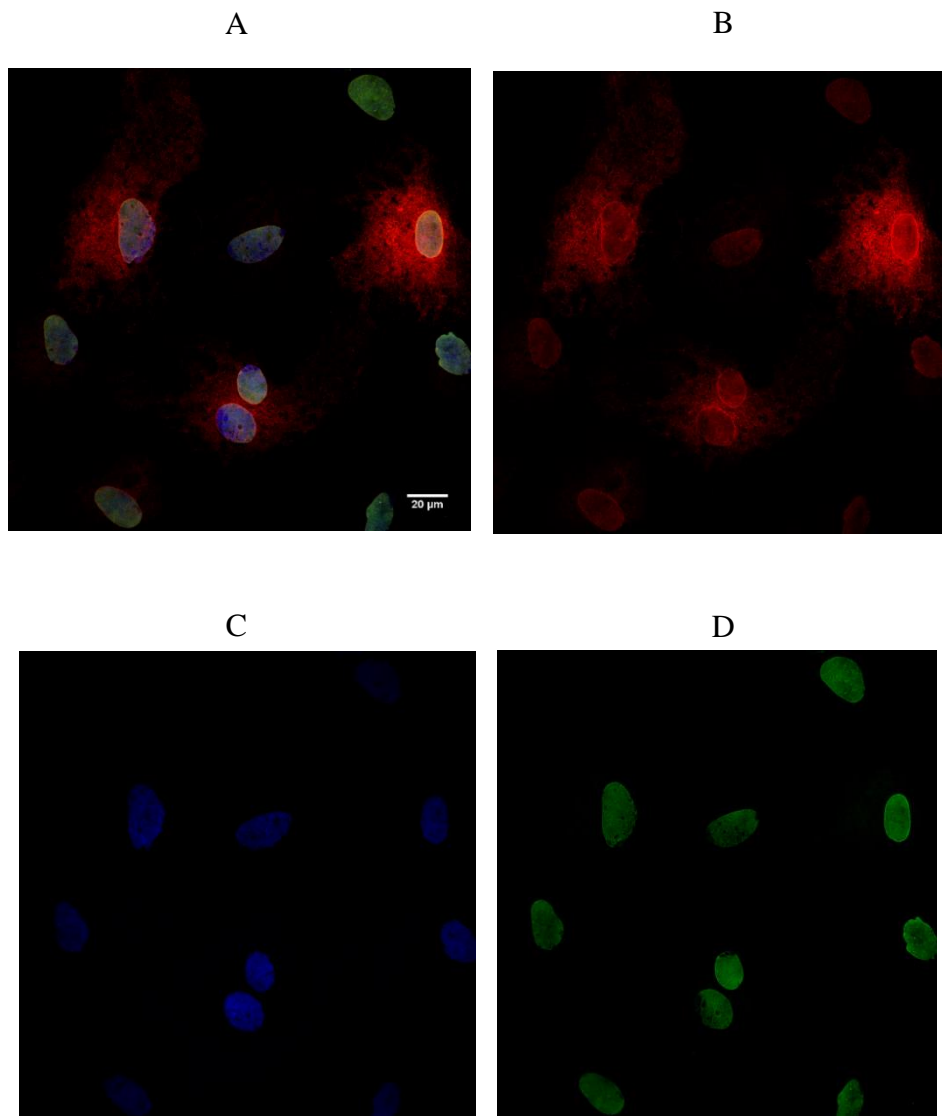


Figure 4.25 Viral expression of N-terminus HA-tagged ABHD6 in rat neonatal cortical astrocytes. A-Merge. B- HA (red). C- DAPI (blue) and D- Lamin β 1 (green). Scale bar = 20 μ m.

4.5 Discussion

This part of the project focussed on attempting to determine cellular and subcellular locations of MAGL and ABHD6 in rat tissues and in heterologous expression.

4.5.1 Exploring mRNA in rat tissues

One of the aims of the investigations in this Chapter was to compare the genetic expression of MAGL splice variants and ABHD6 in 19 different rat tissues. Normalization of gene expression was conducted to the geometric mean of the three reference genes (β -actin, TBP and GAPDH) as the use of two or three house-keeping genes should reduce the influence of experimental conditions (Bookout *et al.*, 2003; Bustin, 2002).

A pilot investigation of MAGL and ABHD6 gene expression was conducted in tissue extracts from a single male rat (Figure 4.1). Although these data are limited in terms of not reflecting variation between different animals, or indeed different sexes, ages, nutritional or disease states, the data confirmed the previously reported information about the widespread distribution of MAGL and ABHD6 (Chon *et al.*, 2007; Dinh *et al.*, 2002a; Karlsson *et al.*, 1997; Tsou *et al.*, 1998). Analysis of individual rank orders of expression of the three genes indicated they were all relatively abundant in adipose tissue followed by cerebral cortex, which prompts questions about the potential role of ABHD6 in adipose tissue. Indeed elevation of both ABHD6 and MAGL mRNA has been observed in response to a high fat diet (Thomas *et al.*, 2013; Viader *et al.*, 2016).

Figure 4.2 compared the ranking of expression levels of the three enzymes on a visual scale. Where the ranking is identical or close-to-identical, points lie on or close to the line of unity. The good correlation between MAGL and X1MAGL (as many tissues lie on or close to the line of unity) is indicative of some relationship between expressions of the two splice variants. The plots for ABHD6 compared to either MAGL or X1MAGL were not so well aligned, implying these gene products are more independent of one another. Further analysis indicated that small and large intestines were the highest ranking for ABHD6 relative to the

MAGL isoforms. This reinforced the need for attention on these tissues for investigating ABHD6 enzymatic activity, as in the previous Chapter.

One study with similar results to this pilot found that there were relatively high levels of MAGL expression in testis, kidney and white adipose tissue in comparison to ABHD6 (Zhao *et al.*, 2014). MAGL expression was also high in heart and (presumably skeletal) muscle. The expression of ABHD6 was higher than MAGL in brain and liver. Very low levels of MAGL and low ABHD12 expression in pancreatic islets and INS832/13 cells (β - cells model) was observed compared to that of ABHD6. In that study, ABHD6 was suggested to control MAG signalling for insulin secretion as its inhibition enhanced glucose accumulation and insulin secretion (Zhao *et al.*, 2014). Similarly high ABHD6 expression was found in mouse liver and small intestine (Thomas *et al.*, 2013).

Only one human study of ABHD6 gene expression (using multiple tissue cDNA panels) appears in the literature, with confirmation of its wide distribution in different tissues (Li *et al.*, 2009). ABHD6 was relatively high in liver, kidney, ovary and small intestine. It was also screened in some human tumour cell lines; it appeared extremely elevated in U2OS (bone osteosarcoma), PC-3 (prostate cancer), and Jurkat (T-lymphocyte leukaemia) cells with no detection in Hela (cervical adenocarcinoma) and U251 (human glioblastoma) cells.

To summarize, the data reported in this study were in line with previous published work for MAGL and ABHD6 gene expressions. This is the first study to investigate expression of the X1 variant of MAGL. The significance of high mRNA levels of a particular gene in particular tissues can be used to focus on a potential role of that protein there, for example, for MAGL in adipose tissue and testes and ABHD6 in intestines and pancreatic secretion.

4.5.2 Subcellular localization of human MAGL1, MAGL2 and ABHD6 in transfected cells and primary cell culture

The presence of two isoforms of MAGLs underlines the importance of cellular and subcellular localization studies and raises the possibility of tissue-selective targeting of the two isoforms in the future. There are a limited number of studies

on the subcellular distribution of MAGL and ABHD6, however, this is the first to study the subcellular distribution of MAGL2.

Two tagged versions of both MAGL variants and ABHD6 were visualized in immunoblots and shown to be functionally active in the radiometric assay, indicating that tagging did not affect enzyme activities. MAGL1 and MAGL2 were shown to have a similar high level of activity and were inhibited in both fractions by 100 nM JJKK048, while ABHD6 transfects were inhibited by 1 μ M WWL70 (Table 4.1 and 4.2).

MAGL1 staining in transfected HEK293 cells showed that this protein appeared widely across the cell fractions (Figure 4.4 and 4.5). Nuclear extraction also demonstrated the presence of MAGL1 activity and immunoreactivity. This cytoplasmic and membrane distributions were in line with previous studies (Blankman *et al.*, 2007; Dinh *et al.*, 2002a; Dinh *et al.*, 2004; Saario *et al.*, 2005; Woodhams *et al.*, 2012) while the nuclear and microsomal existence were also reported, but only once (Sakurada *et al.*, 1981). MAGL2 (Figure 4.6 and 4.7) seemed to be more associated with membranes, consistent with observations from Chapter 3 using the radiometric enzyme assay. In another study, the rat MAGL was tagged with V5 (14 amino acids) and the construct transiently introduced into HEK293 cells. The images showed MAGL was distributed all over the cells (Straiker *et al.*, 2009), while HA-tagged mouse ABHD6 was found as cytoplasmic and peri-nuclear locations in transfects. This study failed to make clear to which terminal the tag was applied. Interestingly, Straiker et al cultured hippocampal preparations, principally neurons, and found ABHD6 within some populations of astrocytes, juxtaposed to synapses and co-localized with some dendritic spines. COS-7 cells overexpressed with C-terminus tagged ABHD6-ECFP (fluorescent protein tag) showed a perinuclear concentration of ABHD6, and also in the endoplasmic reticulum (Pribasnig *et al.*, 2015). In the same study, ABHD6 was found to co-localize with late endosomes/lysosomes within the cell, which are organelles responsible for lipid sorting.

In this Chapter, ABHD6 protein showed an interesting distribution with different tags. While the C-terminus tagged-version appeared to be distributed around the

plasma membrane, the N-terminus-tagged version appeared to be expressed around the nucleus. Both versions showed cytoplasmic distribution. This was very clear in difference interference contrast images (Figures 4.13 and 4.14). A transmembrane domain within the ABHD6 sequence has been described near the N-terminus (Hsu *et al.*, 2010; Lord *et al.*, 2013). In a recent study, with the intention to study different mutations of ABHD6 in transfected HEK293T cells, ABHD6 was tagged to Myc (polypeptide protein tag of 10 amino acids) at both terminals. The results showed that when N-tagged myc-ABHD6 was stained, the distribution appeared to be in the plasma membrane mainly and in the cytoplasm. While in C-tagged ABH6-myc, the protein appeared located more around the nuclear membrane and cytoplasm (Wei *et al.*, 2016). Thus, consistent with this present study, the enzyme appeared to locate in different positions in the cell dependent on the different location of the tag, at least with recombinant system.

The detection of MAGL and ABHD6 proteins in the soluble and membrane fractions observed in this Chapter were in line with radiometric results generated in Chapter 3. For example: MAGL1, in comparison to MAGL2, expressed stronger fluorescent signals in ICC which might parallel the higher total 2OG activity detected in the previous Chapter. Similarly, the greater proportion of MAGL2 associated with membranes in ICC, in comparison to its cytosolic partition, might reflect the higher total 2OG hydrolysis detected in MAGL2 transfected HEK293 membranes than its soluble fraction. Another example: ABHD6 evident in the soluble fraction of these host cells (in ICC) were consistent with the -relatively low-activity detected in the soluble fraction of ABHD6-HEK293 transfects (in radiometric assay).

It is not uncommon when trying to blot or stain a sample, to encounter problems with non-specific binding and/or antibody selectivity, particularly with polyclonal antibodies. In this study, many attempts to detect ABHD6 immunoreactivity using commercially available antibodies (with many different optimization trials) ended with multiple non-specific binding and no obvious immunoreactivity for ABHD6. Previous studies have made use of locally-generated antibodies (Marrs *et al.*, 2010; Pribasnig *et al.*, 2015; Straiker *et al.*,

2009; Thomas *et al.*, 2013). The authors of the study were approached but had no stocks available for further investigations. Recently, Wei *et al.* were successful in using a commercial ABHD6 antibody (Abcam, 87532) (Wei *et al.*, 2016), although it was no longer available on the website. To overcome this issue, a HA-tag was cloned and attached to MAGL and ABHD6. Because tagging might cause changes into the protein, tagging was conducted at both termini and assessed by different methods.

Na⁺/K⁺-ATPase, an integral membrane protein, was chosen in this study as it has long been a marker for plasma membranes (Holtbäck *et al.*, 1999; Meier PJ *et al.*, 1984; Pohl *et al.*, 2005; Van Dyke, 2004) and can be detected with a monoclonal specific antibody (Abcam, EP1845Y). However, Na⁺/K⁺-ATPase was also found to be present and functionally active in the nuclear envelope of HEK293 cells (Galva *et al.*, 2012). This observation may explain the extensive appearance of this marker in the nuclear fractions in Figures 4.19 and 4.20, which suggest that it was not an appropriate marker to distinguish between nuclear and plasma membranes. This was not the case for lamin β1 and α-tubulin, which might indicate a greater specificity of these markers for nuclear membrane and cytosol labelling, respectively, thus highly referred to the presence of ABHD6 in the nuclear membrane and cytosol of the selected cells as shown in Figures in this Chapter.

4.5.3 Focus on primary cell culture and viral infection

One of the limitations in this Chapter was the use of cultured cells from different species. Immunostaining was conducted on neonatal cortical astrocytes from rat and neonatal cortical neuronal primary cells from mice, as these were available locally in Nottingham. Mouse ABHD6 shares high sequence identity with human (94%) and rat (97%) orthologues (Thomas *et al.*, 2013), indicating a high degree of overlap across the species. ABHD6 localization in neurons and astrocytes appeared to be distinct. In neuronal cells, it appeared more a cytoplasmic than a membrane-associated protein, while in astrocytes, it appeared associated more with the nuclear membrane with a minor cytoplasmic expression.

This distribution of ABHD6 in primary cells (using N-tag) was not the same when the same tag was introduced in HEK293 cells. The use of immortalized/un-specialized cell lines are often standard in biological experiments for many reasons, for example, ready availability, low manipulation time, unlimited expansion capacity and a step toward minimized animal experimentation (Pan *et al.*, 2009b). However, cell lines may miss tissue-specific properties and be subject to genetic drift quite different from cells *in vivo* (Pan *et al.*, 2009b). In contrast, primary cell culture retains greater *in vivo* tissue genetic makeup and function, thus, more closely mimics the physiology of cells *in vivo* (Primary Cell Culture online). This might explain the discrepancy of tagged ABHD6 in HEK293 cells from primary cell culture. Particularly and in support of such a notion, a similar pattern of expression (membrane and nuclear) was reported with myc-ABHD6 and ABHD6-myc, respectively, in HEK293 cells (Wei *et al.*, 2016).

Introducing the genes of interest into primary cells was possible by conducting the powerful and efficient tool of viral infection (Hwang *et al.*, 1984). To take advantage of this ABHD6- virus, it could be possible, in the future, to study ABHD6 cellular and subcellular localization in real tissues, *in vivo*. According to our data in Chapter 3, intestine may be the best tissue to be explored first. As this ABHD6-virus was cloned with HA- tags, it could also be possible to visualize its distribution in live cells taking advantage of a highly selective monoclonal anti-HA antibody and the power of confocal microscopy. However, it should be kept in mind that there is a risk of photo-toxicity (interaction between a fluorescent dye and excitation light) caused by this type of microscopy (Dobrucki *et al.*, 2007).

4.5.4 Implication of ABHD6 distribution

Although more research is needed, it is interesting to note here that ABHD6 (specifically, the soluble fraction) seemed to be complemented by ECB receptors: CB₁ and CB₂, intracellularly (see below), which might give clue about how all of these components could control level of ECBs (in this case 2-AG) away from its lipid environment (plasma membrane). It is well-known that a large proportion

of CB₁ -and to less extent CB₂ -receptors in brain cells were primarily positioned as pre-synaptic (plasma membrane associated) to inhibit neurotransmission often through inhibition of voltage gated calcium channels, although post-synaptic expression (Atwood *et al.*, 2012; Lovinger, 2008) was also well described in literature (Busquets-Garcia *et al.*, 2017). Surprisingly, CB₁ (Delgado-Peraza *et al.*, 2016; Freund *et al.*, 2003; Thibault *et al.*, 2013) and CB₂ (den Boon *et al.*, 2012) receptors were both found intracellularly. In addition, mitochondrial expression of CB₁ receptors, whether centrally (in hippocampus) (Benard *et al.*, 2012) or peripherally (in sperm) (Aquila *et al.*, 2010), were reported. Recently, cytosolic expression of CB₁ and CB₂ receptors has been reported in human malignant thyroid lesions (Lakiotaki *et al.*, 2015). These studies referred to the presence of cannabinoid receptors within the soluble fraction of the cells alongside ECB degrading enzymes, for example: MAGL (Blankman *et al.*, 2007; Dinh *et al.*, 2002a) and ABHD6 (as shown in this Chapter). Thus, this might help in understating spatial network constraints responsible for regulating 2-AG bioavailability within different cellular compartments.

It is tempting to speculate that ABHD6 distribution in the nuclear compartment might be linked to the recently published nuclear DAGL localization (specifically DAGL α) in rat brain cortical neurons (Caño *et al.*, 2015) (by high resolution fluorescence microscopy, nuclear fractionation and western blot analysis) in that ABHD6 and DAGL are enzymes responsible for 2-AG degradation and production, respectively. This close proximity might mediate regulatory processes such as gene transcription (Caño *et al.*, 2015). In addition, despite the significant MAGL like activity recently reported in isolated rat brain cortical nuclei (by using 10 μ M NAM as a MAGL inhibitor by liquid chromatography and mass spectrometry), it was found that MAGL was not the “main” enzyme responsible for 2-AG hydrolysis in nuclear compartments in those cells (Caño *et al.*, 2015). This might implicate ABHD6 expression (as a 2-AG metabolising enzyme) in nuclear membranes.

While this study does not address the issue of ABHD6 within the synaptic area (whether pre-or post-synaptic), a link to DAGL distribution is plausible. Two

DAGL isoforms were identified in 2003 (Jain *et al.*, 2013): DAGL β -which is thought to be more predominant in the developing central nervous system-(Bisogno *et al.*, 2003; Jain *et al.*, 2013; Wu *et al.*, 2010) and DAGL α , predominant in adult brain (Gao *et al.*, 2010; Tanimura *et al.*, 2010; Yoshino *et al.*, 2011). For neuronal DAGL β , the precise localization within the synapse is still unknown (Reisenberg *et al.*, 2012); probably at presynaptic terminals or post-synaptically reported in mature autaptic hippocampal neurons (Jain *et al.*, 2013). In contrast, it has been recognised that DAGL α exhibited an “exquisite mirrored pattern” of the CB₁ receptor throughout synapses in the nervous system, with the CB₁ receptor restricted to the presynaptic terminal and DAGL α to the complementary postsynaptic site (Katona *et al.*, 2006; Reisenberg *et al.*, 2012; Uchigashima *et al.*, 2007; Yoshino *et al.*, 2011). In parallel, it has been reported that neuronal ABHD6 sits post-synaptically juxtaposed with presynaptic CB₁ receptors, while MAGL is found as a pre-synaptic enzyme (Savinainen *et al.*, 2012). This spatial expression of the enzymes reveals a well-designed molecular picture to allow privileged access of 2-AG to the CB₁ receptor (Reisenberg *et al.*, 2012).

In the same context, COX-2 has been reported also to be expressed by excitatory neurons at post-synaptic sites in rat cerebral cortex (Caño *et al.*, 2015; Kaufmann *et al.*, 1996; Slanina *et al.*, 2005) and it was expressed “exclusively” in neurons rather than glia or microglia (Kaufmann *et al.*, 1996; Yamagata *et al.*, 1993). In addition, COX-2 was detected in the nuclear membrane (Morita *et al.*, 1995; Yuan *et al.*, 2015) . Keeping in mind the reported link between ECB and the eicosanoid system (see Sections 1.6.4, 1.6.5 and 1.7.1 in Chapter 1), in particular the very recent description link with ABHD6 (Tanaka *et al.*, 2017; Wen *et al.*, 2018), this shared pattern of intracellular compartmentalization of ABHD6 and COX-2 (around nucleus and post-synaptic site) might explain the interplay between them. Thus, the relative expression of COX-2 and ABHD6 might control or direct 2-AG levels toward prostaglandin production, or might point to the role of COX-2 in controlling the level of 2-AG available at CB₁ receptor. This implies a role for prostaglandin signalling in brain synaptic plasticity.

Another proposed molecular target for ABHD6 in brain could be glutamate and GABA neurotransmission (see below). AMPA receptors, dynamically, control synaptic transmission and plasticity and deficit in these processes are strongly linked to psychiatric and neurodegenerative disorders, for example: Alzheimer's disease, schizophrenia and autism (Henley *et al.*, 2016; Haganir *et al.*, 2013; Wei *et al.*, 2017). It has been reported that ABHD6 is one of the putative auxiliary proteins for native AMPA receptor complexes (regulatory proteins) for which an exact function remains to be elucidated (Schwenk *et al.*, 2012; Wei *et al.*, 2016). Overexpression of ABHD6 inhibited AMPA receptor-mediated synaptic transmission and post-synaptic surface AMPA receptors of three types of AMPA (GluA1, GluA2 and GluA3) in neurons and in recombinant system, as well as, a loss of ABHD6 in cultured neurons elevated AMPA receptor-mediated synaptic transmission (Wei *et al.*, 2017; Wei *et al.*, 2016). On the other hand, it has been shown that ABHD6 was a potential therapeutic target for epilepsy by interacting with brain GABA receptors (Naydenov *et al.*, 2014). ABHD6 inhibition by the brain penetrant inhibitor, WWL123, alleviated epileptic symptoms during pentylenetetrazole- induced seizures (seizure evoking drug) and this blockade was absent in the presence of picrotoxin (GABA_A receptor antagonist). The authors reported the lack of tolerance or motor or cognitive impairment on chronic ABHD6 blockade and attributed this “non CB₁ receptor” effects to the spatiotemporal specificity of ABHD6 blockade and its weak enzymatic activity that controls only local levels of 2-AG (Naydenov *et al.*, 2014). 2-AG potentiates GABA_A receptors at low concentrations of GABA, see Sigel *et al.*, (2011).

It is also important to consider ABHD6 substrates. Interestingly, a number of potential physiological substrates for ABHD6 have been uncovered. Recently, ABHD6 has been found to degrade about 90% of bis(monoacylglycero)phosphate with high specific activity in liver (Pribasniig *et al.*, 2015) (see Section 1.6.1 in Chapter 1). In addition, phospholipids and lysophospholipids have found to accumulate in ABHD6 ASO-treated mice livers (Thomas *et al.*, 2013), suggesting ABHD6 can act both as a monoacylglycerol lipase and lysophospholipase (Thomas *et al.*, 2013). Lysophospholipids are

known to play various roles as mediators (Makide *et al.*, 2009). These studies might be taken as evidence for the presence of other potential endogenous substrates and/or functions for ABHD6 waiting to be explored.

In this Chapter, it has been shown that ABHD6 was detected in the soluble fraction of transfected HEK293 and infected primary cell cultures- Figure 4.13, 4.23 and 4.25. This mean that this enzyme is in contact with hydrophobic nature of substrate/s. This would raise the question of how it hydrolyses various lipid substrates. On one hand, it might be explained by a phenomenon named interfacial activation which has been postulated for lid domain lipases (Berg *et al.*, 2001; Verger, 1997). Basically when lipase comes into contact with water-lipid surfaces, a conformational rearrangement would result in displacement of the lid which in turn makes the active site accessible to the substrate for lipolysis (Kingsley *et al.*, 2013). On the other hand, it might indicate the presence of specific carriers or transport proteins to convey substrates to ABHD6. Future studies should address this intriguing hypothesis. This hypothesis could be applied also to an artificial, surrogate substrate, for example, MUH, which will be discussed in the following Chapter as a novel HTS for ABHD6.

To summarize, versions of MAGL1, MAGL2 and ABHD6 were generated tagged at both termini and expressed in both cultured and primary cell preparations. For some of these enzymes, the location of the tag appeared to influence the subcellular location of the protein.

Chapter Five

MAGL and ABHD6 high throughput assays

5. MAGL and ABHD6 high throughput assays

5.1 Introduction

MAGL, ABHD12 and ABHD6 belong to the serine α/β -hydrolase fold superfamily (Karlsson *et al.*, 1997; Lord *et al.*, 2013). This family shares a common motif made up of 8 parallel β -sheet strands (except for the second strand) surrounded by α -loops and helices (Figure 5.1). Since their identification, there has been an interest in the potential therapeutic benefits of these enzymes. MAGL and/or ABHD6 inhibition has been suggested to have potential benefit in many pathologies and diseases (Sections 1.6 and 1.7). Thus, identifying assays, substrates and inhibitors can aid in identifying the enzymes' patho/physiological role/s and hence therapeutic potential in the future.

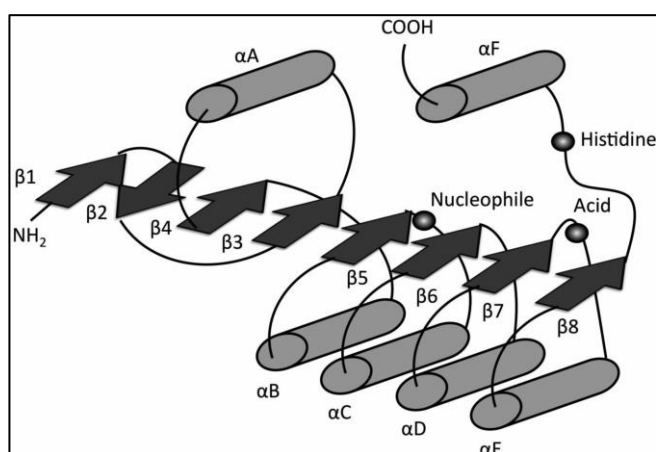


Figure 5.1 A schematic of the α/β hydrolase fold protein superfamily. Adapted from (Nardini *et al.*, 1999)

One of the common methods used to measure MAGL activity has been gas or liquid chromatography mass spectrometry of the products of catalysis, where 2-AG has been used as the substrate (Muccioli *et al.*, 2008b).

A “gold standard” method used to measure MAGL activity has been the radiometric assay as it provides accurate and sensitive readings. It is based on the use of a radiolabelled substrate (in this study, 2OG labelled in the glycerol moiety of the compound) incubated for a set period of time with a tissue preparation. Then, organic solvent (or in this study, charcoal) is used to stop the

reaction and to separate two phases: aqueous and organic fractions (or charcoal pellet and supernatant layer). The radiolabelled glycerol liberated by hydrolytic action of the enzyme is retained in the aqueous phase (or supernatant layer) and can be sampled and measured using liquid scintillation spectroscopy. Both methods are considered laborious, time consuming, expensive, and not suitable for high throughput inhibitor screening.

The first reported non-radiometric enzyme assay for MAGL made use of 7-hydroxycoumarinyl arachidonate as a fluorogenic substrate, which could be hydrolysed into arachidonic acid and the highly fluorescent 7-hydroxycoumarin (Wang *et al.*, 2008). This assay had a Z' score (which is used as a measure of quality and suitability for high throughput screening, HTS, assay) of 0.7-0.9, which indicates very good assay properties. However, later on, it was found that this assay was highly affected by the presence of BSA (it had an esterase like activity exaggerating measurement) indicating it was less suitable for biological samples (Savinainen *et al.*, 2010).

Another example of a fluorescent product employed in assessing hydrolytic activity of lipases is 4-methylumbelliferone, 4MU (Dolinsky *et al.*, 2004; Gilham *et al.*, 2005). A variety of its esters are available and have been tested in enzymatic hydrolysis assays. Among them, the heptanoyl ester, 4-methylumbelliferyl heptanoate (MUH), seemed to show a similar affinity, $K_m = 100 \mu\text{M}$, in different species (porcine, wheat, castor and peanut) for undefined esterases (Jacks *et al.*, 1967). MUH as a substrate, had been recommended previously for lipase assays as it is not hydrolysed by other esterases (Guilbault *et al.*, 1969). MUH has been suggested to be highly sensitive as low rates of hydrolysis can be accurately detected because of the intense fluorescent nature of the reaction product, 4MU, and because of a monomolecular detection basis as only one fatty acid is esterified to 4MU (Jacks *et al.*, 1967). The degradation of MUH requires an enzyme that could metabolise substrates with a hydrophobic character and an extended alkyl chain (Dolinsky *et al.*, 2004).

Another method for measuring MAGL activity uses colorimetric reaction products, which are attractive for HTS methodologies, first conducted with

human recombinant MAGL (Muccioli *et al.*, 2008a) then using native tissue (Muccioli *et al.*, 2008a; Patel, 2009). 4-nitrophenylacetate (4-NPA) is a chromogenic substrate hydrolysed to produce a yellow coloured product that can be monitored over time in a kinetic assay. This 4-NPA assay does not need stopping solutions allowing a kinetic approach to assays (Gilham *et al.*, 2005). It is simple, inexpensive and can have a Z' score of 0.84 (Patel, 2009). A major disadvantage is that it is a nonspecific substrate for esterases and so a previous investigation suggested that follow up investigations by conventional assays were required to confirm specificity (Patel, 2009).

ABPP is a relatively new strategy for measuring enzyme activity in relatively physiological conditions. It relies on covalently linking a probe to the active site of an enzyme where the probe has a reporter tag (Liu *et al.*, 1999a). It was the assay used to detect the roles of ABHD6 and ABHD12 in 2-AG hydrolysis (Blankman *et al.*, 2007), and is useful for screening multiple members of the same protein family simultaneously. Probes have been designed with a deliberate lack of selectivity, so are not suitable to screen individual enzymes in different tissues and cells.

A further alternative method used a glycerol detection assay as a highly sensitive method to provide kinetic information (Navia-Paldanius *et al.*, 2012). It measures glycerol liberated using an enzymatic cascade coupled to hydrogen peroxide to generate fluorescent resorufin (Figure 5.2). It was used successfully to investigate MAGL, ABHD6 and ABHD12 in a recombinant system (Navia-Paldanius *et al.*, 2012). A drawback of this assay is that the kits commercially available are relatively expensive.

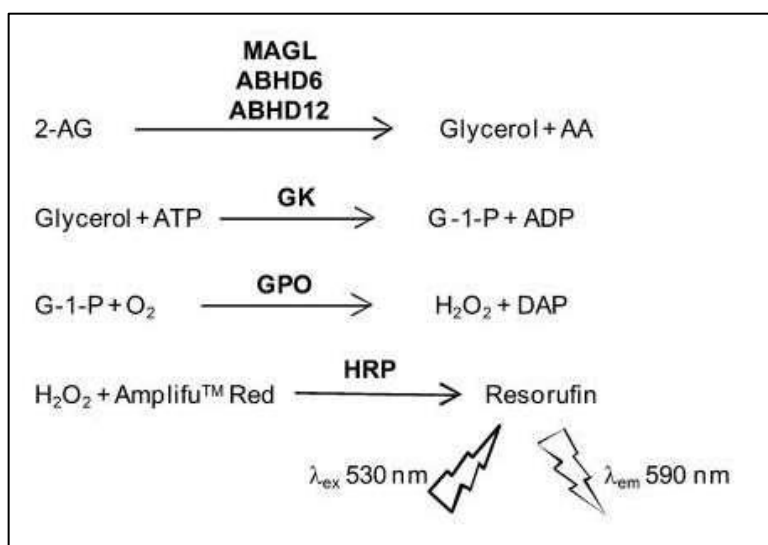


Figure 5.2 The glycerol detection assay of endocannabinoid hydrolysing enzymes. Adapted from (Navia-Paldanius *et al.*, 2012)). Glycerol is converted to glycerol-1-phosphate (G-1-P) in the presence of adenosine triphosphate (ATP) and glycerol kinase (GK), which is further converted to hydrogen peroxide H₂O₂ in the presence of glycerol 3-phosphate oxidase (GPO). Horseradish peroxidase (HRP) converts Amplifu™ Red to resorufin which can be measured kinetically at the wavelengths indicated.

5.2 Aim of this Chapter

The aim in this Section was to develop *in vitro* HTS assays that were simple, inexpensive (in terms of time and cost), reproducible and sensitive enabling measurement of human recombinant MAGL1, MAGL2, ABHD6 and ABHD12 and the screening of a large library of potential inhibitors. The objectives were:

- Screening of these enzymes using a chromogenic substrate 4-nitrophenyl acetate (NPA).
- Screening of these enzymes using two fluorogenic substrates: 4-methylumbelliferyl heptanoate (MUH) and its analogue 4-methylumbelliferyl oleate (MUO).
- Development of a local version of a glycerol detection assay.

5.3 Methods

The previously described transfects were used in this Chapter, MAGL1, MAGL2, ABHD6 and ABHD12. A negative control, empty vector pcDNA3.1 transfection was also used in parallel. Reagent details were mentioned in Methodology Chapter, Section 2.1. All data were analysed by GraphPad Prism 7 and presented either as absorbance units, relative fluorescent units or percentage control of hydrolysis. Log IC₅₀ values and residual activities were calculated from non-linear regression curves fitted to inhibitor concentration-effect data using the four parameter logistic equation (where the top was constrained to values in the absence of inhibitor, 100 %).

5.3.1 4-NPA assay

200 µl of freshly prepared 2 mM NPA was mixed with 20 µl transfect preparations (cytosolic and membrane fractions) in 96-well microtitre plates at 37 °C with occasional shaking and monitored at 405 nm continuously using a microplate spectrophotometer (Spectra MAX 340pc plate reader (Molecular Devices, CA)) for up to two hours. Appropriate blanks were used alongside.

NPA is a substrate for many esterases (Muccioli *et al.*, 2008a) including MAGL. Upon incubation with the enzyme source, hydrolysis of NPA generates 4-nitrophenol (yellow product absorbing at 405 nm) and acetic acid (Figure 5.3).

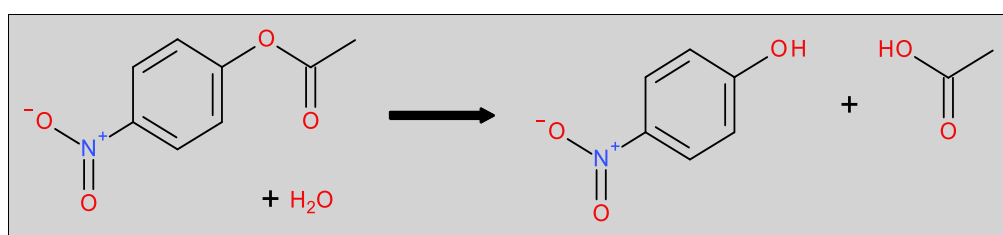


Figure 5.3 Schematic clarify the chemical reaction of 4-NPA hydrolysis.

5.3.2 4-Methylumbelliferyloleate and 4-methylumbelliferylheptanoate assays

MUO hydrolysis was conducted in a total reaction volume of 100 µl at a final concentration of 12.5 µM MUO. The MUH assay consisted of the same volume but with varying substrate concentrations. Soluble and membrane fractions were

incubated with the substrate with occasional shaking at 37 °C. The fluorescent 4MU product (Figures 5.4 and 5.5) was read at excitation/ emission wavelengths of 355/460 nm (Guilbault *et al.*, 1969; Jacks *et al.*, 1967).

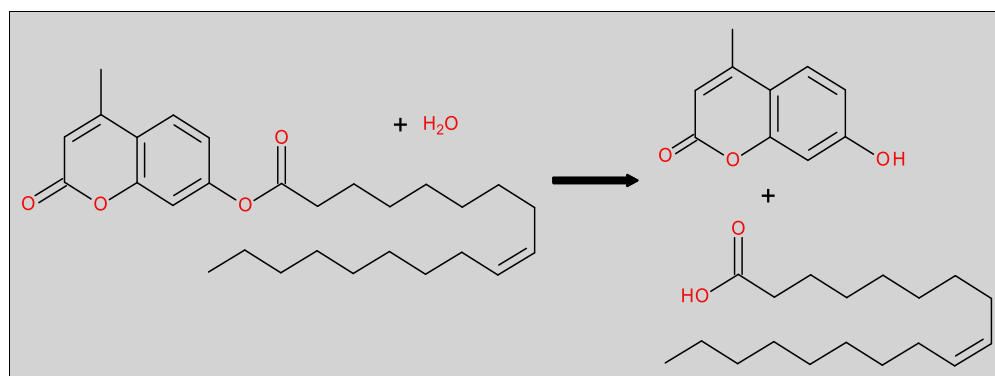


Figure 5.4 Schematic clarify the chemical reaction of 4-MUO hydrolysis.

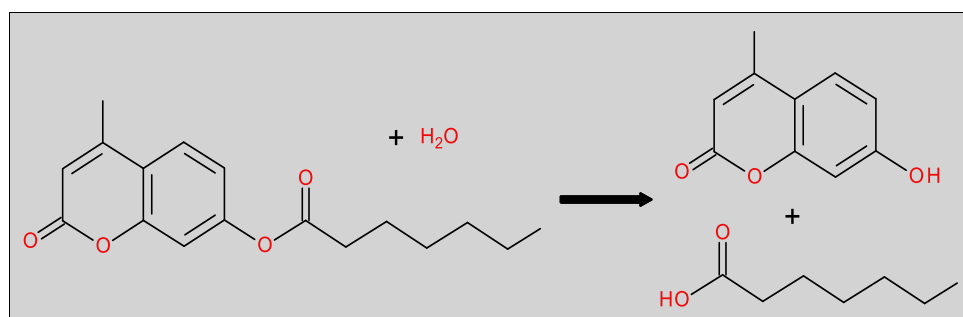


Figure 5.5 Schematic clarify the chemical reaction of 4-MUH hydrolysis.

5.3.3 Glycerol detection assay

The glycerol detection kit (MAK117) and individual glycerol assay materials were bought from Sigma Chemical Company (Dorset, UK). Monoacylglycerol substrates were purchased from Tocris (Bristol, UK). The protocol applied here followed that of Savinainen *et al.* (Savinainen *et al.*, 2010) but with minor modifications. In this study, the assay volume of 100 μ l was made up from 25 μ l substrate, 25 μ l enzyme (membrane fraction) and 25 μ l buffer incubated at 37 °C for 30 minutes followed by the addition of 25 μ l master mix of detection enzymes, kinetically assayed at room temperature. Final concentrations of enzymes and substrates are indicated in Table 5.1).

Table 5.1 Master mix component and final concentrations in glycerol detection assay.

Component	Final concentration
HRP, GPO and GK	0.4 unit/ ml
ATP	0.25 mM
Amplifu™ Red	20 μM
Substrate	25 μM

5.4 Results

Much of the data reported in this Section were produced in collaboration with Yousra Adel and Sadia Shabnam, whilst they were conducting research projects under my supervision on the MSc. in Drug Discovery and Pharmaceutical Sciences at the University of Nottingham.

5.4.1 4-NPA assay

A pilot study was conducted using a range of NPA concentrations with membrane and soluble fractions of a MAGL1 transfect and an empty vector transfect (Figure 5.6). Attempts to fit Michaelis-Menten (rectangular hyperbola) curves to the data from the mock-transfected preparation failed due to low rates of hydrolysis (Figure 5.6). In contrast, K_m values could be calculated of 1.0 mM for both cytosolic and membrane fractions of the MAGL1 transfect with V_{max} values of 1.1 and 0.8 AU, respectively (Figure 5.6).

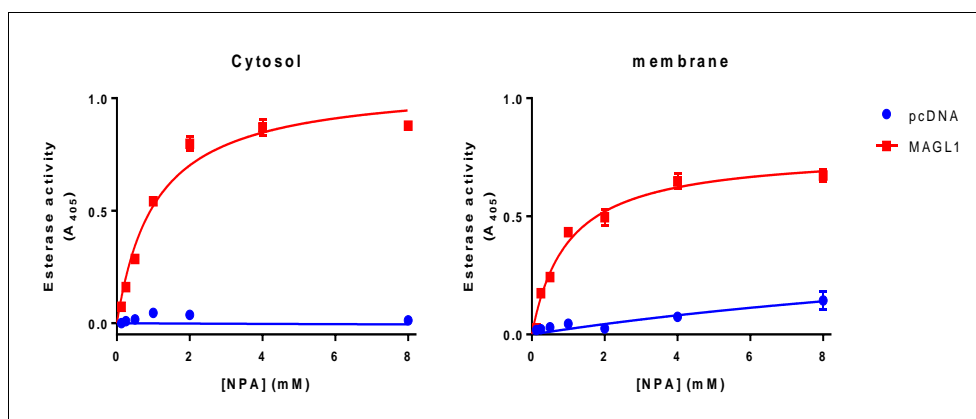


Figure 5.6 Michaelis-Menten analysis of 4-NPA hydrolysis by two fractions of recombinant MAGL1 transiently expressed in HEK293 cells.

Data are mean \pm SEM from a single experiment performed in quadruplicate. Background absorbance (in the absence of added protein) was subtracted.

Using NPA at a concentration twice the K_m value, screening of cytosolic and membrane fractions of transfected enzymes was conducted (Figure 5.6). Basal levels of hydrolysis (NPA in the absence of enzyme source) were relatively constant during the incubation period, indicating a stable substrate. Elevated basal readings were observed upon using substrate solutions which had undergone freezing and thawing, and so fresh preparations were made up with each experiment.

Preparations from HEK293 cells transfected with the pcDNA empty vector showed a linear increase with time, with higher activity in the membrane fraction (Figure 5.7). Membrane fractions from ABHD6 or ABHD12 transfects failed to show increased levels of hydrolysis relative to the empty vector. MAGL1 showed the highest activity in this screen for both cytosolic and membrane fractions, with a non-linear profile, suggestive of a saturation phenomenon. MAGL2 also showed elevated rates of hydrolysis compared to the pcDNA transfect in both cytosol and membrane fractions. Cytosolic extract from the ABHD6 transfect showed an apparently linear increase in hydrolysis with time (Figure 5.7).

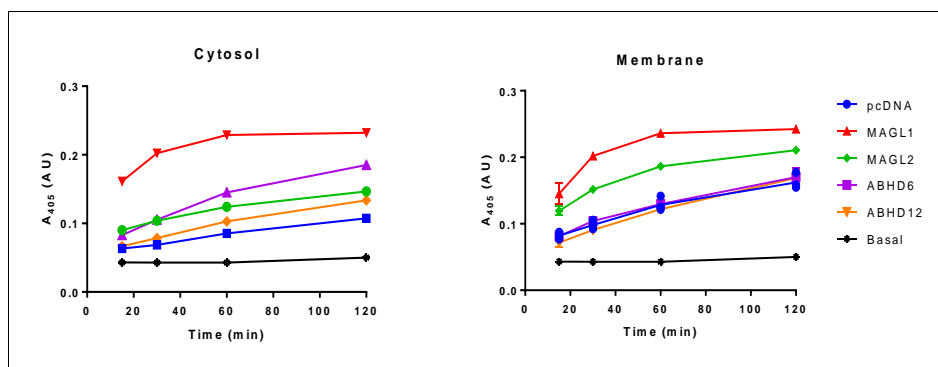


Figure 5.7 Hydrolysis of 2mM 4-NPA by two fractions of recombinant enzymes. Data represent mean \pm SEM of a single experiment performed in quadruplicate, representative of 5 transfection repeats.

In these initial examinations, the cellular lysate was undiluted, therefore, the next step was to explore serial dilutions of MAGL1 to identify a useable condition for screening of potential inhibitors. Diluting the mock transfected cytosolic preparation made little difference to the rate of NPA hydrolysis (Figure 5.8), while dilution of the MAGL1 cytosolic fraction eight-fold appeared to have levels of hydrolysis similar to the background. The membrane fraction of the pcDNA-transfected cells exhibited a modest dilution-dependent reduction in the rate of hydrolysis (Figure 5.8). Similarly, to the cytosolic fraction, dilutions of the MAGL membrane fractions to eight-fold or more appeared not different to background.

Further studies using this substrate were, therefore, discontinued due to the poor rates of hydrolysis, which would require relatively large quantities of the transfected MAGL isoforms.

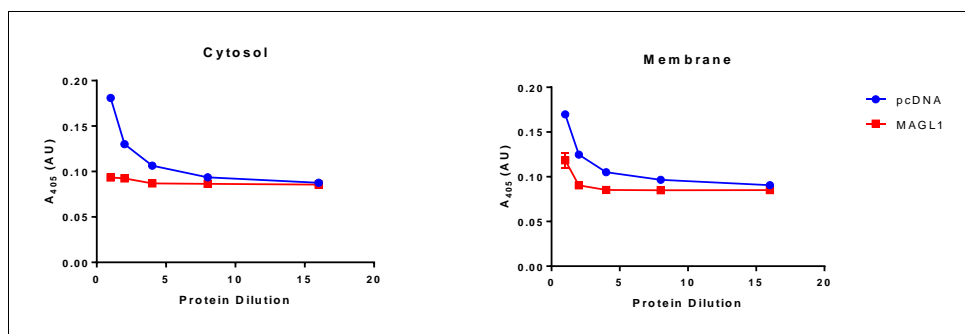


Figure 5.8 Hydrolysis of 4-NPA by 5 points protein dilution of recombinant MAGL1 and control. Data represent mean \pm SEM of a single experiment performed in quadruplicate, representative of 5 transfection repeats.

5.4.2 4-MUO assay

To characterise MUO as a substrate, the time course of hydrolysis of different substrate dilutions with a soluble fraction from rat liver was conducted (Figure 5.9 & 5.10). Background hydrolysis of MUO (in the absence of an enzyme source) was low and relatively constant over the incubation period, indicative of a stable substrate. The lowest concentration of substrate ($1.56 \mu\text{M}$) was not hydrolysed at a rate much different from the background, while $12.5 \mu\text{M}$ MUO appeared elevated (relative to background) and linear with time, while $25 \mu\text{M}$ MUO was elevated (relative to $12.5 \mu\text{M}$ MUO) and appeared to show a saturation phenomenon. Serial dilutions of the rat liver soluble fraction showed the rate of hydrolysis was relatively constant at around 40 fold increase over background even at 64 fold dilution (Figure 5.10).

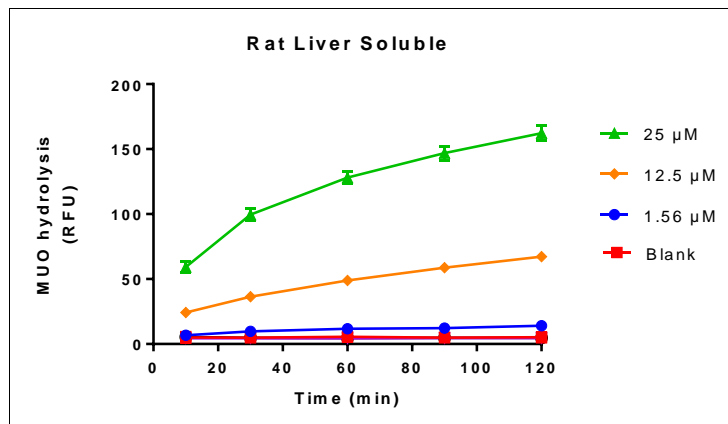


Figure 5.9 Hydrolysis of different concentrations of 4-MUO by rat liver soluble fraction. Data represent mean \pm SEM of a single experiment performed in quadruplicate.

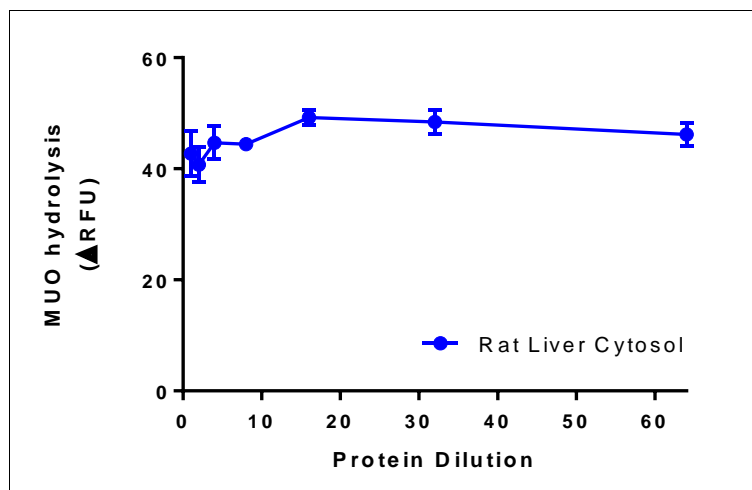


Figure 5.10 Hydrolysis of 4-MUO by doubling protein dilutions of rat liver and control. Data represent mean \pm SEM of a single experiment performed in quadruplicate.

The next step was to screen the recombinant enzymes in this assay using the concentration of MUO identified to retain linearity of hydrolysis with the rat liver soluble fraction (12.5 μ M, Figure 5.9 & 5.10). As in the first experiments, the enzyme blanks were stable over time (Figure 3.11). MUO hydrolysis in the presence of the samples from the pcDNA-transfected cells was linear over time. Fractions from the enzyme-transfected cells were not substantially different from the pcDNA control, although the membrane fraction from the ABHD6 transfect was modestly elevated compared to the background (Figure 3.11).

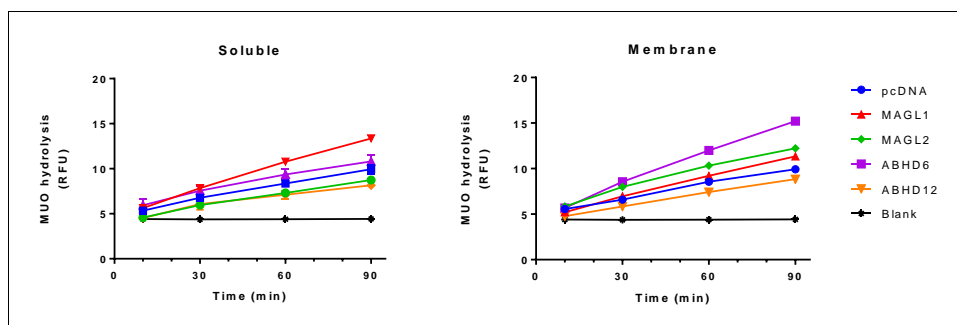


Figure 5.11 Hydrolysis of 4-MUO by two fractions of recombinant enzymes. Data represent mean \pm SEM of a single experiment performed in quadruplicate.

Given the poor rates of hydrolysis of MUO, further studies using this substrate were discontinued.

5.4.3 Glycerol detection assay

The previous substrates were synthetic and, although useful for screening purposes, might have a distinct profile to the endogenous substrate/s. A glycerol detection assay would allow the hydrolysis of endogenous monoacylglycerols to be measured. The assay uses a cascade of enzymes to produce hydrogen peroxide which, in the presence of horseradish peroxidase (HRP), converts Amplifu™ Red to the fluorescent product resorufin. The enzymes included in the coupled system are glycerol kinase and glycerol 3-phosphate oxidase (Figure 5.2). As part of the preliminary validation, a glycerol standard curve was constructed using a commercial kit and a much cheaper assay mix making use of the same enzymes bought separately (Figure 5.12). The commercial assay kit generated a linear glycerol standard plot at different time points ranging from 10-90 min. For the self-generated kit, the glycerol standard curve appeared non-linear. At 30 min, the lab version revealed high signals of more than 250 RFU at a much lower glycerol level of 0.75 nanomoles while the commercial kit had around 100 RFU at 5 nanomoles of added glycerol.

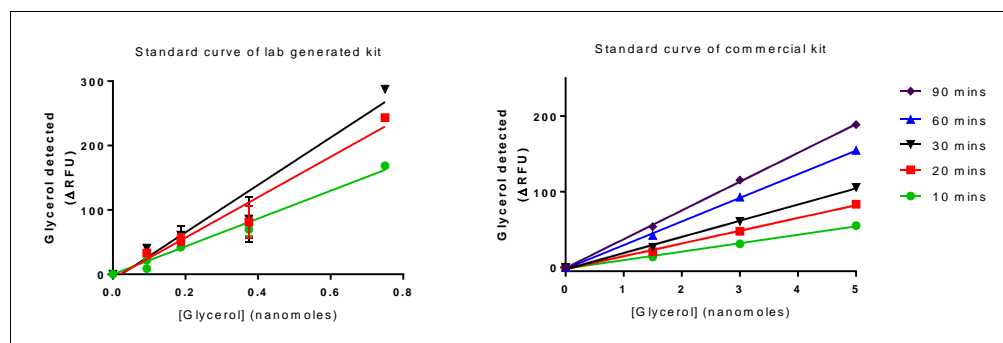


Figure 5.12 Linearity of glycerol standard plot in lab generated kit and commercial kit assays at various time points.

Data represents a single experiment performed in duplicate. Background glycerol (at zero time) has been subtracted from each time point.

Three commercially available 2-monoacylglycerols (2-arachidonylglycerol, 2-palmitolglycerol and 2-oleolyglycerol) were tested as substrates in this assay (Figure 5.13). Detection of hydrolysis of 2OG using the commercial kit identified time-dependent activity with membrane preparations from pcDNA and enzyme-transfected HEK293 cells, with the enzyme transfects having greater activity than the mock transfect (Figure 5.13-D). The fluorescent signal detected from the self-generated kit was much lower than the commercial one (Figure 5.13-A-B-C). Further, the self-generated detection method showed low rates of hydrolysis for the mock transfect and no increase with the enzyme transfects.

Given the lack of reproducibility of the commercial kit using the lab-generated version and the cost of the commercial kit, this assay method was discontinued.

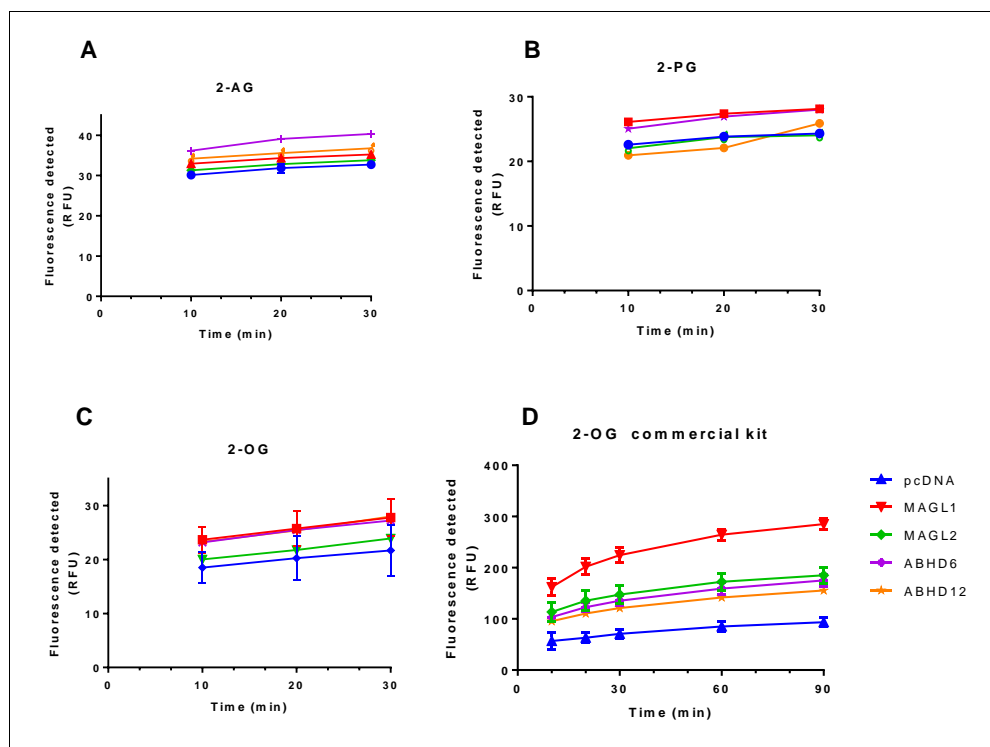


Figure 5.13 Hydrolysis of three 2-monoacylglycerol substrates in lab generated kit. The hydrolysis of 100 μ M of (A) 2OG, (B) 2-PG and (C) 2-AG by membrane fractions of the recombinant enzymes using the lab mix kit while (D) with 2OG using the commercial kit. Data represent a single experiment performed in duplicate, representative of 3-4 separate transfection preparations.

5.4.4 4-MUH assay

The chromogenic substrate MUH proved to be usable for measuring ABHD6 activity (Figure 5.14) compared to other selected enzymes. This was shown by the MSc students at a final concentration of 250 μ M substrate (Mahmood *et al.*, 2017). There was a low background activity over time (indicating a stable substrate) along with a larger signal window between ABHD6 and other transfects (including mock transfects), although with an apparent saturation phenomena in both soluble and membrane fractions (Figure 5.14). There was a modest increase in hydrolysis in the presence of ABHD12. Therefore, further work was conducted to characterize the use of MUH as a substrate for ABHD6.

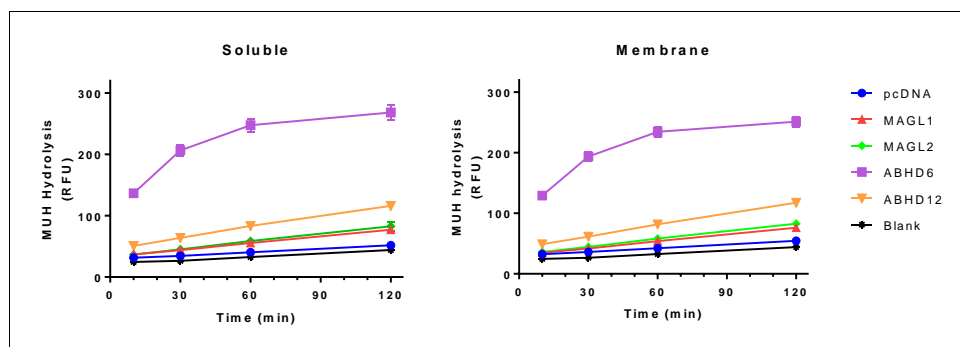


Figure 5.14 Hydrolysis of 4-MUH by two fractions of recombinant enzymes at 250 μ M final concentration.

Data represents mean \pm SEM of a single experiment performed in 8 replicates.

The experimental setup allowed comparison of enzyme activities to two types of blanks: MUH blanks and tissue blanks, where either the substrate or the enzyme preparation, respectively, were omitted. Michaelis-Menten analysis was conducted using 75 μ l MUH dilutions and 25 μ l of ABHD6-HEK293 membrane preparations (1:100 fold diluted), kinetically assayed at room temperature. Assessing inhibitor effects was conducted using 50 μ l of MUH, 40 μ l enzyme and 10 μ l buffer vehicle or inhibitor.

Using a range of MUH concentrations, saturation of hydrolysis rates was apparent (Figure 5.15, B), allowing calculation of a K_m value of 32 ± 8 μ M (from at least 5 separate transfection preparations). Subsequent experiments were conducted using 50 μ M MUH.

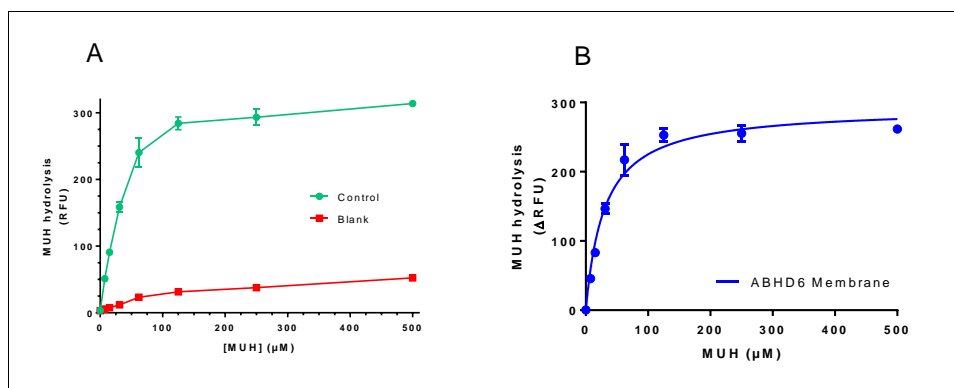


Figure 5.15 Michaelis-Menten analysis of 4-MUH in ABHD6-HEK293 membrane preparations.

(A) Represents “raw” data while (B) after background MUH hydrolysis subtraction (blank). Data represent mean \pm SEM of a single experiment performed in triplicate, representative of 5 separate transfection preparations.

The next step was screening of different compounds to validate the assay for ABHD6 screening. Figure 5.16 shows 11 selected inhibitors used to identify MUH hydrolysis; these were:

- MAFP as a non-selective irreversible serine hydrolase family inhibitor (Deutsch *et al.*, 1997),
- JJKK048 (Aaltonen *et al.*, 2013), JZL184 (Long *et al.*, 2009a), pristimerin (King *et al.*, 2009) and URB602 (Hohmann *et al.*, 2005) as reportedly-selective MAGL inhibitors,
- WWL123 and WWL70 as reportedly-selective ABHD6 inhibitors,
- JNJ1661010 (Karbarz *et al.*, 2009), URB597 (Piomelli *et al.*, 2006) and PF3845 (Ahn *et al.*, 2009b) as FAAH inhibitors and
- benzil as carboxylesterases inhibitor (Hyatt *et al.*, 2006).

The screening assay started with a 15 min pre-incubation of the ABHD6 transfect with the inhibitors, followed by 60 min of incubation at 37 °C at a final inhibitors concentration of 1 μM. Due to variability in baseline activity (controls) between transfects, it was not possible to apply parametric analysis of the data. MAFP, JJKK048 and WWL70 produced significant inhibition, as expected. Other inhibitors were ineffective (Figure 5.16).

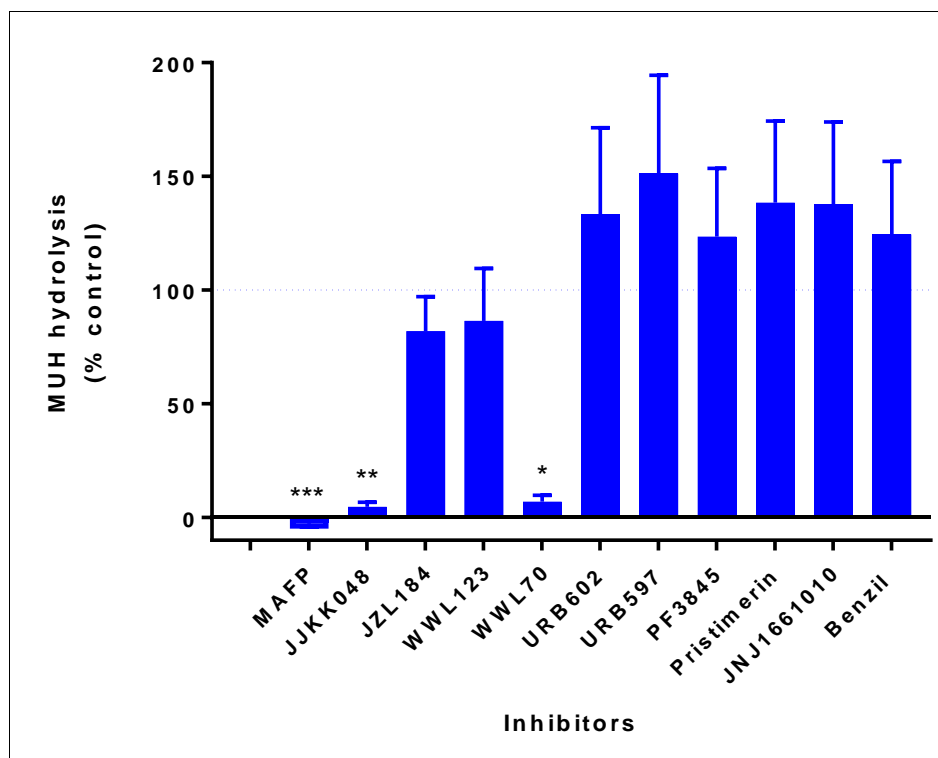


Figure 5.16 Hydrolysis of MUH by 1 μ M concentrations of eleven different inhibitors in ABHD6-HEK293 membrane preparation.

Data represents mean \pm SEM from seven separate preparations performed in duplicate. * $P \leq 0.01$, ** $P \leq 0.001$ and *** $P \leq 0.0001$ (Freidman analysis with uncorrected Dunn's test). Statistical analysis was conducted by a colleague (SPH Alexander) blinded to the construction of the assay.

The concentration dependence of the most effective inhibitors MAFP, JJKK048, and WWL70 was assessed further. WWL123 was also included in this analysis given the unexpected lack of inhibition in the preliminary screen (Figure 5.17). pIC_{50} values of four inhibitors were 8.0 ± 0.01 and 7.1 ± 0.06 for MAFP and JJKK048, respectively with no residual activity, while for WWL123 and WWL70, values were 6.3 ± 0.1 (residual activity of $45 \pm 2\%$ control) and 7.3 ± 0.05 (residual activity of $6 \pm 1\%$ control), respectively (Figure 5.17).

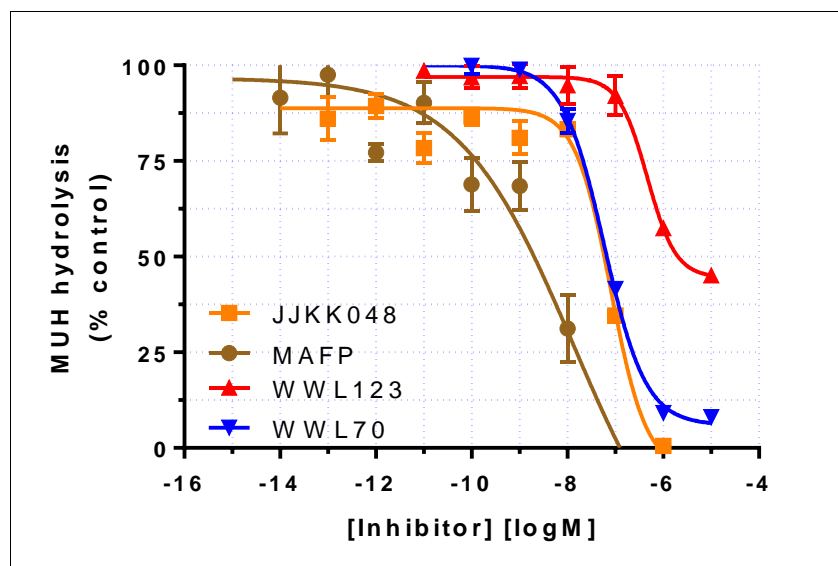


Figure 5.17 Concentration inhibition curves of MAFP, JJKK048, WWL123 and WWL70 for 4-MUH hydrolysis in ABHD6-HEK293 membrane preparations.

Curve fitting to the four parameter logistic equation was conducted by a colleague (SPH Alexander) blinded to the construction of the assay. Data are mean \pm SEM from four (MAFP and JJKK048) or five (WWL70 and WW123) separate transfection preparations performed in duplicate.

The Z' score is a simple statistical coefficient that has been recommended for evaluation and comparison of the quality of assays, and the optimization and validation of high throughput screening assays (Zhang *et al.*, 1999). It is used to indicate the suitability of an assay for large scale compound screening. It involves four parameters: means and standard deviations of both positive (p) and negative (n) controls: \bar{X}_p and \bar{X}_n , and σ_p and σ_n respectively in the following equation:

$$Z = 1 - ((3 * \bar{X}_p + 3 * \bar{X}_n) / (\sigma_p - \sigma_n))$$

If the result is between 0.5-1, the interpretation is considered an excellent assay; between 0-0.5 means a marginal assay which would require independent confirmation for any 'hits'.

Using 1 μ M WWL70 as a positive control allowed calculation of a Z' score of 0.42. Consequently, screening of 36 different compounds was conducted at 10 μ M final concentration (Figure 5.18) after 60 min of simultaneous incubation with 80 μ l ABHD6 preparation and 10 μ l MUH. The screening was conducted

blindly; inhibitor solutions were prepared by a third party and results were analysed by someone not involved in the construction of the experiment.

The majority of the compounds were ineffective. Some had a small, but statistically significant, inhibition. Typically, the level of inhibition by these agents was less than 10 %, so no further analysis was conducted. Greater levels of inhibition were observed with orlistat (31 ± 13 % control) and palmitic acid (53 ± 12 % control). Orlistat was further investigated in a serial dilution inhibition curve (Figure 5.19) revealing pIC₅₀ value of 6.5 ± 0.3 with almost complete inhibition of enzyme activity.

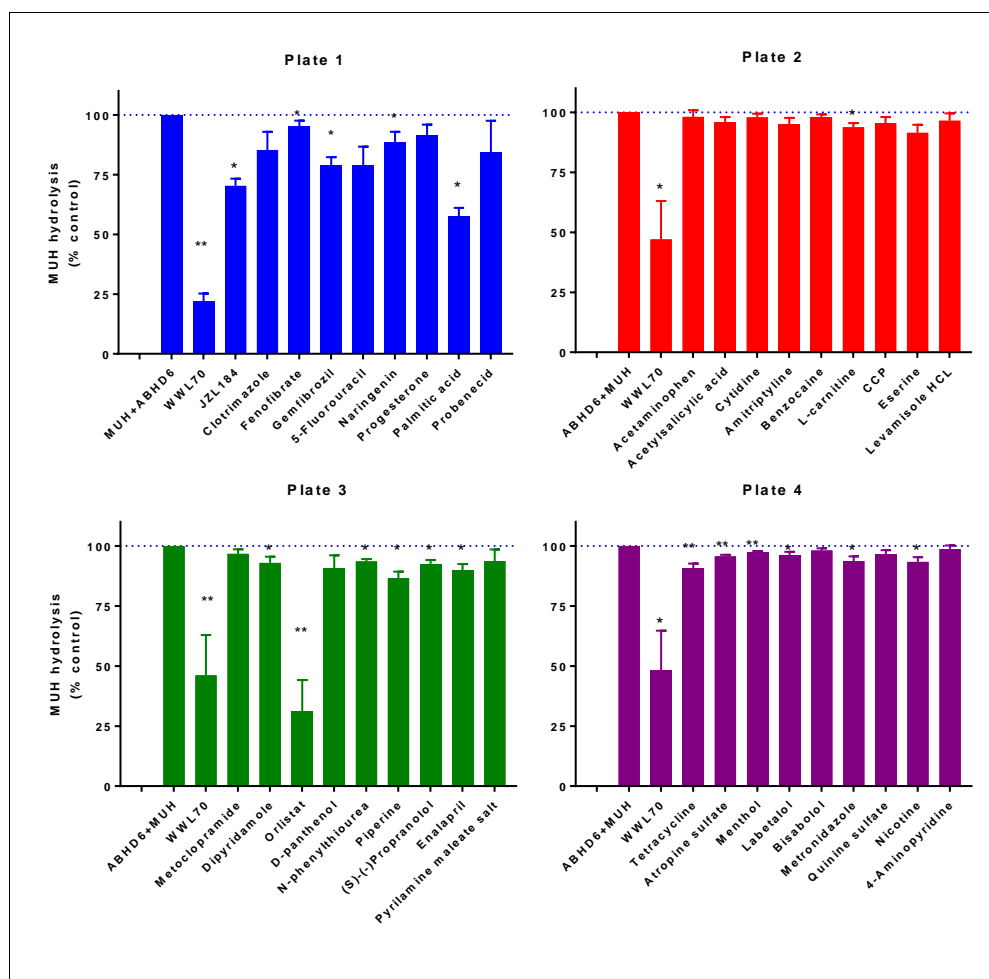


Figure 5.18 Blind screening of a range of drugs as potential inhibitors of MUH hydrolysis in ABHD6-HEK293 membrane preparations.

WWL70 at 1 µM was used as a positive control on every plate assessed. The final concentration of other drugs was 10 µM. Data represent mean ± SEM from four separate preparations performed in duplicate. Note: CCP in second plate is *N*-cyclohexane carbonyl pentadecylamine, an inhibitor of NAAA. * $P \leq 0.01$, ** $P \leq 0.001$, *** $P \leq 0.0001$ repeated measures ANOVA with Dunnett's multiple comparisons test.

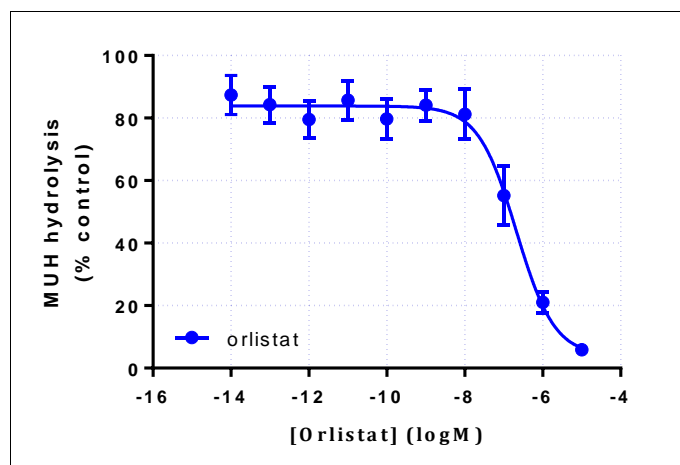


Figure 5.19 Concentration inhibition curve of orlistat for MUH Hydrolysis in ABHD6-HEK293 membrane preparation. Data represent mean \pm SEM from four separate transfection Preparations performed in duplicate.

To further characterise the assay, six “alternative” substrates were screened at 100 μ M final concentration (Figure 5.20), and 60 min of co-incubation. 1-OG, AEA and 2-PG were without effect, while 2OG, 2-AG and *N*-arachidonylglycine (NAGLY) evoked significant inhibitions of MUH hydrolysis. 100 μ M 2-AG appeared to have the greatest impact but still failed to elicit inhibition greater than 50 % (68 ± 4 % control), so further investigation of its potency was not conducted.

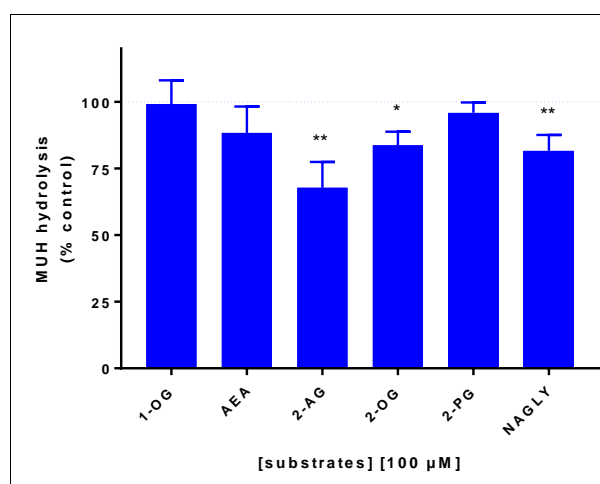


Figure 5.20 Hydrolysis of 4-MUH by putative substrates (at 100 μ M) In ABHD6-HEK293 membrane preparation.

Data represent mean \pm SEM from seven separate preparations performed in duplicate. * $P \leq 0.01$, and ** $P \leq 0.001$ repeated measures ANOVA with Dunnett's multiple comparisons test conducted by a colleague blinded to the construction of the experiment.

Given that MUH was a poor substrate for other recombinant esterases investigated in this study (Figure 5.14), this substrate was used to investigate ABHD6 activity in rat tissues. Rat intestine was the first choice to establish this exploration, based on the results from Chapter 3 using the radiometric assay. In particular, female small intestine particulate preparations showed a higher ABHD6 activity in comparison to male preparations. Therefore, it was chosen for the subsequent experiments.

Serial protein dilutions with and without 1 μ M (final concentration) WWL70 and orlistat (potentially to detect other lipase activities) displayed an unexpected time course profile. Figure 5.21 illustrates results in the presence of tissue diluted 125-fold. The control (intestine preparation in the absence of inhibitors) exhibited a very high basal hydrolytic level (at $t=0$) which rose after 10 min and then gradually declined over time till 60 min when there were no differences between the control and the presence of the two inhibitor (Figure 5.21). A potential confounding effect of another enzyme/s present in the intestine that would also metabolise MUH or potentially the product 4MU was considered. Michaelis-Menten analysis in the absence and presence of 1 μ M WWL70 was difficult as there was no major inhibitory effect of WWL70 until higher concentrations of MUH were reached (225 and 250 μ M, Figure 5.22). The pattern of activity was not consistent with the ABHD6 transfects (Figure 5.15).

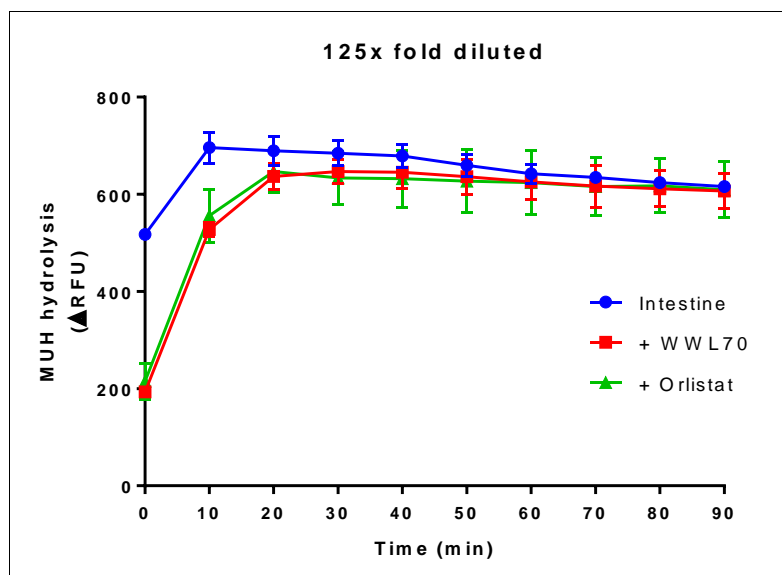


Figure 5.21 Hydrolysis of 4-MUH by 125X fold protein dilution of rat intestine membranes. Final concentration of WWL70 and Orlistat was 1 μ M. Data represent mean \pm SEM of a single experiment performed in triplicate. Background MUH hydrolysis has been subtracted.

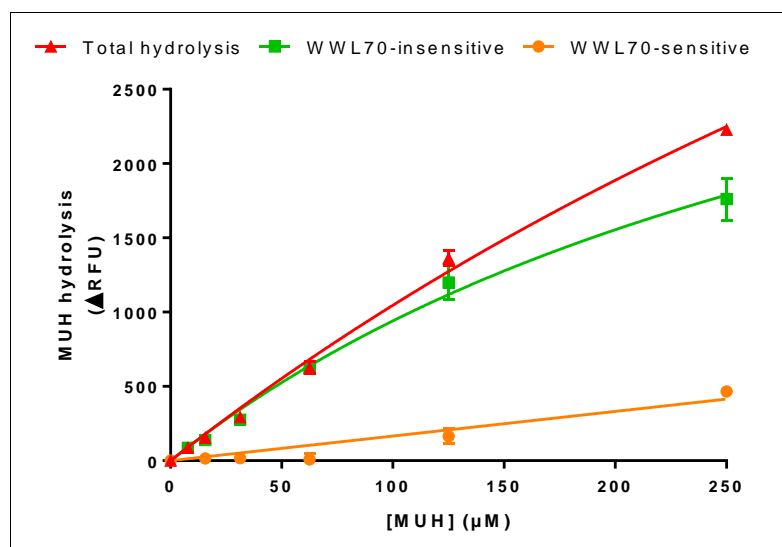


Figure 5.22 Michaelis-Menten analysis of 4-MUH in rat intestine membranes. Data represents mean \pm SEM of a single experiment performed in triplicate, representative of 5 separate preparations. Background MUH hydrolysis has been subtracted.

Several optimization experiments were conducted, designed to characterise MUH hydrolysis in rat intestine including assessing soluble and membrane fractions and both sexes. All these experiments, however, failed to establish a solid base for further investigation in this tissue. To exclude any role for the presence of an

esterase or any other enzymes in intestine that could interfere with this assay and to have a better separation of particulate and soluble fractions in centrifugation, the next step was to investigate ABHD6 activity in a tissue where activity had previously been reported in the literature, namely the brain, and specifically, hippocampus membranes (Figure 5.23). Based on pilot experiments, a protein dilution was selected at 150-fold in all experiments.

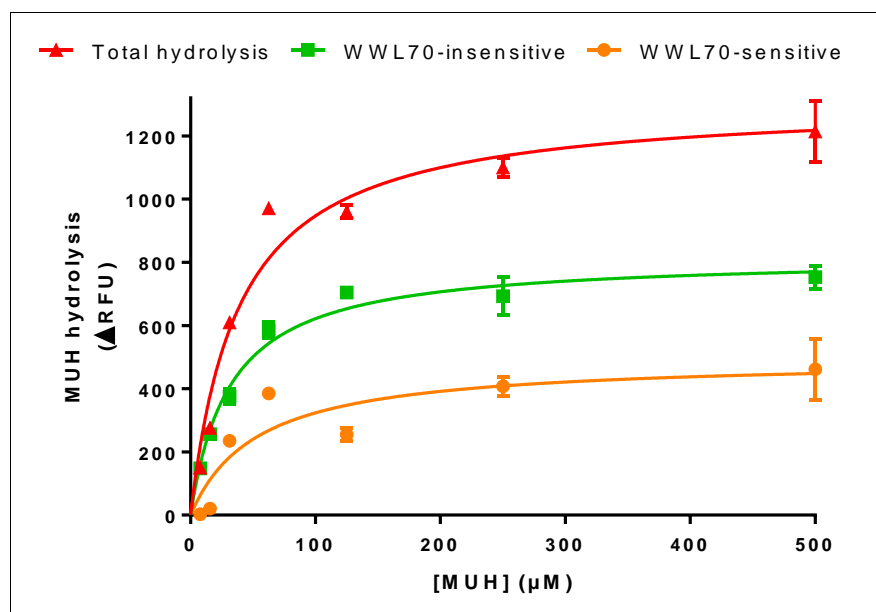


Figure 5.23 Michaelis-Menten analysis of 4-MUH hydrolysis in rat hippocampus membranes. Data represent mean \pm SEM of a single experiment performed in triplicate, representative of five separate preparations. Background MUH hydrolysis has been subtracted.

Table 5.2 K_m values for MUH hydrolysis in rat hippocampal membranes. Data from five separate preparations presented as mean \pm SEM.

	K_m (μM)
Total hydrolysis	31 ± 5
Sensitive to WWL70	45 ± 7
Insensitive to WWL70	25 ± 4

Using a range of MUH concentrations in the absence and presence of $1 \mu\text{M}$ WWL70, activity sensitive to WWL70 (potentially equivalent to ABHD6 activity) was calculated by subtracting WWL7-insensitive activity from total hydrolytic activity (Figure 5.23). In all three cases, a rectangular hyperbola could be fitted allowing determination of apparent K_m values of 25-45 μM (Table 5.2). The WWL-sensitive portion of MUH hydrolysis represented about 40 % of total

hydrolysis. Investigating the total enzyme activity for one- or two-site fits (single vs double rectangular hyperbolae), Prism preferred a single site fit, indicating a failure to distinguish multiple sites, with a calculated K_m value of $31 \pm 5 \mu\text{M}$.

The same 11 inhibitors tested in ABHD6 transfects above (Figure 5.16) were also tested using rat hippocampal particulate preparations. Although JJKK048 and PF3845 produced statistically significant inhibitions, they still failed to elicit inhibition greater than 50 % (69 ± 10 and 88 ± 7 , respectively) (Figure 5.24). Only MAFP produced an inhibition greater than half ($22 \pm 11\%$ control). WWL70 was investigated further using a range of concentrations (Figure 5.25). Consequently, a pIC_{50} value of 7.4 could be calculated with a maximal inhibition of only about 30%. However, this non-linear fitting in Prism showed high variability among the 5 animal tissues tested in terms of individual pIC_{50} values calculated (ranging from 6.6 to 10), slope (-0.17 to -10.14) and maximum inhibition (20% up to 50%). These results highlight major inter-individual variation, as well as the presence of abundant MUH hydrolysis caused by a serine hydrolase enzyme/s (Figure 5.24) distinct from ABHD6 (Figure 5.25).

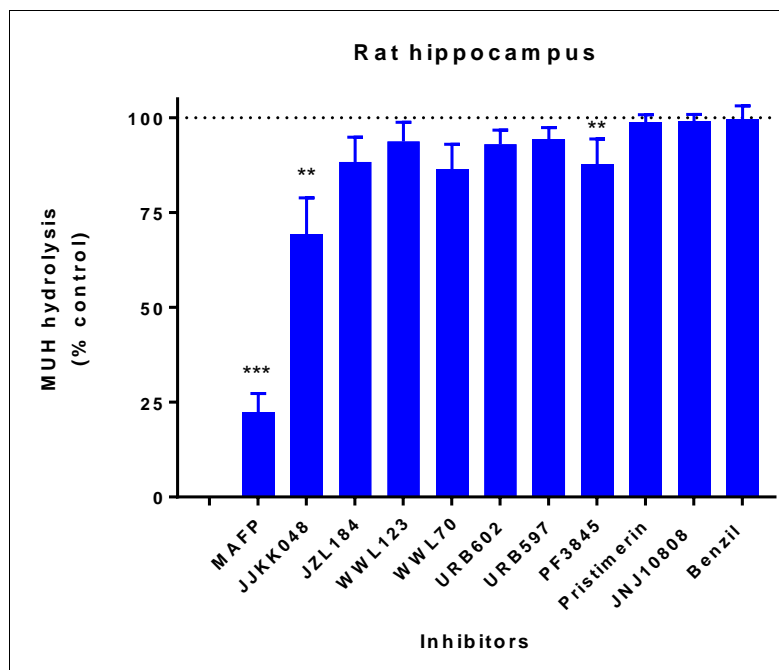


Figure 5.24 MUH Hydrolysis in rat hippocampus membranes in the presence of 1 μM concentrations of eleven different inhibitors. Data are mean \pm SEM from five separate preparations conducted in duplicate. ** $P \leq 0.001$, *** $P \leq 0.0001$, repeated measures ANOVA with Friedman test conducted by a colleague blinded to the construction of the experiment.

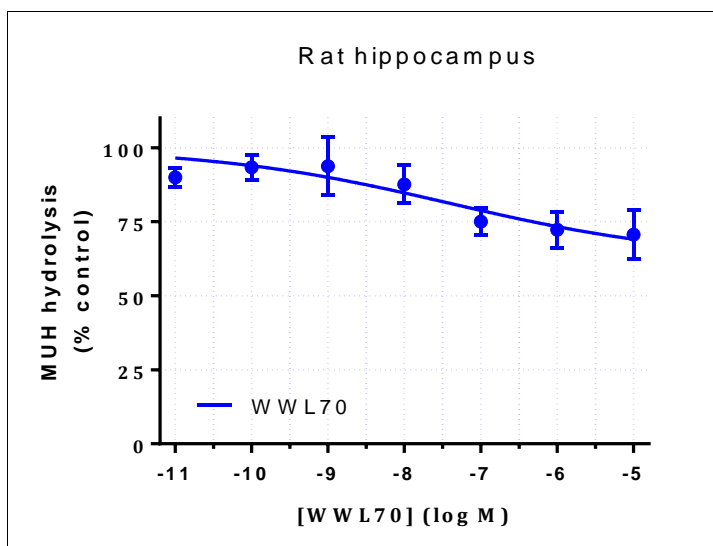


Figure 5.25 Concentration inhibition curve of WWL70 for 4-MUH hydrolysis in rat hippocampus membranes. Data are mean \pm SEM from five separate preparations performed in duplicate.

In order to try to isolate the other enzyme activity/activities responsible for the majority of MUH hydrolysis in this tissue, a number of inhibitors were assessed

in the presence and absence of WWL70 (Figure 5.26). In this assay, 5 μ l of all inhibitors at 1 μ M final concentration were screened without pre-incubation (due to the practical nature of distributing the different additions; to allow mixing, the last component added was tissue rather than substrate). A distinct inhibitory profile was observed from that obtained in Figure 5.24. The experimental design was constructed to answer the following three questions:

- 1- Do the inhibitors have an effect on rat hippocampal MUH hydrolysis?
- 2- Do they have an effect when combined with WWL70 (anticipated to inhibit ABHD6 selectively)?
- 3- Is the effect of WWL70 maintained in the presence of those inhibitors?

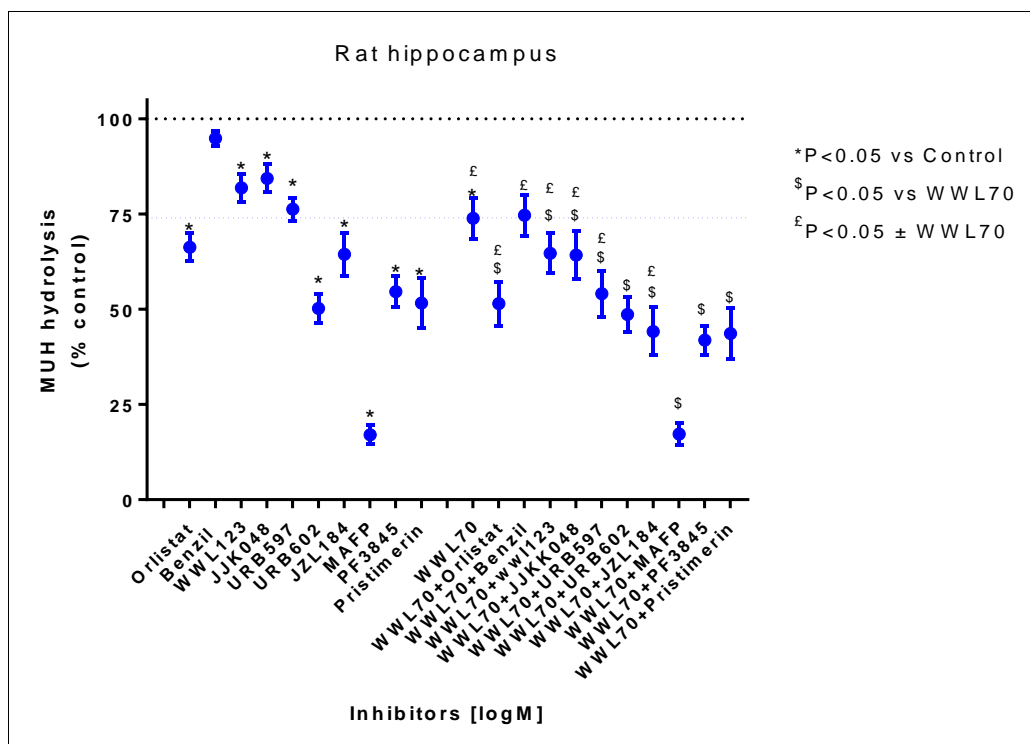


Figure 5.26 MUH hydrolysis in rat hippocampus membranes in the presence of 11 inhibitors with and without WWL70.

The final concentration of each inhibitor was 1 μ M. Data are mean \pm SEM from five separate preparations performed in duplicate. Data were analysed by one way ANOVA and Uncorrected Fisher's Least Significant Difference by a colleague blinded to the construction of the experiment.

To answer the first question, all of the inhibitors were used without further combination and were compared statistically with a control (an absence of inhibitor). All of the inhibitors examined evoked a significant reduction in MUH

hydrolysis except benzil. Given the selectivity profile of benzil (Hyatt *et al.*, 2006), this suggests that carboxylesterases do not contribute to MUH hydrolysis in this tissue. WWL70 was only capable of evoking ~25 % inhibition of hydrolysis, while MAFP evoked the largest inhibition of MUH hydrolysis (to 17 ± 2 % control). Three inhibitors showed an inhibitory effect of approximately half: URB602 (50 ± 4 % control), pristimerin (52 ± 7 % control) and PF3845 (55 ± 4 % control). The level of inhibition by those agents were different from that shown in Figure 5.24.

The next step was to use a combination of the inhibitors with WWL70 to investigate whether the inhibitor was still able to evoke a significant effect. The hypothesis being tested was that if WWL70 inhibits ABHD6 selectively (and completely) and a second agent still has an inhibitory effect (in combination), this would indicate the presence of multiple MUH hydrolysing activities other than ABHD6. For benzil, which failed to inhibit MUH hydrolysis in this tissue directly, there was no further effect in the presence of WWL70, which might be taken as further evidence for the absence of carboxylesterases. In contrast to benzil, WWL70 failed to cause a significant inhibition in the presence of MAFP. This is consistent with MAFP acting to inhibit multiple serine hydrolases, including ABHD6 (see Chapter 3, Figure 3.12 and Table 3.12). For the other inhibitors, the hypothesis being tested was whether they were still able to evoke a significant inhibition in the presence of WWL70 (identified as the dashed line in Figure 5.26); that is, whether MAGL, FAAH, etc. could also contribute to MUH hydrolysis. Thus, significant effects of JJKK048, URB602, JZL184 and pristimerin were observed, suggesting a potential contribution of MAGL to MUH hydrolysis in this tissue. Further, PF3845 and URB597 also displayed significant effects in the presence of WWL70, implying a role for FAAH in MUH hydrolysis. Orlistat was able to maintain a significant inhibitory effect in the presence of WWL70. Thus, although orlistat was observed to evoke a concentration-dependent of ABHD6 activity in transfects (see Figure 5.19), it is primarily identified as an inhibitor of pancreatic lipase and DAG lipases (Lunagariya *et al.*, 2014). The mechanism of orlistat action should be the focus of further investigation with more selective DAGL inhibitors (currently not commercially

available). Unexpectedly, WWL123 in the presence of WWL70 caused a further inhibition, indicating WWL123 is not inhibiting the same activity as WWL70. Again this possibility could be tested further, possibly using the ABPP technique. Finally, in the third comparison, the hypothesis investigated was whether the presence of these inhibitors altered the inhibitory effects of WWL70. Benzil did not alter the inhibitory effect of WWL70 upon combination, suggesting these agents have divergent targets. Activities in the presence of orlistat, WWL123, JKKK048, URB597 and JZL184 also retained sensitivity to WWL70, suggesting a divergence of molecular targets. As expected, WWL70 showed no further effect upon combination with MAFP as the latter is known to inhibit ABHD6 as well as multiple other serine hydrolases. Combination with URB602, PF3845 and pristimerin failed to allow a significant effect of WWL70, suggesting a potential overlap in the molecular action of these agents.

5.5 Discussion

No single assay could be applied for screening of all the recombinant enzymes under scrutiny. NPA and MUO appear to be of limited value in the investigation of MAGL activities *in vitro* while MUH hydrolysis, by contrast, could be a promising assay for screening modulators of ABHD6 in recombinant system. In terms of assaying ABHD6 activity in ‘real’ tissues, MUH requires further optimisation to be useful.

5.5.1 4-NPA

MAGL1 was the only enzyme which showed a clearly elevated NPA hydrolytic activity compared to the vector control. This activity was apparent in both membrane and soluble fractions and in multiple biological repeats.

Background hydrolysis of NPA appeared higher in the membranes of MAGL1-HEK293 compared to the cytosolic fraction (Figure 5.6), while the cytosol appeared to be more active for similar dilution levels. This combination would make the soluble fraction the preferred source for inhibitor screening.

The binding cavity of MAGL1 seemed to accommodate the nitrophenol group, an effect not observed with the other enzymes. Notably, JZL184, a MAGL-

selective inhibitor, has a nitrophenyl substituent adjacent to the carbamate, which is the site for covalent attachment to MAGL (Long *et al.*, 2009b).

MAGL2 showed a lower level of activity compared to equivalent dilutions of MAGL1 transfects, consistent with previous radiometric enzyme assay results obtained in Chapter 1 which could be attributed to a change in the lid area of MAGL2 or a reduced efficiency of expression.

A previous report used 250 μ M 4-NPA as a final concentration for inhibitor screening in the presence of BSA (Muccioli *et al.*, 2008a). A separate study reported that MAGL activity increased with increasing BSA concentration, although using a different substrate: 7-hydroxycoumarinyl-arachidonate (7-HCA) (Wang *et al.*, 2008). It would be potentially useful in the future to investigate the effect of BSA with this NPA assay.

The results described in this report are inconsistent with a previous publication using 4-NPA as a substrate for MAGL activity inhibitor screening (Muccioli *et al.*, 2008a; Patel, 2009). The report from Muccioli *et al.* (2008a) indicated a higher affinity for hydrolysis of NPA under their conditions (0.2 mM compared to 1 mM in the current investigation). Whether this difference is a consequence of the dual tagged enzyme expressed in *E. coli* (Muccioli *et al.*, 2008) compared to the untagged enzyme expressed in mammalian HEK293 cells (this study) remains to be tested.

Although this HTS assay is cheap and practical in terms of sample handling and ease of quantification, there was an important drawback which was the high cost in terms of enzyme production, given that there was a limited dilution range over which enzymatic activity was distinguishable from background.

5.5.2 4-MUO assay

Through the use of the radiometric assay, it was apparent that all the selected enzymes recognized oleate esters since they hydrolysed 2OG. However, the lipases appeared less active with MUO as a substrate and the overall production of fluorescence was clearly low. It might be because of the difference between

the relatively small glycerol head group of 2OG compared to the very much larger 4MU of MUO, which might impede binding to the active site of these enzymes.

Although MUO appears not to have been previously used as a substrate for MAG hydrolyses, there are reports of its use for other enzymes. For example, it was investigated as a substrate of acid lipase in preparations of human leucocytes, fibroblasts and liver where it was tested at pH 4 (Koster *et al.*, 1980). Similarly, an acid lipase from human spinal cord and cerebellum was assessed with MUO as substrate at pH 5 (Hirsch *et al.*, 1977). In the current investigation, a more neutral pH of 7.4 was used to more closely mimic physiological conditions. It is possible that the assay might be more successful at lower pH, but the deviation from physiological conditions would be less likely to generate valid data.

5.5.3 Glycerol detection assay

The glycerol assay has been described as a valuable real time fluorescent based assay that can detect picomole quantities of end products (Navia-Paldanius *et al.*, 2012). A commercial kit is available for glycerol detection, but it proved impractical from an economic point of view. Attempts to replace it with a lab-made kit using simple and cheap materials, many from the same vendor, were unsuccessful. The lab generated kit, however, exhibited a reduced detection capacity with no differences between different substrates (Figure 5.13). A number of individual elements were tested and replaced to attempt to recover detection capacity without success so further investigations were discontinued. Independent investigation found that the commercial sources of Amplifu™ Red have different characteristics outcome in terms of the capacity for signal detection in the enzyme assay (personal communication with SPH Alexander).

5.5.4 4-MUH assay

It has been suggested that MUH as a substrate is much more suitable for measuring lipase activity as it is not easily hydrolysed by non-lipolytic esterases (Gilham *et al.*, 2005). Previously, MUH was used for screening lipases and esterases at a final concentration of 100 μ M (Gilham *et al.*, 2005) based on modification of the Dolinsky method (Dolinsky *et al.*, 2004). However, this is the

first study to apply the MUH assay for measuring ABHD6 activity. In transfects, this assay exhibited a marginal Z' score providing a valuable method for initial high-throughput screening for libraries of ABHD6 modulators or compounds. From a practical perspective, it is one of the more straightforward assays to put together.

Results of inhibitor screening in ABHD6 transfects (Figure 5.16 and 5.17) showed complete inhibition by JJKK048 which was also described in Chapter 3 using the radio-metric assay. JJKK048 was reported to be a selective inhibitor of MAGL with a potency (IC_{50} value) less than 0.4 nM- ($pIC_{50} \sim 9.3$) -in human (Aaltonen *et al.*, 2013). It produced a complete ABHD6 inhibition (Figure 5.17), although with lower potency (pIC_{50} value of 7.1 ± 0.06); a selectivity ratio of greater than 100-fold. WWL70 was previously described as a selective and potent ABHD6 inhibitor in human recombinants ($pIC_{50} 7.07 \pm 0.05$) (Navia-Paldanius *et al.*, 2012) and in mouse brain membrane proteasome (pIC_{50} of ~ 7.15) (Blankman *et al.*, 2007). Similarly, in MUH assay, it produced a pIC_{50} value of 7.3 ± 0.05 with slight residual activity of 6 ± 1 % control (Figure 5.17). Regarding WWL123, a previous study for the concentration inhibition curve of human ABHD6 transfects showed a complete inhibition caused by WWL123 with IC_{50} value 0.43 μ M ($pIC_{50} \sim 6.4$) using ABPP (Bachovchin *et al.*, 2010). In our study, WWL123 showed incomplete inhibition of MUH hydrolysis (residual activity of $45 \pm 2\%$ control) in the transfects with a potency of 6.3 ± 0.1 , identical to literature values. A more detailed examination using conventional Michaelis-Menten approaches might identify mechanistic differences between the different inhibitors (competitive vs non-competitive, for example). Whether the residual activity reflects the presence of an additional enzyme activity in this tissue could be explored through the application of the ABPP technique.

Orlistat (also known as tetrahydrolipostatin) is documented as a DAGL inhibitor with a pIC_{50} value of 7.2 in recombinant expression (Bisogno *et al.*, 2003). It was reported to have a pIC_{50} value of 7.32 in a glycerol detection assay for ABHD6 activity (Navia-Paldanius *et al.*, 2012). In the present study, we observed a similar potency of 6.5 ± 0.3 in this assay.

On the other hand, the inhibitor profiles in the rat hippocampus appeared to be different from that of ABHD6-transfects and the inhibitor profile in the hippocampus was itself highly variable, as shown in Figure 5.24 and 5.26. At the current time, there is no obvious explanation for this variation. A minor point of variation between the two Figures was that there was no pre-incubation between enzyme and inhibitors in Figure 5.26. Another possible explanation is that there might be some consequence of the complex mixture of proteins present in the rat hippocampus, while the transfect will have fewer non-contributing proteins. Interestingly, both circumstances identified a major inhibition by MAFP, suggesting serine hydrolases were responsible for the majority of MUH hydrolysis. Therefore, it would be useful to apply ABPP to investigate which rat hippocampal membrane proteins are tagged by the FP-rhodamine and sensitive to MUH (and WWL70, WWL123, 2OG, etc).

Despite the complicated interpretation of Figure 5.26, there were certain points worthy of focus. Benzil was an inhibitor that failed to alter MUH hydrolysis whether it was applied alone or in combination with WWL70. This is indicative that carboxylesterases do not contribute to hippocampal MUH hydrolysis.

MAFP, on the other hand, caused a significant inhibition in which was not altered in combination with WWL70. The major effect of MAFP suggests a predominant role for serine hydrolases, although a more precise definition could not be made as MAFP is a potent non-selective lipase inhibitor.

The inhibitory effects of URB597 and PF3845 suggest that FAAH might also hydrolyse MUH. This could be tested with the recombinant enzyme. Additionally, inhibition by JZL184, JJKK048, URB602 and pristimerin suggests that MAGL might also be capable of hydrolysing MUH. This contrasts with the data from the expression of MAGL isoforms, both of which were poorly active as MUH hydrolysing activities (Figure 5.14). Potentially, there might be species differences between rat and human MAGL, or the post-translational modifications in the different cellular contexts might have some influence. The application of ABPP might resolve this issue.

The effect of orlistat was independent of the effect of WWL70 and could indicate a role for DAGL in MUH hydrolysis.

A similar substrate, 6,8-difluoro-4-methylumbelliferyl octanoate (DiFMUO), has been used to screen DAGL activity in recombinant assays (Singh *et al.*, 2016). It showed that there is the potential for similar substrate being metabolized by DAGL. Since DAGL α is present in the adult brain (Gao *et al.*, 2010; Tanimura *et al.*, 2010), it might be some of the hydrolysis is mediated by DAGL. However, the ABPP approach using FP-rhodamine is reported to be unsuccessful with DAGL (Hoover *et al.*, 2008).

Results in Figure 5.26 might highlighted mechanistic differences between different inhibitors. Hypothetically, if WWL70 failed to elicit a further inhibition when combined with any of these selected agents, then the implication is that this agent and WWL70 might have a similar mechanism of action. URB602, pristimerin and PF3845 are examples of such agents.

Another potential interpretation of the data shown in Figure 5.26 is the lack of selectivity of these inhibitors. An expectation for WWL70 and WWL123 is that they should both inhibit ABHD6 selectively, while in combination (in Figure 5.26), there was further inhibition. URB597 and PF3845 (FAAH inhibitors) were anticipate to have the same effect but failed to show a similar level of inhibition. Similarly, JKKK048, JZL184, pristimerin and URB602 (MAGL inhibitors) were able to inhibit MUH hydrolysis but with a variable level indicating a lack of selectivity.

Keeping in mind MUH was not a good substrate for hMAGL (in transfects cells) (Figure 5.14) and the implications of multiple enzymes involvement with MUH in rat (as discussed above) including MAGL, this might reflect species variation. It would be useful to investigate MUH in a recombinant rat enzymes. In particular JZL184 (a gold standard inhibitor for human MAGL but not in rat (Long *et al.*, 2009a)) which caused a significant inhibition in MUH hydrolysis in rat hippocampus, it would be useful to assess its potency in rat by conducting serial inhibition curve.

It would be useful to have tissue available from mice in which the genes encoding ABHD6, ABHD12 and MAGL were disrupted in order to assess whether these inhibitors were acting selectively through these enzymes using the MUH assay in mice hippocampus preparations.

To summarize, as it has been shown above, in intestine and hippocampus, there were unpredicted and difficult to explain data in real tissues making the application of MUH to screen for ABHD6 activity impractical without further characterisation.

Chapter Six

General Discussion

6. General Discussion

6.1 Discussion

A number of key advances in cannabinoid research –aimed at generating therapeutic compounds- have been achieved over the last two decades, particularly in our understanding of the composition of the endocannabinoid system and its complexity. The study of the hydrolase enzymes is projected to be beneficial as their targeting is postulated to have a major influence on the maintenance of ECBs levels. The present thesis aimed principally to identify the biochemical characteristics and distribution (cellular and subcellular) of ABHD6 and MAGL, in recombinant systems, in preparations from animal tissues and in primary cell culture. To achieve this goal, multiple molecular, biochemical and pharmacological techniques were applied, ranging from genetic expression tools, functional activities, immunoblotting and immunostaining to ABPP.

The characterization of ABHD6 in this project suggests that there is a relative abundance of ABHD6 (at both genetic and functional levels) in the intestine, however, its role in digestion/or signalling is yet to be defined. ABHD6 was found to be abundantly active in the soluble fractions of rat small and large intestines with some male: female dimorphism apparent. This soluble ABHD6 activity, when the literature suggests the enzyme to be membrane bound, appeared independent of protease activity. Moreover, Caco-2 cells, often used in the literature as a model for human intestine, showed the highest ABHD6 activity among other screened cell lines (as discussed in Chapter 3). Thus, there is accumulating evidence implicating roles for ABHD6 (and possibly other unidentified monoacylglycerol hydrolases) in the intestine.

The data in this thesis add to the growing evidence-base describing the distribution of ABHD6. Interestingly, ABHD6 showed different subcellular localization with different positions of tags in HEK293 transfects. Using confocal microscopy and with differential interference contrast microscopy, the C terminal-tagged version was visualized around the plasma membrane while the N terminal-tag was localized around the nuclear membrane. Furthermore, using

viral infection of neurons and glial cells, ABHD6 retained activity in these primary cells, albeit to variable extents. In astrocytes, ABHD6 showed a tendency to be distributed around the nuclear membrane more than the plasma membrane using N-tagging. Notably, ABHD6 could be visualized in the cytoplasm of the cells, particularly in neuronal axons. The soluble appearance of ABHD6 was also evident in a number of studied cell lines in this thesis. The different subcellular locations of ABHD6 observed in different cells may result from differential trafficking of protein.

Chapter 4 revealed, as a precursor to rat tissue radiometric assay exploration, new insights regarding the mRNA expression of three target enzymes (ABHD6, MAGL and for the first time, X1 MAGL) in rat tissues. mRNA of ABHD6 and MAGL were extensively expressed in all tissues and consistent with the reports from literature. Generally, there were approximate equivalent levels of mRNA expression between ABHD6 and MAGL in rat neural tissues (Figure 2.1) (or even higher ABHD6 expression, as in spinal cord for example), however, in radiometric assay of these tissues (Chapter 3), the results showed predominant MAGL activity over ABHD6 (under same experimental conditions). The interpretation of this discrepancy between mRNA level and activity is complex but it might reflect that the substrate preferences are different for these two enzymes. A broad unbiased metabolomics approach to investigate the comparative effect of selective inhibitors in cells and tissues on levels of different metabolites might identify novel, ‘preferred’ substrates for these enzymes. Alternatively, mRNA transcribed from these two genes may not be translated into functional protein with the same efficiency. This could be further explored by investigating the stability of mRNA and whether there is a difference in the turnover of one compared to other which might affect the conversion into protein.

Results from the literature suggest expression of MAGL and ABHD6 activities in brain, yet a direct comparison between both enzymes, using 2OG as a substrate and under the same radiometric assay conditions, has not previously been investigated. This study addressed the enzyme distribution in the CNS and in recombinant systems by looking at their activities in the absence and presence of

reportedly-selective inhibitors. Results in Chapter 3 showed that MAGL was the major enzyme responsible for 2OG hydrolysis in different areas within rat CNS tissues (in both soluble and membrane fractions) while ABHD6 could not be reliably quantified.

A further novel aspect of the project was the characterization of the second splice variant of human MAGL. Generally, enzyme isoforms which differ substantially in their amino acid sequence are expected to differ in the kind of reaction they catalyse or reaction rates, in their substrate affinity or other functional properties (Gunning, 2001; Tomaiuolo *et al.*, 2008). In this thesis, it was found that MAGL2 appeared to differ from MAGL1 in terms of reaction rates in recombinant system (under identical experimental conditions) in both radiometric (Chapter 3) and colorimetric assays (Chapter 5).

JJKK048 was found in this study to be a potent MAGL inhibitor consistent with its description in the literature (Aaltonen *et al.*, 2013; Laitinen *et al.*, 2014) with an off target, lower potency action at ABHD6. In contrast to the literature, WWL123 showed a potency of $pIC_{50} \sim 8$ (higher than reported (Bachovchin *et al.*, 2010)) in the radiometric enzyme assay in the recombinant system and in animal tissues. This was not the case using a fluorogenic substrate in the MUH assay (Chapter 3) where WWL123 evoked a concentration-dependent inhibition with a pIC_{50} value of 6.3. The application of different assay techniques and/or conditions could generate different inhibitors potencies and this complicates interpretation of data (Navia-Paldanius *et al.*, 2012; Saario *et al.*, 2004; Woodhams, 2012). Therefore, it would be useful to have a systematic analysis of inhibitors profiles in different enzyme assays to determine whether there is a “real” variation based on enzyme methodology.

It appeared that inhibition of a single enzyme is an attractive and potentially successful approach for therapeutic exploitation of the endocannabinoid system. FAAH inhibitors as a potential drugs have been tried before and showed a failure in the clinical trials (Fowler *et al.*, 2017; Huggins *et al.*, 2012; Wagenlehner *et al.*, 2017), also see (van Esbroeck *et al.*, 2017). Thus, there is a need to explore MAGL inhibitors for a potential focused therapeutic strategies *in vivo* keeping in

mind that MAGL is the main 2-AG hydrolytic enzyme. Developing MAGL inhibitors is considered a promising approach in the treatment of inflammation, cancers, pain and other pathological conditions (see Chapter 1). However, the side effects of chronic treatment with irreversible compounds could be an obstacle toward testing these compounds beyond the pre-clinical level, which is the current status for MAGL inhibitors (Fowler, 2012). This might be possible by developing reversible MAGL inhibitors or causing less potent inhibition to elicit a more subtle effect on 2-AG accumulation at synapses. Indeed, Aghazadeh et al. (2018) have described a new class of reversible MAGL inhibitor, diphenylpyrazole derivatives with IC_{50} 0.5 μ M, with promising anti-proliferative activity in high-grade serous ovarian cancer (OVCAR3) both in *in vitro* and in *in vivo* (Aghazadeh Tabrizi *et al.*, 2018).

ABHD6 inhibitors, although only a limited number of which are currently available and have been studied, also have promising therapeutic potential (as discussed in the Introduction). The use of ABHD6 inhibitors might even have a beneficial role over the use of MAGL inhibitors, as ABHD6 inhibition leads to smaller, potentially more localised, increases in 2-AG accumulation and hence, may be associated with fewer unwanted effects, for example, through receptor desensitization (Long *et al.*, 2009b). The lack of selective ABHD12 inhibitors up to now has impeded its exploration and so the therapeutic potential of targeting this enzyme is largely unknown. Based on these observations, therefore, there was a need to develop HTS assays to facilitate the rapid discovery of useful inhibitors/substrate. However, in our hands, none of the assay methodologies applied in this study were successful for this enzyme. It is worthy to mention that, since the reports of its 2-AG hydrolase activity 10 years ago (Blankman *et al.*, 2007), there has been no further evidence to support ABHD12 belonging to ECB family. This raises questions regarding the enzymes “real” endogenous substrate preference.

In the last part of this project -Chapter 5-, a number of different substrates were assessed for *in vitro* assays for the three enzymes. Among them, MUH hydrolysis assay (with a Z score of 0.42 as an indication of assay quality and its suitability

for HTS (Wang *et al.*, 2008)) proved to be useful for ABHD6 screening in recombinant systems. However, the use of MUH as a substrate in tissue screening of ABHD6 was complicated and proved difficult to interpret.

6.2 Limitations

This work has a number of limitations. ABPP represents a useful functional enzymatic activity-based technique used to a limited extent in this study as a confirmatory tool. It was used to identify MAGL1, MAGL2 and ABHD6 with and without relevant inhibitors. However, studies were limited due to technical problems with the gel scanner. It would be useful if the soluble fraction of rat intestine could be visualized alongside the membranes in ABPP gel. This could serve to highlight the presence of ABHD6 activity in this tissue with the benefit of identifying the molecular size of the functional entity. It could also provide information about the level of inhibition by selective ABHD6 inhibitors (as a comparison) or as an off target by other non-selective inhibitors.

The paucity of primary cell availability during the project time frame limited the numbers of repetitions and further exploration of ICC. It would be useful to determine distribution of the C-tagged version of ABHD6 in these cells. This could also be applied to the tagged MAGL versions, especially MAGL2, to see if there is spatial and temporal distribution distinct from MAGL1.

Assays using 4-NPA, 4-MUO and a home-made glycerol detection method (described in Chapter 3) had drawbacks associated with their use for these enzymes and still need further optimization steps to improve their selectivity and sensitivity. Especially for the lab-made glycerol detection assay, it seemed there were subtle but relevant factors affecting its sensitivity, although it was apparently identical in terms of component final concentrations to the original reported assay. However, within the limited time of the project period, optimization could not be completed.

Finally, despite the difficulties and challenges in cloning and transfection steps (mentioned in Chapter 3), it was rewarded by providing successful sustainable resources of MAGL1, MAGL2, ABHD6, ABHD12, FAAH1 and FAAH2. The

characterization of FAAH1 and FAAH2 is to be continued by Master students. A second variant of ABHD12 (NM_015600.4, NCBI with 404 aa) was not successfully cloned, despite many optimization attempts. It is described as having an alternate 3' terminal exon compared to variant 1, resulting in a longer isoform with a distinct C-terminus compared to the one cloned in this thesis (NM_001042472.2, NCBI with 398 aa). Only one report predicted the presence of a second ABHD12 isoform (Lord *et al.*, 2013), that is of shorter length to our cloned ABHD12 (362 aa) and the authors acknowledge that it was not confirmed at the protein level. Whether a second variant is present or not, the lack of selective inhibitors limits further investigation of ABHD12.

6.3 Future perspectives

It is now widely accepted that endocannabinoids have multiple physiological, psychological and pathological effects. One area of research is now looking into how to increase endogenous ECB levels for potential therapeutic benefit by pharmacological or genetic inhibition. Generally, in order to be able to develop ABHD6/MAGLs as drug targets, it is imperative to investigate their subcellular distribution and expression in different cellular and tissue contexts and whether tissue-selective inhibitors will be crucial for effective and safe therapeutic purposes. This thesis has explored most of these aspects. However, based on our novel information regarding ABHD6/MAGL potential biochemical roles in small and large intestines (which are one of the key sites for dietary energy metabolism and transformation) and based on previous reports regarding ABHD6 involvement in metabolic diseases (Fisette *et al.*, 2016; Thomas *et al.*, 2013; Zhao *et al.*, 2016), it would be of potential benefit to focus on the roles of these enzymes in metabolic diseases. Chronic metabolic disorder is caused by impaired lipid metabolism and is associated with “low grade inflammation” (Poursharifi *et al.*, 2017); ABHD6 and MAGL are regulators of lipid metabolism so it is not difficult to propose a wider involvement for them in different metabolic diseases: obesity, cardiac disease, diabetes and insulin resistance and in non-alcoholic fatty liver disease (Pribasnig *et al.*, 2015).

Pharmacological inhibition serves as a useful investigative tool to disclose pharmacological properties of ECB (Owens et al., 2017). It increases the endogenous tone of ECB or preserves exogenously administered cannabinoids by delaying degradation (Patel, 2009). Thus, to explore how inhibition of these enzymes, *in vivo*, could affect dietary lipid metabolism in the gut, determination of MAGs species levels before and after a meal containing a selective ABHD6/MAGL inhibitor in blood plasma or specific tissues would be valuable. It would be of interest to examine orlistat, which is known to inhibit pancreatic lipase (Lunagariya *et al.*, 2014) and in our hands (Chapter 3) ABHD6 at a reasonable potency but inactive against MAGL (Bisogno *et al.*, 2006). This could be further extended in assessing acute doses of these inhibitors versus repeated chronic doses.

In particular, if a selective ABHD6 inhibitor could be synthesized that is not well absorbed but still has an activity in gut, how it might be related on long repeated administration to an animal model of inflammatory bowel disorders (ulcerative colitis and Crohn's disease model, for example), especially after a recent report describing anti-inflammatory effect of pharmacological ABHD6 inhibition in an animal model of multiple sclerosis (Wen *et al.*, 2015).

Projecting forward, it would be also useful to run similar experiments (assuming inhibitors safety) in human, especially for patients with gut diseases like inflammatory bowel diseases. It would be worthy to investigate the potential role of ABHD6 inhibition on bowel lesions and to assess the effect from acute vs repeated drug exposure including any potential side effects. The intestinal epithelium can be easily disrupted during gut inflammation (Martini *et al.*, 2017). If a comparison is made between healthy volunteers and patients by giving low doses of osmotic laxatives (such as lactulose) which are normally not absorbed by the bowel. Measurement of urinary excretion for those agents - which would indicate some absorption of lactulose- would provide an indirect index of the tightness of the gut epithelium. Imaging studies using fluorinated version (¹⁸F) of ABHD6 inhibitor/s Positron emission tomography (PET) scans can show the distribution of these agent/s, whether they stay in the gut or get absorbed.

Alternatively, we can investigate any potential therapeutic role of ABHD6 inhibition in those patients by comparing inflammatory markers such as: C-reactive protein, prostaglandins, and cytokines before and after treatment, for example.

On other hand, genetic inhibition could also represent new platform for further studies. For example, generation of conditional knockout animal models (intestinal knockouts or knockout in specific cells) would be useful to investigate changes in metabolic parameters like: MAGs species (centrally and peripherally) or appetite affection, body weight, etc.

In parallel, it would be useful to compare ABHD6 knockout animals with wildtypes to investigate WWL123 as a brain penetrant inhibitor (Naydenov et al., 2014) (on repeated administrations) on signalling pathway/s in epilepsy (as ABHD6 inhibition has been shown to be effective *in vivo*, by reducing seizures in an epilepsy model).

It is also desirable to assess whether there are genetic variation of ABHD6 in human and if there are natural variants which associate with disease/drug susceptibility/etc. For example, it would be valuable to investigate the sequences and expression levels of ABHD6 in the gut of normal volunteers and those with metabolic diseases or epilepsy.

In addition, this thesis supplies information about the expression of these enzymes in cells of the nervous system: astrocytes, microglia and neurons. However, the physiological roles in these cells were not inspected. It would be beneficial if ABHD6/MAGL were investigated *in vivo* to address its primary role in those cells using viral infection (which was successfully applied for ABHD6 in this study) as an efficient tool for gene transfer to various cells and tissues.

It is now accepted that ABHD6 is able to hydrolyse specific pools of 2-AG in brain (Blankman et al., 2007; Marris et al., 2010; Marris et al., 2011). It was stated that ABHD6 preferred 2-AG over 2OG (Navia-palidus 2012) in a glycerol detection assay. Clearly, a focus of future research must be to determine if ABHD6 has other physiological substrates *in vivo*. Therefore, it would be useful

to investigate other MAGs, in particular 2-AG and bis(monoacylglyceryl)phosphate (Pribasni \acute{c} *et al.*, 2015). However, radiolabelled 2-AG is commercially available but it is not the case for bis(monoacylglyceryl)phosphate. It may also be worthwhile to try the 1 (3)-isomer of 2-AG (as it is the preferred structure of MAGs to hABHD6)(Navia-Paldanius *et al.*, 2012). Alternatively, 1-PG was also reported to be a useful ABHD6 substrate in INS82/13 β cell extracts by HPLC (Zhao *et al.*, 2014). Screening would best be achieved with a generalised metabolomics investigation in the presence and absence of a selective inhibitors of ABHD6 (and MAGL, ABHD12, etc.) in miscellaneous cell types, for example: brain slices and liver slices. Furthermore, multiple glycerides can be detected in rat tissues ranging from palmitate, oleate, stearate to the polyunsaturated fatty acids (PUFAs) such as Docosahexaenoic acid (DHA), Eicosapentaenoic acid (EPA) (although DHA and EPA (omega-3 fats) are commercially not available but they could be synthesised).

Developing an HTS method is important in the next step of investigation for these ECB metabolising enzymes. This is especially true for MAGL2 and ABHD12, which have been characterised in only a very limited manner. I would suggest to apply MUH assay to screen for selective ABHD6 inhibitors in the recombinant system as it would be crucial for the next step of ABHD6 exploration. It would also be useful to test other substrates, for ABHD6 and other lipases. For example: screening different fatty acid esters side chain (butyryl, hexanoyl, palmitoyl, oleoyl, etc) of 4-MU (as a common substrate for all lipases (Gilham *et al.*, 2005) would be useful as well as the thioester analogue of 2-arachidonoyl glycerol: arachidonoyl-1-thioglycerol (Figure 6.1).



Figure 6.1 Chemical structure of arachidonoyl-1-thioglycerol.

The availability of relevant high throughput screening assays for compound libraries to identify inhibitors will pave the way for further investigation of different biochemical and pharmacological aspects of these enzymes and will open the door for further *in vivo* studies. Furthermore, physiological studies of all of these enzymes, with specific mutations and the use of selective enzyme inhibitors, in intact cells to study the acute regulation of enzyme activity (phosphorylation and SUMOylation, for example) in these transfects would be of high interest. Eventually, it is hoped that further studies will discover compounds with a good balance between potency and selectivity toward other potential off-targets and with therapeutic efficacy.

To conclude, this project characterized ABHD6 and MAGL1 and identified a novel MAGL2 in different host contexts. This study set up and developed a high throughput screening *in vitro* assay for ABHD6 to test and broaden its substrate/inhibitor library profile in the future. It is anticipated that the information from these studies will aid in more complete understanding of the role of endocannabinoid system and provide significant bearing on the therapeutic potential of these enzymes.

7. References:

Aaltonen N, Savinainen Juha R, Ribas Casandra R, Rönkkö J, Kuusisto A, Korhonen J, *et al.* (2013). Piperazine and Piperidine Triazole Ureas as Ultrapotent and Highly Selective Inhibitors of Monoacylglycerol Lipase. *Chem. Biol.* **20**(3): 379-390.

Abelaira HM, Reus GZ, Neotti MV, Quevedo J (2014). The role of mTOR in depression and antidepressant responses. *Life sciences* **101**(1-2): 10-14.

Aboud ME, Sorensen RG, Stella N (2012). *endoCANNABINOIDS: Actions at Non-CB1/CB2 Cannabinoid Receptors*. edn. Springer New York.

Adams IB, Martin BR (1996). Cannabis: pharmacology and toxicology in animals and humans. *Addiction* **91**(11): 1585-1614.

Agarwal N, Pacher P, Tegeder I, Amaya F, Constantin CE, Brenner GJ, *et al.* (2007a). Cannabinoids mediate analgesia largely via peripheral type 1 cannabinoid receptors in nociceptors. *Nat. Neurosci.* **10**(7): 870-879.

Agarwal N, Pacher P, Tegeder I, Amaya F, Constantin CE, Brenner GJ, *et al.* (2007b). Cannabinoids mediate analgesia largely via peripheral type 1 cannabinoid receptors in nociceptors. *Nat. Neurosci.* **10**(7): 870-879.

Aghazadeh Tabrizi M, Baraldi PG, Baraldi S, Ruggiero E, De Stefano L, Rizzolio F, *et al.* (2018). Discovery of 1,5-Diphenylpyrazole-3-Carboxamide Derivatives as Potent, Reversible, and Selective Monoacylglycerol Lipase (MAGL) Inhibitors. *J. Med. Chem.* **61**(3): 1340-1354.

Ahn K, Johnson DS, Cravatt BF (2009a). Fatty acid amide hydrolase as a potential therapeutic target for the treatment of pain and CNS disorders. *Expert opinion on drug discovery* **4**(7): 763-784.

Ahn K, Johnson DS, Mileni M, Beidler D, Long JZ, McKinney MK, *et al.* (2009b). Discovery and characterization of a highly selective FAAH inhibitor that reduces inflammatory pain. *Chem. Biol.* **16**(4): 411-420.

Ahn K, McKinney MK, Cravatt BF (2008). Enzymatic Pathways That Regulate Endocannabinoid Signaling in the Nervous System. *Chem. Rev.* **108**(5): 1687-1707.

Alexander SPH (2014). Cannabinoids and the Brain. In: (ed)^(eds). *eLS*, edn: John Wiley & Sons, Ltd. p^pp.

Alhouayek M, Lambert DM, Delzenne NM, Cani PD, Muccioli GG (2011). Increasing endogenous 2-arachidonoylglycerol levels counteracts colitis and related systemic inflammation. *FASEB journal : official publication of the Federation of American Societies for Experimental Biology* **25**(8): 2711-2721.

Alhouayek M, Masquelier J, Cani PD, Lambert DM, Muccioli GG (2013). Implication of the anti-inflammatory bioactive lipid prostaglandin D2-glycerol ester in the control of macrophage activation and inflammation by ABHD6. *Proceedings of the National Academy of Sciences of the United States of America* **110**(43): 17558-17563.

Alhouayek M, Masquelier J, Muccioli GG (2014). Controlling 2-arachidonoylglycerol metabolism as an anti-inflammatory strategy. *Drug Discovery Today* **19**(3): 295-304.

Ameri A (1999). The effects of cannabinoids on the brain. *Prog. Neurobiol.* **58**(4): 315-348.

Aquila S, Guido C, Santoro A, Perrotta I, Laezza C, Bifulco M, *et al.* (2010). Human Sperm Anatomy: Ultrastructural Localization of the Cannabinoid1 Receptor and a Potential Role of Anandamide in Sperm Survival and Acrosome Reaction. *The Anatomical Record* **293**(2): 298-309.

Atwood BK, Straiker A, Mackie K (2012). CB(2) cannabinoid receptors inhibit synaptic transmission when expressed in cultured autaptic neurons. *Neuropharmacology* **63**(4): 514-523.

Bachovchin DA, Ji T, Li W, Simon GM, Blankman JL, Adibekian A, *et al.* (2010). Superfamily-wide portrait of serine hydrolase inhibition achieved by library-versus-library screening. *Proceedings of the National Academy of Sciences* **107**(49): 20941-20946.

Baggelaar MP, Chameau PJP, Kantae V, Hummel J, Hsu K-L, Janssen F, *et al.* (2015). Highly Selective, Reversible Inhibitor Identified by Comparative Chemoproteomics Modulates Diacylglycerol Lipase Activity in Neurons. *J. Am. Chem. Soc.* **137**(27): 8851-8857.

Baggelaar MP, van Esbroeck ACM, van Rooden EJ, Florea BI, Overkleeft HS, Marsicano G, *et al.* (2017). Chemical Proteomics Maps Brain Region Specific Activity of Endocannabinoid Hydrolases. *ACS Chemical Biology* **12**(3): 852-861.

Basso L, Altier C (2017). Transient Receptor Potential Channels in neuropathic pain. *Current opinion in pharmacology* **32**: 9-15.

Beltramo M, Bernardini N, Bertorelli R, Campanella M, Nicolussi E, Fredduzzi S, *et al.* (2006). CB2 receptor-mediated antihyperalgesia: possible direct involvement of neural mechanisms. *The European journal of neuroscience* **23**(6): 1530-1538.

Benard G, Massa F, Puente N, Lourenco J, Bellocchio L, Soria-Gomez E, *et al.* (2012). Mitochondrial CB(1) receptors regulate neuronal energy metabolism. *Nat. Neurosci.* **15**(4): 558-564.

Benito C, Tolón RM, Pazos MR, Núñez E, Castillo AI, Romero J (2008). Cannabinoid CB(2) receptors in human brain inflammation. *Br. J. Pharmacol.* **153**(2): 277-285.

Berdan CA, Erion KA, Burritt NE, Corkey BE, Deeney JT (2016). Inhibition of Monoacylglycerol Lipase Activity Decreases Glucose-Stimulated Insulin Secretion in INS-1 (832/13) Cells and Rat Islets. *PLoS One* **11**(2): e0149008.

Berg OG, Gelb MH, Tsai M-D, Jain MK (2001). Interfacial Enzymology: The Secreted Phospholipase A2-Paradigm. *Chem. Rev.* **101**(9): 2613-2654.

Bertrand T, Auge F, Houtmann J, Rak A, Vallee F, Mikol V, *et al.* (2010). Structural basis for human monoglyceride lipase inhibition. *Journal of molecular biology* **396**(3): 663-673.

Biegon A (2004). Cannabinoids as neuroprotective agents in traumatic brain injury. *Curr. Pharm. Des.* **10**(18): 2177-2183.

Biosystems A (2008). Guide to Performing Relative Quantitation of Gene Expression Using Real-Time Quantitative PCR.

Bisogno T (2008). Endogenous cannabinoids: structure and metabolism. *J. Neuroendocrinol.* **20 Suppl 1**: 1-9.

Bisogno T, Cascio MG, Saha B, Mahadevan A, Urbani P, Minassi A, *et al.* (2006). Development of the first potent and specific inhibitors of endocannabinoid biosynthesis. *Biochimica et Biophysica Acta (BBA) - Molecular and Cell Biology of Lipids* **1761**(2): 205-212.

Bisogno T, Howell F, Williams G, Minassi A, Cascio MG, Ligresti A, *et al.* (2003). Cloning of the first sn1-DAG lipases points to the spatial and temporal regulation of endocannabinoid signaling in the brain. *The Journal of cell biology* **163**(3): 463-468.

Bisogno T, Petrocellis L, Marzo V (2002). Fatty Acid Amide Hydrolase, an Enzyme with Many Bioactive Substrates. Possible Therapeutic Implications. *Curr. Pharm. Des.* **8**(7): 533-547.

Björklund E, Norén E, Nilsson J, Fowler CJ (2010). Inhibition of monoacylglycerol lipase by troglitazone, N-arachidonoyl dopamine and the irreversible inhibitor JZL184: comparison of two different assays. *Br. J. Pharmacol.* **161**(7): 1512-1526.

Blankman JL, Cravatt BF (2013). Chemical probes of endocannabinoid metabolism. *Pharmacol. Rev.* **65**(2): 849-871.

Blankman JL, Simon GM, Cravatt BF (2007). A comprehensive profile of brain enzymes that hydrolyze the endocannabinoid 2-arachidonoylglycerol. *Chem. Biol.* **14**(12): 1347-1356.

Bliss TVP, Lømo T (1973). Long-lasting potentiation of synaptic transmission in the dentate area of the anaesthetized rabbit following stimulation of the perforant path. *The Journal of Physiology* **232**(2): 331-356.

Boldrup L, Wilson SJ, Barbier AJ, Fowler CJ (2004). A simple stopped assay for fatty acid amide hydrolase avoiding the use of a chloroform extraction phase. *J. Biochem. Biophys. Methods* **60**(2): 171-177.

Bookout AL, Mangelsdorf DJ (2003). Quantitative real-time PCR protocol for analysis of nuclear receptor signaling pathways. *Nuclear Receptor Signaling* **1**: e012.

Bosier B, Muccioli GG, Lambert DM (2013). The FAAH inhibitor URB597 efficiently reduces tyrosine hydroxylase expression through CB1- and FAAH-independent mechanisms. *Br. J. Pharmacol.* **169**(4): 794-807.

Bouaboula M, Poinot-Chazel C, Bourrie B, Canat X, Calandra B, Rinaldi-Carmona M, *et al.* (1995). Activation of mitogen-activated protein kinases by stimulation of the central cannabinoid receptor CB1. *Biochem. J.* **312** (Pt 2): 637-641.

Bridges D, Ahmad K, Rice ASC (2001). The synthetic cannabinoid WIN55,212-2 attenuates hyperalgesia and allodynia in a rat model of neuropathic pain. *Br. J. Pharmacol.* **133**(4): 586-594.

Bronstein R, Torres L, Nissen JC, Tsirka SE (2013). Culturing Microglia from the Neonatal and Adult Central Nervous System. *Journal of visualized experiments : JoVE*(78): 10.3791/50647.

Buczynski MW, Parsons LH (2010). Quantification of brain endocannabinoid levels: methods, interpretations and pitfalls. *British journal of pharmacology* **160**(3): 423-442.

Busquets-Garcia A, Bains J, Marsicano G (2017). CB1 Receptor Signaling in the Brain: Extracting Specificity from Ubiquity. *Neuropsychopharmacology* **43**: 4.

Bustin SA (2002). Quantification of mRNA using real-time reverse transcription PCR (RT-PCR): trends and problems. *J. Mol. Endocrinol.* **29**(1): 23-39.

Caño GGd, Aretxabala X, González-Burguera I, Montaña M, Jesús MLd, Barrondo S, *et al.* (2015). Nuclear diacylglycerol lipase- α in rat brain cortical neurons: evidence of 2-arachidonoylglycerol production in concert with phospholipase C- β activity. *J. Neurochem.* **132**(5): 489-503.

Chakrabarti A, Onaivi ES, Chaudhuri G (1995). Cloning and sequencing of a cDNA encoding the mouse brain-type cannabinoid receptor protein. *DNA Seq.* **5**(6): 385-388.

Chang JW, Coggnetta AB, 3rd, Niphakis MJ, Cravatt BF (2013). Proteome-wide reactivity profiling identifies diverse carbamate chemotypes tuned for serine hydrolase inhibition. *ACS chemical biology* **8**(7): 1590-1599.

Chang JW, Niphakis MJ, Lum KM, Coggnetta AB, 3rd, Wang C, Matthews ML, *et al.* (2012). Highly selective inhibitors of monoacylglycerol lipase bearing a reactive group that is bioisosteric with endocannabinoid substrates. *Chem. Biol.* **19**(5): 579-588.

Chen R, Zhang J, Wu Y, Wang D, Feng G, Tang Y-P, *et al.* (2012). Monoacylglycerol lipase is a new therapeutic target for Alzheimer's disease. *Cell reports* **2**(5): 1329-1339.

Chesworth R, Long LE, Weickert CS, Karl T (2018). The Endocannabinoid System across Postnatal Development in Transmembrane Domain Neuregulin 1 Mutant Mice. *Frontiers in Psychiatry* **9**: 11.

Chicca A, Nicolussi S, Bartholomäus R, Blunder M, Aparisi Rey A, Petrucci V, *et al.* (2017). Chemical probes to potently and selectively inhibit endocannabinoid cellular reuptake. *Proc. Natl. Acad. Sci. U. S. A.* **114**(25): E5006-E5015.

Chon SH, Zhou YX, Dixon JL, Storch J (2007). Intestinal monoacylglycerol metabolism: developmental and nutritional regulation of monoacylglycerol lipase and monoacylglycerol acyltransferase. *The Journal of biological chemistry* **282**(46): 33346-33357.

Croft W, Reusch K, Tilunaite A, Russell NA, Thul R, Bellamy TC (2016). Probabilistic encoding of stimulus strength in astrocyte global calcium signals. *Glia* **64**(4): 537-552.

Cunha P, Romão AM, Mascarenhas-Melo F, Teixeira HM, Reis F (2011). Endocannabinoid system in cardiovascular disorders - new pharmacotherapeutic opportunities. *Journal of Pharmacy and Bioallied Sciences* **3**(3): 350-360.

Dajas-Bailador F, Jones EV, Whitmarsh AJ (2008). The JIP1 Scaffold Protein Regulates Axonal Development in Cortical Neurons. *Curr. Biol.* **18**(3): 221-226.

Delgado-Peraza F, Ahn KH, Nogueras-Ortiz C, Mungrue IN, Mackie K, Kendall DA, *et al.* (2016). Mechanisms of Biased β -Arrestin-Mediated Signaling Downstream from the Cannabinoid 1 Receptor. *Mol. Pharmacol.* **89**(6): 618-629.

den Boon FS, Chameau P, Schaafsma-Zhao Q, van Aken W, Bari M, Oddi S, *et al.* (2012). Excitability of prefrontal cortical pyramidal neurons is modulated by activation of intracellular type-2 cannabinoid receptors. *Proceedings of the National Academy of Sciences of the United States of America* **109**(9): 3534-3539.

Deutsch DG, Chin SA (1993). Enzymatic synthesis and degradation of anandamide, a cannabinoid receptor agonist. *Biochem. Pharmacol.* **46**(5): 791-796.

Deutsch DG, Omeir R, Arreaza G, Salehani D, Prestwich GD, Huang Z, *et al.* (1997). Methyl arachidonyl fluorophosphonate: a potent irreversible inhibitor of anandamide amidase. *Biochem. Pharmacol.* **53**(3): 255-260.

Devane WA, Dysarz FA, 3rd, Johnson MR, Melvin LS, Howlett AC (1988). Determination and characterization of a cannabinoid receptor in rat brain. *Mol. Pharmacol.* **34**(5): 605-613.

Devane WA, Hanus L, Breuer A, Pertwee RG, Stevenson LA, Griffin G, *et al.* (1992). Isolation and structure of a brain constituent that binds to the cannabinoid receptor. *Science* **258**(5090): 1946-1949.

Di Marzo V (2008). Targeting the endocannabinoid system: to enhance or reduce? *Nature reviews. Drug discovery* **7**(5): 438-455.

Di Marzo V, Fontana A, Cadas H, Schinelli S, Cimino G, Schwartz JC, *et al.* (1994). Formation and inactivation of endogenous cannabinoid anandamide in central neurons. *Nature* **372**(6507): 686-691.

Di Marzo V, Petrosino S (2007). Endocannabinoids and the regulation of their levels in health and disease. *Curr. Opin. Lipidol.* **18**(2): 129-140.

Dinh TP, Carpenter D, Leslie FM, Freund TF, Katona I, Sensi SL, *et al.* (2002a). Brain monoglyceride lipase participating in endocannabinoid inactivation. *Proceedings of the National Academy of Sciences of the United States of America* **99**(16): 10819-10824.

Dinh TP, Freund TF, Piomelli D (2002b). A role for monoglyceride lipase in 2-arachidonoylglycerol inactivation. *Chem. Phys. Lipids* **121**(1-2): 149-158.

Dinh TP, Freund TF, Piomelli D (2002c). A role for monoglyceride lipase in 2-arachidonoylglycerol inactivation. *Chem. Phys. Lipids* **121**(1-2): 149-158.

Dinh TP, Kathuria S, Piomelli D (2004). RNA interference suggests a primary role for monoacylglycerol lipase in the degradation of the endocannabinoid 2-arachidonoylglycerol. *Mol. Pharmacol.* **66**(5): 1260-1264.

Dobrucki JW, Feret D, Noatynska A (2007). Scattering of exciting light by live cells in fluorescence confocal imaging: phototoxic effects and relevance for FRAP studies. *Biophys. J.* **93**(5): 1778-1786.

Dolinsky VW, Douglas DN, Lehner R, Vance DE (2004). Regulation of the enzymes of hepatic microsomal triacylglycerol lipolysis and re-esterification by the glucocorticoid dexamethasone. *Biochem. J.* **378**(3): 967-974.

Douglass JD, Zhou YX, Wu A, Zadrogra JA, Gajda AM, Lackey AI, *et al.* (2015). Global deletion of MGL in mice delays lipid absorption and alters energy homeostasis and diet-induced obesity. *J. Lipid Res.* **56**(6): 1153-1171.

Duncan M, Thomas AD, Cluny NL, Patel A, Patel KD, Lutz B, *et al.* (2008). Distribution and function of monoacylglycerol lipase in the gastrointestinal tract. *American journal of physiology. Gastrointestinal and liver physiology* **295**(6): G1255-1265.

Earleywine M (2002). *Understanding marijuana : a new look at the scientific evidence.* edn. Oxford University Press: New York.

Egertova M, Elphick MR (2000). Localisation of cannabinoid receptors in the rat brain using antibodies to the intracellular C-terminal tail of CB. *The Journal of comparative neurology* **422**(2): 159-171.

Elphick MR, Egertova M (2001). The neurobiology and evolution of cannabinoid signalling. *Philos. Trans. R. Soc. Lond. B. Biol. Sci.* **356**(1407): 381-408.

Farquhar-Smith WP, Egertova M, Bradbury EJ, McMahon SB, Rice AS, Elphick MR (2000). Cannabinoid CB(1) receptor expression in rat spinal cord. *Mol. Cell. Neurosci.* **15**(6): 510-521.

Fisette A, Tobin S, Decarie-Spain L, Bouyakdan K, Peyot ML, Madiraju SRM, et al. (2016). alpha/beta-Hydrolase Domain 6 in the Ventromedial Hypothalamus Controls Energy Metabolism Flexibility. *Cell Rep* **17**(5): 1217-1226.

Fiskerstrand T, H'Mida-Ben Brahim D, Johansson S, M'Zahem A, Haukanes BI, Drouot N, et al. (2010). Mutations in ABHD12 cause the neurodegenerative disease PHARC: An inborn error of endocannabinoid metabolism. *Am. J. Hum. Genet.* **87**(3): 410-417.

Fisyunov A, Tsintsadze V, Min R, Burnashev N, Lozovaya N (2006). Cannabinoids modulate the P-type high-voltage-activated calcium currents in purkinje neurons. *Journal of neurophysiology* **96**(3): 1267-1277.

Fowler CJ (2007). The contribution of cyclooxygenase-2 to endocannabinoid metabolism and action. *Br. J. Pharmacol.* **152**(5): 594-601.

Fowler CJ (2014). Has FLAT fallen flat? *Trends Pharmacol. Sci.* **35**(2): 51-52.

Fowler CJ (2012). Monoacylglycerol lipase – a target for drug development? *Br. J. Pharmacol.* **166**(5): 1568-1585.

Fowler CJ, Doherty P, Alexander SPH (2017). Endocannabinoid Turnover. *Adv. Pharmacol.* **80**: 31-66.

Fowler CJ, Jonsson KO, Tiger G (2001). Fatty acid amide hydrolase: biochemistry, pharmacology, and therapeutic possibilities for an enzyme hydrolyzing anandamide, 2-arachidonoylglycerol, palmitoylethanolamide, and oleamide. *Biochem. Pharmacol.* **62**(5): 517-526.

Fredrikson G, Stralfors P, Nilsson NO, Belfrage P (1981). Hormone-sensitive lipase of rat adipose tissue. Purification and some properties. *The Journal of biological chemistry* **256**(12): 6311-6320.

Fredriksson R, Lagerstrom MC, Lundin LG, Schioth HB (2003). The G-protein-coupled receptors in the human genome form five main families. Phylogenetic analysis, paralogon groups, and fingerprints. *Mol. Pharmacol.* **63**(6): 1256-1272.

Freund TF, Katona I, Piomelli D (2003). Role of endogenous cannabinoids in synaptic signaling. *Physiol. Rev.* **83**(3): 1017-1066.

Fu J, Bottegoni G, Sasso O, Bertorelli R, Rocchia W, Masetti M, *et al.* (2011). A catalytically silent FAAH-1 variant drives anandamide transport in neurons. *Nat. Neurosci.* **15**(1): 64-69.

Galiegue S, Mary S, Marchand J, Dussosoy D, Carriere D, Carayon P, *et al.* (1995). Expression of central and peripheral cannabinoid receptors in human immune tissues and leukocyte subpopulations. *Eur. J. Biochem.* **232**(1): 54-61.

Galva C, Artigas P, Gatto C (2012). Nuclear Na(+)/K(+)-ATPase plays an active role in nucleoplasmic Ca(2+) homeostasis. *J. Cell Sci.* **125**(24): 6137-6147.

Gantz I, Muraoka A, Yang YK, Samuelson LC, Zimmerman EM, Cook H, *et al.* (1997). Cloning and chromosomal localization of a gene (GPR18) encoding a novel seven transmembrane receptor highly expressed in spleen and testis. *Genomics* **42**(3): 462-466.

Gao Y, Vasilyev DV, Goncalves MB, Howell FV, Hobbs C, Reisenberg M, *et al.* (2010). Loss of retrograde endocannabinoid signaling and reduced adult neurogenesis in diacylglycerol lipase knock-out mice. *The Journal of neuroscience : the official journal of the Society for Neuroscience* **30**(6): 2017-2024.

Gaoni Y, Mechoulam R (1964). Isolation, Structure, and Partial Synthesis of an Active Constituent of Hashish. *J. Am. Chem. Soc.* **86**(8): 1646-1647.

Gerard CM, Mollereau C, Vassart G, Parmentier M (1991). Molecular cloning of a human cannabinoid receptor which is also expressed in testis. *Biochem. J.* **279** (Pt 1): 129-134.

Gertsch J, Pertwee RG, Di Marzo V (2010). Phytocannabinoids beyond the Cannabis plant - do they exist? *British journal of pharmacology* **160**(3): 523-529.

Ghafouri N, Tiger G, Razdan RK, Mahadevan A, Pertwee RG, Martin BR, *et al.* (2004). Inhibition of monoacylglycerol lipase and fatty acid amide hydrolase by analogues of 2-arachidonoylglycerol. *Br. J. Pharmacol.* **143**(6): 774-784.

Gilham D, Lehner R (2005). Techniques to measure lipase and esterase activity in vitro. *Methods* **36**(2): 139-147.

Gonsiorek W, Lunn C, Fan X, Narula S, Lundell D, Hipkin RW (2000). Endocannabinoid 2-arachidonyl glycerol is a full agonist through human type 2 cannabinoid receptor: antagonism by anandamide. *Mol. Pharmacol.* **57**(5): 1045-1050.

Grabner GF, Eichmann TO, Wagner B, Gao Y, Farzi A, Taschler U, *et al.* (2016). Deletion of Monoglyceride Lipase in Astrocytes Attenuates Lipopolysaccharide-induced Neuroinflammation. *The Journal of biological chemistry* **291**(2): 913-923.

Grabner GF, Zimmermann R, Schicho R, Taschler U (2017). Monoglyceride lipase as a drug target: At the crossroads of arachidonic acid metabolism and endocannabinoid signaling. *Pharmacol. Ther.* **175**: 35-46.

Griebel G, Pichat P, Beeské S, Leroy T, Redon N, Jacquet A, *et al.* (2015). Selective blockade of the hydrolysis of the endocannabinoid 2-arachidonoylglycerol impairs learning and memory performance while producing antinociceptive activity in rodents. *Scientific Reports* **5**: 7642.

Gruner BM, Schulze CJ, Yang D, Ogasawara D, Dix MM, Rogers ZN, *et al.* (2016). An in vivo multiplexed small-molecule screening platform. *Nature methods* **13**(10): 883-889.

Guilbault GGa, Hieserman J (1969). Fluorometric substrate for sulfatase and lipase. *Anal. Chem.* **41**(14): 2006-2009.

Guindon J, Guijarro A, Piomelli D, Hohmann AG (2011). Peripheral antinociceptive effects of inhibitors of monoacylglycerol lipase in a rat model of inflammatory pain. *Br. J. Pharmacol.* **163**(7): 1464-1478.

Gunning PW (2001). Protein Isoforms and Isozymes. In: (ed)^(eds). *eLS*, edn: John Wiley & Sons, Ltd. p^pp.

Hall W, Solowij N (1998). Adverse effects of cannabis. *Lancet* **352**(9140): 1611-1616.

Hansen KB, Rosenkilde MM, Knop FK, Wellner N, Diep TA, Rehfeld JF, *et al.* (2011). 2-Oleoyl Glycerol Is a GPR119 Agonist and Signals GLP-1 Release in Humans. *The Journal of Clinical Endocrinology & Metabolism* **96**(9): E1409-E1417.

Hanus LO (2009). Pharmacological and therapeutic secrets of plant and brain (endo)cannabinoids. *Med. Res. Rev.* **29**(2): 213-271.

Hanus LO, Mechoulam R (2010). Novel natural and synthetic ligands of the endocannabinoid system. *Curr. Med. Chem.* **17**(14): 1341-1359.

Hartley JL, Temple GF, Brasch MA (2000). DNA cloning using in vitro site-specific recombination. *Genome research* **10**(11): 1788-1795.

Henley JM, Wilkinson KA (2016). Synaptic AMPA receptor composition in development, plasticity and disease. *Nature Reviews Neuroscience* **17**: 337.

Herkenham M, Lynn AB, Little MD, Johnson MR, Melvin LS, de Costa BR, *et al.* (1990). Cannabinoid receptor localization in brain. *Proceedings of the National Academy of Sciences of the United States of America* **87**(5): 1932-1936.

Hillard CJ, Harris RA, Bloom AS (1985). Effects of the cannabinoids on physical properties of brain membranes and phospholipid vesicles: fluorescence studies. *The Journal of pharmacology and experimental therapeutics* **232**(3): 579-588.

Hirsch HE, Wernicke JF, Myers LW, Parks ME (1977). ACID LIPASE-ESTERASE (4-METHYLUMBELLIFERYL OLEATE HYDROLASE) OF WHITE MATTER LOCALIZED IN OLIGODENDROCYTE CELL BODIES1. *J. Neurochem.* **29**(6): 979-985.

Ho SY, Delgado L, Storch J (2002). Monoacylglycerol metabolism in human intestinal Caco-2 cells: evidence for metabolic compartmentation and hydrolysis. *The Journal of biological chemistry* **277**(3): 1816-1823.

Ho WS, Randall MD (2007). Endothelium-dependent metabolism by endocannabinoid hydrolases and cyclooxygenases limits vasorelaxation to anandamide and 2-arachidonoylglycerol. *Br. J. Pharmacol.* **150**(5): 641-651.

Hohmann AG (2007). Inhibitors of monoacylglycerol lipase as novel analgesics. *Br. J. Pharmacol.* **150**(6): 673-675.

Hohmann AG, Suplita RL, Bolton NM, Neely MH, Fegley D, Mangieri R, *et al.* (2005). An endocannabinoid mechanism for stress-induced analgesia. *Nature* **435**(7045): 1108-1112.

Holmquist M (2000). Alpha/Beta-hydrolase fold enzymes: structures, functions and mechanisms. *Current protein & peptide science* **1**(2): 209-235.

Holtbäck U, Brismar H, DiBona GF, Fu M, Greengard P, Aperia A (1999). Receptor recruitment: A mechanism for interactions between G protein-coupled receptors. *Proceedings of the National Academy of Sciences* **96**(13): 7271-7275.

Hoover HS, Blankman JL, Niessen S, Cravatt BF (2008). Selectivity of inhibitors of endocannabinoid biosynthesis evaluated by activity-based protein profiling. *Bioorg. Med. Chem. Lett.* **18**(22): 5838-5841.

Howlett AC, Barth F, Bonner TI, Cabral G, Casellas P, Devane WA, *et al.* (2002). International Union of Pharmacology. XXVII. Classification of cannabinoid receptors. *Pharmacol. Rev.* **54**(2): 161-202.

Howlett AC, Qualy JM, Khachatrian LL (1986). Involvement of Gi in the inhibition of adenylate cyclase by cannabimimetic drugs. *Mol. Pharmacol.* **29**(3): 307-313.

Hsu KL, Tsuboi K, Chang JW, Whitby LR, Speers AE, Pugh H, *et al.* (2013). Discovery and optimization of piperidyl-1,2,3-triazole ureas as potent, selective, and in vivo-active inhibitors of alpha/beta-hydrolase domain containing 6 (ABHD6). *Journal of medicinal chemistry* **56**(21): 8270-8279.

Hsu KL, Tsuboi K, Speers AE, Brown SJ, Spicer T, Fernandez-Vega V, *et al.* (2010). Optimization and characterization of triazole urea inhibitors for abhydrolase domain containing protein 6 (ABHD6). In: (ed)^(eds). *Probe Reports from the NIH Molecular Libraries Program*, edn. Bethesda MD. p^pp.

Hu W-R, Lian Y-F, Peng L-X, Lei J-J, Deng C-C, Xu M, *et al.* (2014). Monoacylglycerol lipase promotes metastases in nasopharyngeal carcinoma. *International Journal of Clinical and Experimental Pathology* **7**(7): 3704-3713.

Huang SM, Bisogno T, Trevisani M, Al-Hayani A, De Petrocellis L, Fezza F, *et al.* (2002). An endogenous capsaicin-like substance with high potency at recombinant and native vanilloid VR1 receptors. *Proceedings of the National Academy of Sciences of the United States of America* **99**(12): 8400-8405.

Huganir RL, Nicoll RA (2013). AMPARs and Synaptic Plasticity: The Last 25 Years. *Neuron* **80**(3): 704-717.

Huggins JP, Smart TS, Langman S, Taylor L, Young T (2012). An efficient randomised, placebo-controlled clinical trial with the irreversible fatty acid amide hydrolase-1 inhibitor PF-04457845, which modulates endocannabinoids but fails to induce effective analgesia in patients with pain due to osteoarthritis of the knee. *Pain* **153**(9): 1837-1846.

Hwang LH, Gilboa E (1984). Expression of genes introduced into cells by retroviral infection is more efficient than that of genes introduced into cells by DNA transfection. *J. Virol.* **50**(2): 417-424.

Hyatt JL, Tsurkan L, Wierdl M, Edwards CC, Danks MK, Potter PM (2006). Intracellular inhibition of carboxylesterases by benzil: modulation of CPT-11 cytotoxicity. *Molecular cancer therapeutics* **5**(9): 2281-2288.

Ibrahim MM, Deng H, Zvonok A, Cockayne DA, Kwan J, Mata HP, *et al.* (2003). Activation of CB(2) cannabinoid receptors by AM1241 inhibits experimental

neuropathic pain: Pain inhibition by receptors not present in the CNS. *Proc. Natl. Acad. Sci. U. S. A.* **100**(18): 10529-10533.

Irving AJ, Rae MG, Coutts AA (2002). Cannabinoids on the Brain. *TheScientificWorldJOURNAL* **2**.

Iwasaki Y, Saito O, Tanabe M, Inayoshi K, Kobata K, Uno S, *et al.* (2008). Monoacylglycerols Activate Capsaicin Receptor, TRPV1. *Lipids* **43**(6): 471-483.

Jacks TJ, Kircher HW (1967). Fluorometric assay for the hydrolytic activity of lipase using fatty acyl esters of 4-methylumbelliferone. *Anal. Biochem.* **21**(2): 279-285.

Jain T, Wager-Miller J, Mackie K, Straiker A (2013). Diacylglycerol Lipase α (DAGL α) and DAGL β Cooperatively Regulate the Production of 2-Arachidonoyl Glycerol in Autaptic Hippocampal Neurons. *Mol. Pharmacol.* **84**(2): 296-302.

Jiang W, Hua R, Wei M, Li C, Qiu Z, Yang X, *et al.* (2015). An optimized method for high-titer lentivirus preparations without ultracentrifugation. *Scientific Reports* **5**: 13875.

Johnson DE, Heald SL, Dally RD, Janis RA (1993). Isolation, identification and synthesis of an endogenous arachidonic amide that inhibits calcium channel antagonist 1,4-dihydropyridine binding. *Prostaglandins Leukot. Essent. Fatty Acids* **48**(6): 429-437.

Kano M (2014). Control of synaptic function by endocannabinoid-mediated retrograde signaling. *Proceedings of the Japan Academy. Series B, Physical and biological sciences* **90**(7): 235-250.

Karbarz MJ, Luo L, Chang L, Tham CS, Palmer JA, Wilson SJ, *et al.* (2009). Biochemical and biological properties of 4-(3-phenyl-[1,2,4] thiadiazol-5-yl)-piperazine-1-carboxylic acid phenylamide, a mechanism-based inhibitor of fatty acid amide hydrolase. *Anesth. Analg.* **108**(1): 316-329.

Karlsson M, Contreras JA, Hellman U, Tornqvist H, Holm C (1997). cDNA cloning, tissue distribution, and identification of the catalytic triad of monoglyceride lipase. Evolutionary relationship to esterases, lysophospholipases, and haloperoxidases. *The Journal of biological chemistry* **272**(43): 27218-27223.

Karlsson M, Reue K, Xia Y-R, Lusi AJ, Langin D, Tornqvist H, *et al.* (2001). Exon-intron organization and chromosomal localization of the mouse monoglyceride lipase gene. *Gene* **272**(1): 11-18.

Kathuria S, Gaetani S, Fegley D, Valino F, Duranti A, Tontini A, *et al.* (2003). Modulation of anxiety through blockade of anandamide hydrolysis. *Nat. Med.* **9**(1): 76-81.

Katona I, Urbán GM, Wallace M, Ledent C, Jung K-M, Piomelli D, *et al.* (2006). Molecular Composition of the Endocannabinoid System at Glutamatergic Synapses. *The Journal of neuroscience : the official journal of the Society for Neuroscience* **26**(21): 5628-5637.

Kaufmann WE, Worley PF, Pegg J, Bremer M, Isakson P (1996). COX-2, a synaptically induced enzyme, is expressed by excitatory neurons at postsynaptic sites in rat cerebral cortex. *Proceedings of the National Academy of Sciences of the United States of America* **93**(6): 2317-2321.

Kaur J (2014). A comprehensive review on metabolic syndrome. *Cardiology research and practice* **2014**: 943162.

Kim J, Alger BE (2004). Inhibition of cyclooxygenase-2 potentiates retrograde endocannabinoid effects in hippocampus. *Nat. Neurosci.* **7**(7): 697-698.

King AR, Dotsey EY, Lodola A, Jung KM, Ghomian A, Qiu Y, *et al.* (2009). Discovery of Potent and Reversible Monoacylglycerol Lipase Inhibitors. *Chem. Biol.* **16**(10): 1045-1052.

King AR, Duranti A, Tontini A, Rivara S, Rosengarth A, Clapper JR, *et al.* (2007). URB602 inhibits monoacylglycerol lipase and selectively blocks 2-arachidonoylglycerol degradation in intact brain slices. *Chem. Biol.* **14**(12): 1357-1365.

Kingsley KA, Yuval B, Barbara JR, Bradley CP, Donna LP, Robert GG, *et al.* (2013). Identification of Small Molecules That Selectively Inhibit Diacylglycerol Lipase- α Activity. *Journal of biomolecular screening* **19**(4): 595-605.

Kinsey SG, Long JZ, O'Neal ST, Abdullah RA, Poklis JL, Boger DL, *et al.* (2009). Blockade of endocannabinoid-degrading enzymes attenuates neuropathic pain. *The Journal of pharmacology and experimental therapeutics* **330**(3): 902-910.

Kinsey SG, O'Neal ST, Long JZ, Cravatt BF, Lichtman AH (2011). Inhibition of endocannabinoid catabolic enzymes elicits anxiolytic-like effects in the marble burying assay. *Pharmacology, biochemistry, and behavior* **98**(1): 21-27.

Kinsey SG, Wise LE, Ramesh D, Abdullah R, Selley DE, Cravatt BF, *et al.* (2013). Repeated Low-Dose Administration of the Monoacylglycerol Lipase Inhibitor JZL184 Retains Cannabinoid Receptor Type 1-Mediated

Antinociceptive and Gastroprotective Effects. *The Journal of pharmacology and experimental therapeutics* **345**(3): 492-501.

Klein TW (2005). Cannabinoid-based drugs as anti-inflammatory therapeutics. *Nature reviews. Immunology* **5**(5): 400-411.

Kopp F, Komatsu T, Nomura DK, Trauger SA, Thomas JR, Siuzdak G, *et al.* (2010). The glycerophospho metabolome and its influence on amino acid homeostasis revealed by brain metabolomics of GDE1(-/-) mice. *Chem. Biol.* **17**(8): 831-840.

Koster JF, Vaandrager H, Van Berkel TJC (1980). Study of the hydrolysis of 4-methylumbelliferyl oleate by acid lipase and cholesteryl oleate by acid cholesteryl esterase in human leucocytes, fibroblasts and liver. *Biochimica et Biophysica Acta (BBA) - Lipids and Lipid Metabolism* **618**(1): 98-105.

Kozak KR, Gupta RA, Moody JS, Ji C, Boeglin WE, DuBois RN, *et al.* (2002). 15-Lipoxygenase metabolism of 2-arachidonylglycerol. Generation of a peroxisome proliferator-activated receptor alpha agonist. *The Journal of biological chemistry* **277**(26): 23278-23286.

Labar G, Bauvois C, Borel F, Ferrer JL, Wouters J, Lambert DM (2010a). Crystal structure of the human monoacylglycerol lipase, a key actor in endocannabinoid signaling. *Chembiochem : a European journal of chemical biology* **11**(2): 218-227.

Labar G, Wouters J, Lambert DM (2010b). A review on the monoacylglycerol lipase: at the interface between fat and endocannabinoid signalling. *Curr. Med. Chem.* **17**(24): 2588-2607.

Lafontan M, Langin D (2009). Lipolysis and lipid mobilization in human adipose tissue. *Prog. Lipid Res.* **48**(5): 275-297.

Laitinen T, Navia-Paldanius D, Ryttilahti R, Marjamaa JJ, Karizkova J, Parkkari T, *et al.* (2014). Mutation of Cys242 of human monoacylglycerol lipase disrupts balanced hydrolysis of 1- and 2-monoacylglycerols and selectively impairs inhibitor potency. *Mol. Pharmacol.* **85**(3): 510-519.

Lakiotaki E, Giaginis C, Tolia M, Alexandrou P, Delladetsima I, Giannopoulou I, *et al.* (2015). Clinical Significance of Cannabinoid Receptors CB1 and CB2 Expression in Human Malignant and Benign Thyroid Lesions. *BioMed Research International* **2015**: 839403.

Landy A (1989). Dynamic, structural, and regulatory aspects of lambda site-specific recombination. *Annu. Rev. Biochem.* **58**: 913-949.

Leung D, Saghatelian A, Simon GM, Cravatt BF (2006). Inactivation of N-acyl phosphatidylethanolamine phospholipase D reveals multiple mechanisms for the biosynthesis of endocannabinoids. *Biochemistry (Mosc)*. **45**(15): 4720-4726.

Li F, Fei X, Xu J, Ji C (2009). An unannotated alpha/beta hydrolase superfamily member, ABHD6 differentially expressed among cancer cell lines. *Molecular biology reports* **36**(4): 691-696.

Li W, Blankman JL, Cravatt BF (2007). A functional proteomic strategy to discover inhibitors for uncharacterized hydrolases. *Journal of the American Chemical Society* **129**(31): 9594-9595.

Lichtman AH, Leung D, Shelton CC, Saghatelian A, Hardouin C, Boger DL, et al. (2004). Reversible Inhibitors of Fatty Acid Amide Hydrolase That Promote Analgesia: Evidence for an Unprecedented Combination of Potency and Selectivity. *J. Pharmacol. Exp. Ther.* **311**(2): 441-448.

Liu J, Wang L, Harvey-White J, Osei-Hyiaman D, Razdan R, Gong Q, et al. (2006). A biosynthetic pathway for anandamide. *Proceedings of the National Academy of Sciences* **103**(36): 13345-13350.

Liu Y, Patricelli MP, Cravatt BF (1999a). Activity-based protein profiling: the serine hydrolases. *Proceedings of the National Academy of Sciences of the United States of America* **96**(26): 14694-14699.

Liu Y, Patricelli MP, Cravatt BF (1999b). Activity-based protein profiling: The serine hydrolases. *Proc. Natl. Acad. Sci. U. S. A.* **96**(26): 14694-14699.

Loading Control Guide (Abcam, <https://www.abcam.com/primary-antibodies/loading-control-guide>).

Long JZ, Cravatt BF (2011). The metabolic serine hydrolases and their functions in mammalian physiology and disease. *Chem. Rev.* **111**(10): 6022-6063.

Long JZ, Li W, Booker L, Burston JJ, Kinsey SG, Schlosburg JE, et al. (2009a). Selective blockade of 2-arachidonoylglycerol hydrolysis produces cannabinoid behavioral effects. *Nature chemical biology* **5**(1): 37-44.

Long JZ, Nomura DK, Cravatt BF (2009b). Characterization of monoacylglycerol lipase inhibition reveals differences in central and peripheral endocannabinoid metabolism. *Chem. Biol.* **16**(7): 744-753.

Lord CC, Thomas G, Brown JM (2013). Mammalian alpha beta hydrolase domain (ABHD) proteins: lipid metabolizing enzymes at the interface of cell signaling and energy metabolism. *Biochim. Biophys. Acta* **1831**(4): 792-802.

Lovinger DM (2008). Presynaptic modulation by endocannabinoids. *Handbook of experimental pharmacology*(184): 435-477.

Lowry OH, Rosebrough NJ, Farr AL, Randall RJ (1951). Protein measurement with the Folin phenol reagent. *J Biol Chem* **193**(1): 265-275.

Lunagariya NA, Patel NK, Jagtap SC, Bhutani KK (2014). Inhibitors of pancreatic lipase: state of the art and clinical perspectives. *EXCLI Journal* **13**: 897-921.

Mahmood N, Abdul Maqsood Y, Shabnam S, Bennett A, Steve A (2017). In vitro esterase assays for human recombinant monoacylglycerol hydrolases (MAGL, ABHD6, ABHD12). *International Cannabinoid Research Society (2017 Symposium Final Programme), ICRS posters*.

Maier S, Staffler G, Hartmann A, Hock J, Henning K, Grabusic K, *et al.* (2006). Cellular target genes of Epstein-Barr virus nuclear antigen 2. *J. Virol.* **80**(19): 9761-9771.

Makide K, Kitamura H, Sato Y, Okutani M, Aoki J (2009). Emerging lysophospholipid mediators, lysophosphatidylserine, lysophosphatidylthreonine, lysophosphatidylethanolamine and lysophosphatidylglycerol. *Prostaglandins Other Lipid Mediat.* **89**(3): 135-139.

Manna JD, Wepy JA, Hsu KL, Chang JW, Cravatt BF, Marnett LJ (2014). Identification of the major prostaglandin glycerol ester hydrolase in human cancer cells. *The Journal of biological chemistry* **289**(49): 33741-33753.

Maresz K, Carrier EJ, Ponomarev ED, Hillard CJ, Dittel BN (2005). Modulation of the cannabinoid CB2 receptor in microglial cells in response to inflammatory stimuli. *J. Neurochem.* **95**(2): 437-445.

Marrs, Blankman JL, Horne EA, Thomazeau A, Lin YH, Coy J, *et al.* (2010). The serine hydrolase ABHD6 controls the accumulation and efficacy of 2-AG at cannabinoid receptors. *Nat. Neurosci.* **13**(8): 951-957.

Marrs W, Stella N (2007). 2-AG + 2 new players = forecast for therapeutic advances. *Chem. Biol.* **14**(12): 1309-1311.

Marrs WR, Horne EA, Ortega-Gutierrez S, Cisneros JA, Xu C, Lin YH, *et al.* (2011). Dual inhibition of alpha/beta-hydrolase domain 6 and fatty acid amide hydrolase increases endocannabinoid levels in neurons. *The Journal of biological chemistry* **286**(33): 28723-28728.

Martini E, Krug SM, Siegmund B, Neurath MF, Becker C (2017). Mend Your Fences: The Epithelial Barrier and its Relationship With Mucosal Immunity in

Inflammatory Bowel Disease. *Cellular and Molecular Gastroenterology and Hepatology* **4**(1): 33-46.

Mathew RJ, Wilson WH, Turkington TG, Coleman RE (1998). Cerebellar activity and disturbed time sense after THC. *Brain research* **797**(2): 183-189.

Matias I, Di Marzo V (2007). Endocannabinoids and the control of energy balance. *Trends in Endocrinology & Metabolism* **18**(1): 27-37.

Matsuda LA, Lolait SJ, Brownstein MJ, Young AC, Bonner TI (1990). Structure of a cannabinoid receptor and functional expression of the cloned cDNA. *Nature* **346**(6284): 561-564.

Matuszak N, Hamtiaux L, Baldeyroux B, Muccioli GG, Poupaert JH, Lansiaux A, *et al.* (2012). Dual inhibition of MAGL and type II topoisomerase by N-phenylmaleimides as a potential strategy to reduce neuroblastoma cell growth. *European journal of pharmaceutical sciences : official journal of the European Federation for Pharmaceutical Sciences* **45**(3): 263-271.

Max D, Hesse M, Volkmer I, Staeger MS (2009). High expression of the evolutionarily conserved alpha/beta hydrolase domain containing 6 (ABHD6) in Ewing tumors. *Cancer science* **100**(12): 2383-2389.

McHugh D, Hu SSJ, Rimmerman N, Juknat A, Vogel Z, Walker JM, *et al.* (2010). N-arachidonoyl glycine, an abundant endogenous lipid, potently drives directed cellular migration through GPR18, the putative abnormal cannabidiol receptor. *BMC Neuroscience* **11**: 44-44.

Mechoulam R, Ben-Shabat S, Hanus L, Ligumsky M, Kaminski NE, Schatz AR, *et al.* (1995). Identification of an endogenous 2-monoglyceride, present in canine gut, that binds to cannabinoid receptors. *Biochem. Pharmacol.* **50**(1): 83-90.

Meerbrey KL, Hu G, Kessler JD, Roarty K, Li MZ, Fang JE, *et al.* (2011). The pINDUCER lentiviral toolkit for inducible RNA interference in vitro and in vivo. *Proceedings of the National Academy of Sciences* **108**(9): 3665-3670.

Meier PJ, Sztul ES, Reuben A, JL. B (1984). Structural and functional polarity of canalicular and basolateral plasma membrane vesicles isolated in high yield from rat liver. *The Journal of cell biology* **98**(3): 991-1000.

Melvin LS, Johnson MR, Harbert CA, Milne GM, Weissman A (1984). A cannabinoid derived prototypical analgesic. *Journal of medicinal chemistry* **27**(1): 67-71.

Morita I, Schindler M, Regier MK, Otto JC, Hori T, DeWitt DL, *et al.* (1995). Different Intracellular Locations for Prostaglandin Endoperoxide H Synthase-1 and -2. *J. Biol. Chem.* **270**(18): 10902-10908.

Muccioli GG, Labar G, Lambert DM (2008a). CAY10499, a novel monoglyceride lipase inhibitor evidenced by an expeditious MGL assay. *Chembiochem : a European journal of chemical biology* **9**(16): 2704-2710.

Muccioli GG, Stella N (2008b). An optimized GC-MS method detects nanomole amounts of anandamide in mouse brain. *Anal. Biochem.* **373**(2): 220-228.

Muccioli GG, Xu C, Odah E, Cudaback E, Cisneros JA, Lambert DM, *et al.* (2007). Identification of a Novel Endocannabinoid-Hydrolyzing Enzyme Expressed by Microglial Cells. *The Journal of Neuroscience* **27**(11): 2883-2889.

Muldoon PP, Chen J, Harenza JL, Abdullah RA, Sim-Selley LJ, Cravatt BF, *et al.* (2015). Inhibition of monoacylglycerol lipase reduces nicotine withdrawal. *British journal of pharmacology* **172**(3): 869-882.

Mulvihill MM, Nomura DK (2013). Therapeutic Potential of Monoacylglycerol Lipase Inhibitors. *Life Sci.* **92**(8-9): 492-497.

Murataeva N, Straiker A, Mackie K (2014). Parsing the players: 2-arachidonoylglycerol synthesis and degradation in the CNS. *Br. J. Pharmacol.* **171**(6): 1379-1391.

Nardini M, Dijkstra BW (1999). Alpha/beta hydrolase fold enzymes: the family keeps growing. *Curr. Opin. Struct. Biol.* **9**(6): 732-737.

Navia-Paldanius D, Savinainen JR, Laitinen JT (2012). Biochemical and pharmacological characterization of human alpha/beta-hydrolase domain containing 6 (ABHD6) and 12 (ABHD12). *J. Lipid Res.* **53**(11): 2413-2424.

Naydenov AV, Horne EA, Cheah CS, Swinney K, Hsu KL, Cao JK, *et al.* (2014). ABHD6 blockade exerts antiepileptic activity in PTZ-induced seizures and in spontaneous seizures in R6/2 mice. *Neuron* **83**(2): 361-371.

Nomura DK, Hudak CS, Ward AM, Burston JJ, Issa RS, Fisher KJ, *et al.* (2008). Monoacylglycerol lipase regulates 2-arachidonoylglycerol action and arachidonic acid levels. *Bioorg. Med. Chem. Lett.* **18**(22): 5875-5878.

Nomura DK, Lombardi DP, Chang JW, Niessen S, Ward AM, Long JZ, *et al.* (2011a). Monoacylglycerol lipase exerts dual control over endocannabinoid and fatty acid pathways to support prostate cancer. *Chem. Biol.* **18**(7): 846-856.

Nomura DK, Long JZ, Niessen S, Hoover HS, Ng SW, Cravatt BF (2010). Monoacylglycerol lipase regulates a fatty acid network that promotes cancer pathogenesis. *Cell* **140**(1): 49-61.

Nomura DK, Morrison BE, Blankman JL, Long JZ, Kinsey SG, Marcondes MCG, *et al.* (2011b). Endocannabinoid hydrolysis generates brain prostaglandins that promote neuroinflammation. *Science (New York, N.Y.)* **334**(6057): 809-813.

Nurmikko TJ, Serpell MG, Hoggart B, Toomey PJ, Morlion BJ, Haines D (2007). Sativex successfully treats neuropathic pain characterised by allodynia: a randomised, double-blind, placebo-controlled clinical trial. *Pain* **133**(1-3): 210-220.

O'Sullivan SE (2007). Cannabinoids go nuclear: evidence for activation of peroxisome proliferator-activated receptors. *British journal of pharmacology* **152**(5): 576-582.

Okine BN, Norris LM, Woodhams S, Burston J, Patel A, Alexander SP, *et al.* (2012). Lack of effect of chronic pre-treatment with the FAAH inhibitor URB597 on inflammatory pain behaviour: evidence for plastic changes in the endocannabinoid system. *British journal of pharmacology* **167**(3): 627-640.

online ap Subcellular fractionation protocol.

Oparina NY, Delgado-Vega AM, Martinez-Bueno M, Magro-Checa C, Fernandez C, Castro RO, *et al.* (2014). PDK locus in systemic lupus erythematosus: fine mapping and functional analysis reveals novel susceptibility gene ABHD6. *Ann. Rheum. Dis.*

Overton HA, Babbs AJ, Doel SM, Fyfe MC, Gardner LS, Griffin G, *et al.* (2006). Deorphanization of a G protein-coupled receptor for oleoylethanolamide and its use in the discovery of small-molecule hypophagic agents. *Cell metabolism* **3**(3): 167-175.

Oz M, Tchugunova Y, Dinc M (2004). Differential effects of endogenous and synthetic cannabinoids on voltage-dependent calcium fluxes in rabbit T-tubule membranes: comparison with fatty acids. *Eur. J. Pharmacol.* **502**(1-2): 47-58.

Oz M, Tchugunova YB, Dunn SM (2000). Endogenous cannabinoid anandamide directly inhibits voltage-dependent Ca²⁺ fluxes in rabbit T-tubule membranes. *Eur. J. Pharmacol.* **404**(1-2): 13-20.

Pan B, Zucker RS (2009a). A General Model of Synaptic Transmission and Short-Term Plasticity. *Neuron* **62**(4): 539-554.

Pan C, Kumar C, Bohl S, Klingmueller U, Mann M (2009b). Comparative Proteomic Phenotyping of Cell Lines and Primary Cells to Assess Preservation of Cell Type-specific Functions. *Molecular & cellular proteomics : MCP* **8**(3): 443-450.

Patel A (2009). Endocannabinoid Turnover And Function. *Ph.D. University of Nottingham*.

Patel JZ, Nevalainen TJ, Savinainen JR, Adams Y, Laitinen T, Runyon RS, *et al.* (2015). Optimization of 1,2,5-Thiadiazole Carbamates as Potent and Selective ABHD6 Inhibitors. *ChemMedChem* **10**(2): 253-265.

Patel KD, Davison JS, Pittman QJ, Sharkey KA (2010). Cannabinoid CB(2) receptors in health and disease. *Curr. Med. Chem.* **17**(14): 1393-1410.

Pertwee RG (2006). Cannabinoid pharmacology: the first 66 years. *British journal of pharmacology* **147 Suppl 1**: S163-171.

Pertwee RG (2009). Emerging strategies for exploiting cannabinoid receptor agonists as medicines. *Br. J. Pharmacol.* **156**(3): 397-411.

Pertwee RG (1999). Pharmacology of cannabinoid receptor ligands. *Curr. Med. Chem.* **6**(8): 635-664.

Pertwee RG (2010). Receptors and Channels Targeted by Synthetic Cannabinoid Receptor Agonists and Antagonists. *Curr. Med. Chem.* **17**(14): 1360-1381.

Pertwee RG, Howlett AC, Abood ME, Alexander SP, Di Marzo V, Elphick MR, *et al.* (2010). International Union of Basic and Clinical Pharmacology. LXXIX. Cannabinoid receptors and their ligands: beyond CB(1) and CB(2). *Pharmacol. Rev.* **62**(4): 588-631.

Piomelli D, Tarzia G, Duranti A, Tontini A, Mor M, Compton TR, *et al.* (2006). Pharmacological profile of the selective FAAH inhibitor KDS-4103 (URB597). *CNS drug reviews* **12**(1): 21-38.

Planès R, Ben Haij N, Leghmari K, Serrero M, BenMohamed L, Bahraoui E (2016). HIV-1 Tat Protein Activates both the MyD88 and TRIF Pathways To Induce Tumor Necrosis Factor Alpha and Interleukin-10 in Human Monocytes. *J. Virol.* **90**(13): 5886-5898.

Pohl J, Ring A, Korkmaz Ü, Eehalt R, Stremmel W (2005). FAT/CD36-mediated Long-Chain Fatty Acid Uptake in Adipocytes Requires Plasma Membrane Rafts. *Mol. Biol. Cell* **16**(1): 24-31.

Poling JS, Rogawski MA, Salem N, Vicini S (1996). Anandamide, an Endogenous Cannabinoid, Inhibits Shaker-related Voltage-gated K⁺ Channels. *Neuropharmacology* **35**(7): 983-991.

Poursharifi P, Madiraju SRM, Prentki M (2017). Monoacylglycerol signalling and ABHD6 in health and disease. *Diabetes, Obesity and Metabolism* **19**: 76-89.

Prasad-Reddy L, Isaacs D (2015). A clinical review of GLP-1 receptor agonists: efficacy and safety in diabetes and beyond. *Drugs in context* **4**: 212283.

Pribasniig MA, Mrak I, Grabner GF, Taschler U, Knittelfelder O, Scherz B, *et al.* (2015). alpha/beta Hydrolase Domain-containing 6 (ABHD6) Degrades the Late Endosomal/Lysosomal Lipid Bis(monoacylglycerol)phosphate. *The Journal of biological chemistry* **290**(50): 29869-29881.

Primary Cell Culture online (SIGMA-ALDRICH, <https://www.sigmaaldrich.com/technical-documents/articles/biology/primary-cell-culture.html>).

Ramesh D, Ross GR, Schlosburg JE, Owens RA, Abdullah RA, Kinsey SG, *et al.* (2011). Blockade of endocannabinoid hydrolytic enzymes attenuates precipitated opioid withdrawal symptoms in mice. *The Journal of pharmacology and experimental therapeutics* **339**(1): 173-185.

Reisenberg M, Singh PK, Williams G, Doherty P (2012). The diacylglycerol lipases: structure, regulation and roles in and beyond endocannabinoid signalling. *Philosophical Transactions of the Royal Society B: Biological Sciences* **367**(1607): 3264-3275.

Riccardi L, Arencibia JM, Bono L, Armirotti A, Girotto S, De Vivo M (2017). Lid domain plasticity and lipid flexibility modulate enzyme specificity in human monoacylglycerol lipase. *Biochimica et Biophysica Acta (BBA) - Molecular and Cell Biology of Lipids* **1862**(5): 441-451.

Rinaldi-Carmona M, Barth F, Heaulme M, Shire D, Calandra B, Congy C, *et al.* (1994). SR141716A, a potent and selective antagonist of the brain cannabinoid receptor. *FEBS letters* **350**(2-3): 240-244.

Rouzer CA, Marnett LJ (2011). Endocannabinoid oxygenation by cyclooxygenases, lipoxygenases, and cytochromes P450: cross-talk between the eicosanoid and endocannabinoid signaling pathways. *Chem. Rev.* **111**(10): 5899-5921.

Saario SM, Salo OM, Nevalainen T, Poso A, Laitinen JT, Jarvinen T, *et al.* (2005). Characterization of the sulfhydryl-sensitive site in the enzyme

responsible for hydrolysis of 2-arachidonoyl-glycerol in rat cerebellar membranes. *Chem. Biol.* **12**(6): 649-656.

Saario SM, Savinainen JR, Laitinen JT, Jarvinen T, Niemi R (2004). Monoglyceride lipase-like enzymatic activity is responsible for hydrolysis of 2-arachidonoylglycerol in rat cerebellar membranes. *Biochem. Pharmacol.* **67**(7): 1381-1387.

Sakurada T, Noma A (1981). Subcellular localization and some properties of monoacylglycerol lipase in rat adipocytes. *J Biochem* **90**(5): 1413-1419.

Samson MT, Small-Howard A, Shimoda LM, Koblan-Huberson M, Stokes AJ, Turner H (2003). Differential roles of CB1 and CB2 cannabinoid receptors in mast cells. *Journal of immunology* **170**(10): 4953-4962.

Savinainen JR, Saario SM, Laitinen JT (2012). The serine hydrolases MAGL, ABHD6 and ABHD12 as guardians of 2-arachidonoylglycerol signalling through cannabinoid receptors. *Acta physiologica* **204**(2): 267-276.

Savinainen JR, Yoshino M, Minkkila A, Nevalainen T, Laitinen JT (2010). Characterization of binding properties of monoglyceride lipase inhibitors by a versatile fluorescence-based technique. *Anal. Biochem.* **399**(1): 132-134.

Scalvini L, Piomelli D, Mor M (2016). Monoglyceride lipase: Structure and inhibitors. *Chem. Phys. Lipids* **197**: 13-24.

Schalk-Hihi C, Schubert C, Alexander R, Bayoumy S, Clemente JC, Deckman I, et al. (2011). Crystal structure of a soluble form of human monoglyceride lipase in complex with an inhibitor at 1.35 Å resolution. *Protein Sci.* **20**(4): 670-683.

Schatz AR, Lee M, Condie RB, Pulaski JT, Kaminski NE (1997). Cannabinoid receptors CB1 and CB2: a characterization of expression and adenylate cyclase modulation within the immune system. *Toxicol. Appl. Pharmacol.* **142**(2): 278-287.

Schlosburg JE, Blankman JL, Long JZ, Nomura DK, Pan B, Kinsey SG, et al. (2010). Chronic monoacylglycerol lipase blockade causes functional antagonism of the endocannabinoid system. *Nat. Neurosci.* **13**(9): 1113-1119.

Schlosburg JE, Carlson BL, Ramesh D, Abdullah RA, Long JZ, Cravatt BF, et al. (2009). Inhibitors of endocannabinoid-metabolizing enzymes reduce precipitated withdrawal responses in THC-dependent mice. *The AAPS journal* **11**(2): 342-352.

Schwenk J, Harmel N, Brechet A, Zolles G, Berkefeld H, Muller CS, *et al.* (2012). High-resolution proteomics unravel architecture and molecular diversity of native AMPA receptor complexes. *Neuron* **74**(4): 621-633.

Shimasue K, Urushidani T, Hagiwara M, Nagao T (1996). Effects of anandamide and arachidonic acid on specific binding of (+) -PN200-110, diltiazem and (-) -desmethoxyverapamil to L-type Ca²⁺ channel. *Eur. J. Pharmacol.* **296**(3): 347-350.

Simon GM, Cravatt BF (2010). Activity-based proteomics of enzyme superfamilies: serine hydrolases as a case study. *The Journal of biological chemistry* **285**(15): 11051-11055.

Singh Praveen K, Markwick R, Howell Fiona V, Williams G, Doherty P (2016). A novel live cell assay to measure diacylglycerol lipase α activity. *Biosci. Rep.* **36**(3): e00331.

Slanina KA, Schweitzer P (2005). Inhibition of cyclooxygenase-2 elicits a CB1-mediated decrease of excitatory transmission in rat CA1 hippocampus. *Neuropharmacology* **49**(5): 653-659.

Smith PK, Krohn RI, Hermanson GT, Mallia AK, Gartner FH, Provenzano MD, *et al.* (1985). Measurement of protein using bicinchoninic acid. *Anal. Biochem.* **150**(1): 76-85.

Snider NT, Nast JA, Tesmer LA, Hollenberg PF (2009). A Cytochrome P450-Derived Epoxygenated Metabolite of Anandamide Is a Potent Cannabinoid Receptor 2-Selective Agonist. *Mol. Pharmacol.* **75**(4): 965-972.

Sostres C, Gargallo CJ, Lanas A (2013). Nonsteroidal anti-inflammatory drugs and upper and lower gastrointestinal mucosal damage. *Arthritis research & therapy* **15**(Suppl 3): S3-S3.

Staton PC, Hatcher JP, Walker DJ, Morrison AD, Shapland EM, Hughes JP, *et al.* (2008). The putative cannabinoid receptor GPR55 plays a role in mechanical hyperalgesia associated with inflammatory and neuropathic pain. *Pain* **139**(1): 225-236.

Stella N (2010). Cannabinoid and cannabinoid-like receptors in microglia, astrocytes and astrocytomas. *Glia* **58**(9): 1017-1030.

Stella N (2004). Cannabinoid signaling in glial cells. *Glia* **48**(4): 267-277.

Sticht MA, Long JZ, Rock EM, Limebeer CL, Mechoulam R, Cravatt BF, *et al.* (2012). Inhibition of monoacylglycerol lipase attenuates vomiting in *Suncus murinus* and 2-arachidonoyl glycerol attenuates nausea in rats. *Br. J. Pharmacol.* **165**(8): 2425-2435.

Storch J, Zhou YX, Lagakos WS (2008). Metabolism of apical versus basolateral sn-2-monoacylglycerol and fatty acids in rodent small intestine. *J. Lipid Res.* **49**(8): 1762-1769.

Straiker A, Hu SS, Long JZ, Arnold A, Wager-Miller J, Cravatt BF, *et al.* (2009). Monoacylglycerol lipase limits the duration of endocannabinoid-mediated depolarization-induced suppression of excitation in autaptic hippocampal neurons. *Mol. Pharmacol.* **76**(6): 1220-1227.

Sugiura T, Kishimoto S, Oka S, Gokoh M (2006). Biochemistry, pharmacology and physiology of 2-arachidonoylglycerol, an endogenous cannabinoid receptor ligand. *Prog. Lipid Res.* **45**(5): 405-446.

Sugiura T, Kondo S, Sukagawa A, Tonegawa T, Nakane S, Yamashita A, *et al.* (1996). Transacylase-mediated and phosphodiesterase-mediated synthesis of N-arachidonylethanolamine, an endogenous cannabinoid-receptor ligand, in rat brain microsomes. Comparison with synthesis from free arachidonic acid and ethanolamine. *Eur. J. Biochem.* **240**(1): 53-62.

Sumislawski JJ, Ramikie TS, Patel S (2011). Reversible gating of endocannabinoid plasticity in the amygdala by chronic stress: a potential role for monoacylglycerol lipase inhibition in the prevention of stress-induced behavioral adaptation. *Neuropsychopharmacology* **36**(13): 2750-2761.

Tanaka M, Moran S, Wen J, Affram K, Chen T, Symes AJ, *et al.* (2017). WWL70 attenuates PGE(2) production derived from 2-arachidonoylglycerol in microglia by ABHD6-independent mechanism. *Journal of neuroinflammation* **14**: 7.

Tanimura A, Yamazaki M, Hashimoto-dani Y, Uchigashima M, Kawata S, Abe M, *et al.* (2010). The endocannabinoid 2-arachidonoylglycerol produced by diacylglycerol lipase alpha mediates retrograde suppression of synaptic transmission. *Neuron* **65**(3): 320-327.

Taschler U, Radner FPW, Heier C, Schreiber R, Schweiger M, Schoiswohl G, *et al.* (2011). Monoglyceride Lipase Deficiency in Mice Impairs Lipolysis and Attenuates Diet-induced Insulin Resistance. *The Journal of biological chemistry* **286**(20): 17467-17477.

Tchantchou F, Zhang Y (2013). Selective inhibition of alpha/beta-hydrolase domain 6 attenuates neurodegeneration, alleviates blood brain barrier breakdown, and improves functional recovery in a mouse model of traumatic brain injury. *Journal of neurotrauma* **30**(7): 565-579.

Thibault K, Carrel D, Bonnard D, Gallatz K, Simon A, Biard M, *et al.* (2013). Activation-Dependent Subcellular Distribution Patterns of CB1 Cannabinoid Receptors in the Rat Forebrain. *Cereb. Cortex* **23**(11): 2581-2591.

Thomas G, Betters JL, Lord CC, Brown AL, Marshall S, Ferguson D, *et al.* (2013). The serine hydrolase ABHD6 Is a critical regulator of the metabolic syndrome. *Cell Rep* **5**(2): 508-520.

Thomas SG (2014). The Serine Hydrolase Abhd6 Is A Critical Regulator Of The Metabolic Syndrome. *Ph.D Thesis*.

Tiscornia G, Singer O, Verma IM (2006). Production and purification of lentiviral vectors. *Nat. Protocols* **1**(1): 241-245.

Todd AE, Orengo CA, Thornton JM (2001). Evolution of function in protein superfamilies, from a structural perspective. *Journal of molecular biology* **307**(4): 1113-1143.

Tomaiuolo M, Bertram R, Houle D (2008). ENZYME ISOFORMS MAY INCREASE PHENOTYPIC ROBUSTNESS. *Evolution; international journal of organic evolution* **62**(11): 2884-2893.

Tominaga M, Caterina MJ, Malmberg AB, Rosen TA, Gilbert H, Skinner K, *et al.* (1998). The cloned capsaicin receptor integrates multiple pain-producing stimuli. *Neuron* **21**(3): 531-543.

Tsou K, Brown S, Sanudo-Pena MC, Mackie K, Walker JM (1998). Immunohistochemical distribution of cannabinoid CB1 receptors in the rat central nervous system. *Neuroscience* **83**(2): 393-411.

Turcotte C, Chouinard F, Lefebvre JS, Flamand N (2015). Regulation of inflammation by cannabinoids, the endocannabinoids 2-arachidonoyl-glycerol and arachidonoyl-ethanolamide, and their metabolites. *J. Leukoc. Biol.* **97**(6): 1049-1070.

Uchigashima M, Narushima M, Fukaya M, Katona I, Kano M, Watanabe M (2007). Subcellular arrangement of molecules for 2-arachidonoyl-glycerol-mediated retrograde signaling and its physiological contribution to synaptic modulation in the striatum. *The Journal of neuroscience : the official journal of the Society for Neuroscience* **27**(14): 3663-3676.

Valenzano KJ, Tafesse L, Lee G, Harrison JE, Boulet JM, Gottshall SL, *et al.* (2005). Pharmacological and pharmacokinetic characterization of the cannabinoid receptor 2 agonist, GW405833, utilizing rodent models of acute and chronic pain, anxiety, ataxia and catalepsy. *Neuropharmacology* **48**(5): 658-672.

van der Stelt M, Hansen HH, Veldhuis WB, Bar PR, Nicolay K, Veldink GA, *et al.* (2003). Biosynthesis of endocannabinoids and their modes of action in neurodegenerative diseases. *Neurotoxicity research* **5**(3): 183-200.

Van Dyke RW (2004). Heterotrimeric G protein subunits are located on rat liver endosomes. *BMC physiology* **4**(1): 1.

van Esbroeck ACM, Janssen APA, Cognetta AB, 3rd, Ogasawara D, Shpak G, van der Kroeg M, *et al.* (2017). Activity-based protein profiling reveals off-target proteins of the FAAH inhibitor BIA 10-2474. *Science* **356**(6342): 1084-1087.

Vandesompele J, De Preter K, Pattyn F, Poppe B, Van Roy N, De Paepe A, *et al.* (2002). Accurate normalization of real-time quantitative RT-PCR data by geometric averaging of multiple internal control genes. *Genome biology* **3**(7): RESEARCH0034.

Vandevoorde S, Jonsson KO, Labar G, Persson E, Lambert DM, Fowler CJ (2007). Lack of selectivity of URB602 for 2-oleoylglycerol compared to anandamide hydrolysis in vitro. *Br. J. Pharmacol.* **150**(2): 186-191.

Vaughan M, Berger JE, Steinberg D (1964). HORMONE-SENSITIVE LIPASE AND MONOGLYCERIDE LIPASE ACTIVITIES IN ADIPOSE TISSUE. *The Journal of biological chemistry* **239**: 401-409.

Verger R (1997). 'Interfacial activation' of lipases: facts and artifacts. *Trends Biotechnol.* **15**(1): 32-38.

Viader A, Blankman JL, Zhong P, Liu X, Schlosburg JE, Joslyn CM, *et al.* (2015). Metabolic Interplay between Astrocytes and Neurons Regulates Endocannabinoid Action. *Cell reports* **12**(5): 798-808.

Viader A, Ogasawara D, Joslyn CM, Sanchez-Alavez M, Mori S, Nguyen W, *et al.* (2016). A chemical proteomic atlas of brain serine hydrolases identifies cell type-specific pathways regulating neuroinflammation. *eLife* **5**: e12345.

Volk DW, Siegel BI, Verrico CD, Lewis DA (2013). Endocannabinoid metabolism in the prefrontal cortex in schizophrenia. *Schizophr. Res.* **147**(1): 53-57.

Wagenlehner FME, van Till JWO, Houbiers JGA, Martina RV, Cerneus DP, Melis J, *et al.* (2017). Fatty Acid Amide Hydrolase Inhibitor Treatment in Men With Chronic Prostatitis/Chronic Pelvic Pain Syndrome: An Adaptive Double-blind, Randomized Controlled Trial. *Urology* **103**: 191-197.

Walter L, Dinh T, Stella N (2004). ATP induces a rapid and pronounced increase in 2-arachidonoylglycerol production by astrocytes, a response limited by monoacylglycerol lipase. *The Journal of neuroscience : the official journal of the Society for Neuroscience* **24**(37): 8068-8074.

Wang Y, Chanda P, Jones PG, Kennedy JD (2008). A fluorescence-based assay for monoacylglycerol lipase compatible with inhibitor screening. *Assay and drug development technologies* **6**(3): 387-393.

Warrington JA, Nair A, Mahadevappa M, Tsyganskaya M (2000). Comparison of human adult and fetal expression and identification of 535 housekeeping/maintenance genes. *Physiological genomics* **2**(3): 143-147.

Wei BQ, Mikkelsen TS, McKinney MK, Lander ES, Cravatt BF (2006). A second fatty acid amide hydrolase with variable distribution among placental mammals. *The Journal of biological chemistry* **281**(48): 36569-36578.

Wei M, Jia M, Zhang J, Yu L, Zhao Y, Chen Y, *et al.* (2017). The Inhibitory Effect of α/β -Hydrolase Domain-Containing 6 (ABHD6) on the Surface Targeting of GluA2- and GluA3-Containing AMPA Receptors. *Frontiers in Molecular Neuroscience* **10**: 55.

Wei M, Zhang J, Jia M, Yang C, Pan Y, Li S, *et al.* (2016). α/β -Hydrolase domain-containing 6 (ABHD6) negatively regulates the surface delivery and synaptic function of AMPA receptors. *Proc. Natl. Acad. Sci. U. S. A.* **113**(19): E2695-E2704.

Wen J, Jones M, Tanaka M, Selvaraj P, Symes AJ, Cox B, *et al.* (2018). WWL70 protects against chronic constriction injury-induced neuropathic pain in mice by cannabinoid receptor-independent mechanisms. *Journal of neuroinflammation* **15**(1): 9.

Wen J, Ribeiro R, Tanaka M, Zhang Y (2015). Activation of CB2 receptor is required for the therapeutic effect of ABHD6 inhibition in experimental autoimmune encephalomyelitis. *Neuropharmacology* **99**: 196-209.

Woodhams SG (2012). Modulation of Spinal Hyper-Excitability by the Cannabinoid & Vanilloid systems. *PhD thesis University of Nottingham.*

Woodhams SG, Wong A, Barrett DA, Bennett AJ, Chapman V, Alexander SPH (2012). Spinal administration of the monoacylglycerol lipase inhibitor JZL184 produces robust inhibitory effects on nociceptive processing and the development of central sensitization in the rat. *Br. J. Pharmacol.* **167**(8): 1609-1619.

Wu CS, Zhu J, Wager-Miller J, Wang S, O'Leary D, Monory K, *et al.* (2010). Requirement of cannabinoid CB(1) receptors in cortical pyramidal neurons for appropriate development of corticothalamic and thalamocortical projections. *The European journal of neuroscience* **32**(5): 693-706.

Xu J-Y, Chen C (2015). Endocannabinoids in Synaptic Plasticity and Neuroprotection. *The Neuroscientist : a review journal bringing neurobiology, neurology and psychiatry* **21**(2): 152-168.

Yamagata K, Andreasson KI, Kaufmann WE, Barnes CA, Worley PF (1993). Expression of a mitogen-inducible cyclooxygenase in brain neurons: regulation by synaptic activity and glucocorticoids. *Neuron* **11**(2): 371-386.

Yang H, Zhou J, Lehmann C (2016). GPR55 - a putative "type 3" cannabinoid receptor in inflammation. *J. Basic Clin. Physiol. Pharmacol.* **27**(3): 297-302.

Ye L, Zhang B, Seviour EG, Tao KX, Liu XH, Ling Y, *et al.* (2011). Monoacylglycerol lipase (MAGL) knockdown inhibits tumor cells growth in colorectal cancer. *Cancer letters* **307**(1): 6-17.

Yin H, Chu A, Li W, Wang B, Shelton F, Otero F, *et al.* (2009). Lipid G protein-coupled receptor ligand identification using beta-arrestin PathHunter assay. *The Journal of biological chemistry* **284**(18): 12328-12338.

Yip PK, Kaan TK, Fenesan D, Malcangio M (2009). Rapid isolation and culture of primary microglia from adult mouse spinal cord. *Journal of neuroscience methods* **183**(2): 223-237.

Yoshino H, Miyamae T, Hansen G, Zambrowicz B, Flynn M, Pedicord D, *et al.* (2011). Postsynaptic diacylglycerol lipase mediates retrograde endocannabinoid suppression of inhibition in mouse prefrontal cortex. *J Physiol* **589**(Pt 20): 4857-4884.

Yu CB, Zhu LY, Wang YG, Li F, Zhang XY, Dai WJ (2016). Systemic transcriptome analysis of hepatocellular carcinoma. *Tumour biology : the journal of the International Society for Oncodevelopmental Biology and Medicine* **37**(10): 13323-13331.

Yu Z, Z. H, L. LM (2013). Subcellular Fractionation of Cultured Human Cell Lines. *Bio-protocol* **3**(9).

Yuan C, Smith WL (2015). A Cyclooxygenase-2-dependent Prostaglandin E2 Biosynthetic System in the Golgi Apparatus. *J. Biol. Chem.* **290**(9): 5606-5620.

Zhang D, Saraf A, Kolasa T, Bhatia P, Zheng GZ, Patel M, *et al.* (2007). Fatty acid amide hydrolase inhibitors display broad selectivity and inhibit multiple carboxylesterases as off-targets. *Neuropharmacology* **52**(4): 1095-1105.

Zhang J, Hoffert C, Vu HK, Groblewski T, Ahmad S, O'Donnell D (2003). Induction of CB2 receptor expression in the rat spinal cord of neuropathic but not inflammatory chronic pain models. *Eur. J. Neurosci.* **17**(12): 2750-2754.

Zhang JH, Chung TD, Oldenburg KR (1999). A Simple Statistical Parameter for Use in Evaluation and Validation of High Throughput Screening Assays. *Journal of biomolecular screening* **4**(2): 67-73.

Zhao S, Mugabo Y, Ballentine G, Attane C, Iglesias J, Poursharifi P, *et al.* (2016). alpha/beta-Hydrolase Domain 6 Deletion Induces Adipose Browning and Prevents Obesity and Type 2 Diabetes. *Cell Rep* **14**(12): 2872-2888.

Zhao S, Mugabo Y, Iglesias J, Xie L, Delghingaro-Augusto V, Lussier R, *et al.* (2014). alpha/beta-Hydrolase domain-6-accessible monoacylglycerol controls glucose-stimulated insulin secretion. *Cell metabolism* **19**(6): 993-1007.

Zhao S, Poursharifi P, Mugabo Y, Levens EJ, Vivot K, Attane C, *et al.* (2015). α/β -Hydrolase domain-6 and saturated long chain monoacylglycerol regulate insulin secretion promoted by both fuel and non-fuel stimuli. *Molecular Metabolism* **4**(12): 940-950.

Zhong P, Wang W, Pan B, Liu X, Zhang Z, Long JZ, *et al.* (2014). Monoacylglycerol lipase inhibition blocks chronic stress-induced depressive-like behaviors via activation of mTOR signaling. *Neuropsychopharmacology* **39**(7): 1763-1776.

Zhu W, Zhao Y, Zhou J, Wang X, Pan Q, Zhang N, *et al.* (2016). Monoacylglycerol lipase promotes progression of hepatocellular carcinoma via NF- κ B-mediated epithelial-mesenchymal transition. *Journal of Hematology & Oncology* **9**(1): 127.

Zvonok N, Pandarinathan L, Williams J, Johnston M, Karageorgos I, Janero DR, *et al.* (2008). Covalent Inhibitors of Human Monoacylglycerol Lipase: Ligand-assisted Characterization of the Catalytic Site by Mass Spectrometry and Mutational Analysis. *Chem. Biol.* **15**(8): 854-862.

Zygmunt PM, Ermund A, Movahed P, Andersson DA, Simonsen C, Jonsson BA, *et al.* (2013). Monoacylglycerols activate TRPV1--a link between phospholipase C and TRPV1. *PLoS One* **8**(12): e81618.

8. Appendix

8.1 Section A

This section encompassing various Tables, maps and Figures.

Table A.1: Detailed cloning information of MAGL1, MAGL2, ABHD6, ABHD12, FAAH1 and FAAH2 and their vectors and maps.

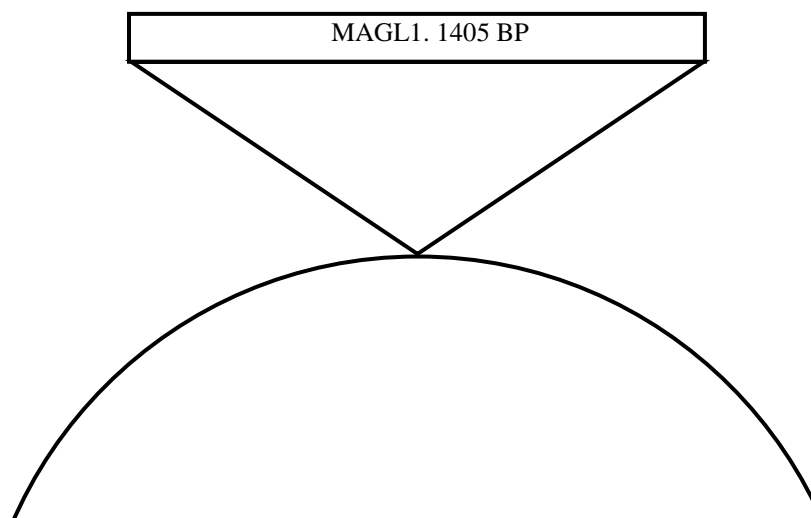
Plasmid Name	MAGL1 -pcDNA3.1(-)zeo
Protein	Monoacylglycerol lipase1
Species	Human
Genbank ID	NM_007283.6
Vector	pcDNA3.1(-)zeo
Restriction sites used	BamHI and HINDIII
Forward primer sequence	ACA GGATCC GGCTGAGCGCCCCAGCCCGA
Reverse primer sequence	ACA AAGCTT GGAGAGGCAGGGCAGAGGCTTGGC
Insert Source	Human brain RNA
Antibiotic selection	Ampicillin
DNA insert size (bp)	1405 bp

DNA sequence of insert	<pre> ggctgag cgccccagcc cgaaggcag ggtctgggtg cgggaagagg gctcggagct gccttcctgc tccttggggccgccagat gagggaacag cccgattgc ctggttctga ttctccaggc tctcgtggtt gtggaatgca aacgccagcacataatgaa acaggacctg aagaccttc cagcatgccagaggaaagt cccccaggcg gaccccagc agcattcct accaggacct cctcacctggtcaatgcag aeggacagta cctctctgc aggfactgga aaccacagg cacaccaag gccctcatc ttgtgccca tggagccgga gagcacagt gccgctatga agagctggctcggatgctga tgggctgga cctgctggtg ttgccccag accatgttg ccacggacag agcgaagggg agaggatgt agtgtctgac ttccacttt tctcagggga tgtttgcagcatgtgatt ccatcgaaa agactacct gggttctctg tctctctt gggacctccatggggaggcg ccatcgccat cctcacggc gacagaggc cgggcaact cgcggcatgtactcatt cgcctctggt tctgccaat cctgaatctg caacaactt caagtccttctgctgaaaag tctcaacct tctgctgcca aactgtccc tgggcccac cgactcagcgtctctc ggaataagac agaggctgac attataact cagaccct gatctgcccgcagggctga aggtgtgctt cggcatcaa ctgctgaat ccgtctcag ggtggagcgcgccctccca agctgactgt gccctctctg ctgctccagg gctctgccga tgcctatgt gacagcaaag gggctacct gctcatggag ttagccaaga gccaggacaa gactctcaagattatgaag gtgctacca tctctccac aaggagctc ctgaagtcac caactcgtcttccatgaaa taacatgtg ggtctctcaa aggacagcca cggcaggaac tgcgtccca cctgaatgc attggccgtt gccggctca tggctgggg gatgcaggca ggggaagggc agagatggct ttcagatat ggcttccaa aaaaaaaaa aaaaaaaat cagaaattgg agaattcct agcacaattt tcaaaaaat aacagacatt tttgtatac attagactat cagacactgg acctaccta atggttagac actttatgca aaaaaagaga aaggcccag gtgattttcc acaaagaatg tctaaaatg tccactgaaa aaaaagccaa gcctctgcctctctcc </pre>
Protein sequence	<pre> Met ETGPEDPSS Met PEESP RRT PQSIPYQD LPHLVNADGQYLF CRYWKPTGTPKALIFV SHGAGEHSGRYEELAR Met L Met GLDLLVF AHDHVGHGQSEGER Met VVSDFHVFVRDV LQHVDS Met QKDY PGLPVFLLGHS Met GGA IAILTAERPGHFAG Met VLISPLVLANPES ATTFK VLA AKVLN LVL PNL SLGPIDSSVL SRNKTEVDIYNSDPLICRAGLKVCFGIQL LNAVSRVERALPKLTVPFLLLQGSADRLC DSKGA YLL Met ELAKS QDKTLKIYEGAYH VLHKELPEVTNSVFHEIN Met WVSQRTATA GTASPP </pre>
Calc Mol Weight (kDa)	34270.57 KDa
General Description	The purple colour indicates the forward and reverse primers while the blue colour indicates the starting and stopping codons.

Map:

5' site BamHI

3' site HINDIII



pcDNA3.1 (-)zeo,

5428 bp

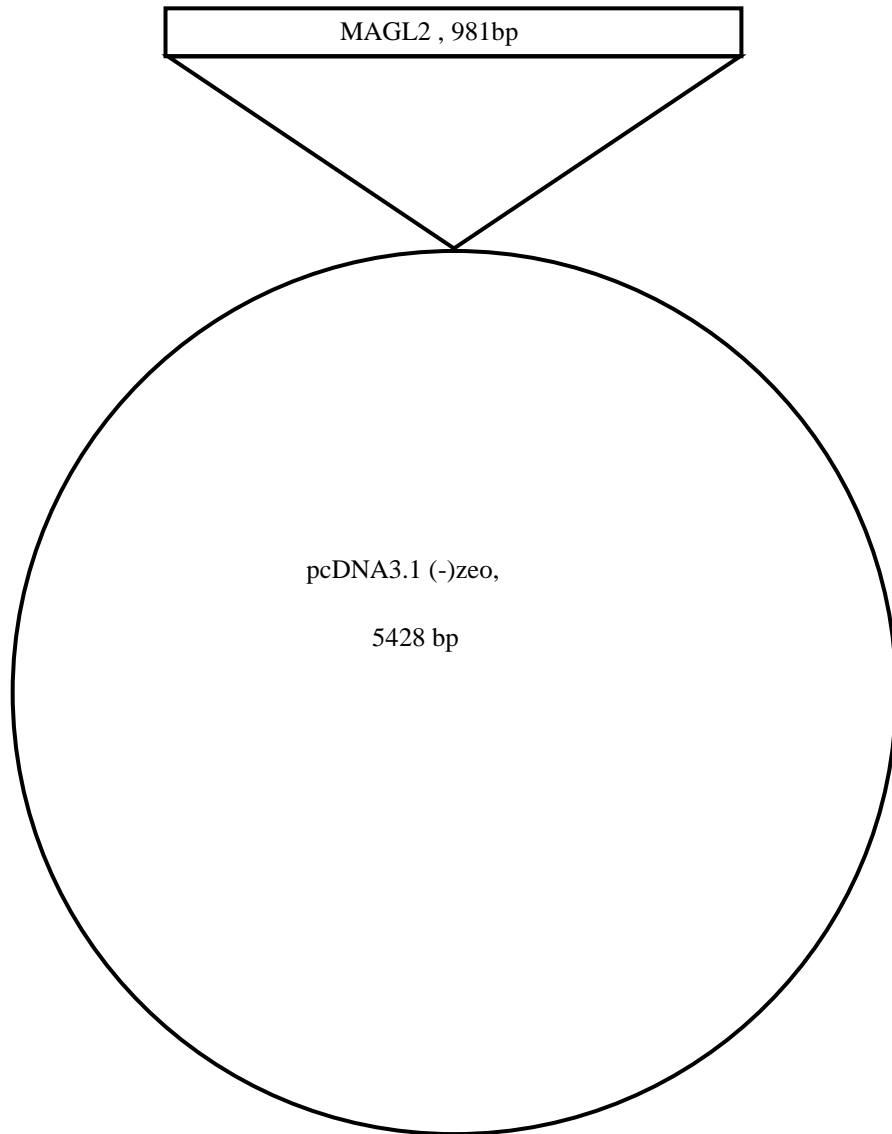
Plasmid Name	MAGL2 –pcDNA3.1(-)zeo
Protein	Monoacylglycerol lipase 2
Species	Human
Genbank ID	NM: 001003794.2
Vector	pcDNA3.1(-)zeo
Restriction sites used	BamHI and HINDIII
Forward primer sequence	ACAGGATCCGCGCTCGTGGCCCCGGACCT
Reverse primer sequence	ACAAGCTTCCCCAGACCATGAGCCGGGCA
Insert Source	Human brain RNA
Antibiotic selection	Ampicillin
DNA insert size (bp)	981
DNA sequence of insert	gcgctcgt ggccccggac ctgaagaccc ttccagcatg ccagaggaaa gttccccag gcggaccccg cagagcattc cctaccagga cctccctcac ctggtcaatg cagacggaca gtacctctc tgcaggactt ggaaccacac aggcacacc aaggccctca tctttgtgc ccatggagcc ggagagcaca gtggccgcta tgaagagctg gctcggatgc tgatggggct ggacctgctg gtgtcgccc acgaccatgt tggccacgga cagagcgaag ggagagaggat ggtagtgtct gactccacg tttcgtcag ggatgtgtg cagcatgtgg attccatgca gaaagactac cctgggcttc ctgtcttct tctggggccac tccatgggag gcgccatgc catcctcac gccgcagaga ggccggggcca cttcgccggc atggtaacta ttcgcctct ggttcttcc aatcctgaat

	<p>ctgcaacaac ttcaaggtc cttgctgca aagtgtcaa ccttgtctg ccaactgt cctcgggccc catcgactcc agcgtgctct ctggaataa gacagaggtc gacattata actcagaccc cctgatctgc cgggcagggc tgaagggtg cttcggcatc caactgctga atgccgtctc acgggtggag cgcgccctcc ccaagctgac tgtgccctc ctgctgctcc agggctctgc cgatgccta tgtgacagca aaggggccta cctgctcatg gagtagcca agagccagga caagactctc aagattatg aaggtgcta ccatgtctc cacaaggagc ttctgaagt caccaactcc gtctccatg aaataaacat gtgggtctct caaaggacag ccacggcagg aactgcgtcc ccaccctgaa tgcattggcc ggcgccggc tcatggtctg ggggatgcag</p>
Protein sequence	<p>Met PEESPRRTPQSIPYQDLPHLVNADGQ YLFCRYWKPTGTPKALIFVSHGAGEHSG RYEELARMetLMetGLDLLVFAHDHVGHG QSEGERMetVVSDFHVFVRDVLQHVD SMetQKDYPLPVFLLGHSMetGGAIAILT AAERP GHFAGMetVLISPLVLANPESATT FKVLA AKVLNLVLPNLSLGPIDSSVLSR NKTEVDIYNSDPLICRAGLKVCFGIQLLN AVSRVERALPKLTVPFLLLQGSADRLCD SKGAYLLMetELAKSQDKTLKIYEGAYHV LHKELPEVTNSVFHEINMetWVSQRTATA GTASPP</p>
Calc Mol Weight (kDa)	33240.18 KDa
General Description	The purple colour indicates the forward and reverse primers while the blue colour indicates the starting and stopping codons.

Map:

5' site BamHI

3' site HINDIII

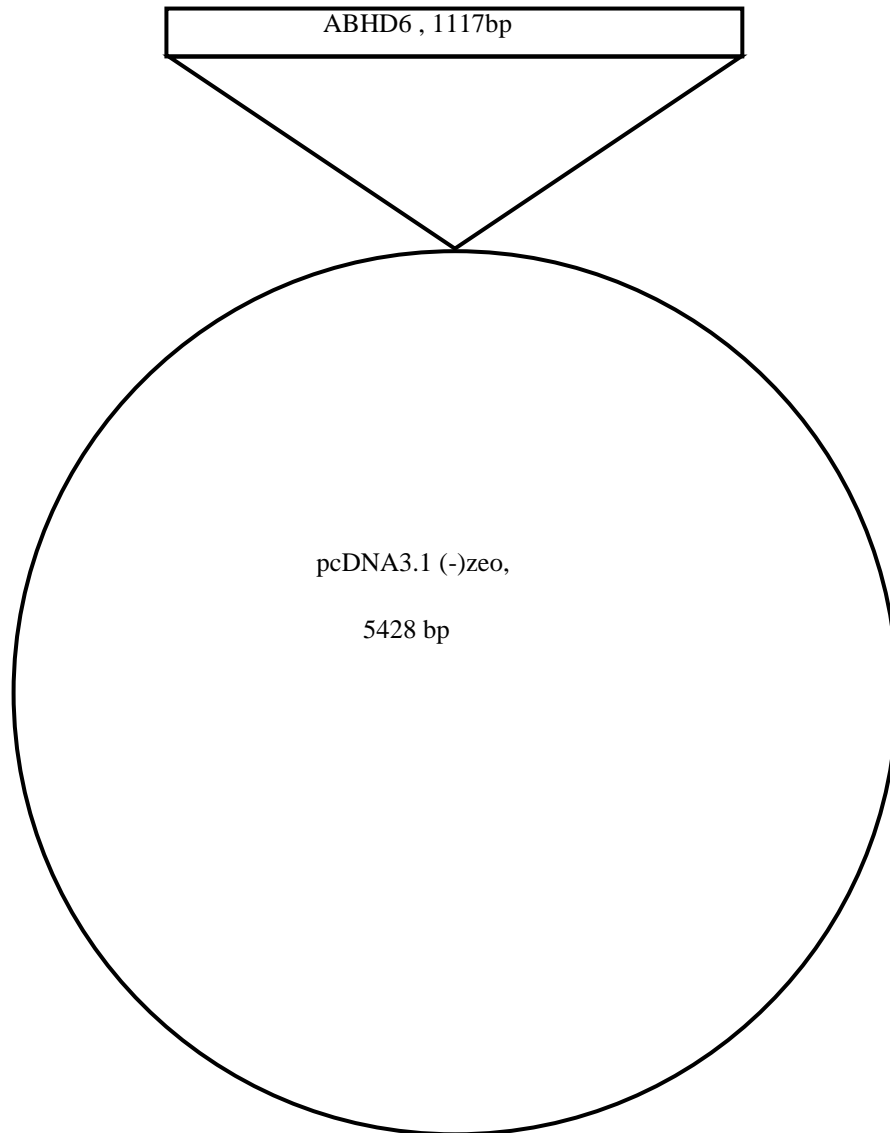


Plasmid Name	ABHD6 –pcDNA3.1(-)zeo
Protein	Alpha – beta hydrolase domain -6
Species	Human
Genbank ID	NM: 020676.5
Vector	pcDNA3.1(-)zeo
Restriction sites used	BamHI and HINDIII
Forward primer sequence	ACAGGATCCGGCTGGTCAGGAGTCAGCCAGCCT
Reverse primer sequence	ACAAGCTTTGGTGGCTGCGTCAGACTTGGGGG
Insert Source	Human adipose tissue
Antibiotic selection	Ampicillin
DNA insert size (bp)	1117 bp
DNA sequence of insert	<pre> ggctg gtcaggagtc agccagcctg aaagagcagg atggatctg atgtggttaa catgttttg attgcccgcg gcacgctggc catccaatc ctggcattg tgcttcatt tctctgtgg ccttcagcac tgataagaat ctattattgg tactggcggg ggacattggg catgcaagtc cgctatgttc accatgaaga ctatcagttc tgttattct tccggggcag gctggggcac aaacctcca tctcatgct ccacggatc ctgcccaca aggatatgtg gctcagtgtg gtcaagtcc ttccaaagaa cctgcactg gctgctgtgg acatgccagg acatgagggc accaccgct ctccctgga tgacctgtcc atagatgggc aagttaagag gatacaccag ttgtagaat gcctgaagct gaacaaaaa ccttccacc ttgttaggcac ctccatgggt ggccagggtg ctggggtgta tgctgcttac taccatcgg atgtctccag cctgtgtctc gtgtgtcctg ctggcctgca gtactcaact gacaatcaat ttgtacaacg gctcaaagaa ctgcagggct ctgccgccgt ggagaagatt ccctgated cgtctacccc agaagagatg agtgaaatgc ttcagetctg ctctatgtc cgttcaagg tgccccagca gatcctgcaa ggccttctg atgtccgat cctcataac aactctacc gaaagtgtt ttggaaatc gtcagtgaga agtccagata ctctccat cagaacatgg acaagatcaa ggttccgacg cagatcatct gggggaaca agaccaggtg ctggatgtgt ctggggcaga catgttgcc aagtcaattg ccaactgcca ggtggagctt ctgaaaact gtgggcactc agtagtgatg gaaagacca ggaagacagc caagctcata atcgacttt tagcttctgt gcacaacaca gacaacaaca agaagctgga ctgggcccc gactgcagcc tgcattctgc acacagcatc tgctccatc cccaagctc gacgcagcca cca </pre>
Protein sequence	<p>Met D L D V V N Met F V I A G G T L A I P I L A F V A S F L L W P S A L I R I Y Y W Y W R R T L G Met Q V R Y V H H E D Y Q F C Y S F R G R P G H K P S I L Met L H G F S A H K D Met W L S V V K F L P K N L H L V C V D Met P G H E G T T R S S L D D L S I D G Q V K R I H Q F V E C L K L N K K P F H L V G T S Met G G Q V A G V Y A A Y Y P S D V S S L C L V C P A G L Q Y S T D N Q F V Q R L K E L Q G S A A V E K I P L I P S T P E E Met S E Met L Q L C S Y V R F K V P Q Q I L Q G L V D V R I P H N N F Y R K L F L E I V S E K S R Y S L H Q N Met D K I K V P T Q I I W G K Q D Q V L D V S G A D Met L A K S I A N C Q V E L L E N C G H S V V Met E R P R K T A K L I I D F L A S V H N T D N N K K L D yellow: transmembrane domain</p>
Calc Mol Weight (kDa)	38305.70 KDa
General Description	The purple colour indicates the forward and reverse primers while the blue colour indicates the starting and stopping codons.

Map:

5' site BamHI

3' site HINDIII

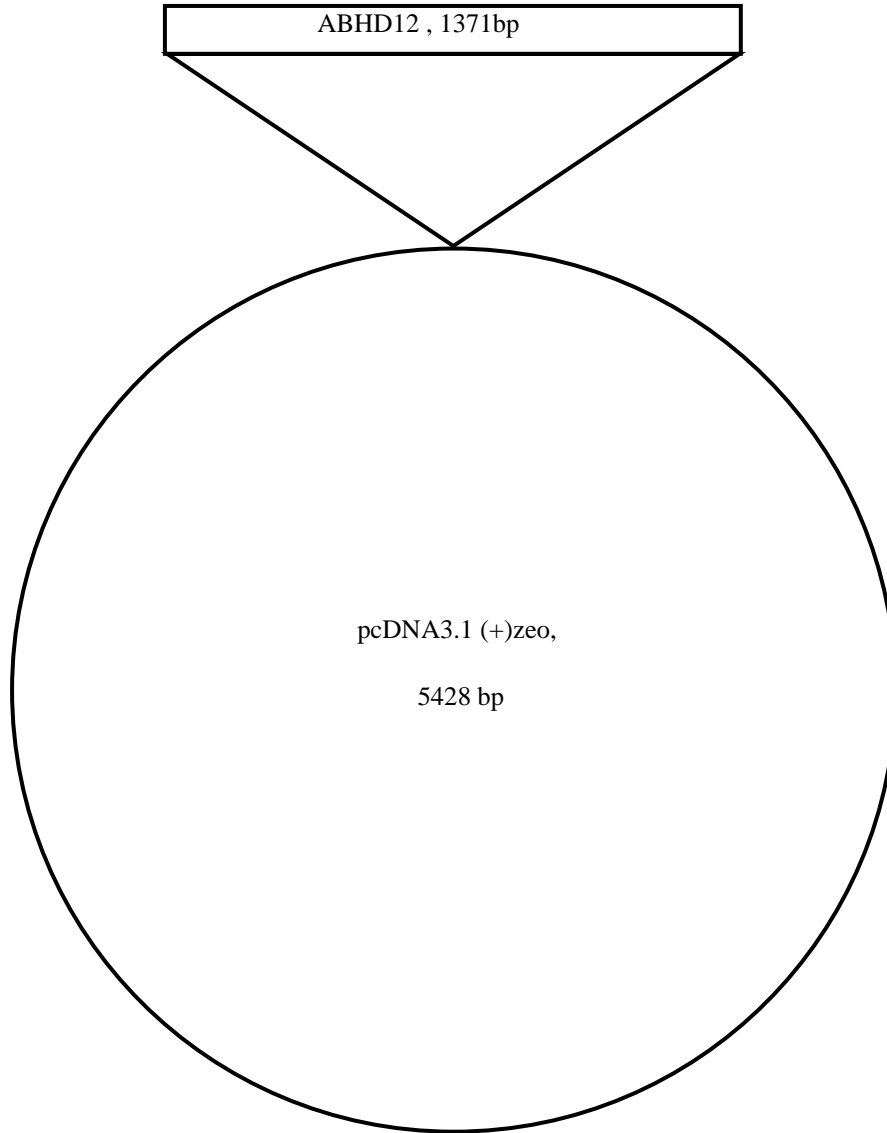


Plasmid Name	ABHD12 -pcDNA3.1(+)-zeo
Protein	Alpha- beta hydrolase domain 12
Species	Human
Genbank ID	NM: 001042472.2
Vector	pcDNA3.1(+)-zeo
Restriction sites	BamHI and XhoI
Forward primer sequence	ACA GGATCC GCGGCCTGGGCTGGGATGTGAGG
Reverse primer sequence	ACA CTCGAG ACGGGAGGAGGGCAGAGGTCTTA
Insert Source	Human brain RNA
Antibiotic selection	Ampicillin
DNA insert size (bp)	1371 bp
DNA sequence of insert	<p>gggcctggg ctgggatgtg aggagcgcg ggttccgggc tccgggctct gggtggcggc ggctgtgagc ggcggcactg cggcgcaggc cagcggggcg cgtcggcggc tggccctgtc ggccgcggga tgaggaagcg gaccgagccc gtcgccttgg agcatgagcg ctgcgcgcc gcgggctcgt cctctcagg ctggccgcc gcggcgctgg acgccactg ccgcctgaag cagaacctac gcctgacggg cccggcggcg gctgagccgc gctgcgcagc cgacgcggga atgaagcggg cgctggcag gcgaagggc gtgtggttc gctgaggaa gatacttct tgtgtttgg ggtgtacat tgccattcca tttctcatca aactatgccc tggaaatcac gccaactga tttttgaa ttcgtaaga gttccctatt teattgattt gaaaaacca caggatcaag gttgaaatca cacgtgaac tactacctgc agccagagga agacgtgacc attgagctc ggcacaccgt cctgcagtc tggtggaaga acgccaagg caagaccag atgtggtatg aggatgcctt ggcttcagc caccctata tctgtacct gcattgggaa gcaggtacca gaggaggcga ccaccgctg gagctttaca aggtgctgag ttccttgggt taccatgtgg tcaccttga ctacagaggt tggggtgact cagtgggaa gccatctgag cggggcatga cctatgacgc actccagtt tttgactgga taaagcaag aagtgggtac aaccctgtg acatctgggg ccactctg ggcactggcg tggcgacaaa tctggtgagg cgctctgtg agcgagagac gctccagat gccttata tggaaatccc attactaat atccgcgaag aagctaagag ccattcatt tcagtgatat atcgatact cctggggtt gactggtct tcttgatcc tattacaagt agtggaaata aattgcaaa tgatgaaac gtgaagcaca tctctgtcc cctgctatc ctgcacgctg aggacgacc ggtggtgccc tccagcttg gcagaaagct ctatagcatc gccgaccag ctggaagctt ccgagattc aaagttagt tttgccctt teattcagac cttgggtaca ggcacaata cattacaag agcctgagc tgccacggat actgagggaa ttctgggga agtcggagcc tgagcaccag cactgagcct gcctggga aggaagcatg aagacctctg ccctctccc gt</p>
Protein sequence	Met RKRTEPVALEHERCAAAGSSSSGSA LDADCRLKQNLRLTGPAAEPRCAADAG Met KRALGRRKGVWLRRLRKILFCVLGLYIAIPFLI KLCPGIQAKLIFLNFVRVPYFIDLKKPQDQG LNHTCNYYLQPEEDVTIGVWHTVPAVWVK NAQKDKQMet WYEDALASSHPHILYLHGNAG TRGGDHRVELYKVLSSLGYHVVTFDYRGW GDSVGTPSERGMet TYDALHVFDWIKARSGD NPVYIWGHSLGTGVATNLVRRLCERETPPD ALILESPFTNIREEAKSHPFSVIYRYFPGFDW FFLDPITSSGIKFANDENVKHISCPILLHAE DDPVVPFQLGRKLYSIAAPARSFRDFKVF VPFHSDLGYRHKYIYKSPELPRILREFLGKS EPEHQH
Calc Mol Weight (kDa)	45068.18 KDa
General Description	The purple colour indicates the forward and reverse primers while the blue colour indicates the starting and stopping codons.

Map:

5' site BamHI

3' site XhoI

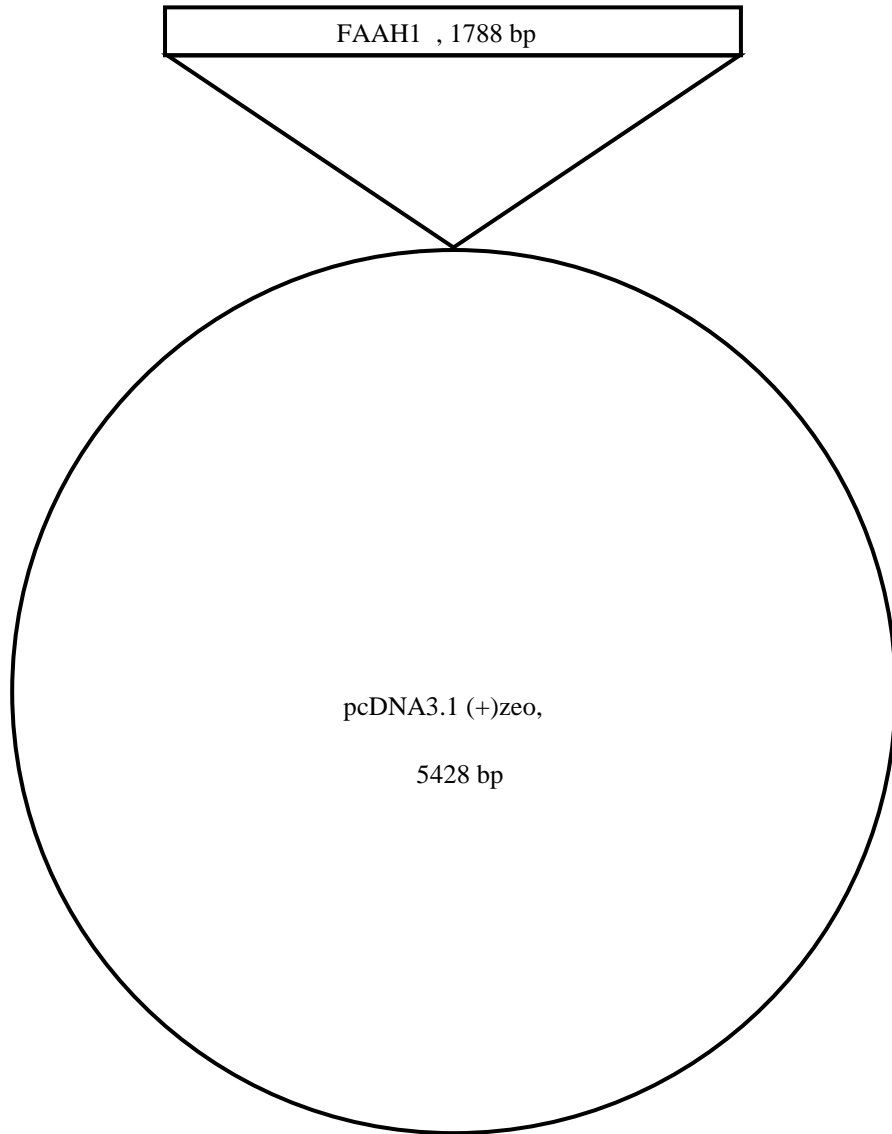


	<p>CETQLSQAPR QGLLYGVPVS LKECFYKGGQ DSTLGLSLNE GVPAECDSVV VHVLKLGAV PFVHTNVPQS MFSYDCSNPL FGQTVNPWKS SKSPGGSSGG EGALIGSGGS PLGLGTDIGG SIRFPSSFSG ICGLKPTGNR LSKSGLKGCV YGQEAURLSV GPMARDVESL ALCLRALLCE DMFRLDPTVP PLPFREEVYT SSQPLRVGY ETDNYTMPSP AMRRVLETQ QSLEAAGHTL VPFLPSNIPH ALETSTGGL FSDGGHTFLQ NFKGDFVDPC LGDLVSILKL PQWLKGLLAF LVKPLLRLS AFLSNMKSRS AGKLWELQHE IEVYRKTVIA QWRALDLVV LTPMLAPALD LNAPGRATGA VSYTMLYNCL DFPAGVVPVT TVTAEDEAQM EHYRGYFGDI WDKMLQKGMK KSVGLPVAVQ CVALPWQEEL CLRFMREVER LMTPEKQSS</p>
Calc Mol Weight (Da)	66519.14 Da
General Description	The purple colour indicates the forward and reverse primers while the blue colour indicates the starting and stopping codons.

Map:

5' site KpnI

3' site BamHI



Plasmid Name	FAAH2 pcDNA3.1(+) zeo
Protein	Fatty acid amide hydrolase 2
Species	Human
Genbank ID	NM: NM_174912.3
Vector	pcDNA3.1(+) zeo
Restriction sites used	KpnI and BamHI
Forward primer sequence	gatc GGTACC ctgcgatggcaccttcattacc
Reverse primer sequence	gata GGATCC gctggtgcttgattcacc
Insert Source	cDNA of hepatocyte and liver
Antibiotic selection	Ampicillin
DNA insert size (bp)	1689 bp
DNA sequence of insert	ACTCACTATAGGGAGACCCAAGCTGGCTAGCGTT TAAACTTAAGCTT GGTACC ctgcgatggcaccttcattaccgcc cgcattcagttgtcctcttggggcgctaggttctcataggttagtagccgag cagctttagtcttaggggtccaaagttgctcaaacacctcggccggtgact gaaccattgcttctgcttgggatgagctgccaagctgatccgacagagaa agggtgaaatgatagatgtgttcaggcttatcaacagaatcaaggacgtgaacc caatgatcaatgaattgtcaagtacaggttgagggaagcgaagaggctcat gctgtagatcaaaagcttcagagaaagcaggaagatgaagccacctggaaaat aatggcccttcttggggttcttggacagtcaggaagcttccagctacaagga atgcccaattcttggactcatgaaccgtcgtgatccattgccccaaacagatgcc actgtggtggcattactgaaggagctggtgccattccttggcacaaccaactgt agtgagttgtgtatggtatgaatccagtaacaagatctatggccgatcaaacac ccatagattacagcatattgaggtggaagttctggtggtgagggctgcacactg gcagctgcctgctcagttattggtgtggctctgatattggtgtagcattcgaatgc ctgcttctcaatggtatattggacacaagccttccaggtggttccccaaaa ggtcagttcccttggctgtgggagcccaggagttgttctgtcactggtcctatgt gccgttatgctgaagacctggccccatgtgaaggtcatggcaggacctgggat caaaaggftaaaactagacacaaaaggtacattaaaaactaaaatttactggat ggaacatgatggaggctcattttatgtccaaagtgaccaagatctcattatgact cagaaaaaggtgtgttcacctgaactattctaggacctcagttcaacatgta aactgaagaaaatgaagtacttttcagttgtggatgcaatgatgcagcaaaag gacatgatgggaaggaacctgtgaaattgtagattgcttggtagacctgggaaa catgtcagtcctctgtgggagttgatcaaatggtgcctgggtctgcagttacacc atccttccattgactggcttgggaagaaagctcagatataccaatgagaaa taccaaaagtttaaggcagtggaagaaagcctcgtaaaagagctggtgatagc taggtgatgatggtgttcttatatccctcacatcccacagttggcacctaaagcatca tgtcccttaacacggccttcaacttcttacacaggtgtctcagtcacctgggtt tgctgtgacccaatgccactgggactgaatgcaaaagactccctttaggcatc caggttgtgctggacctttaatgatcatctgacctggctgtggccagctacttg gagaaaactttggggctgggtctgtccaggaaagtttaggagacctctgca aggttaatgtgtgtgtgtttgtgttcgtgtggtggttcttattaattgggtgaaatc aagcaccagcGGATCC ACTAGTCCAGTGTGGTGGGAATT CTGCAGATATCCAGCACAGTGGCGGCCGCTCGAG TCTAGAGGGCCCCG
Protein sequence	MAPSFTARIQLFLLRALGFLIGLVGRAALVLGGPKF ASKTPRPVTEPLLLLSGMQLAKLIRQRKVKCIDVVQ AYINRIKDVNPMINGIVKYRFEEAMKEAHA VDQKL AEKQEDEATLENKWPFLGVPLTVKEAFQLQGMPNS SGLMNRDAIAKTDATVVALLKGAGAIPLGITNCSE LCMWYESSNKIYGRSNNPYDLQHIVGGSSGEGCT LAAACSVIGVGS DIGGSIRMPAFFNGIFGHKPSGVV PNKGQFPLAVGAQELFLCTGPMCRYAEDLAPMLKV MAGPGIKRLKLDTKVHLKDLKIFYWMEHDGGSFLM

	SKVDQDLIMTQKKVVVHLETILGASVQHVKLKKMK YSFQLWIAMMSAKGHDGKEPVKFVDLLGDHGKHV SPLWELIKWCLGLSVYTIPSIGLALLEEKLRYSNEKY QKFKAVEESLRKELVDMLGDDGVFLYPSHPTVAPK HHVPLTRPFNFAYTGVFSALGLPVTQCPLGLNAKGL PLGIQVVAGPFNDHLTLAVAQYLEKTFGGWVCPGF
Calc Mol Weight (Da)	58303.52 Da
General Description	The purple colour indicates the forward and reverse primers while the blue colour indicates the starting and stopping codons.

Map:

5' site KpnI

3' site BamHI

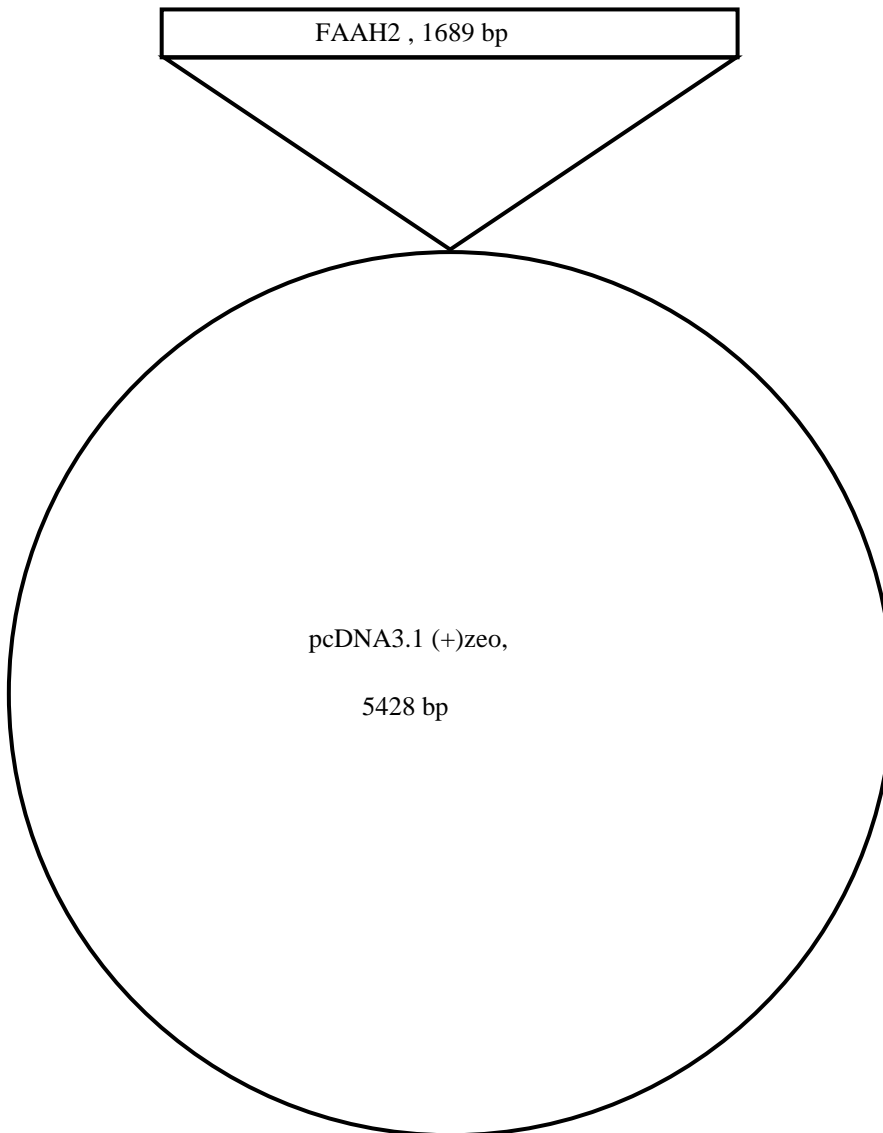


Table A.2: Detailed cloning information about tagged MAGL1, MAGL2 and ABHD6 from C and N terminal sites.

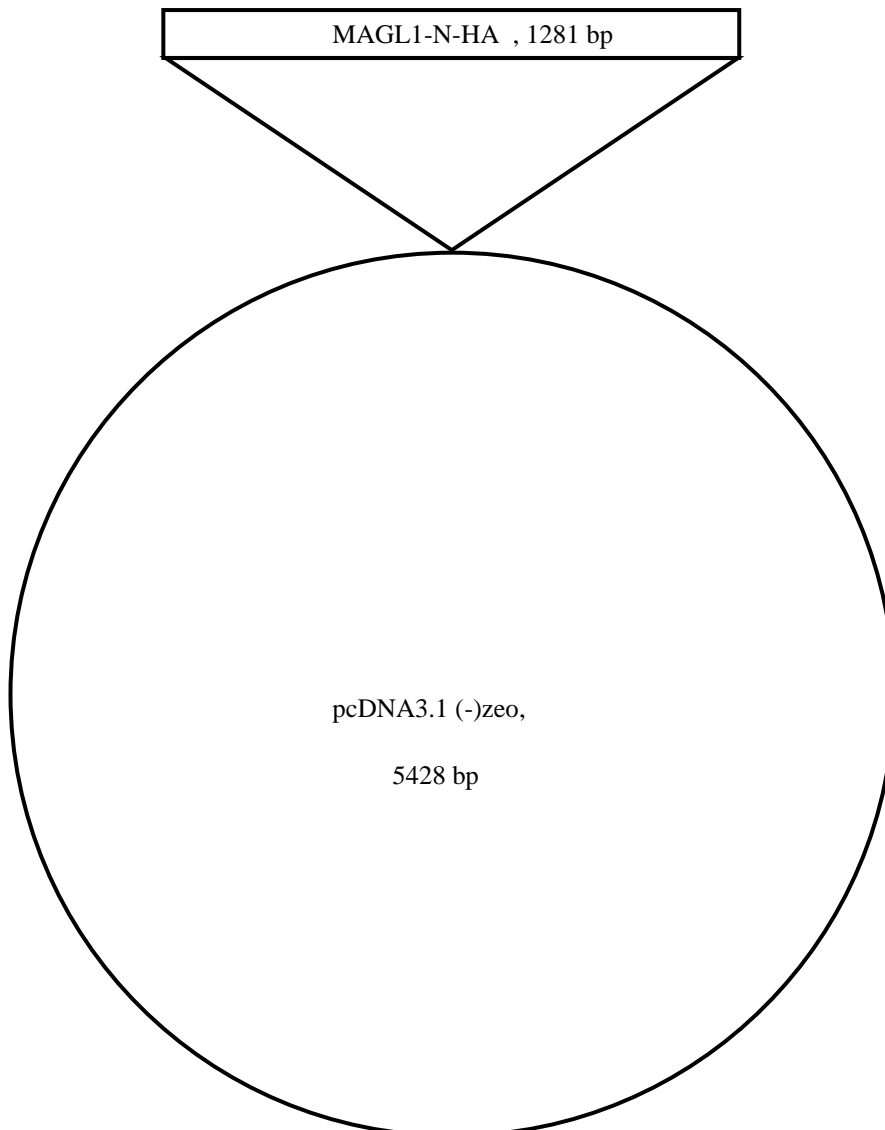
Plasmid Name	MAGL1 –HA- N- terminus tag pcDNA3.1(-)zeo
Protein	MAGL1 tagged to HA protein from the N end
Species	Human
Genbank ID	NM: NM_007283.6
Vector	pcDNA3.1(-)zeo
Restriction sites	KpnI and HindIII
Forward primer sequence	gatcGGTACCATGTACCCATACGATGTTCCAGATTACGC TGGAAAGTGGTgaaacaggacctgaagaccct
Reverse primer sequence	ACAAAGCTTGGAGAGGCAGGGCAGAGGCTTGGC (original)
Insert Source	MAGL1 untagged plasmid
Antibiotic selection	Ampicillin
DNA insert size (bp)	1281 bp
DNA sequence of insert	TAATACGACTCACTATAGGGA GACCCAAGCTGGCTAG CGTTTAAACGGGCCCTCTAGACTCGAGCGGCCGCCAC TGTGCTGGATATCTGCAGAATTCCACCACACTGGACTA GTGGATCCGAGCTCGGTACCATGTACCCATACGATGTT CCAGATTACGCTGGAAGTGGTgaaacaggacctgaagaccctccag catccagaggaaagtccccaggcggaccccgcagagcattccctaccaggacctcc ctcacctgtcaatcgacacggacagtacctctctgcaggtactgaaacccacaggca cacccaaggccctcatcttgtgtccatggagccggagagcacagtgccgctatgaag agctgctcggatgctgatgggctggacctgctggtgtcggccacgacctgttgcc acggacagagcgaaggggagaggatgtagtctgactccacgtttcgtcagggatg tgttcagcatgtgattccatgcagaaagactaccctgggcttctgtcttctctggg actccatgggaggcgcctatgcatcctcacggccgcagagaggccgggacccttgc cgcatggtactcatttgcctctggttcttccaactctgaatctgcaacaacttcaagg cttctgctgcaagtgctcaacctgtgctgccaactgtccctcgggcccacgactccag cgtgctctctcgaataagacagaggctgacattataactcagacccctgatctcggg gcagggtgaaagtgctcggcatccaactgctgaatccgctcaggggtggagcg cgccctcccaagtgactgtgccctctctgctcagggctctgccgatgcctatgt gacagcaaaagggcctacctgctcatggagtagccaagagccaggacaagactc gatttatgaaagtgctaccatgttccacaaggagcttctgaagtcaccaactccgt ccatgaaataaacatgtgggtctcacaaggacagccacggcaggaactgctcccac cctgaatgcattggcgggtcccggctcaggtctgggggatgcaggcaggggaaagg cagagatggcttctcagatgctgctgcaaaaaaaaaaaaaaaaaaaatcagaaattg gagaaatccttagcacaatttctaaaaataacagacattttgtatacattagactatc cagactgacctacctaaggttagacactttatgcaaaaaagagaaaggtccagtgat ttccacaagaatgtgtaaatgtccactgaaaacaaagccaaagcctctgacctgct ccAAGCTTAAGTTTAAACCGCTGATCAGCCTCGACTGT GCCTTCTA
Protein sequence	MYPYDVEDYAGSEETGPEDPSSMPEESSPRRTPQSIPYQD LPHLVNADGQYLFCRYWKPTGTPKALIFVSHGAGEHSG RYEELARMLMGLDLLVFAHDHVGHGQSEGERMVVSD HVFVRDVLQHVDSMQKDYPGLPVFLLGHSMGGAIALT AARPGHFAGMVLISPLVLANPESATTFKVLAAKVLNLV LPNLSLGPIDSSVLSRNKTEVDIYNSDPLICRAGLKVCFGI QLLNAVSRVERALPKLTVPFLLQGSADRLCDKSGAYLL

	MELAKS QDK TLKI YEG AYHVL HKEL PEVTNS VFHE INM WVSQRTATAGTASPP*(MHWPV PGSWGGCR QGKGR DG FSDMAC QKKKKK IRNWRNP* HNFLK NNRH FCY TLDYQ TL DLP * WLD TLCKKRERSQ VIFHKE CAKMSTEN KAK PLP CLS)
Calc Mol Weight (kDa)	35577.81 KDa
General Description	The yellow colour indicates T7 and BGH-R primers. The red colour indicates cutting enzymes. Light grey colour is for starting and stopping codon while dark one is for CDS. The blue colour is for reverse primer. The purple colour indicates HA tag sequence while the green colour indicates flexor linker sequence.

Map:

5' site KpnI

3' site HINDIII



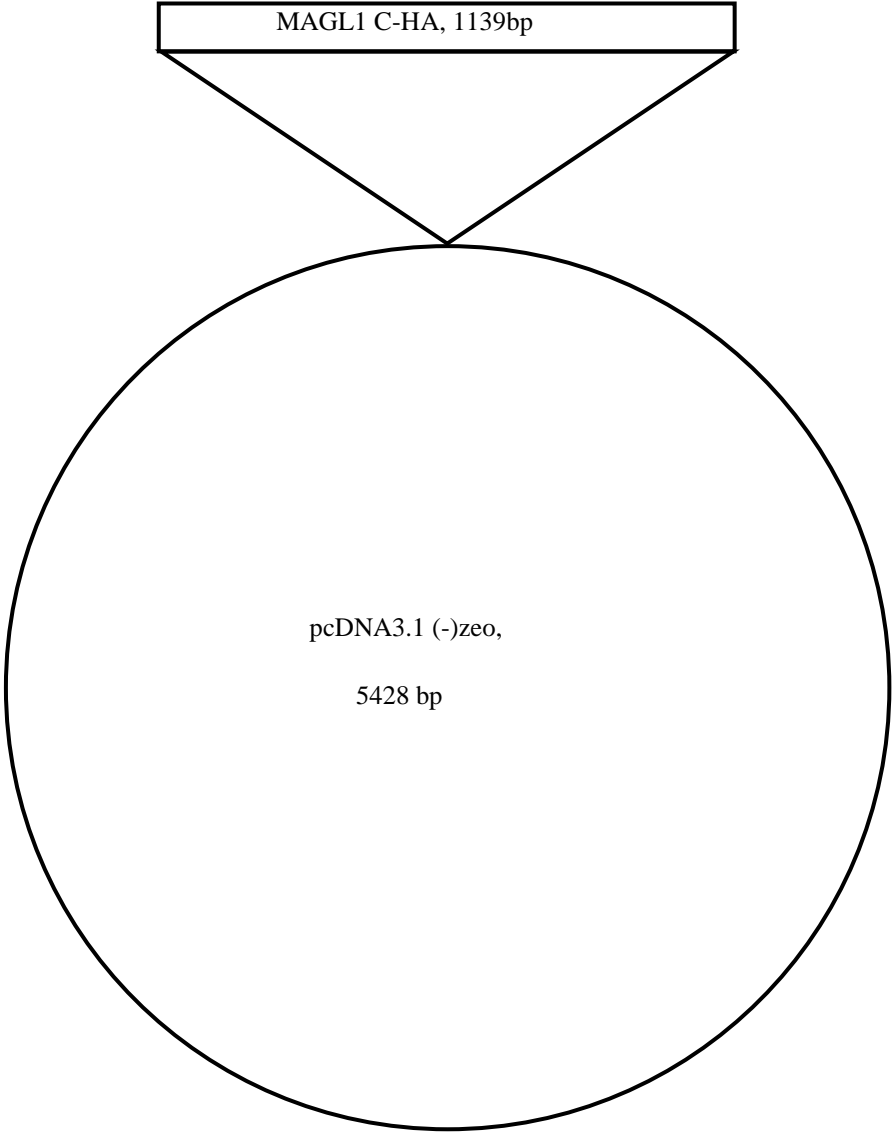
Plasmid Name	MAGL1 –HA- C- terminus tag pcDNA3.1(-)zeo
Protein	MAGL1 tagged to HA protein from the C end.
Species	Human
Genbank ID	NM: NM_007283.6
Vector	pcDNA3.1(-)zeo
Restriction sites used	BamHI and KpnI
Forward primer sequence	ACAGGATCCggctgagcgccccagcccgaaggcag (original)
Reverse primer sequence	gatcGGTACC TTAAGCGTAATCTGGAACATCGTATGGGTA ACCACTTCGGGTGGGGACGCAGTTCCTGC
Insert Source	MAGL1 untagged plasmid
Antibiotic selection	Ampicillin
DNA insert size (bp)	1139 bp
DNA sequence of insert	TAATACGACTCACTATAGGGAGACCCAAGCTGGCTAGC GTTTAAACGGGCCCTCTAGACTCGAGCGGCCCACTGT GCTGGATATCTGCAGAATTCCACCACACTGGACTAGT GATCCggctgagcgccccagcccgaaggcagggtctgggtgcgggaagggtc ggagctgcctctctgctgccttggggccgccagatgagggaacagcccgattgcctggt ctgattctccaggctctgctggttggatgcaaacgccagcacataatgaaacaggacc tgaagaccctccagcatgccagaggaaagtccccaggcggaccgccagagcattcc ctaccaggacctccctcacctggtcaatgcagacggacagctacctctctcaggtactgga aaccacaggcacaccaaggccctcatcttgtgccatggagccggagagcacagtgg ccgetatgaagagctggctcggatgctgatgggctggacctgctggtgtgccacgac catgttgccacggacagagcgaaggggagaggatgtagtctgactccagcttctgt cagggatgtgtgcagatgtgattccatgcagaagactaccctgggtctctgtctctt ctggccactccatggaggcgcctatccatcctcagggccgagagggccgggcca cttcgccgcatggtactcatttcgctctgttctgccaatctgaatctgcaacaacttcaa ggtccttctgctgcaaggtgctcaacctgtgctgccaactgtcctcgggccatgactc cagcgtgctctcgaataagacagaggtgcacattataactagaccctgatctgccg ggcagggtgaaggtgtcttcggcatccaactgctgaatgccgtctcaggggtgagcgc gccctcccaagctgactgtccctctctgctcagggctctgccgatgcctatgtgac agcaaggggcctacctgctcatggagttagccaagagccaggacaagactctcaagatt atgaaggtgctaccatgttccacaaggagcttctgaagtccaactccgtcttccatga aataaacatgtgggtctctcaaaggacagccagggcaggaactgcgtccccaccGGA AGTGGT TACCCATACGATGTTCCAGATTACGCTTAA GGT ACCAAGCTTAAAGTTTAAACCGCTGATCAGCCTCGACTGT GCCTTCTA
Protein sequence	METGPEDPSSMPEESSPRRTPQSIPYQDLPHLVNADGQYLF CRYWKPTGTPKALIFVSHG AGEHSGRYEELARMLMGLDLLVFAHDHVGHGQSEGERM VVSDFHVFVRDVLQHVDSMQKD YPGLPVFLLGHSMGGAIAILTAAERPGHFAGMVLISPLVLA NPESATTFKVLAAKVLNLV LPNLSLGPIDSSVLSRNKTEVDIYNSDPLICRAGLKVCFGIQ LLNAVSRVERALPKLTV FLLQGSADRLCDSKGYLLMELAKSQDKTLKIYEGAYH VLHKELPEVTNSVFHEINMWV SQRATAGTASPPGSGYPYDVPDYA*
Calc Mol Weight (kDa)	35555.10 KDa
General Description	The yellow colour indicates T7 and BGH-R primers. The red colour indicates cutting enzymes.

	Light grey colour is for starting and stopping codon while dark one for CDS. The blue is for forward primer. The purple colour indicates HA tag sequence while the green colour indicates flexor linker sequence.
--	--

Map:

5' site BamHI

3' site KpnI

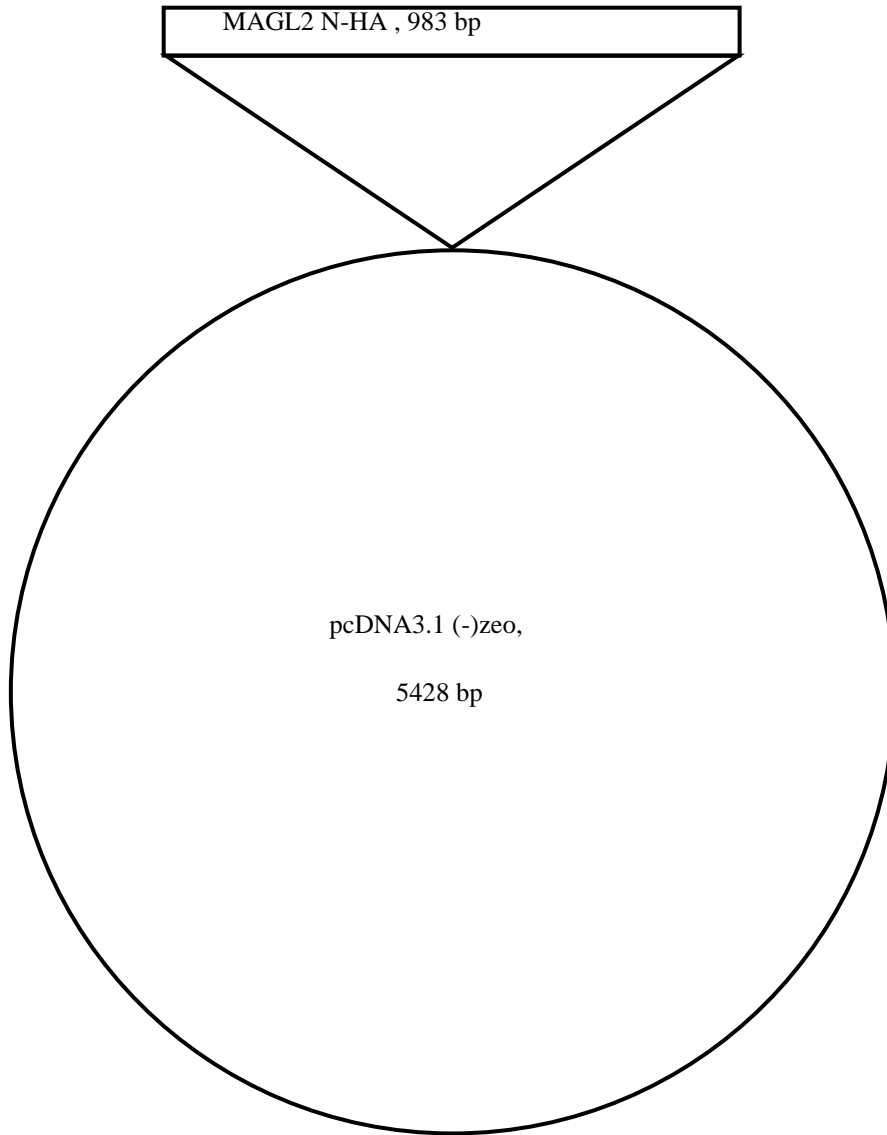


Plasmid Name	MAGL2 –HA- N- terminus tag pcDNA3.1(-)zeo
Protein	MAGL2 tagged to HA protein from the N end
Species	Human
Genbank ID	NM: 001003794.2
Vector	pcDNA3.1(-)zeo
Restriction sites used	KpnI and HindIII
Forward primer sequence	gatcGGTACCATGTACCCATACGATGTTCCAGATTACGC TGAAGTGGTCCAGAGGAAAGTTCCCCCAGG
Reverse primer sequence	ACAAAGCTTCCCCAGACCATGAGCCGGGCA (original)
Insert Source	MAGL2 untagged plasmid
Antibiotic selection	Ampicillin
DNA insert size (bp)	983 bp
DNA sequence of insert	TAATACGACTCACTATAGGGAGACCCAAGCTGGCTAG CGTTTAAACGGGCCCTCTAGACTCGAGCGGCCGCCAC TGTGCTGGATATCTGCAGAATTCCACCACACTGGACTA GTGGATCCGAGCTCGGTACCATGTACCCATACGATGTT CCAGATTACGCTGGAAGTGGTccagaggaaagttccccaggcggga ccccgcagagcattccctaccaggacccctcacctgtgcaatgcagacggacagtacc tctctgcaggtactgaaaccacaggcacaccaaggccctcatcttctgtgccatgg agccggagagcacagtggccgctatgaagagctggctggatgctgatgggctggac ctgctggtttcccccacaccatgttgccacggacagagcgaaggggagaggatggt agtgtctgactccacgtttctgtagggatgtgtgcagcatgtggattccatgcagaaaga ctaccctgggcttctgtcttctctggccactccatgggaggcgcaccatccatcctca cggccgcagagaggccggccacttcgccgcatggtactcatttcgcctctggttctgc caatcctgaatctgcaacaacttcaaggctcttctgctcgaaagtgtcaacctgtgctgcc aaactgtccctcgggccatcgactccagcgtgctctctcggaaataagacagaggtcga catttataactcagaccctgatctgccggcagggtgaaggtgcttcggcatccaa ctgctgaatgccgtctcacgggtgagcgcacctccccaaagctgactgtgccctctctg ctgctccagggtctgcccgatgcctatgtgacagcaaagggcctacctgctcatggag ttagccaagagccaggacaagactctcaagattatgaaggtcctaccatgttctccaca aggagctcctgaagtccaactccgtcttccatgaaataaacatgtgggtctctcaagg acagccacggcaggaaactgcgtccccaccctgaatgcattggcggggtccccgctcag gtctgggggAAGCTTAAGTTTAAACCGCTGATCAGCCTCGA CTGTGCCTTCTA
Protein sequence	MYPDVPDYAGSGPEESSPRRTPQSIPYQDLPHLVNADG QYLFRCRYWKPTGTPKALIFVS HGAGEHSGRYEELARMLMGLDLLVFAHDHVGHGQSEG ERMVVSDFHVFVRDVLQHVDSMQ KDYPGLPVFLLGHSMGGAIAILTAAERPGRHFGMVLISPL VLANPESATTFKVLAAKVLN LVLPNLSLGPIDSSVLSRNKTEVDIYNSDPLICRAGLKVCF GIQLLNAVSRVERALPKLT VPFLLQGSADRLCDSKGYLLMELAKSQDKTLKIYEGA YHVLHKELPEVTNSVFHEINM WVSQRTATAGTASPP*
Calc Mol Weight (kDa)	34524.71 KDa
General Description	The yellow colour indicates T7 and BGH-R primers. The red colour indicates cutting enzymes. Light grey colour is for starting and stopping codon while dark one for CDS. The blue colour is for reverse primer. The purple colour indicates HA tag sequence while the green colour indicates flexor linker sequence.

Map:

5' site KpnI

3' site HINDIII

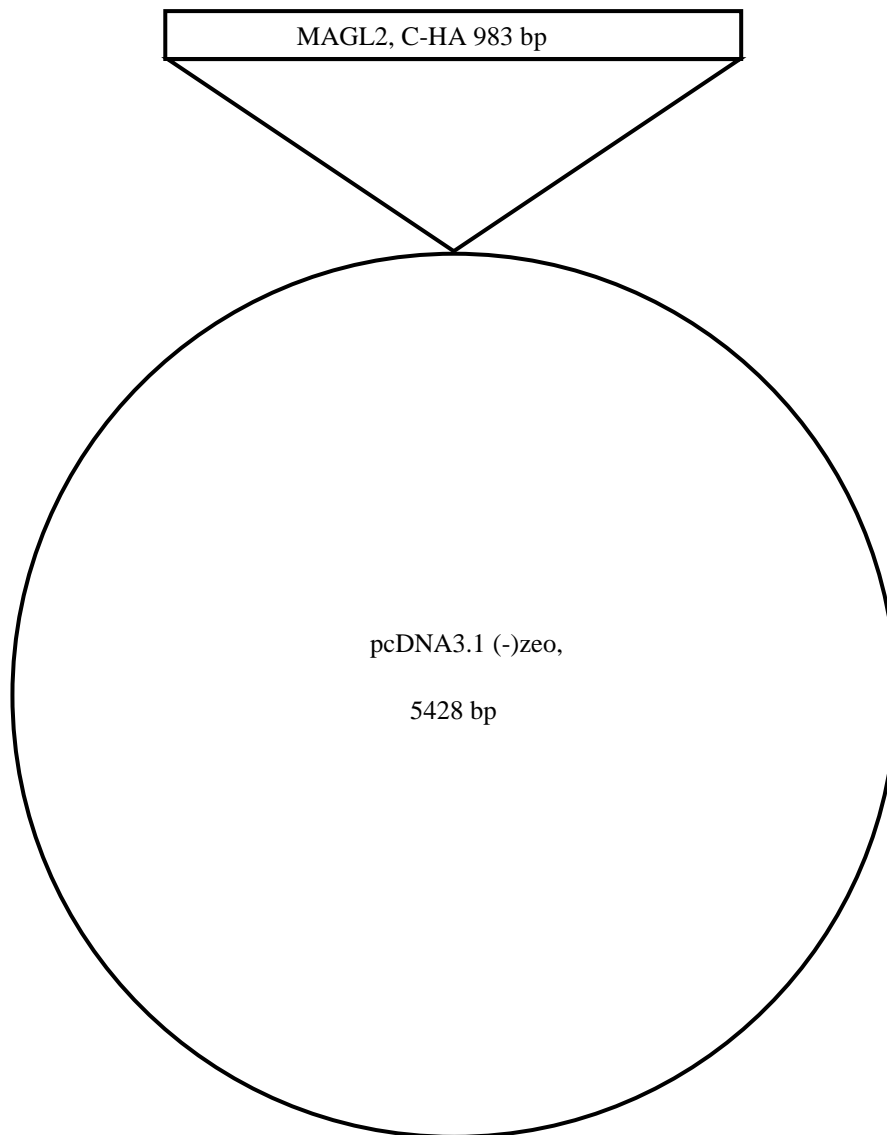


Plasmid Name	MAGL2 –HA- C- terminus tag pcDNA3.1(-)zeo
Protein	MAGL2 tagged to HA protein from the C end.
Species	Human
Genbank ID	NM: 001003794.2
Vector	pcDNA3.1(-)zeo
Restriction sites used	BamHI and KpnI
Forward primer sequence	ACAGGATCCGCGCTCGTGGCCCCGGACCT (original)
Reverse primer sequence	gacGGTACCTTAAGCGTAATCTGGAACATCGTATGGG TAACCACTTCgggtgggacgcagttcctgc
Insert Source	MAGL2 untagged plasmid
Antibiotic selection	Ampicillin
DNA insert size (bp)	983 bp
DNA sequence of insert	AATACGACTCACTATAGGGAGACCCAAGCTGGCTAG CGTTTAAACGGGGCCCTCTAGACTCGAGCGGCCGCCA CTGTGCTGGATATCTGCAGAATTCCACCACACTGGAC TAGTGGATCGgcgctcgtggccccggacctgaagaccctccagcatgccag aggaaagtccccagggcggacccgcagagcattccctaccaggacctccctacct ggtcaatgcagacggacagtacctctctcgaggtactggaaccacagggcacacce aaggccctcatctttgtgccatggagccggagagcacagtggccgctatgaagagc tgctcggatgctgatgggctggacctgctgtgttcgccacgacctgttgccac ggacagagcgaaggggagagatgtagtctgactccacgtttcgtcagggatg tgtgcagcatgtggattccatgcagaaagactaccctgggcttctcttctctggg ccactccatgggagggccatcgccatcctcacggccgcagagagggccgactt cgccggcatgtactcatttcgctctggttctgccaatcctgaatctgcaacaacttca aggtccttctcgcgaaagtctcaacctgtctgccaactgtccctcgggccatcg actccagcgtctctcggataagacagagtcgacattataactcagacccctg atctccgggagggctgaaggtgtcttcgcatccaactgctgaatgccgtctcacg ggtggagcggccctccccagctgactgtcccttctgctgctccagggtctcgc gatcgctatgtgacagcaaggggcctacctgctcatggatgccaagaccagg acaagactctcaagattatgaagtgctaccatgttccacaaggagcttctgaagt caccaactccttccatgaataaacatgtgggtctcctcaaggacagccacggcag gaactcgtccccaccGGAAGTGGTACCCATACGATGTTCC AGATTACGCTTAAAGGTACCAAGCTTAAAGTTTAAACC GCTGATCAGCCTCGACTGTGCCTTCTA
Protein sequence	MPEESSPRRTPQSIPYQDLPHLVNADGQYLFRCRYWKPT GTPKALIFVSHGAGEHSGRYEE LARMLMGLDLLVFAHDHVGHGQSEGERMVVSDFHVF VRDVLQHVDSMQKDYPGLPVFLLG HSMGGAIAILTAAERPGHFAGMVLISPLVLANPESATTF KVLAAKVLNLVLPNLSLGPID SSVLSRNKTEVDIYNSDPLICRAGLKVCFGIQLLNAVSR VERALPKLTVPFLLLQGSADR LCDSKGAYLLMELAKSQDKTLKIYEGAYHVLHKELPE VTNSVFHEINMWVSQRTATAGTA SPPGSGYPYDVPDYA*
Calc Mol Weight (kDa)	34524.71 KDa
General Description	The yellow colour indicates T7 and BGH-R primers. The red colour indicates cutting enzymes. Light grey colour is for starting and stopping codon while dark one for CDS. The blue is for forward primer. The purple colour indicates HA tag sequence while the green colour indicates flexor linker sequence.

Map:

5' site BamHI

3' site KpnI

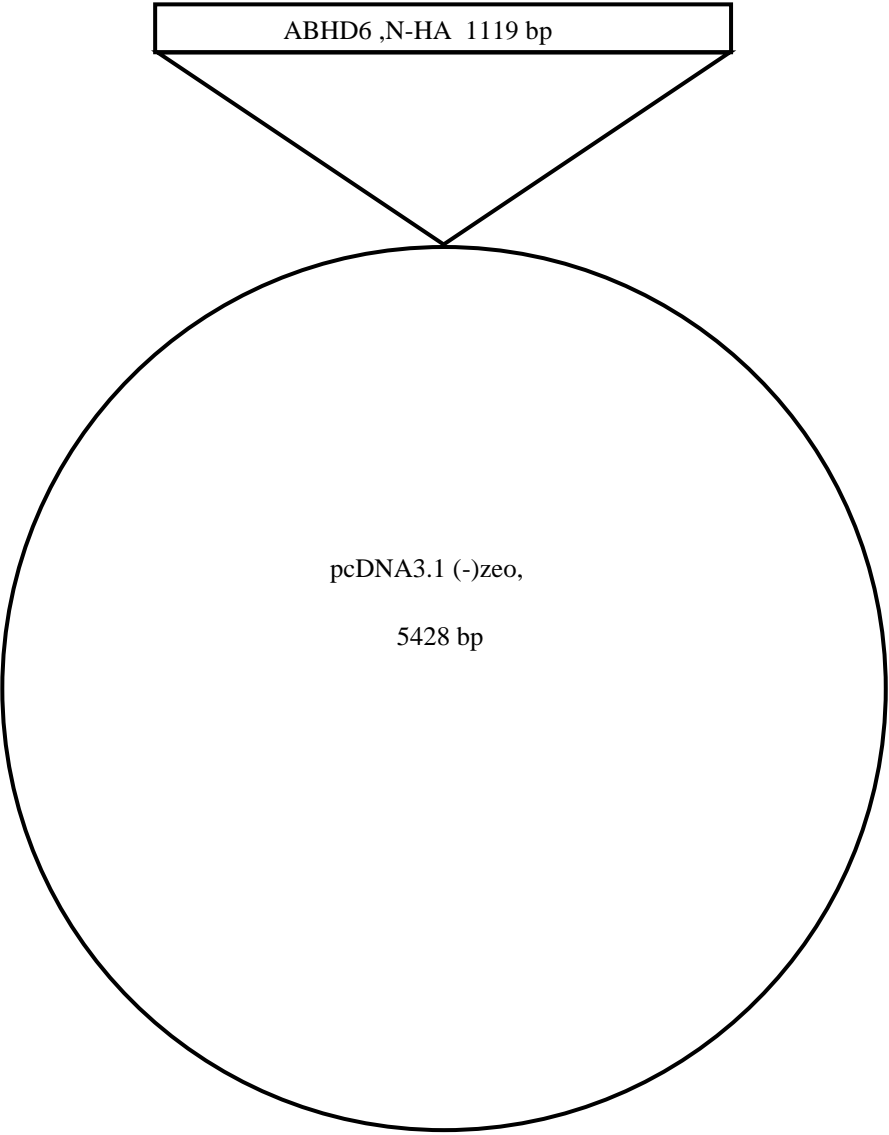


	Light grey colour is for starting and stopping codon while dark one for CDS. The blue colour is for reverse primer. The purple colour indicates HA tag sequence while the green colour indicates flexor linker sequence.
--	--

Map:

5' site KpnI

3' site HINDIII



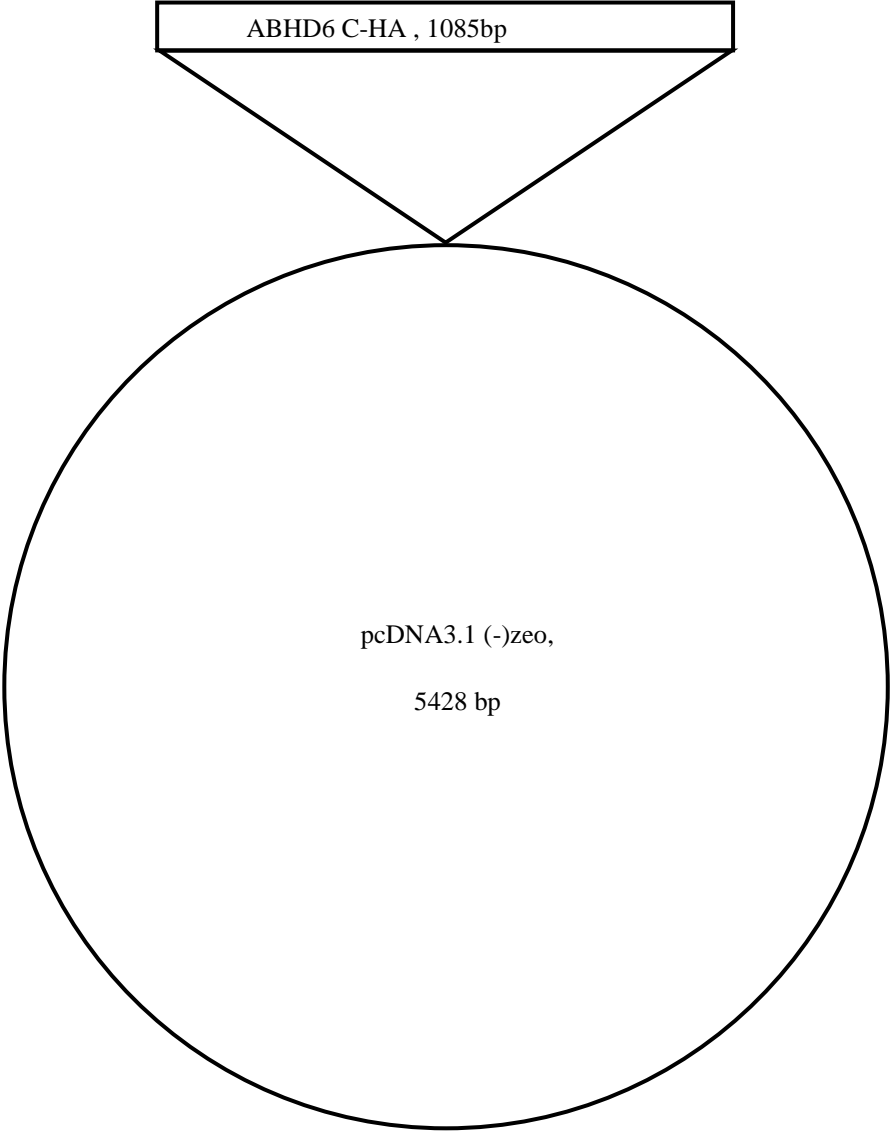
Plasmid Name	ABHD6 –HA- C- terminus tag pcDNA3.1(-)zeo
Protein	Alpha – beta hydrolase domain -6 tagged to HA protein from the C end.
Species	Human
Genbank ID	NM: 020676.5
Vector	pcDNA3.1(-)zeo
Restriction sites used	BamHI and KpnI
Forward primer sequence	ACAGGATCCGGCTGGTCAGGAGTCAGCCAGCCT (original)
Reverse primer sequence	gacGGTACCTTAAGCGTAATCTGGAACATCGTATGGGTA ACCACTTCCgtccagctcttgtgtgtgc
Insert Source	Abhd6 untagged plasmid
Antibiotic selection	Ampicillin
DNA insert size (bp)	1085 bp
DNA sequence of insert	TAATACGACTCACTATAGGGAGACCCAAGCTGGCTAGC GTTTAAACGGGCCCTCTAGACTCGAGCGGCCCGCCACTGT GCTGGATATCTGCAGAATTCCACCACACTGGACTAGT GATCCggctggtcagagtcagccagccgaaagagcaggatggatcttgatggtta acatgtttgtgattcggggcgacgctggccatccaatcctggcatttggcttcatttctt ctgtggcctcagcactgataagaatctatttggactggcggaggacattggcctgca gtccgctatgttaccatgaagactatcagttctgttattcctccggggcagcctgggcaca aacctccatcctcatgctccacggattctctgccacaaggatatgtgctcagtggtca gttcctccaagaacctgcacttggctgctgacatgccaggacatgagggcaccaccc gctcctccctggatgactgcatagatgggcaagttaagagatacaccagttgtagaat gcctgaagctgaacaaaaaccttccacctgtaggcacctccatgggtggccaggtggct gggtgtatgctgctactaccatcggatgctccagcctgtgctcgtgtgctcgtggcct gcagtactcaactgacaatcaattgtacaacggctcaagaactgcaggcctctccgccg tgagaagatccctgatcccgtctaccccagaagagatgagtgaatgctcagctctgct cctatgtccgctcaaggtgccccagcagatcctgcaaggcctgtcgtatgctccgcatcctc ataacaactctaccgaaagtgttttgaaatgctcagtgagaagtcagatactctccat cagaacatggacaagatcaaggtccgacgagatcatctgggggaaacaagaccaggtg ctggatgtctggggcagacatgttgccaagtcaattgccaactgccagtggtgagcttctg gaaaactgtgggcactcagtagtgatgaaagaccaggaagacagccaagctcataatcg acttttagcttctgtgcacaacacagacaacaagaagctggacGGAAGTGGTI ACCCATACGATGTTCCAGATTACGCTTAAAGTACCAAGC TTAAGTTTAAACCGCTGATCAGCCTCGACTGTGCCTTCT A
Protein sequence	MDLDVVNMFVIAAGGTLAIPILAFVASFLLWPSALIRIYYWY WRRTLGMQVRYVHHEDYQF CYSFRGRPGHKPSILMLHGFSAHKDMWLSVVKFLPKNLHL VCVDMPGHEGTRSSLDL IDGQVKRIHQFVECLKLNKKPFHLVGTSMGGQVAGVYAA YYPDVSSLCLVCPAGLQYST DNQFVQRLKELQGSAAVEKIPLIPSTPEEMSEMLQLCSYVR FKVPQQILQGLVDRIPH NFYRKLFLFIVSEKSRYSLHQNMDKIKVPTQIIWGKQDQVL DVSGADMLAKSIANCQVEL LENCGHSSVVMERPRKTAKLIIDFLASVHNTDNNKKLDGSG YPYDVPDYA*
Calc Mol Weight (kDa)	39615.99 KDa
General Description	The yellow colour indicates T7 and BGH-R primers. The red colour indicates cutting enzymes. Light grey colour is for starting and stopping codon while dark one for CDS. The blue is for forward primer.

	The purple colour indicates HA tag sequence while the green colour indicates flexor linker sequence.
--	--

Map:

5' site BamHI

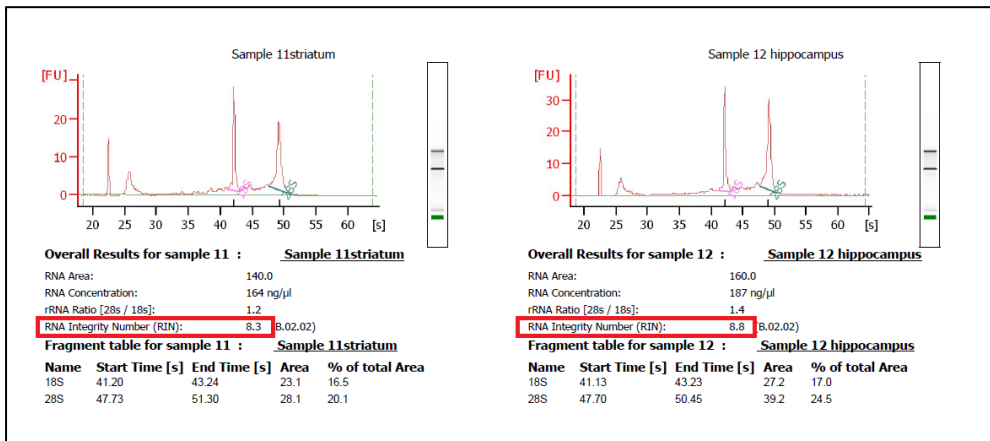
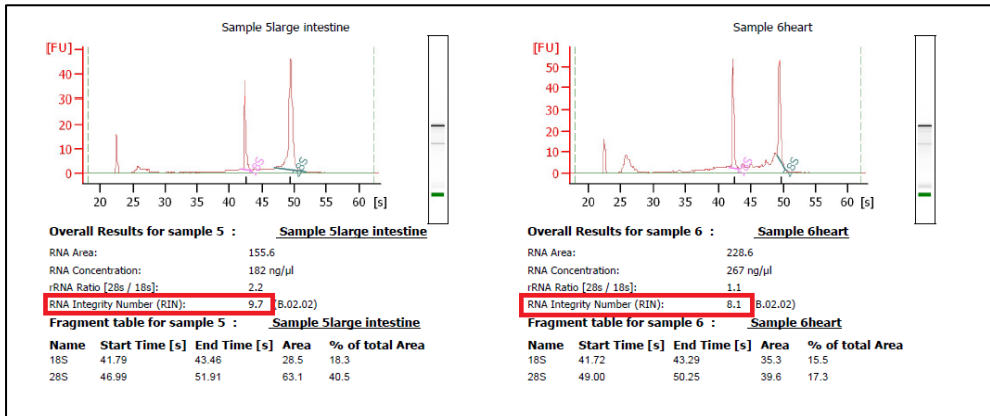
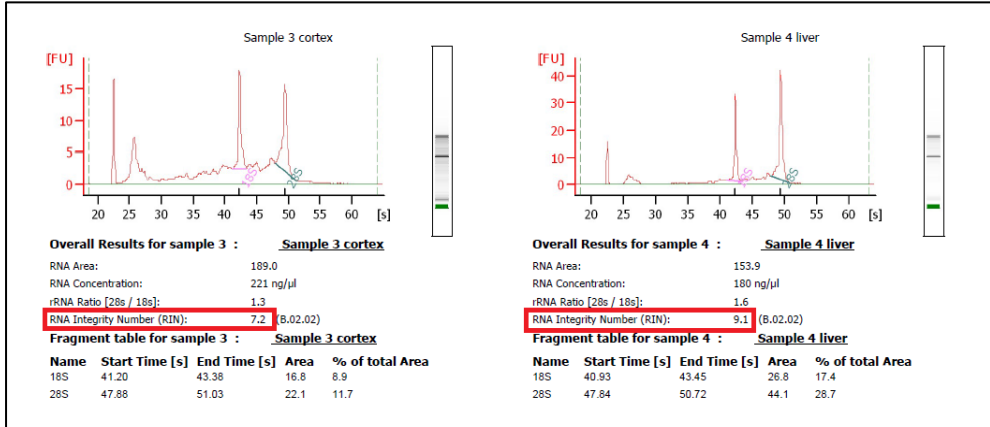
3' site KpnI



CDS of MAGL-1- mRNA
 (Yellow colour is MAGL 1 primers)
 (Green colour is MAGL 3 primers)
 (Brown colour is CDS)
 (Turquoise colour is the supposed missing part in MAGL3: 90 nucleotide)

	CCCAAACCAA	CTTGTCCCA	TCAACTCCAT	CTTTCTAGTC	CCCACCTTCC	CCGGTGACAG
61	CACCCGGCGA	AGCCACCCG	GTTTTCCAG	CGGCATTTC	GATGACAGCT	TCGGGGCTAC
121	GTGTCTGTG	CTGTCCGAGA	CGCACAGGAA	GCAAAGTTG	TGAGAAGCCT	TGGGGGCGAC
181	TTGCCTTGG	GCACCCGCAT	TTGTGCGTCT	GCGAGGTGCC	TCGGTGTGCG	CGGAGCTAGT
241	TTCCAGTTT	CCCGGGCCCC	TCCCTTCTCC	GAGCCCTCT	AGCGATTGT	TTAGGAAAAG
301	TGATGACATG	AACTAGTAGT	GGAGATCGC	AGGCCCGCTC	CCCGCCCTGG	GGAGGGAGGG
361	GAGCCCGGGA	GAGCCTGCGG	GTGGGAGCTG	GAAGCAGGCT	CCCGGCTGAG	CGCCCCAGCC
421	CGAAAGGCAG	GGTCTGGGTG	CGGGAAAGAG	GCTCGGAGCT	GCCTTCCTGC	TGCTTGGGG
481	CGCCCCAGAT	GAGGGAACAG	CCCGATTTCG	CTGGTTCGTA	TTCTCCAGGC	TGTCGTGGTT
541	GTGGAATGCA	AACGCCAGCA	CATAATGGAA	ACAGGACCTG	AAGACCCTTC	CAGCATGCCA
601	GAGGAAAGTT	CCCCCAGGCG	GACCCCGCAG	AGCATTCCCT	ACCAGGACCT	CCCTCACCTG
661	STCAATGCAG	ACGGACAGTA	CCTCTTCTGC	AGGTAAGTGA	AACCCACAGG	CACACCCAAAG
721	GCCCTCATCT	TTGTGTCCCA	TGGAGCCGGA	GAGCACAGTG	GCCGCTATGA	AGAGCTGGCT
781	CGGATGCTGA	TGGGGCTGGA	CCTGCTGGTG	TTCGCCACG	ACCATGTTGG	CCACGGACAG
841	AGCGAAGGGG	AGAGGATGGT	AGTGTCTGAC	TTCCACGTTT	TCGTGAGGGA	TGTGTTGCAG
901	CATGTGGATT	CCATGCAGAA	AGACTACCCT	GGGCTTCCTG	TCTTCCTTCT	GGGCCACTCC
961	ATGGGAGGGG	CCATCGCCAT	CCTCACGGCC	GCAGAGAGGC	CGGGCCACTT	CGCCGGCATG
1021	STACTCATT	CGCCTCTGGT	TCTTGCCAAT	CCTGAATCTG	CAACAACCTT	CAAGGTCCTT
1081	GCTGCGAAAG	TGCTCAACCT	TGTGCTGCCA	AACCTGTCCC	TCGGGCCCAT	CGACTCCAGC
1141	GTGCTCTCTC	GGAAATAGAC	AGAGGTCGAC	ATTTATAACT	CAGACCCCTT	GATCTGCCGG
1201	SCAGGGCTGA	AGGTGTGCTT	CGGCATCCAA	CTGCTGAATG	CCGTCTCACG	GGTGGAGCGC
1261	GCCCTCCCA	AGCTGACTGT	GCCCTTCCTG	CTGCTCCAGG	GCTCTGCCGA	TCGCTTATGT
1321	SACAGCAAAG	GGCCCTACCT	GCTCATGGAG	TTAGCCAAGA	GCCAGGACAA	GACTCTCAAG
1381	ATTTATGAAG	GTGCTTACCA	TGTTCTCCAC	AAGGAGCTTC	CTGAAGTCAC	CAACTCCGTC
1441	TTCCATGAAA	TAAACATGTG	GGTCTCTCAA	AGGACAGCCA	CGGCAGGAAC	TGCGTCCCA
1501	CCCTGATGC	ATTGGCCGGT	GCCCGGCTCA	TGGTCTGGGG	GATGCAGGCA	GGGGAAGGGC
1561	AGAGATGGCT	TCTCAGATAT	GGCTTGCCAA	AAAAAAAAAA	AAAAAAAAAT	CAGAAATTGG
1621	AGAAATCCTT	AGCACAAATT	TCTAAAAAAT	AACAGACATT	TTGTTATAC	ATTAGACTAT
1681	CAGACACTGG	ACCTACCTTA	ATGTTAGAC	ACTTTATGCA	AAAAAAGAGA	AAGGTCCCAG
1741	GTGATTTTCC	ACAAAGAATG	TGCTAAAATG	TCCACTGAAA	ACAAAAGCCAA	GCCTCTGCCC
1801	TGCCTCTCCC	AGCTCCACAA	AGGTTCCAG	GAATTCCTGG	TGTTCCAGG	ACACCAGACT
1861	GCAATAACTG	GAGGCGCCTC	CTTCCTGCC	ACCCCTCGCT	CACGCCCCAG	CGCCCTCTCT
1921	GACCAGCCTC	CGCTTGGTGG	CCTTCCTCTG	GCCGTGTGAT	GAGGTGGTTG	CTGTCTCCAT
1981	AGGGGCCAGC	TCCCCAGGGC	AGACTCACGT	GCCCTCTGTA	GGCTCAGAAA	ATGCCAGCC

Figure A.1: CDS of MAGL1 and MAGL3 according to NCBI. Turquoise colour represent the missing part in MAGL3 isoform in comparison to MAGL1.



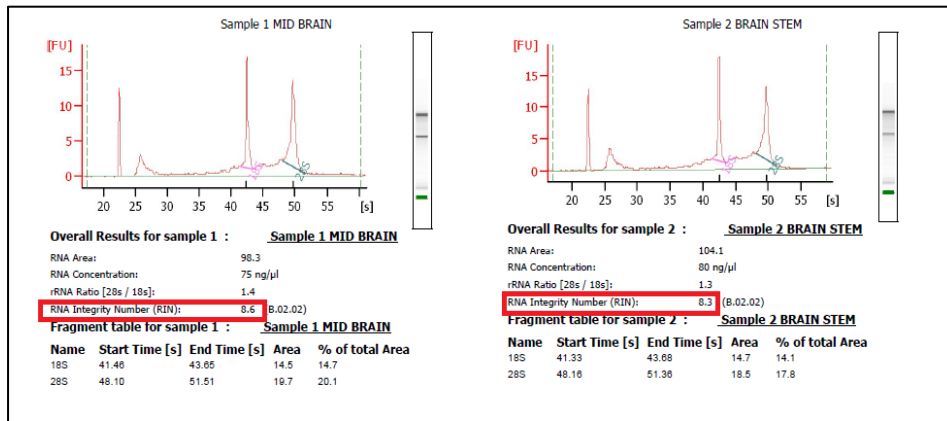


Figure A.2: Representative images from the results of Agilent test showed that high quality RNA from different rat tissues which was used in Taqman mRNA quantification.

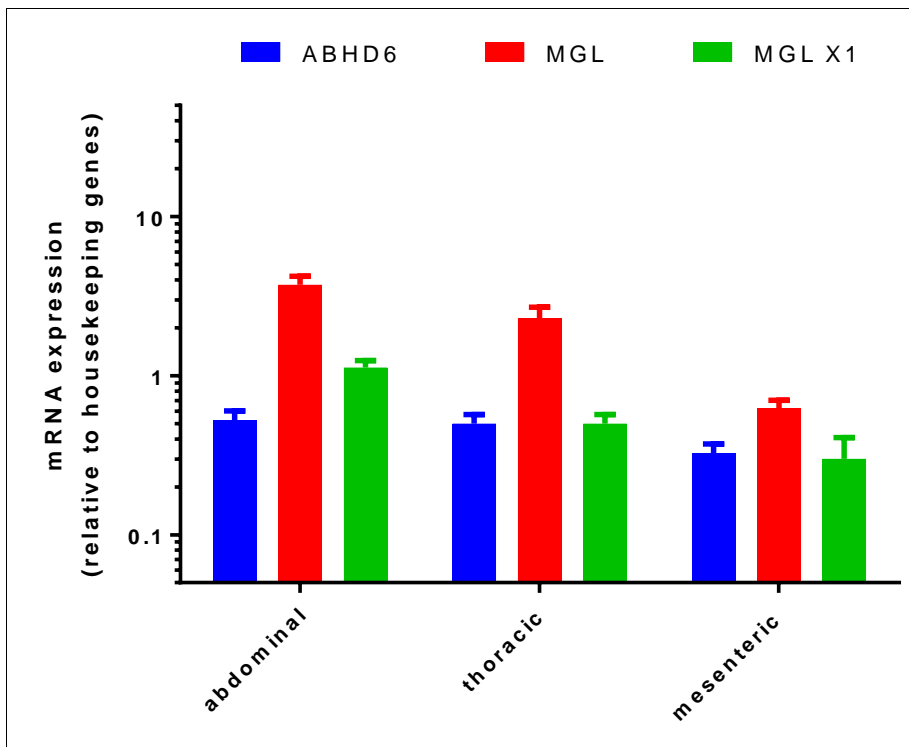


Figure A.3: RT-qPCR analysis of the distribution of rat MAGL, X1MAGL and ABHD6 mRNAs in rat abdominal, thoracic and mesenteric aorta. Data were normalized to the geometric mean of three reference genes (β -actin, TBP and GAPDH). Data represent means \pm SEM of three separate technical experiments from a single male rat.

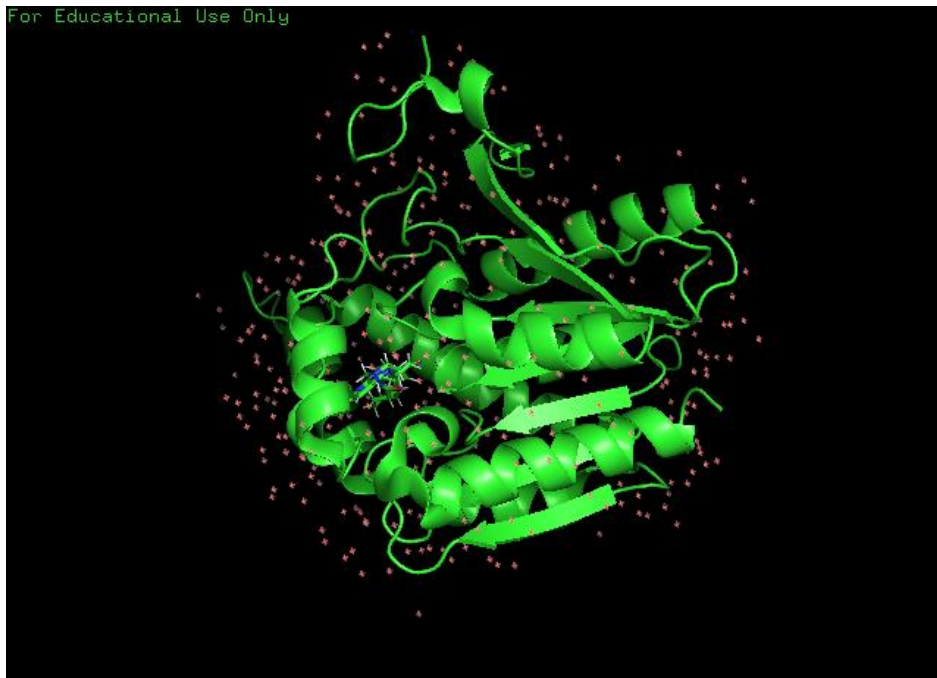


Figure A.4: A pseudo-3D representation of MAGL1 (3PE6), with an inhibitor bound, illustrated using PyMOL. Adapted from (Schalk-Hihi *et al.*, 2011)

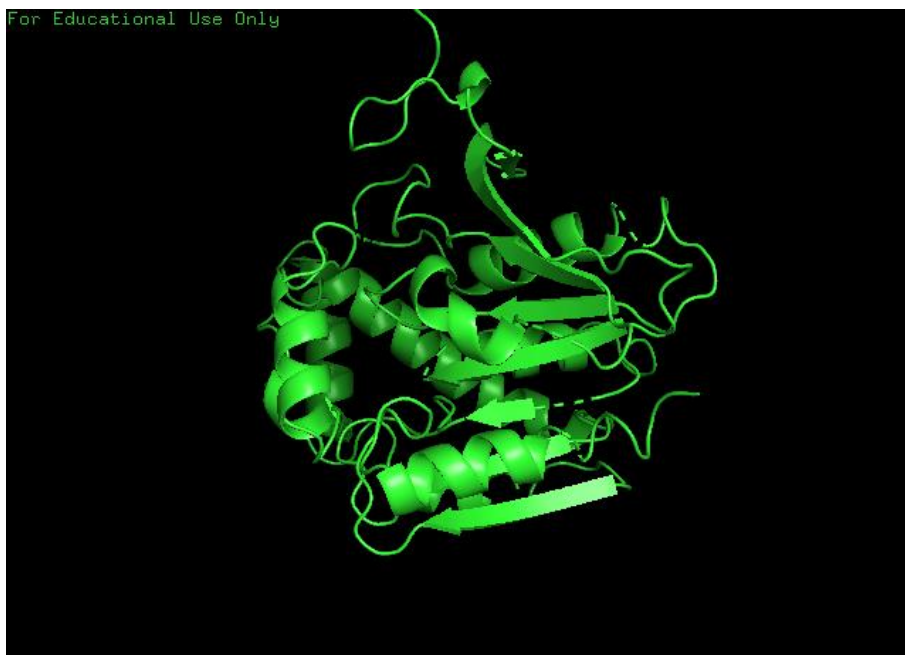


Figure A.5: A pseudo-3D representation of MAGL1 generated by Phyre and illustrated using PyMOL (SPH Alexander).

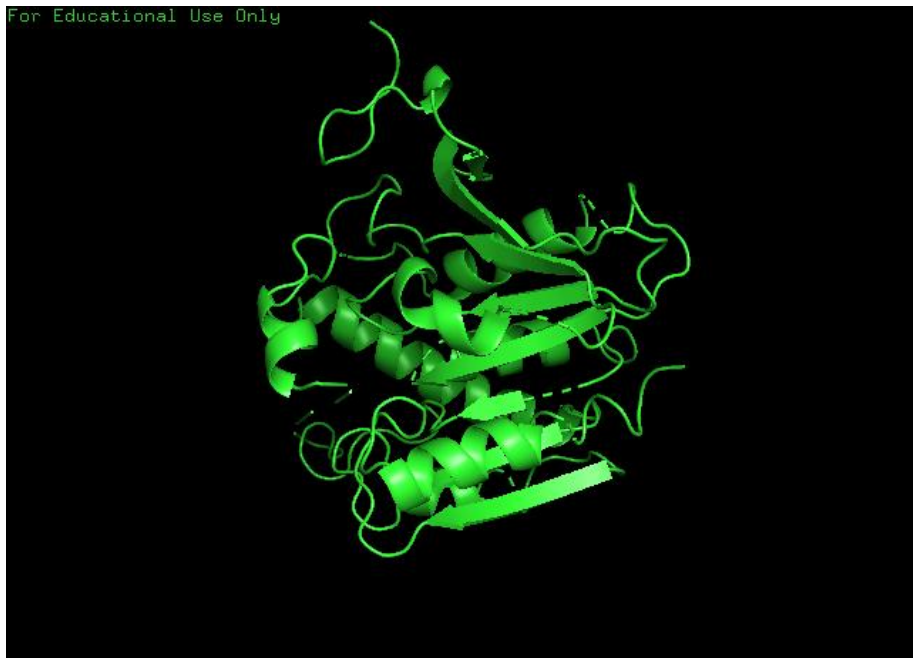


Figure A.6: A pseudo-3D representation of MAGL2 generated by Phyre and illustrated using PyMOL (SPH Alexander).

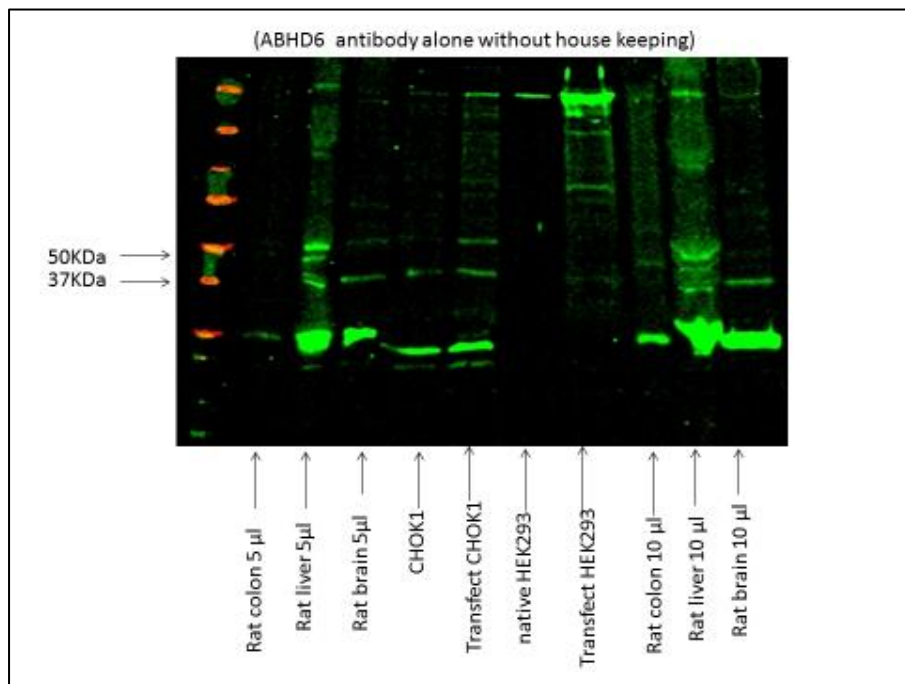


Figure A.7: A representative image for non-specific binding of ABHD6 antibody (GTx87697).

8.2 Section B

The two most common reasons endorse the usage of viral vector in research are: it is a powerful tool of transferring a gene into a hosting genome (Hwang *et al.*, 1984) and its efficiency to delivery gene of interest into primary and other hard-to-transfect mammalian cells. Therefore, this study was aimed to introduce ABHD6 gene into rat primary cell cultures, namely neurons and astrocytes to study the subcellular localization of this enzyme. N-terminus of ABHD6 was chosen to be the virus as it had shown a nuclear membrane distribution in transfected HEK293.

Gateway[®] Technology is a cloning system that takes the advantage of the site-specific recombination properties of bacteriophage lambda (Landy, 1989) to facilitates the integration of lambda into the *E. coli* chromosome. Lambda reaction rest on the presence of DNA recombination sequence (*att* site) and an enzyme that mediate the reaction (Clonase).

This is a rapid and highly efficient tool to transfer the gene of interest between multiple vector systems (Hartley *et al.*, 2000) without loss of nucleotides and does not require DNA synthesis. Two DNA recombination reaction occurs between specific attachments (*att* sites) of the two interacting DAN molecules: The first one called BP recombination reaction to create an entry clone; by joining an *attB* from DNA fragment (PCR product) and *attP* site (provided by pDONR™ vectors). This is followed by creating an expression clone by the LR recombination reaction; *attL*-containing entry clone and *attR*-containing destination vectors (pINDUCER system). After each of the above reactions, transformation of specific strains of *E. coli* was followed (accompanied by the usage of appropriate controls and selection antibiotics) and send for sequencing (using the recommended primers for each vector).

pINDUCER system was choose as destination vector in this study as it is well known to provoke a rapid and doxycycline dependent expression of different genes in different cell types (Meerbrey *et al.*, 2011).

In order to produce a lentivirus, transfection of a suitable host cell line (HEK293FT) (Gibco, R700-70) with three types of plasmids is needed: first a plasmid that carry the gene of interest (transfer plasmid; N-ABHD6). The second one is the packaging system plasmid (pxPAX2)(Addgene, 12260) and finally the envelope plasmid (pMD2.G)(Addgene, 12259). The virus type produced here was pseudo particles of retrovirus. From safety point, it is an in active virus (Tiscornia *et al.*, 2006). Nevertheless, disposal of the materials afterward was done following recommended guidelines for Bio Safety Level (BSL-2). After its production, it need viral concentration, although it is sometimes optional (in this project and in (<https://www.cellecta.com/wp-content/uploads/Cellecta-Manual-Construct-Packaging-Transduction-v9a.pdf>) both conditions were working to the same extend). Finally, infection of the hosting cells was done.